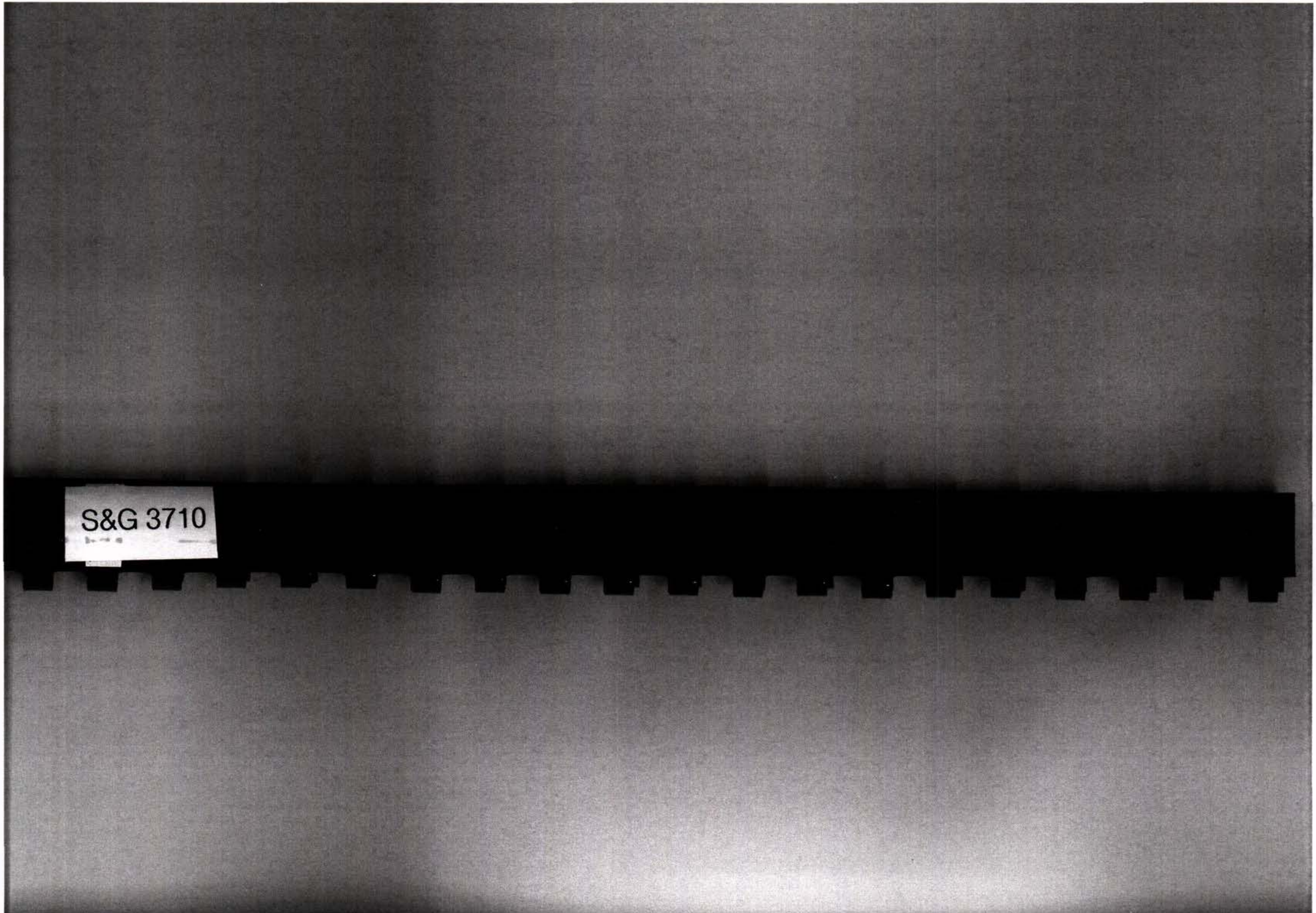
S&G 3710

S+G
3710

STRAIN ACCUMULATION AND EPISODICITY OF FAULT MOVEMENTS IN OTAGO

RESEARCH UNDERTAKEN BY:

Professor Richard J Norris

Ross Nicolls

(Geology Department, Otago University)

Funded by EQC

EQC RESEARCH REPORT 01/445

JUNE 2004

UNIVERSITY of OTAGO

SAPERE AUDE

Te Whare Wānanga o Otāgo

SCIENCES

STRAIN ACCUMULATION AND EPISODICITY OF FAULT MOVEMENTS IN OTAGO

RESEARCH UNDERTAKEN BY:

Professor Richard J Norris

Ross Nicolls

(Geology Department, Otago University)

Funded by EQC

EQC RESEARCH REPORT
01/445

JUNE 2004

Episodic Fault Behaviour in East and Central Otago

Executive Summary

We present the results of a pilot study of episodicity of fault movement among a number of parallel reverse faults in Central and East Otago. South of Jackson Bay, the Alpine Fault exhibits very low dip-slip values, and active deformation east of the fault suggests a high proportion of the orthogonal convergence is partitioned onto structures across Otago. Previous investigations of the Pisa-Grandview and Dunstan Faults in Central Otago, and the Titri and Akatore Faults in coastal Otago produced evidence suggesting periods of enhanced activity followed by long periods of quiescence, with a possible temporal switching of activity between structures. This study places constraints on the timing of the most recent activity on intervening structures by relating surface deformation to datable deposits. In addition, the current rate of regional strain accumulation is established enabling constraint of the total amount of displacement required within the region, and a comparison with geologically determined longer-term rates. This project involved three principal avenues of investigation:

- Obtaining reconnaissance observations of tectonic geomorphology along the southeast range fronts between the Dunstan Range and the east coast and producing more detailed studies of a few selected sites on individual range fronts.
- Obtaining OSL ages on critical horizons that can place age constraints on the timing of the most recent surface deformation associated with rangefront faulting.
- Occupation of two high-precision GPS monitoring sites and comparison with Dunedin continuous base station to establish current strain rate and distribution across the region.

All investigations were carried out successfully and a wealth of new data was obtained which has some interesting implications for seismic hazard assessment and the mechanics of deformation within Otago. The results from the three lines of investigation may be summarised as follows:

- All rangefronts exhibit distributed deformation with no continuous range-scale surface ruptures evident. On a large scale, rangefront deformation is revealed by lineaments formed of stream course deviations and slope breaks. Small-offset range-parallel faulting and folding found both within the ranges and within basin sediments are the norm. These observations are consistent with a model of fold propagation above buried reverse faults. In map view, some of the rangefronts are distinctly sigmoidal and their departure from linearity appears to be structurally controlled. The inflection points are commonly the sites of anomalously-striking stream incision and along-strike extrapolation of known fault segments. Many of the ranges appear to have formed by the amalgamation of en-echelon segments rather than growth on a single continuous structure.

- The Holocene ages of all but one of the sites within deformed rangefront sediments implies the current level of seismic activity in Otago is perhaps higher than previously perceived. This perception is no doubt due in part to the subtle nature of the distributed deformation and lack of prominent continuous fault scarps, combined with a low historical seismicity.

  The amalgamation of OSL ages, geomorphologic and geological data, has enabled tentative estimation of uplift rates of some of the ranges. If it is assumed that the faults dip at around 45°, then heave equals throw, or uplift rate equals shortening rate. These figures are:

  1. Taieri Ridge - 0.6 ± 0.04mm/yr averaged over 12.9 ± 1.1ka
  2. Rock and Pillar Range – 0.15 ± 0.01mm/yr averaged over 8.42 ± 0.83ka
  3. Rough Ridge - 0.18 mm/yr to 0.44 mm/yr averaged over 2.5-1.0Ma (minimum-maximum limits); 0.86mm/yr averaged over 130ka; and 0.27mm/yr averaged over 4ka. These figures for Rough Ridge are comparable with rates obtained in a companion study using ^{10}Be isotopes within sarsen stones (quartzite boulders) to date the timing of peneplain exposure on South Rough Ridge (Jackson *et al.*,2002).

- GPS data indicate a contraction rate of 1.58 ± 0.18 mm/yr between Dunedin and Hyde Rock, and 2.2 ± 0.88 mm/yr between Dunedin and Makarora. Both estimates are subject to uncertainty. These are linear contraction rates which are roughly perpendicular to the strike of the faults in this study, so comparison with shortening determined by dip-slip on these faults is justified. The rate between Dunedin and Makarora is consistent with estimates of long-term contraction across the region based on fault displacement data, but the Dunedin-Hyde Rock rate is faster than might have previously been expected. However, the GPS-derived short term contraction rate across east Otago is compatible with the range-front deformation data and is consistent with the conclusion that east Otago is currently an area of increased activity.

The new data presented raise the likelihood for the contribution of structures other than the Dunstan and Akatore Faults to seismic hazard in Otago. Clearly, Holocene activity has occurred on other structures across the province which offer potential for sizeable earthquakes. Assuming a reasonably constant contraction rate of 1.5mm/yr between Hyde Rock and Dunedin, at least 15m of shortening is required within the region for the Holocene. Documented offsets on the Dunstan and Akatore faults can account for almost half of this requirement and, as this study shows, at least some of the balance has resulted in activity on intervening structures. Currently therefore, all faults in east Otago except for the Titri Fault must be viewed as potentially active.

Whereas there are faults which exhibit long periods of quiescence strongly indicating episodic behaviour, the new data presented here show that several faults in east Otago have been active simultaneously during the Holocene and that a simple model of episodicity is unlikely. More

detailed work is required on each of these structures to determine their individual seismic history. OSL dating techniques have proved invaluable in placing age constraints on deformation within materials traditionally difficult to date accurately.

CONTENTS

1 INTRODUCTION

2 INTRODUCTION

The boundary between the Australian and Pacific plates passes through the South Island of New Zealand (*Fig. 1.1*). Movement across the plate boundary in central South Island according to the Nuvel I A plate model (DeMets et al., 1994) is 37 mm/yr on an azimuth of 071°. The major structure accommodating this movement is the Alpine Fault, which strikes on an average bearing of 055° along the western side of the island.

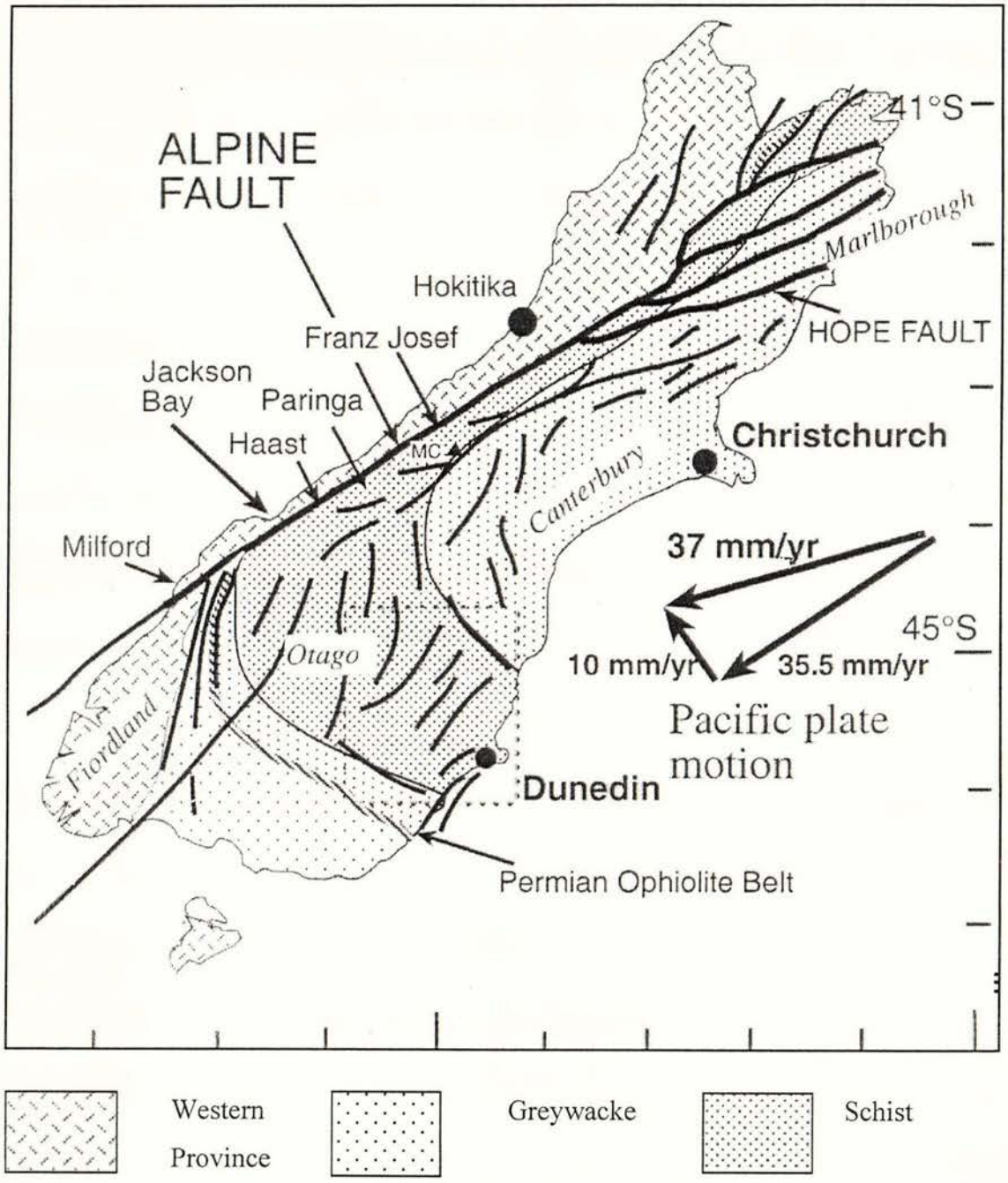

Fig. 1.1 **Map of South Island showing Alpine Fault, smaller faults to the east, and Nuvel 1A plate motion. Box is area in Fig. 1.3.**

The component of plate motion parallel to the Alpine Fault is c. 35 mm/yr with c. 10 mm/yr normal to the fault. Best estimates of late Quaternary slip rates along the fault are compatible with a strike-slip rate of 27±5 mm/yr and a variable dip-slip rate of 0-10 mm/yr (Norris and Cooper, 2001). The maximum rate of dip-slip is in the central part of the fault, where the Southern Alps reach their highest elevation. South of the Glaciers, the dip-slip rates decrease to zero south of Jackson Bay (*Fig. 1.2*). Clearly, a portion of the total plate motion, and to the south, a high proportion of the convergence, is partitioned onto structures other than the Alpine Fault. Deformation, faulting and uplift east of the fault suggests at least some plate motion is being taken up across the South Island within the Pacific plate.

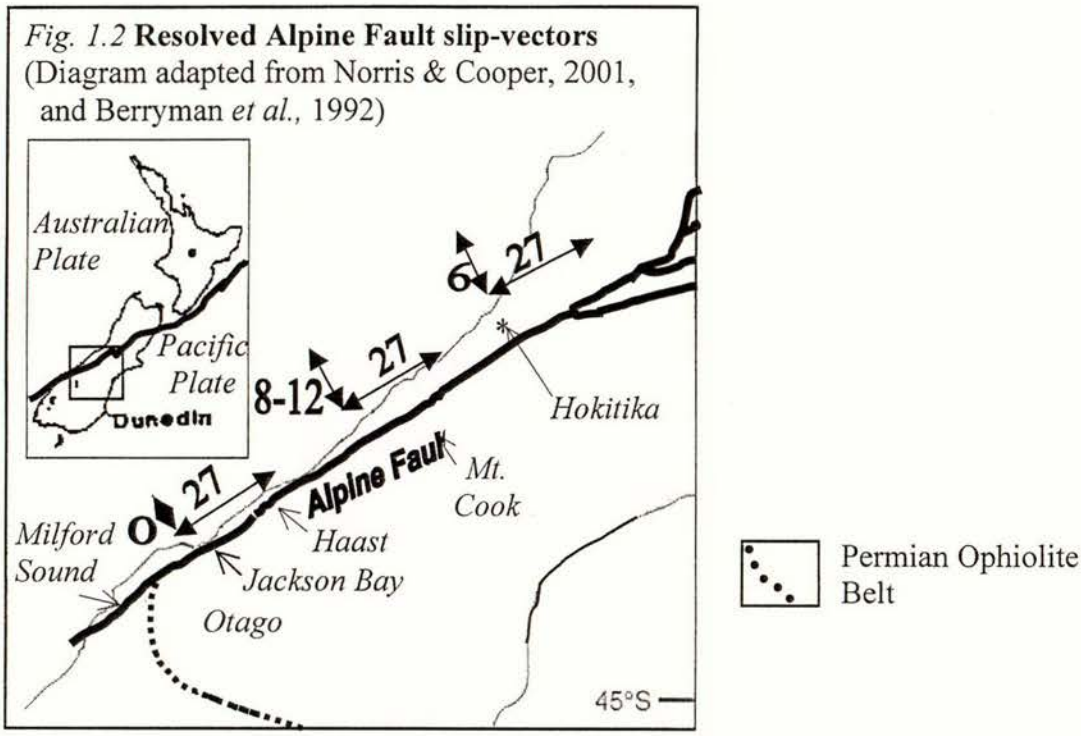

Fig. 1.2 **Resolved Alpine Fault slip-vectors** (Diagram adapted from Norris & Cooper, 2001, and Berryman *et al.*, 1992)

East of the Alpine Fault, the zone of active deformation is widest across Otago, and adjacent to the zone of low dip-slip values on the fault. Central Otago is characterized by a number of parallel, northeast-trending ranges separating broad, flat-bottomed valleys (Fig. 1.3). The ranges are generally asymmetric, with steeper southeast range fronts. Several of the ranges have some evidence of faulting along these steeper sides (e.g. Beanland et al., 1986), and in some instances, also along their northwest flanks (e.g. Markely and Norris, 1999, Thomson, 1996). Most show evidence for range-scale asymmetric folds and may be viewed as large fault-propagation folds above blind reverse faults at depth (Jackson et al., 1996; Markely and Norris, 1999).

The basement rocks of central Otago are schists of the Haast Schist zone. They are mostly within lower greenschist facies, with lower grades to the northeast and southwest (Mortimer, 1993). The schists were uplifted and eroded during the late Cretaceous and early Tertiary to form a peneplain surface on which sediments were subsequently deposited (Bishop, 1994; Le Masurier and Landis, 1996). In Central Otago, these sediments consist of fluvial and lacustrine sediments of the late Miocene Manuherikia Group (Dunstan and Bannockburn Formations, respectively) overlain by Pliocene fluvial conglomerates (Maniototo Conglomerate) derived from uplifting greywacke hills to the north (*Fig.1.1*; Youngson et al., 1998). These sediments have been deformed by faulting and folding of the ranges and mostly stripped off the uplifted ridges (Bishop, 1994). Thus the deformed peneplain surface makes an ideal marker surface for late Cenozoic deformation (Jackson et al., 1996).

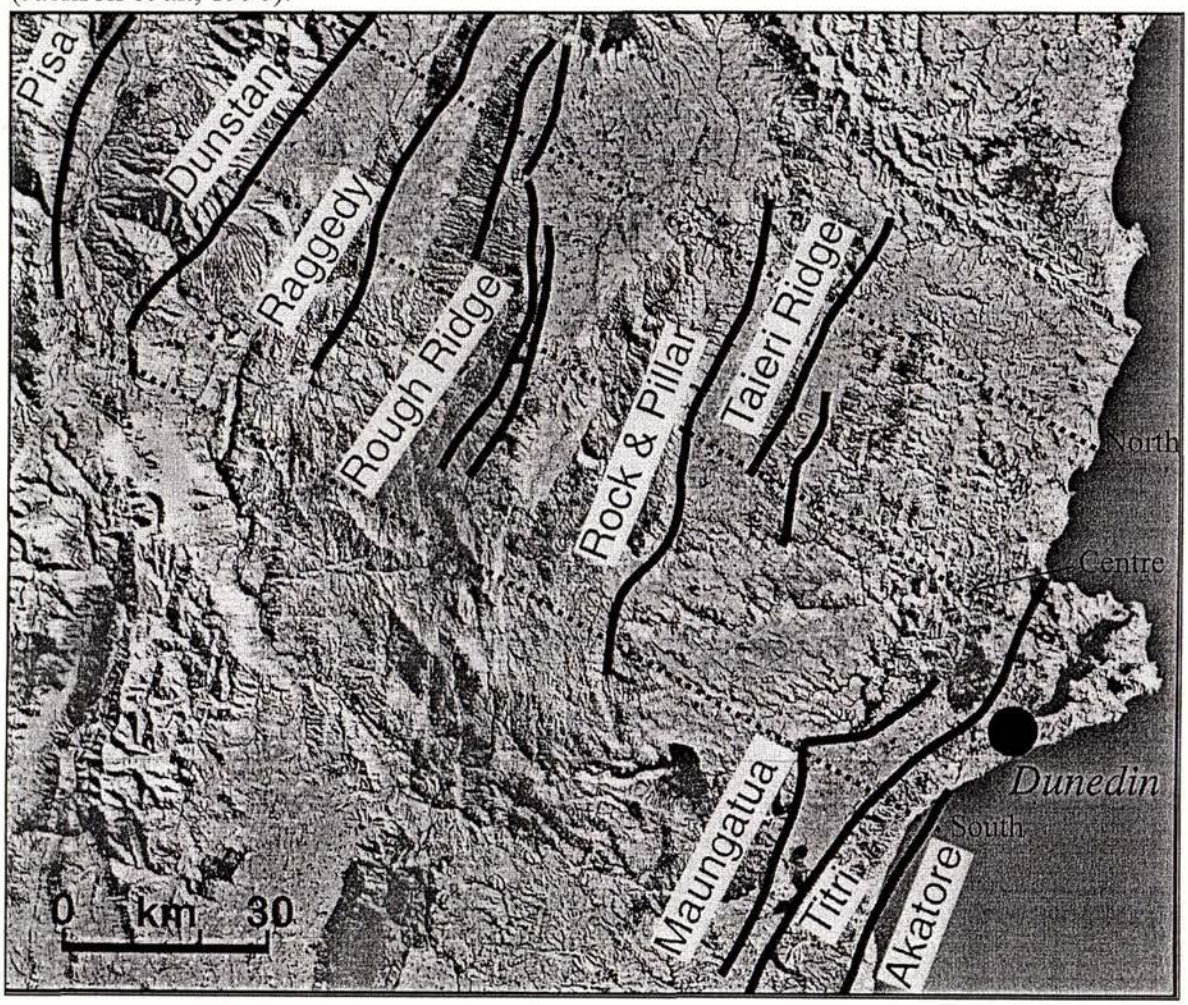

Fig. 1.3 **Otago fault province showing major NE trending ranges and bounding fault structures (note only NE striking faults are highlighted as these are the subject of this project; Cardrona Fault is off the picture to the NW).**

Cotton (1917, 1919) presented some of the earliest studies of the tectonic geomorphology of the region. Detailed paleoseismological work in the upper Clutha area was undertaken by the N. Z. Geological Survey during the early 1980s as part of the engineering investigations for the Clyde dam project (e.g. Beanland et al., 1986; Beanland and Barrow-Hurlbert, 1988; Beanland and Forsyth, 1988; Beanland and Berryman, 1989). These studies produced a wealth of data on late Quaternary faulting in the region and clearly demonstrated the active nature of the Otago fault province. Based on these investigations, Beanland and Berryman (1989) were the first to suggest that activity on these faults may be episodic, with periods of high activity on one fault being followed by long periods of quiescence while activity transferred to another structure in the region. They reported evidence from deformed alluvial fans along the Pisa-Grandview fault zone that indicated an active period around 250,000 ago followed by a long period of quiescence which gave way to further activity from about 70 to 50 or 35 ka. No evidence was found for activity in the last 23,000 years whereas the Dunstan Fault shows abundant evidence for movement during this period (Beanland et al., 1986; Beanland and Berryman, 1989; Berryman and Beanland, 1991). Berryman and Beanland (1991) referred to this behaviour as intermittently characteristic as distinct from the characteristic model of earthquakes commonly used in hazard assessment.

More recent work on the Titri and Akatore faults along the coast (Litchfield, 2000, 2001; Litchfield and Norris, 2000) has shown that these faults too show evidence for periods of enhanced activity followed by long periods of quiescence. For instance, the Akatore fault has evidence for two substantial ruptures during the past 4000 years but none during the previous 100,000 years. Prior to this, there was an earlier period of fault activity. Similarly, the Titri fault has evidence for a period of high activity prior to 100,000 years ago followed by quiescence. There is little data available on faults between the upper Clutha Valley and the coast although some fault traces are visible (Norris et al., 1995; Thomson, 1996; Jackson et al., 1996; Markley and Norris, 1999). A joint programme with Cambridge University and CNRS Orsay, France, on using cosmogenic isotopes to date the timing of surface uplift and erosion of the Tertiary sedimentary cover from some of the ranges is in progress, and preliminary data from one of the ranges, South Rough Ridge, suggests episodic propagation and uplift of the range over the last 500 ka. (Jackson et al., 2002).

Episodic behaviour of faulting has been described from other parts of the world where sets of parallel faults accommodate strain across a region (e.g. Wallace, 1987; Swan, 1988; Jackson and Leeder, 1994; Lee and Schwartz, 1996). By episodic behaviour, we mean a situation where each fault within a set does not exhibit a semi-regular 'return period'

between ruptures but instead, has periods of activity (i.e. 'clustering' of events) interspersed with long periods of quiescence during which displacement is accommodated on neighbouring faults. If episodic (or 'intermittently characteristic') behaviour is the norm amongst the Otago faults, then this has major implications for seismic hazard analysis (Kneupfer, 1992). Most seismic hazard analyses assume a characteristic event and an average return period for each fault within a region (e.g. Stirling et al., 1999). If faulting is episodic, however, then average return periods may be meaningless as only one or two faults may be active at any one time, but with shorter return periods than the general average. One way to assess this would be to carry out detailed paleoseismological studies on all faults and determine their past histories. The 'currently' active faults could be determined and their 'current' return period ascertained. Also, the probability of activity switching from a 'currently' active fault to a dormant fault could also be estimated. These concepts are discussed further in a later section. Unfortunately, paleoseismic data of any quality is only available for one or two faults (e.g. Dunstan, Pisa, Akatore) and even with these, more data is really needed to establish well-constrained probabilities. Carrying out the detailed paleoseismic work, however, is a long-term programme.

The only two faults in Otago for which there is unequivocal evidence of Holocene displacement are the Dunstan Fault (Beanland et al., 1986) and the Akatore Fault (Litchfield and Norris, 2000). For most faults, we have no data on their activity. Sharply defined surface breaks are rare, although distributed surface deformation is evident (e.g. Thomson, 1996; Markely and Norris, 1999). The ages of deformed surfaces and related sedimentary deposits are poorly known. The recent development of optically stimulated luminescence (OSL) dating in New Zealand (e.g. Rees-Jones *et al.*, 2000) provides a method of dating the younger (say <150ka) surfaces and gaining information on fault activity. Detailed study of range fronts is also needed to relate evidence of deformation to datable deposits. This work in tectonic geomorphology is needed before detailed trenching studies are feasible.

The present project is designed to obtain reconnaissance observations along a number of range fronts in central Otago, to then produce more detailed studies at a few selected sites on different range fronts, and to obtain OSL ages on critical horizons that can place age constraints on timing of surface deformation. This should provide a framework in which the general fault behaviour can be assessed and more detailed work undertaken.

A second, lesser objective is to determine the current rate of shortening across Otago by occupying two survey sites with GPS receivers for a sufficient time to reduce noise. The two sites chosen were Hyde Rock and Makarora Trig . Both these sites were occupied for extended periods in 1995, 1996, 1997, 1998, and 2001, and their positions established relative to the Dunedin continuous GPS station. By comparing the new positions with the previously determined ones, any displacement of the stations with respect to Dunedin can be established within relatively small error limits, and the average rate of elastic strain accumulation determined. This will provide us with some estimate of the rate of regional strain accumulation, which should be released by permanent deformation along the range fronts.

2 REGIONAL BACKGROUND

2.1 Basement History of Central and east Otago

Basement is the Otago Schist, part of the Haast Schist group, which is within the Carboniferous to Cretaceous Torlesse terrane of the South Island's Eastern Province (*Fig. 2.1*; Bradshaw et al., 1981; Yardley, 1982; MacKinnon, 1983; Bishop et al., 1985). The Eastern Province consists of terranes interpreted as being accreted onto the Gondwana margin from the Triassic through the Cretaceous (e.g. MacKinnon, 1983; Bishop et al., 1985; Korsch & Wellman, 1988; Mortimer & Campbell, 1996). During the Early-Middle Jurassic "Rangitata I Orogeny" the amalgamation the Caples and Torlesse Terranes produced the moderately high-pressure metamorphic belt forming the Haast Schist (Wood, 1962; Bradshaw et al., 1981; Yardley, 1982; Roser & Cooper, 1990; Mortimer 1993, 2000; Adams & Graham, 1997; Deckert et al., 2002). This is divided geographically into the Marlborough, Alpine, and Otago Schists.

Fig. 2.1 **Simplified pre-Late Cretaceous basement**
(diagram adapted from Deckert *et al.*, 2002)

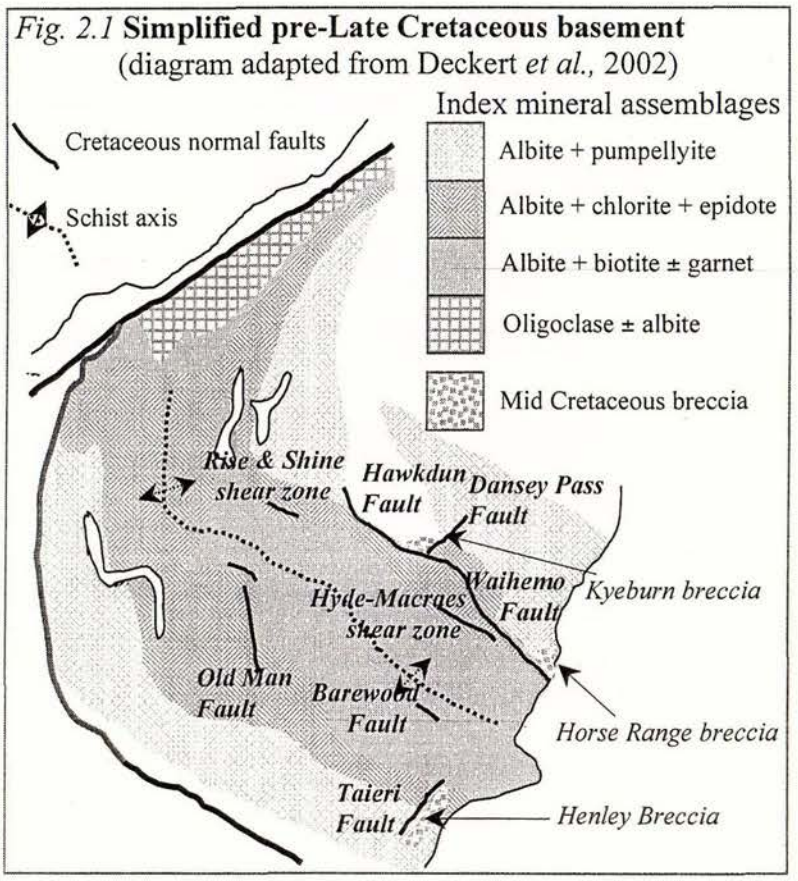

Rifting associated with mid Cretaceous Gondwana break-up produced normal faulting, exhumation, and erosion of the basement and deposition of breccia within rift-related graben of at least 1 km relief (Mutch & Wilson, 1952; Balance, 1993; Le Masurier & Landis, 1996; Deckert *et al.*, 2002). The first appearance of schist clasts in the Kyeburn Formation indicates deep-buried Torlesse rocks were exhumed by 105Ma, during the initial rifting phase (e.g. Bishop & Laird, 1976; Korsch & Wellman, 1988).

There is no evidence of a regional low-relief surface prior to breccia deposition. The extensive near planar erosion surface was formed by fluvial erosion followed by marine transgression and wave planation subsequent to the 85Ma Gondwana break-up (Le Masurier & Landis, 1996). This surface truncates mid-Cretaceous and older rocks including the breccia and is known alternatively as the "Cretaceous peneplain" (Benson, 1935), the "Otago peneplain" (Cotton, 1949; Bishop, 1994), or the "Waipounamu erosion surface" (Le Masurier & Landis, 1996).

Within the Otago Schist, metamorphism increases from prehnite-pumpellyite facies at the peripheries to greenschist facies in the centre, forming a ~150km wide two-sided arch. Peak metamorphic temperatures and pressures of 350-400°C and 8-10kbar in the centre (Mortimer, 2000)(*Fig.2.1*) accompany an increase in deformation as defined by the progressive development of fold generations and foliation transpositions (e.g. Hutton & Turner, 1936; Bishop, 1972; Turnbull *et al.*, 1993; Turnbull, 2000). Textural changes in the schist form zones that parallel metamorphic and deformational changes across the arch. These are used as indicators of post-rnetamorphic faulting (e.g. Craw. 1998).

Fig. 2.2 **Study area and major faults and folds offsetting the Otago peneplain surface**
(Diagram adapted from Forsyth, 2001; Turnbull, 2000)

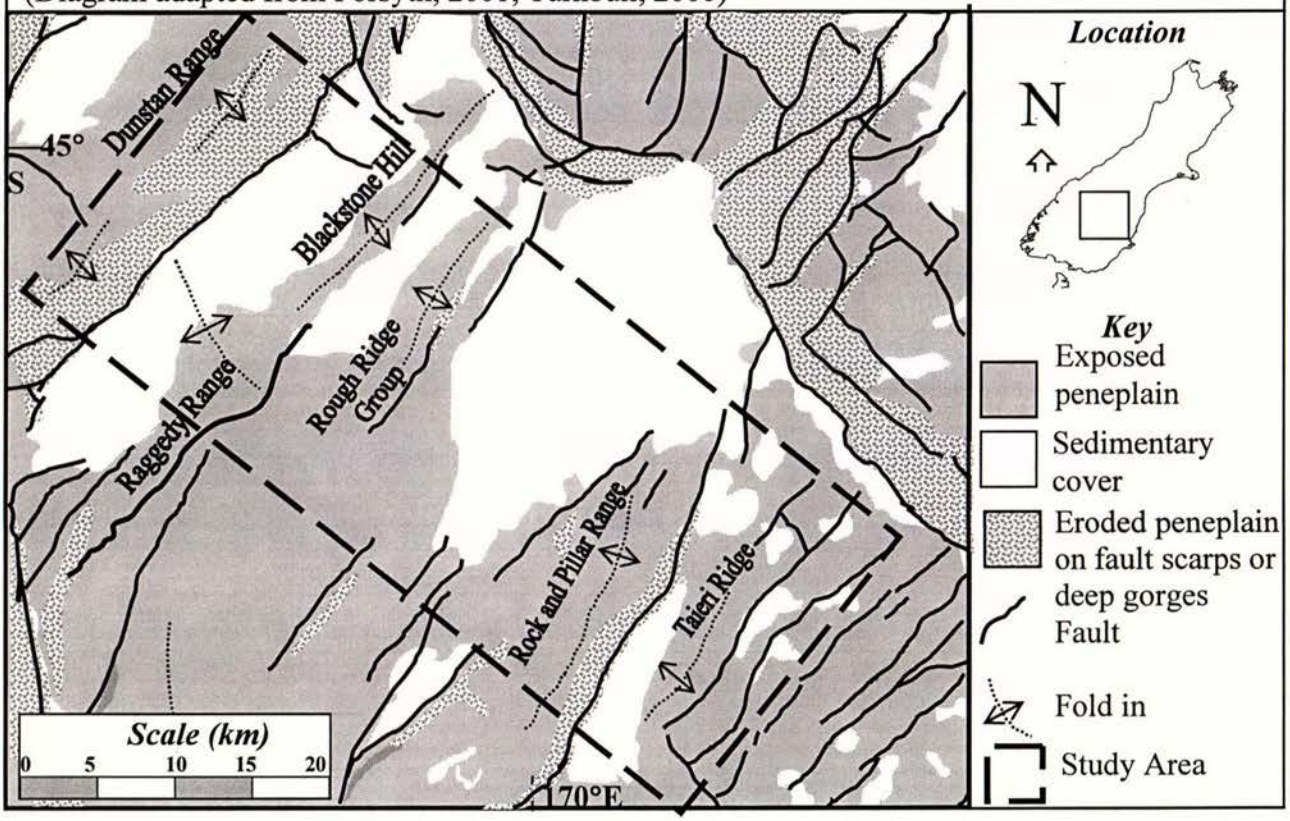

Miocene-Recent deformation related to formation of the Alpine Fault has faulted and folded the erosion surface within central and east Otago to produce the present-day basin and range topography (e.g. Cotton, 1917; Bishop, 1994; Jackson et al., 1996; Turnbull, 2000; Forsyth, 2001: Deckert et al., 2002)(*Fig. 2.2*). The peneplain provides a valuable marker horizon which broadly constrains both total offset and long-term deformation rate of structures (e.g. Cotton, 1917; Bishop, 1972, 1974, 1994; Stirling, 1990; Jackson *et al.*, 1996, 2002; Markley & Norris, 1999).

2.2 Regional Seismicity

Alpine Fault focal plane solutions change from oblique thrusting adjacent to mid-Canterbury towards pure strike-slip adjacent to Otago (Berryman *et al.,* 1992, *Fig.2.3*). There is a coincident increase in the extent of seismicity, normal to the Alpine Fault, from c.100km in mid-Canterbury to c.200km in Otago.

Earthquake epicentres don't delineate known major faults in the Otago region, although the two prominent south-east trending divergent lineaments, at the north-west of the field area (*Fig. 2.3*), are within the Otago Schist basement. These epicentre lineaments approximately map out the boundaries between schist and greywacke (compare *fig.1.1*).

Fig 2.3 **Epicentres for earthquakes shallower than 15km** (Recorded by the NZNSN Jan 1st 1990 - Feb 28th 1993; adapted from Anderson & Webb, 1994, & Berryman *et al.*,, 1992)

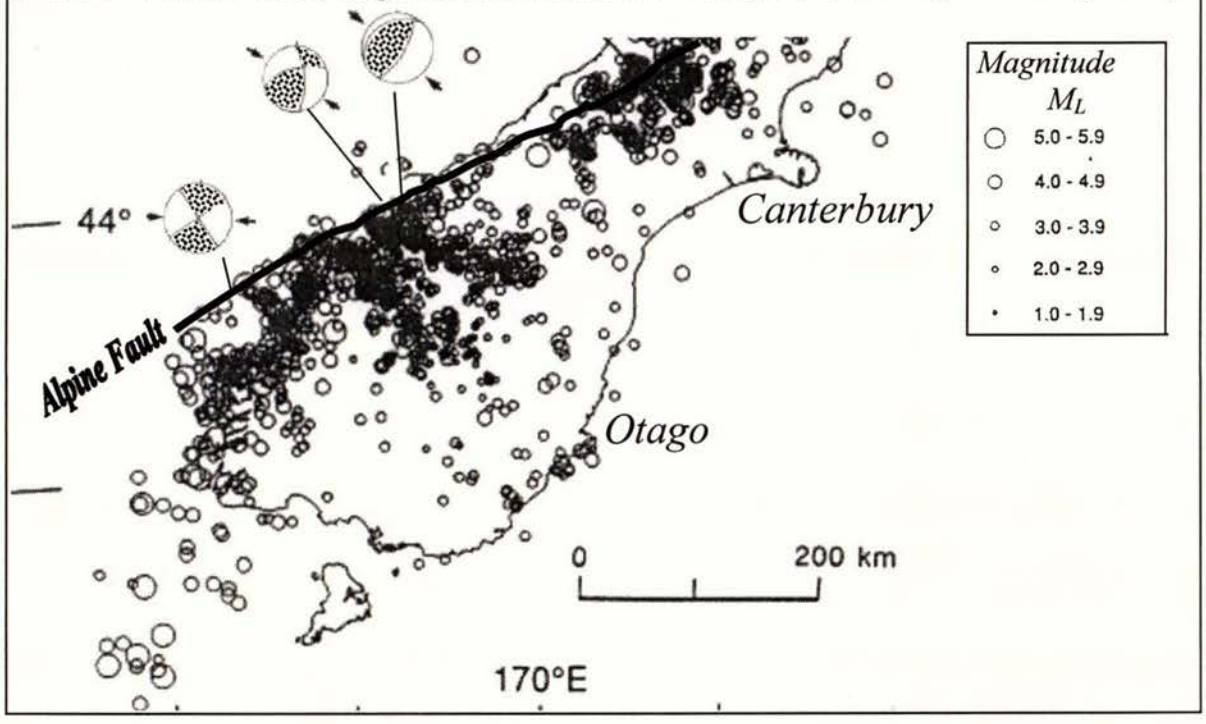

2.3 Previous Work

The actively rising ranges throughout Otago are assumed to be predominantly fault bounded, with long-term deformation rate broadly constrained by disruption of the late Cretaceous-Tertiary peneplain surface (e.g. Cotton, 1917, 1919; Bishop, 1972, 1974, 1994; Yeats, 1986, 1987; Jackson *et al.,* 1996; Le Masurier & Landis, 1996; Forsyth, 2001). Surface evidence of range-scale faulting is equivocal and ranges are interpreted as large fault-propagation folds above blind faults, rather than large rigid fault blocks (Yeats, 1986; Norris *et al.,* 1987; Jackson *et al.,* 1996; Markley & Norris, 1999; Markley & Tikoff, 2003). The existence of faults at depth is supported by the linearity and abruptness of the rangefronts, and the width of the deformation zone associated with each rangefront (e.g. Beanland *et al.,* 1986; Salton, 1993; Markley & Norris, 1999; this study). Consequently, the relative contribution of faulting and folding to overall deformation is hard to ascertain (e.g. Yeats, 1986; Madin, 1988; Salton, 1993; Markley & Norris, 1999; Markley & Tikoff, 2003).

Fig 2.4 **Central and east Otago SPOT image**

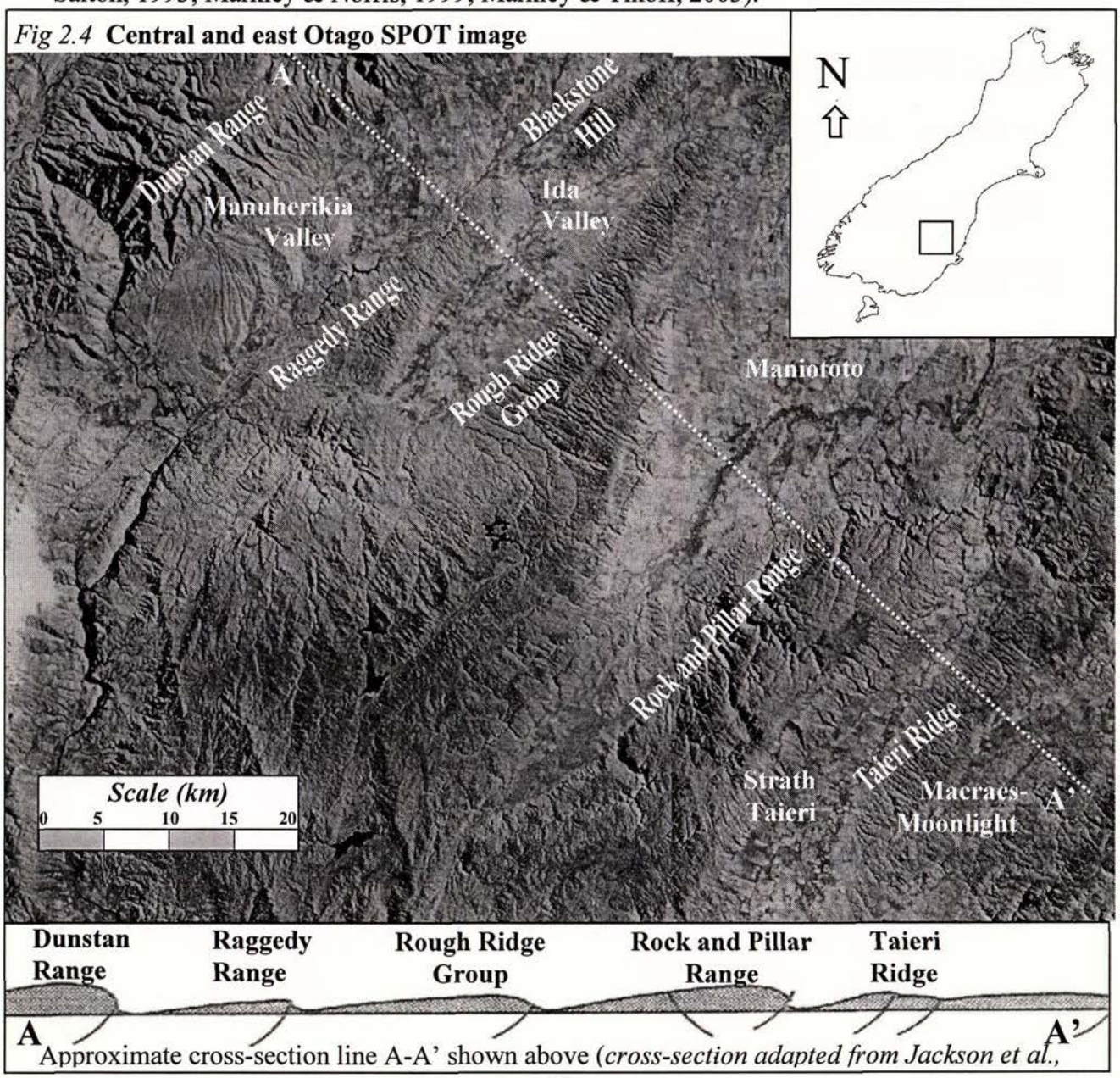

Approximate cross-section line A-A' shown above (*cross-section adapted from Jackson et al.,*

Paleoseismological work undertaken in the 1980s in connection with the Clyde dam project (e.g. Beanland *et al.*, 1986; Beanland & Barrow-Hurlbert, 1988; Beanland & Berryman, 1989) led Beanland & Berryman (1989) to suggest "intermittently characteristic" fault activity on the Pisa-Grandview fault zone. This fault zone bounds the Pisa Range and Lindis Peak mountains and the Cromwell-Tarras basin, immediately west of this study area (*Fig. 1.3*). Increased fault activity was inferred around 250,000 years ago, followed by quiescence until another active period around 70,000 – 35,000. This was achieved primarily by estimation of fault offsets in alluvial fans correlated to glacial end-moraines dated using a late Quaternary glacial chronology (e.g. Beanland & Barrow-Hurlbert, 1988), which was formulated by Officers of the Geological Survey in 1984 (*Table 2.1*). The named glacial advances and best estimates of their ages are based on correlation with the New Zealand record of late Quaternary climatic history (Suggate, 1965). Fans along the Clutha, Nevis, Cardrona, and Kawarau Valleys are correlated with this sequence (Beanland & Barrow-Hurlbert, 1988).

Table 2.1 **Glacial chronology for the Clutha Valley** (Officers of the Geological Survey, 1984)

Glacial Advance	Status	Estimated Age (years)
Northburn	Glaciation	500,000
Lowburn	Glaciation	250,000
Lindis	Penultimate Glaciation	140,000
Luggate	Stadial	70,000
Albert Town	Stadial (last glaciation)	50,000-35,000
Mt. Iron, Hawea	Stadial	18,000

This method of measuring and dating fault movements and surfaces necessarily involves large uncertainties. These are primarily due to;

1. the difficulty of correlating the elevations and identity of lithologically very similar stratigraphic horizons over a large region of known differential uplift;
2. the difficulty in distinguishing fault slip and separation, and thus true fault-related offset;
3. the lack of fault-movement direction indicators, e.g. slickensides, within outwash gravels;
4. the difficulty in assigning an absolute age to offset materials without significant uncertainty (Norris & Cooper, 2000).

Similar problems arise in areas unaffected by glaciation. In the Manuherikia basin, dating of Quaternary pediment surfaces is based largely on relative elevations and degree of weathering of schist clasts (e.g. Madin, 1988). However, in spite of the problems in working with such difficult material, considerable advances have been made.

No evidence of activity within the last 23,000 years was found on the Pisa-Grandview fault zone whereas the Dunstan fault shows abundant evidence of movement for this period (Beanland *et al.,* 1986; Beanland & Berryman, 1989; Berryman & Beanland, 1991). This may represent a temporal switching of activity from the Pisa-Grandview fault zone to the Dunstan fault (Beanland & Berryman, 1989).

Recent work on the sub-parallel Titri and Akatore faults, near the east coast, has shown that these faults also exhibit temporal switching of activity (Litchfield, 2000, 2001; Litchfield & Norris, 2000). The Akatore fault has evidence of two substantial ruptures during the past 4000 years but none in the preceding 100,000 years. There was an earlier period of fault activity prior to this. Conversely, the Titri fault has evidence for a period of high activity prior to 100,000 years, followed by quiescence.

Broad temporal relationships between fault and fold propagation and interaction have been established across Otago by assessing drainage pattern evolution (e.g. Jackson *et al.,* 1996). Topographic variations are attributed to structure, rather than differential erosion because of the consistency of metamorphic and textural grade between ridge-tops and rangefronts.

More recently, dating the duration of exposure of the peneplain surface using in situ cosmogenic ^{10}Be dating techniques on quartzite boulders has yielded growth and propagation rates for South Rough Ridge (Jackson *et al.,* 2002). Their data showed indications of episodic ridge growth with periods of activity in two clusters at around 150-100ka and 600-400ka, with the period between 400ka and 200ka being one of relative inactivity. There is little data available between the Dunstan and Titri faults and table 2.2 (next page) is a summary of fault data to date with a location diagram of faults proximate to this study.

Table 2.2 **Collective summary fault data from Otago**

Fault	Last activity date (yrs B. P.)	Recurrence interval	Long-term slip-rate (mm/yr)	Evidence OL=optical luminescence	Reference
Nevis-Cardrona fault system	<10,000	<3,600 av.		$^{13}C/^{12}C$ paleosol dates Fan & terrace scarps	Beanland & Barrow-Hurlbert, 1988
Pisa-Grandview fault zone	>23,000		1	folding of alluvial fans	Beanland & Berryman, 1989
Dunstan	1,000-5,000 (varies between segments)	8,000 (averaged over five segments)	-	$^{13}C/^{12}C$ dates from trenches Scarps on glacial terraces and fans	Madin, 1988
Blue Lake	late Quaternary		-	Scarp across modern floodplain	Madin, 1988
Spylaw	<10,000	>3,500	-	· Terrace scarp <10,000yrs	Beanland & Berryman, 1986
Blue Mountain #1	<16,000	>8,000	-	Scarps on fan correlated to 16,000-23,000 yr deposits	Beanland & Berryman, 1986
Hyde	<14,000	Best estimate 4,000-5,000	0.4-0.5	Scarps in alluvial fans overlain by loess	Norris *et al.*, 1994
Akatore	1,200	2,000-3,000	0.8-2.3	$^{13}C/^{12}C$ dates on swamp material Uplifted marine terraces	Litchfield, 2000
Titri fault system segments Allanton, Waihola Moneymore	70,000 40,000	70,000-80,000	0.8-2.3	OL dates in loess Uplifted marine terraces Alluvial fans	Litchfield, 2000

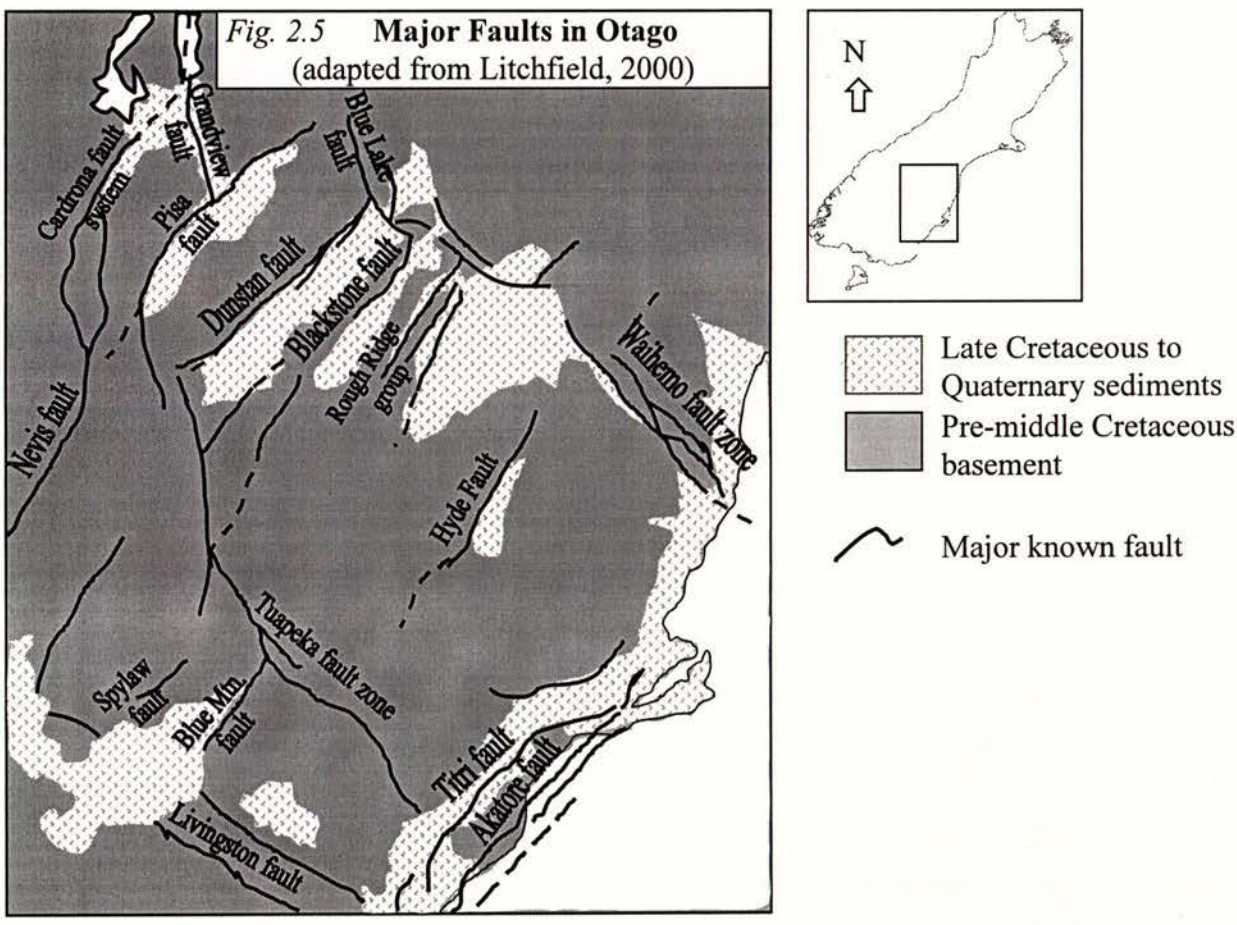

Fig. 2.5 **Major Faults in Otago** (adapted from Litchfield, 2000)

3 Episodic Behaviour in Central Otago

3 Episodic Behaviour in Cental Otago

The set of sub-parallel northeast-striking faults extending across Otago from Lake Wanaka to the Coast (*Fig. 1.3*) generally dip to the west and show reverse movement, with uplift of schist ranges on the western side. The eastern-most two faults, the Titri and Akatore faults, dip east and uplift ranges on their eastern sides (*Fig. 1.3*), The ranges are roughly equally spaced with a spacing of c.15 km. Some of the ranges, such as the Rough Ridge system (*Fig. 2.3*; Jackson et al., 1996), are composite and consist of several, probably linked structures. The spacing of the faults may be related to the thickness of the seismogenic, elastico-frictional part of the crust (Jackson et al., 1996), and would suggest a thickness also of about 15 km, a value compatible with the depth distribution of earthquakes in central South Island away from the Alpine Fault (Leitner *et al.*, 2000).

We estimated the total offset of the peneplain across each of the ranges along three transects and summed these to provide estimates of the total vertical displacement (*Fig. 1.3*). The peneplain was projected down to the fault plane where later sediments infilled valleys. Timing of onset of movement on the faults is uncertain, but the schist ranges were largely buried by thick deposits of greywacke-derived gravels during the Pliocene (Maniototo Conglomerate, Youngson et al., 1998). These gravels are deformed and rotated during uplift of the ranges, indicating that substantial uplift and stripping of the overlying sediments to expose the schist did not occur until the early Pleistocene. Pleistocene deposits contain abundant schist detritus.

Assuming a beginning of substantial displacement on the faults at c. 2.5 Ma, average vertical displacement rates may be calculated across the three transects as 1.9 mm/yr (south), 2.2 mm/yr (centre) and 2.4 mm/yr (north). These are minima, as they only include displacement across the major structures, and of course, displacement rates may not have been constant during the Pleistocene so they represent averages only. They do not take into account any strike-slip motion on the faults. If we assume that the faults dip at 45°, the vertical displacement (throw) is equal to the horizontal displacement (heave) and hence to the shortening across a reverse fault. Thus the calculated average rates are roughly equal to the average rates of shortening across the region accommodated by the major faults. The shortening rates differ between the three transects, possibly representing a real variation, but also reflecting variable data on individual structures in the different regions. Nevertheless, they suggest an overall average rate of shortening across Otago of 2-3 mm/yr.

There are little data on the size of single fault ruptures in Otago. Beanland *et al.* (1986) produce data suggesting a typical displacement in a single event on the Dunstan Fault of about 2 m. The last two displacements on the Akatore Fault produced offsets of 2-3 m (Litchfield and Norris, 2000). Two metres is compatible with the typical length of fault segments in Central Otago (Wells and Coppersmith, 1994; Stirling et al., 1998). At a rate of 2mm/yr, it would take 1000 yr to accumulate 2 m of shortening. If all 10 faults were slipping at equal, constant rates, then each would have a return period of around 10 ka. Larger faults may of course have shorter return periods. This average value is not incompatible with suggested return periods, although the Dunstan and Akatore Faults may have shorter return periods during their most recent period of activity (Beanland et al., 1986; Litchfield and Norris, 2000). What is remarkable, however, is that all faults investigated to date show long periods of quiescence, of over 10x the average return period. This strongly indicates irregular build-up of strain and its release on individual faults, as pointed out by Beanland and Berryman (1989). An alternative view, therefore, is that all the faults are part of a linked system (Beanland and Berryman, 1989). The whole area is strained elastically and release occurs by rupture on one of the faults. If ruptures are distributed randomly amongst the ten faults, then we can calculate the probabilities of one event being followed by any number of others. These figures are set out in Table 3.1 for a set of 10 faults. A probability of rupture of 0.1 (10%) is constant for the random model. The probability of a cluster of 5 or more events is only 0.01%. Similarly we can calculate the probability of periods of quiescence between ruptures (gaps) corresponding to any number of whole system return periods. From the discussion above, the whole system return period for the 10 Otago faults, for a single slip value of 2m and an average regional convergence value of 2mm/yr, should be around 1000 yr. The probability of a gap of 10 or more such periods (10,000 yr) is 39% and for 50 periods (50 ka) 0.5%. Given that existing data suggest gaps of at least 100 ka on at least four faults, the probability of this occurring under the random model would appear slight.

Table 3.1 **The first column gives the probability of subsequent failure, given a rupture on a fault. For a set often equal faults, 0.1 represents a random model where probability remains constant with time. Increased values represent models in which the probability of a fault rupturing for a second time increases. Probabilities of sequences of events forming clusters, and sequences of no-events, forming gaps, are calculated and tabulated (see text for discussion).**

Probability		1+	2+	3+	4+	5+	10+	20+	50+
0.1	Clusters	1	0.1	0.01	0.001	0.0001	10^{-9}		
0.1	Gaps	1	0. 9	0.81	0.73	0.66	0.39	0.12	0.005
0.2	Clusters	1	0.2	0.04	0.008	0.0016	6.4×10^{-5}		
0.2	Gaps	1	0.91	0.83	0.76	0.69	0.43	0.17	0.01
0.5	Clusters	1	0.5	0.25	0.125	0.0625	0.002		
0.5	Gaps	1	0.94	0.89	0.84	0.80	0.6	0.34	0.06
0.8	Clusters	1	0.64	0.51	0.41	0.33	0.13		
0.8	Gaps	1	0.98	0.96	0.93	0.91	0.82	0.65	0.33

A variation is to assume that, once a fault ruptures, its probability to rupture a second time increases. In Table 3.1, increased probabilities of 20%, 50% and 80% for subsequent rupture are calculated, compared to 10% in the random model. Probability of clustering of 5 or more events increases to 33% for the 80% value. Probability of gaps of 50+ periods also increases to 33%. The probability of long periods of quiescence increases exponentially with increasing weighting of subsequent rupture probability. It would appear from these simple calculations that some form of feedback mechanism following rupture (e.g. weakening of the fault) that increases the probability of further rupture is required to explain the long periods of quiescence reported.

This conclusion is further illustrated by *Fig. 3.1*. This is a simulation of a set of five faults breaking according to the principles outlined above. The top strip represents the rupture history of one fault under conditions of random rupture. The other strips represent the same simulation with weighted probabilities of further rupture on the same fault. Only at high weightings do long periods of quiescence appear.

Fig. 3.1 **Charts of an individual fault history within a set of 5 faults collectively accommodating the regional strain. Time in intervals of average return period per rupture somewhere in the whole system is represented by the horizontal axis. Each thin vertical line represents a rupture on the individual fault. Clusters of events increase with increased weighting factor. More importantly, long periods of quiescence only become frequent at high weighting factors. (See text for discussion.)**

4 Methodology

4.1 Optically Stimulated Luminescence Dating

Optically stimulated luminescence dating (OSL) is a technique used to measure the time elapsed since the last exposure of mineral grains (e.g. quartz and feldspar) to sunlight. The principle relies on natural minerals having structural defects in their crystal lattice, which act as local regions of positive charge forming traps for free electrons. When such minerals are exposed to sufficient sunlight, all light sensitive traps are emptied.

With subsequent burial, the electron traps fill at a rate determined by the dose of ionising radiation received by the minerals in question. Radiation originates from the decay of ^{235}U, ^{238}U, ^{232}Th, and ^{40}K within the minerals and their surroundings, and cosmic rays. In the laboratory, exposure of the minerals to light of controlled energy levels empties the traps. As the freed electrons recombine with regions of positive charge, the excess energy is partly released as luminescence. Provided the minerals were exposed to sufficient sunlight during transport and deposition, and had no subsequent exposure, the intensity of the luminescence is proportional to the age of the sedimentary unit. For a thorough review of the process, the reader is referred to Aitken, 1998.

4.1.1 Sample Collection

Samples for OSL dating were collected in 60 x 100mm stainless steel tubes. A spring-loaded internal plunger holds the sample intact while the sample-tube holder is hammered into the sedimentary unit. This prevents mixing within the tube of sediment from the surface, which may have been exposed to sunlight. The tube full of sample is then extracted and wrapped in two layers of aluminium foil and enclosed in opaque plastic, for transport to the laboratory.

Fig. 4.1 **Diagram of sample collection device**

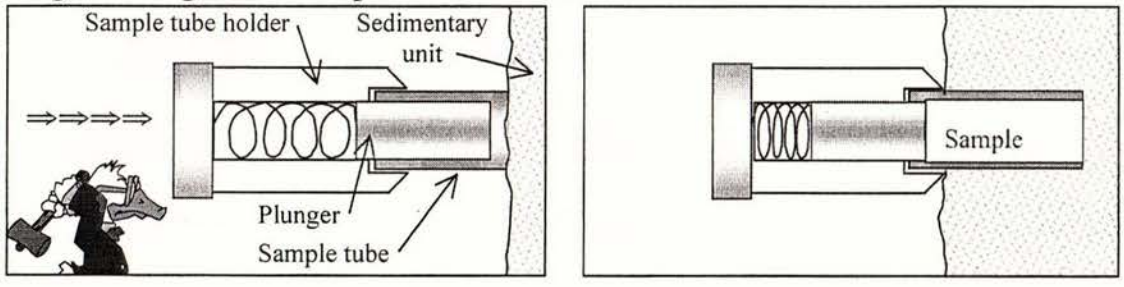

Two sample tubes and a bagged hand sample were taken at each site. Subsequent to collection, all wrapped samples were kept secure and transported to the laboratory by private car. All samples were processed under laboratory monochromatic 'safelight' conditions. Sufficient material was collected, and remains in the laboratory to enable re-processing of any of the samples should this be deemed necessary.

4.1.2 Site selection

Samples were collected from sites chosen to yield as much information as possible while sediment type and sample location must conform to specific requirements to achieve a reliable age determination. Additional data from individual sample sites is also necessary for calculation of correction factors during processing.

Sample requirements

1 Fine-grained silt/mud/sand which has had sufficient exposure to sunlight during protracted transport and/or deposition is required, e.g. loess or overbank river mud and silt. Fine-grained horizons within landslide deposits are contentious in that they may have had no sunlight exposure during transport.

2 Homogeneous material is required to ensure a representative distribution of radioactive ions within the sample. For example granite clasts within quartz sand would cause localised perturbations in the production of ionising radiation.

3 Sample needs to be collected from the centre of a horizon at least 300mm thick. This is in order to minimise the effects of the sample receiving ionising radiation from neighbouring lithologies of possible different composition, provenance and age.

Additional data

1 Depth of burial below ground level and elevation above sea level are required for each sample in order to allow for the small but significant contribution of cosmic rays to the radiation dose rate.

2 An estimate needs to be made of the in-situ water content of the sample to see if it is representative of the water content at the time of deposition. Water in the sediment matrix absorbs some of the radiation that would otherwise reach the grains of the sample. The difference between the in-situ water content and the laboratory sample water content introduces an error in the dose rate determined that needs to be corrected for. In addition the in-situ water content may not be representative of the water content for the burial period. Therefore the water content needs to be evaluated in terms of its in-situ content and the laboratory-induced saturated content. The water content is therefore calculated under the assumption that it is an estimated average value with an uncertainty that covers the extreme cases of dry to water saturated conditions (e.g. Aitken, 1985; Wang, 2001).

4.2 GPS surface mapping

High-precision differential GPS surface mapping of terrace surfaces enables efficient detection of subtle geomorphologic features, namely non-depositional surface tilts and anomalous slope breaks and bulges. Where a bulge in a terrace surface coincides with bedding and stream course disruption it is reasonable to assume a post-depositional tectonic origin for the disturbance, i.e. blind fault movement at depth. Similarly, an alignment of slope breaks and stream course diversions, especially sub-parallel to the rangefront, can be inferred to have a tectonic origin. Surface tilting can be more equivocal and requires closer scrutiny (see section 4.4 below).

4.2.1 Data collection

Three dimensional (x, y, z) surface data was gathered in the field areas using the Trimble GPS Pathfinder Pro-XRS system which comprises a hand-held receiver and back-pack battery and antenna. The antenna was 1.8m above ground surface during traverses, and recording was paused during fence and obstacle climbing. Positions were read at five second epochs during treks of between 2 and 4 hour duration. Treks were generally orthogonal and parallel to rangefronts, except where stream courses (either abandoned or current) were mapped as close as possible to the thalweg. A 'tie-line' was also walked which crossed points on all treks for each field area for the purpose of establishing data continuity. This was to negate the effects of geometric variations in the satellite constellation between individual treks. The elevations measured are height in metres above the ellipsoid plus the1.8m antenna height, but for the purposes of this study it is the relative rather than absolute elevation measurements which are important.

4.2.2 Data processing

At the completion of each trek data was down-loaded into a laptop computer running Trimble GPS Pathfinder Office version 2.7 software. A back-up floppy disc was also written for each trek. These 'rover files' on their own have stated 68% precisions of approximately 30m horizontal and 50m vertical.

4.2.3 Data post-processing

Differential correction processing using Trimble GPS Pathfinder Office version 2.7 software was applied using relevant base files downloaded from Dunedin continuous GPS base station. This uses phase differences between rover and base files of the 1.57GHz GPS carrier signal to remove errors and give (theoretically) sub centimetre positional accuracy. A ±500mm absolute and sub-cm relative accuracy is probably more realistic and more than adequate for the purposes of this study.

4.3 Geological Processes

4.3.1 Differentiating alluvial fan and fluvial deposits

Alluvial fans represent a unique sedimentary environment easily distinguished from gravel-bed rivers on the basis of morphology, hydraulic and sedimentary processes, and resultant facies and assemblages. The semi-conical shape, limited radial extent (generally <10km), plano-convex cross-profile, and comparatively high values of radial slope (2-25°) are a consequence of the transfer of sediment-charged flows from an upland basin through a point source to the fan site at their piedmont setting (Blair & McPherson, 1994). Sediment delivered to the fan site is angular and poorly sorted because of the short transport distance and the rapid and catastrophic nature of sediment transport. They are constructed mainly by catastrophic fluid gravity flows (sheetfloods or incised-channel floods) or sediment gravity flows (rock falls, rock slides, rock avalanches, colluvial slides, and debris flows) generated through failure of bedrock or colluvial slopes in the drainage basin.

Rapid expansion and flow attenuation at the fan apex due to loss of confining channel walls greatly promotes sediment deposition due to rapidly dropping velocity, capacity, and competence (French, 1987). Sheetflood facies consist of vertically alternating planar-bedded couplets 100-300mm thick of boulder, cobble, and pebble gravel regularly interstratified with laminated pebbly gravel or granular coarse sand (Blair & McPherson, 1994; see *Figs. 5.3.10; 5.6.6*). The planar-bedded sets typically dip 2 - 8°, parallel to the fan surface. Incised channels cause the active depositional lobe to be further downstream from the fan apex. The steepness of the fan slope causes large flows to be turbulent and supercritical. The principal facies that results from incised channel deposition is a thick bed of boulder deposits inset within older non-channelized facies such as sheetflood or debris-flow deposits (see *Fig. 5.3.28*).

Fan hydraulic parameters are fundamentally different to those of rivers which generally increase in velocity, competence and capacity for a given channel width. Slopes are <0.5° and typical flow is normally subcritical within a confined channel. The most common gravel-bed river facies are thickly-bedded to crudely and horizontally stratified fining-up clast-supported gravels deposited in longitudinal bars within the active channel tracts. Cross-bedding may be present and overlain by thin flat-bed sheets (McLane, 1995). Gravel clasts are commonly rounded and elongated clasts are imbricated with *a-b* planes oriented perpendicular to slope and dipping upstream. Channel-fill facies sequences are commonly ≤10m thick and pinch out laterally against older channel or overbank sediment. Fine-grained floodplain facies that accumulate from overbank flows are absent in fans.

4.3.2 Differentiating, aeolian, lacustrine and fluvial deposits

Aeolian deposits

Before vegetation establishes itself on the outwash and moraine of receding glaciers, the wind lifts out the fine rock-flour and spreads it as a blanket of loess cover over wide areas. Loess is widespread in Central and east Otago, especially in the lee (southeast) of the ranges. Bodies formed are laterally extensive, homogeneous, fine-grained, well-sorted sandstone. There may be curved or irregular internal erosion surfaces (non-deposition and/or plant growth), and abundant root casts and bioturbation traces. The light brown – light yellow massive sandy silt often possesses a blocky texture with vertical polygonal joint sets and grey veins (see *Figs. 5.4.18; 5.5.5*). Aeolian sands may interfinger with alluvial or lacustrine sediments but do not grade into such sediments (McLane, 1995).

Lacustrine deposits

Late Miocene Bannockburn Formation comprises finely laminated lacustrine silt, mud, and clay inferred to have been deposited in 'Lake Manuherikia', which covered much of what is now Central Otago (Douglas, 1986). Lithology and stratigraphic relationships of sporadic outcrops vary according to locality. Sandy mudstone deposits occur in what were shallow lake margins with clay and mud in more distal areas. Stratigraphic relationships are complex and lacustrine deposits may be interfingered with either Dunstan Formation or Wedderburn Formation (see *Fig. 5.4.2*; Youngson *et al.,* 1998).

Late Quaternary lacustrine deposits occur in both the Strath Taieri and Moonlight Flat areas. Taieri Lake existed at the time of European settlement (Williamson, 1939) but has since been drained. Holocene lacustrine sediments are present in both Taieri Ridge field areas (section 5.2; see *Fig. 5.2.1*). These comprise laterally extensive silt and mud in varve-type mm- and cm-scale laminae, possibly reflecting seasonal freeze-thaw cycles. Distortion of these laminae provides evidence of Holocene tectonism.

Fluvial deposits

Fluvial gravel facies are distinct in the sorting, bedding, rounding, and imbrication of clasts and depositional gradients. Overbank deposits are superficially similar to aeolian and lacustrine deposits, but with significant differences allowing differentiation. Grainsize decreases away from the channel and sandy beds may display ripple cross-lamination. The large-scale distribution of channel and overbank deposits within a large deposit is diagnostic. Long-term avulsion of the valley floor leads to burial of point bar deposits as elongate tabular bodies embedded in or interbedded with finer-grained overbank deposits. Coarse member units may be isolated or erosionally transect each other.

4.3.3 Differentiating erosional and depositional terraces

Erosional terraces form primarily by lateral erosion and depositional terraces represent the un-eroded surface of a valley fill.

Erosional terraces

Erosional terraces have two distinctive properties; 1) they are capped by a uniformly thin layer of alluvium whose thickness is controlled by the scouring depth of the river involved; 2) the surface cut into the bedrock is a flat mirror image of the surface of the capping alluvium. (Ritter *et al.,* 1995) As rivers migrate across the valley floor they erode one bank and simultaneously deposit point bars on the other. The bar sediment becomes the capping of alluvium which is deposited at the same time as the underlying surface is eroded. Formation of erosional terraces requires a long period of tectonic stability.

Depositional terraces

Formation of depositional terraces requires a period of valley filling and subsequent entrenchment into the fill. The tread represents the highest level attained by the valley floor during aggradation (Ritter *et al.,* 1995). Aggradation can be triggered by glacial outwash, changes in stream base level, or increased load due to uplifted source regions. Incision can be triggered by tectonic events or climate change. Two primary distinctions between depositional and erosional terraces are 1) in depositional terraces the tread surface may be flat, but the surface beneath the fill can be very irregular; 2) in depositional terraces the surface beneath the alluvium is an unconformity because it was there before alluvium deposition occurred, in contrast to the simultaneous formation of the base surface and terrace alluvium discussed above.

4.3.4 Differentiating natural surface gradients and post-depositional tectonic movement.

Alluvial fans have average radial surface slope values ranging from 1.5° to 25°, with values of 2° to 12° most typical (Blair & McPherson, 1994). Consequently the bedding within the distinctive sheetflood deposits, which parallels the fan surface, has similar gradients. The sediment gravity-flow deposits, which have poorly developed bedding although sometimes reverse graded, also form at these gradients.

Rivers have longitudinal gradients rarely exceeding 0.4°, even in proximal sections. An exception would be upland rivers whose channel bed is controlled by bedrock. River terrace surfaces therefore (either strath or depositional) have similar gentle downstream gradients. Lacustrine sediments tend to be near-horizontal except where river deltas or alluvial fans are aggrading into the lake. The dip of delta foresets tends to increase with grainsize.

To discern whether valley-fill surface gradients are original or modified by erosion or tectonics or both requires: 1) identification of the depositional environment; 2) accurate measurement of surface gradients; 3) ascertainment of the attitude of bedding or internal structures relative to the surface.

4.3.5 Differentiating local and regional uplift

On a broad scale, localised uplift is manifest in the presence of the ranges (e.g. Cotton, 1917), and regional uplift in uplifted marine terraces and the presence of widespread marine strata at least as far inland as Naseby (Bull & Cooper, 1986; Youngson *et al.,* 1998; Litchfield, 2000). The present elevation of Naseby is approximately 600m.

Localised uplift is superimposed on regional uplift. Regional uplift has caused longitudinal river valleys to become terraced and, locally, tilting and incision of these terraces has occurred proximate to the emerging rangefronts (Jackson *et al.,* 1996). On Blackstone Hill flights of strath terrace remnants whose surface gradients increase with elevation attest to on-going uplift and tilting (Markley & Norris, 1999).

Drainage patterns reveal evidence for growth and interaction of structures because they adapt to changes in surface slopes. This is particularly evident where streams have asymmetric across-valley profiles, i.e. steeper side in the direction of range propagation (e.g. see *Figs. 5.4.10; 5.5.2;* Jackson *et al.,* 1996, 2002).

5 FIELD DATA

5.1 Field area overview

The northeast-trending reverse faults and folds of the field area are shown in *Fig. 5.1*. Ranges become progressively lower and less incised toward the east where larger areas of the unconformity are at least partially preserved (e.g. Youngson & Craw, 1995). The intervening basins become progressively shallower to the east and are generally asymmetrical with steeply dipping or overturned western margins. These contain up to 1000m (commonly much less) of Tertiary to Recent sediments which record ongoing tectonism. The sequence is rarely complete with ongoing deformation inducing much sediment recycling with streams often incising now-tilted or offset terraces they have earlier deposited. Extensive Quaternary alluvial fans overlying older (Eocene-Pleistocene) fluvial and lacustrine sediments with relatively remote provenance are common, especially on the larger ranges. This, combined with deepest fan incision nearest the rangefront, suggests accelerated Quaternary uplift of the ranges. Widespread angular unconformities and divergent bedding attest to progressive deformation. Tilled and elevated strath terrace remnants cut into the schist basement on the sides of many ranges intimate either subsequent uplift or lowering of stream base level. They also suggest lengthy periods of tectonic quiescence during which the river is cutting laterally, rather than incising.

The rangefronts are fairly linear when viewed from a satellite (e.g. Yeats, 1987; Madin. 1988; *Fig. 5.1*), and normally emerge abruptly from beneath sedimentary aprons. Maps traditionally show faults approximately coincident with the rangefront at the folded peneplain-sediment unconformity (e.g. Mutch, 1963; Bishop, 1979; Mortimer, 1993; Turnbull, 2000; Forsyth, 2001). In all cases field evidence for range-scale faulting is equivocal. There is no field evidence for large fault throw as the schist textural grade between range summits and rangefronts, or between ranges, shows no significant difference (Bishop, 1972, 1974, 1979; Mortimer, 1993). Basement schistosity roughly mimics topography (e.g Salton, 1993; Jackson et al., 1996; Markley & Norris; 1999; Markley & Tikoff, 2003), and documented fault segments are located at the foot of the rangefronts (e.g. Beanland et al., 1986; Markley & Norris, 1999). Deformation is distributed across kilometre-scale zones out from the larger ranges (e.g. Beanland *et al.,* 1986, this study), and consists of multiple small offsets with both normal and reverse movements.
These data suggest folding has played an important part in the uplift of the ranges (e.g. Stein & King, 1984; Turnbull *et al.,* 1993; Jackson *et al.,* 1996; Markley & Tikoff, 2003).

5.1 Field area overview

The locations of the five southeast rangefronts selected for investigation and sites for OSL dating are shown below (*Fig.5.1*).

The field locations are at the arrowheads and each asterisk represents an OSL date, which was obtained from that field area.

Fig 5.1 **Central and east Otago field area locations and dating sites**

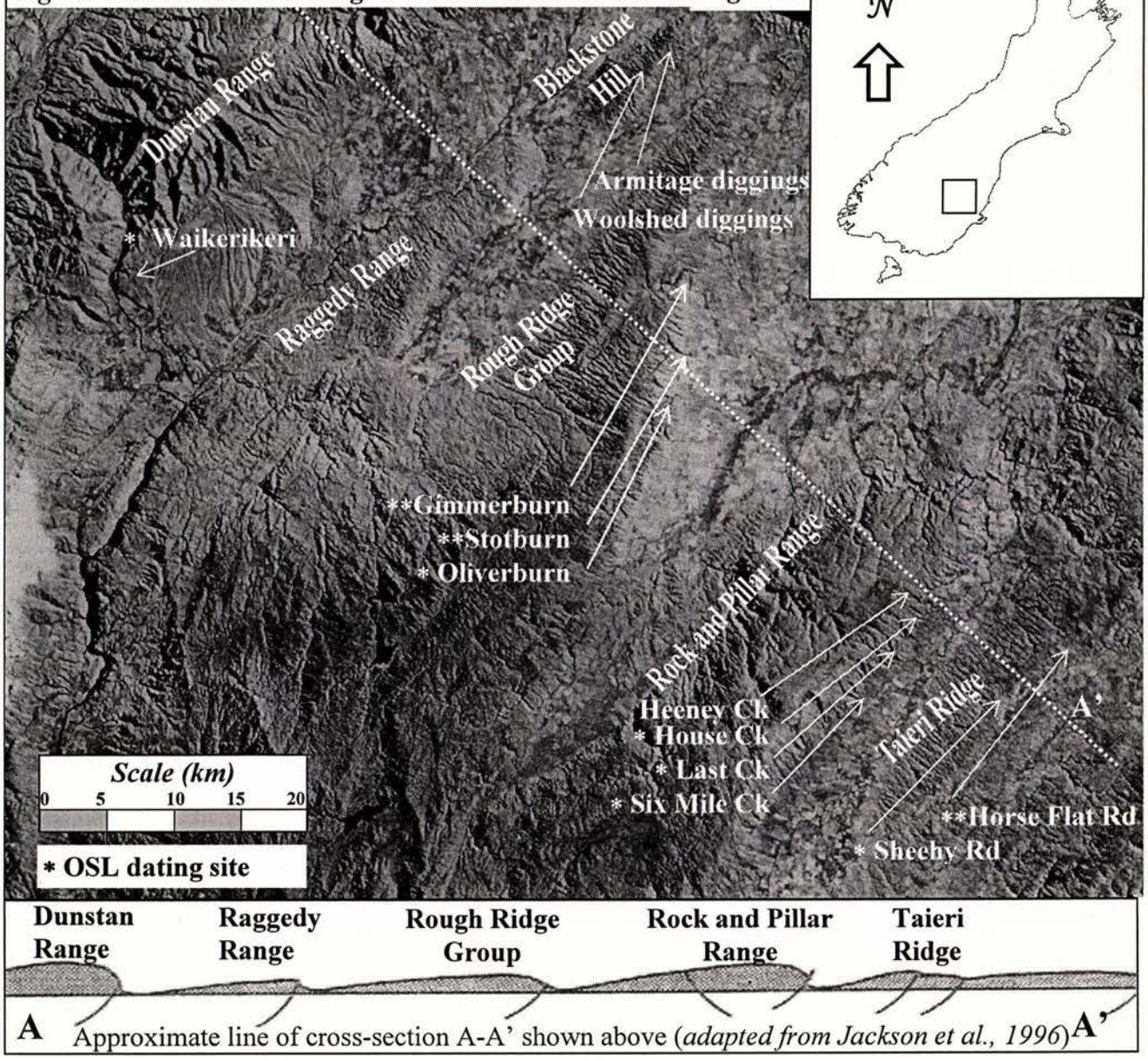

Approximate line of cross-section A-A' shown above (*adapted from Jackson et al., 1996*)

Prospective sites were identified initially by deformation visible in aerial photographs in areas designated Mid to Late Quaternary on Geological and Nuclear Sciences Q-map series QM18 (Turnbull, 2000), and QM19 (Forsyth, 2001). The following sections on five individual rangefronts comprise brief overview, site-specific details of deformation and structure, and rationale for OSL dates, where applicable, for the ten field areas of this study.

Taieri Ridge

5.2 Taieri Ridge Overview

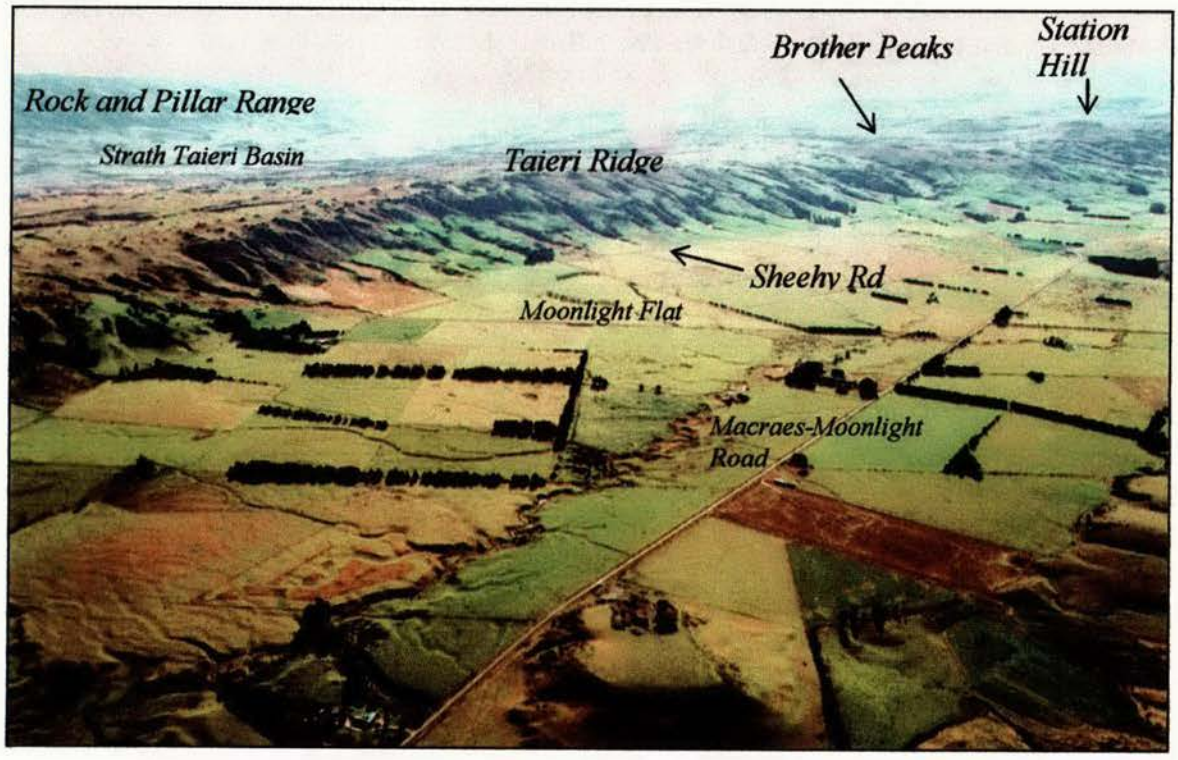

Fig. 5.2.1 **Taieri Ridge and Moonlight district** (Photo CN39443-25: D. L. Homer) North Rock and Pillar Range and Strath Taieri are in left background. Photo looking towards NNE. Note increasing of dip of rangefront towards camera, incision and tilting of fan and terrace surfaces proximate to rangefront, and departure of the rangefront from linearity.

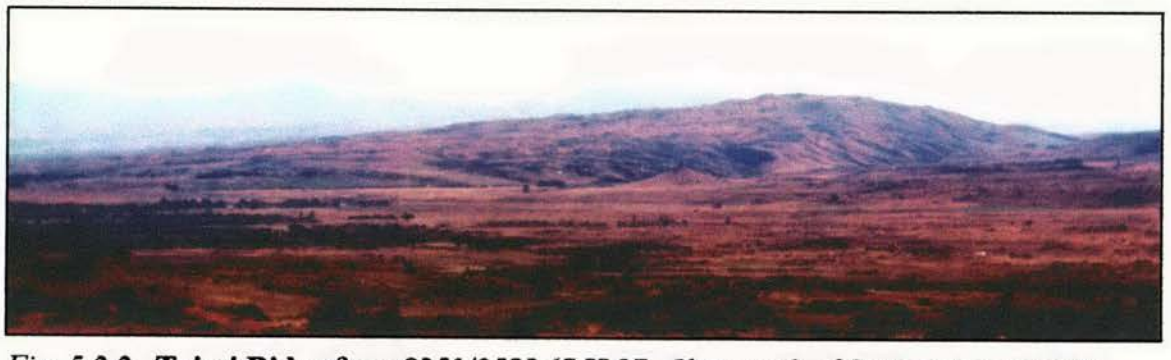

Fig. 5.2.2 **Taieri Ridge** from 8351/0582 (S.H.87 ~8km south of Sutton) towards 35°. Note the asymmetry of the profile, steeper to the southeast. The Kakanui Mountains, in the background, are composed of greywacke and uplifted on northeast side of the northwest-striking Waihemo Fault. This is interpreted as a Cretaceous normal fault reactivated during the Late Cenozoic as a reverse fault (Bishop, 1972), and is still active (e.g. Craw & Chappell, 1999).

5.2 Taieri Ridge Overview

Fig. 5.2.3 **Taieri ridge topography and location of sites**

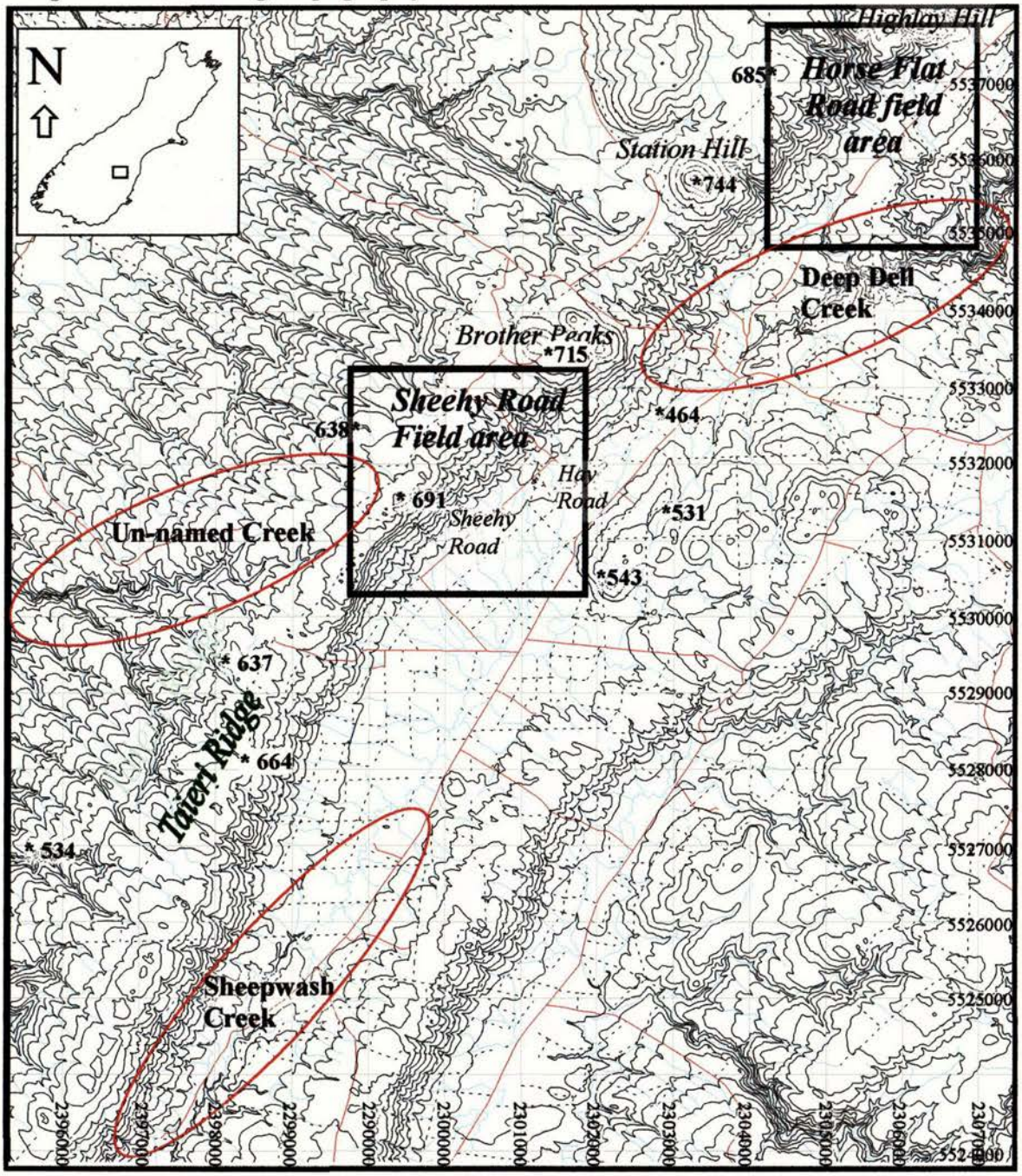

Taieri Ridge is a ~20km long asymmetric schist anticline, steep side to the southeast, and the lowest and eastern-most rangefront in this study. Three Miocene alkali volcanic peaks (Coombs *et al.*, 1986) on the range crest (Brother Peaks, Station Hill, and Highlay Hill) perturb the sub-horizontal range crest (*Fig. 5.2.1*). These overlie and preserve Eocene and Miocene quartz-rich fluvial gravels. Another small intrusion also occurs at the base of the rangefront near the intersection of Sheehy and Hay Roads. In map view the rangefront is distinctly sigmoidal with inflection points aligning with anomalous stream courses (marked with ellipses in *Fig. 5.2.3*), which are oblique to the regional northwest-striking drainage.

5.2.1 Taieri Ridge - Horse Flat Road Section

Fig.5.2.4 **Orthomap and photo locations** (asterisk is location, arrow is camera azimuth)

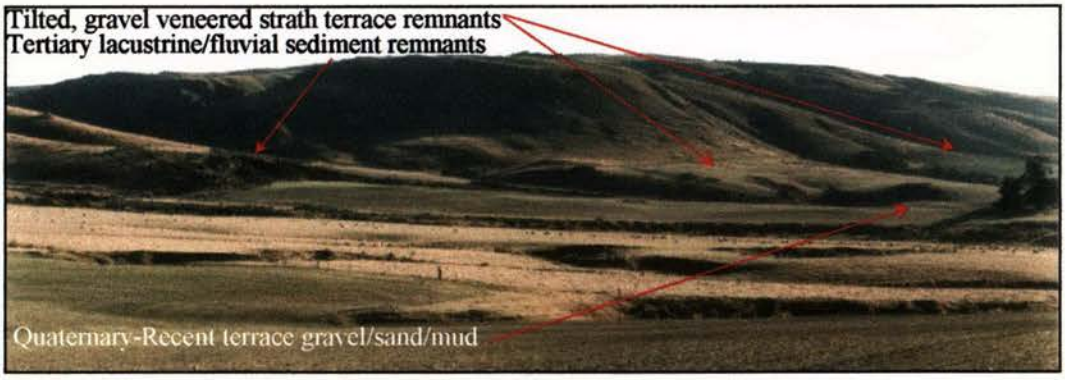

Fig.5.2.5 **Taieri Ridge Rangefront – Horse Flat Road** (from 5601/5875 → ~N)

Surface slopes increase towards the rangefront. Broadly, basin fill is of three types; 1. uplifted and tilted strath terrace remnants covered by a thin (<15m) veneer of fluvial and/or alluvial fan gravels; 2. Tertiary mud (often carbonaceous)/ sand/ gravel remnants; 3. Recent fluvial gravel/sand/mud, with both reworked and contemporary sediment sources.

5.2.1 Taieri Ridge

Horse Flat Road Section

Fig. 5.2.6 **Structure and sample sites**

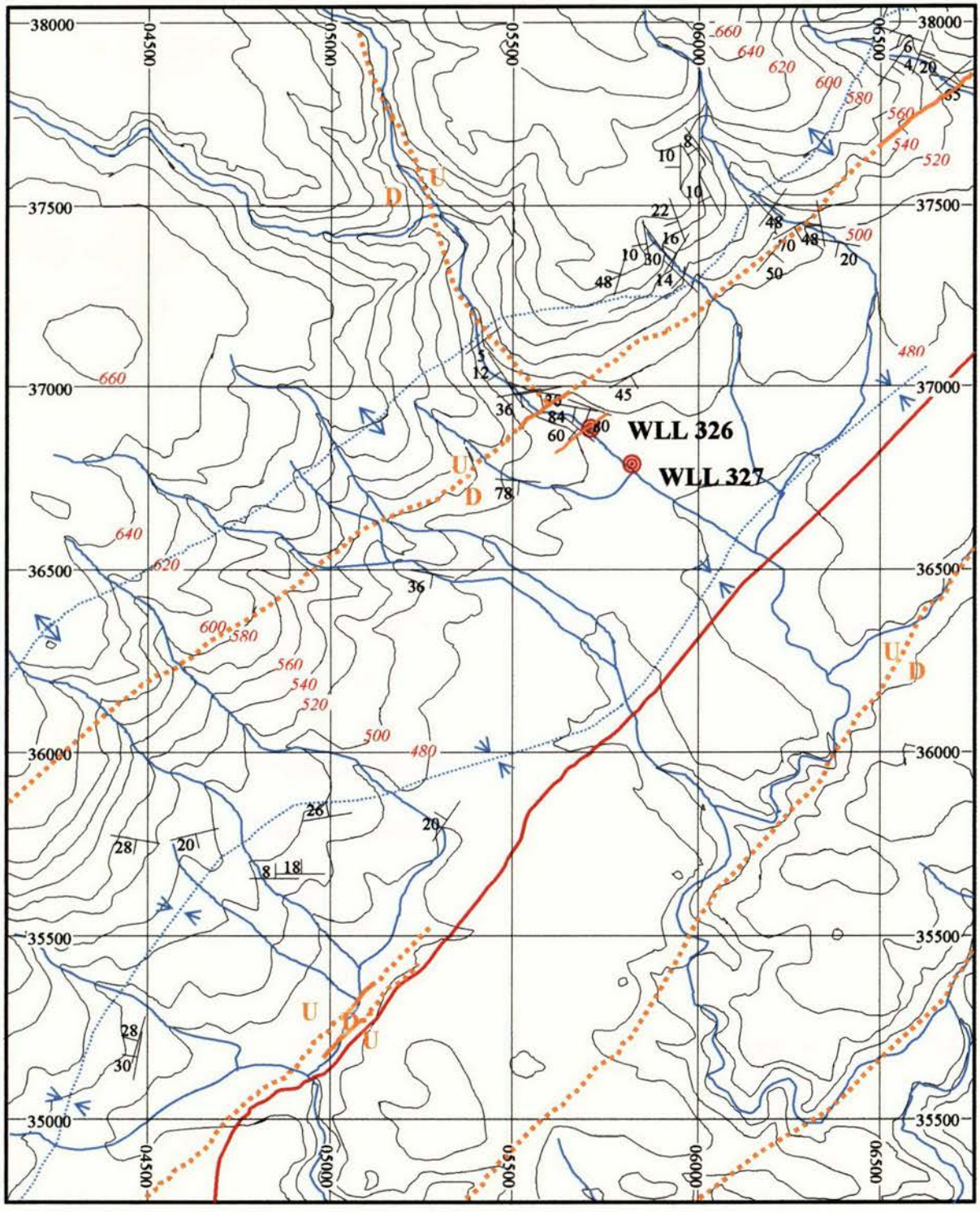

5.2.1 Taieri Ridge - Horse Flat Road Section
Fault exposures

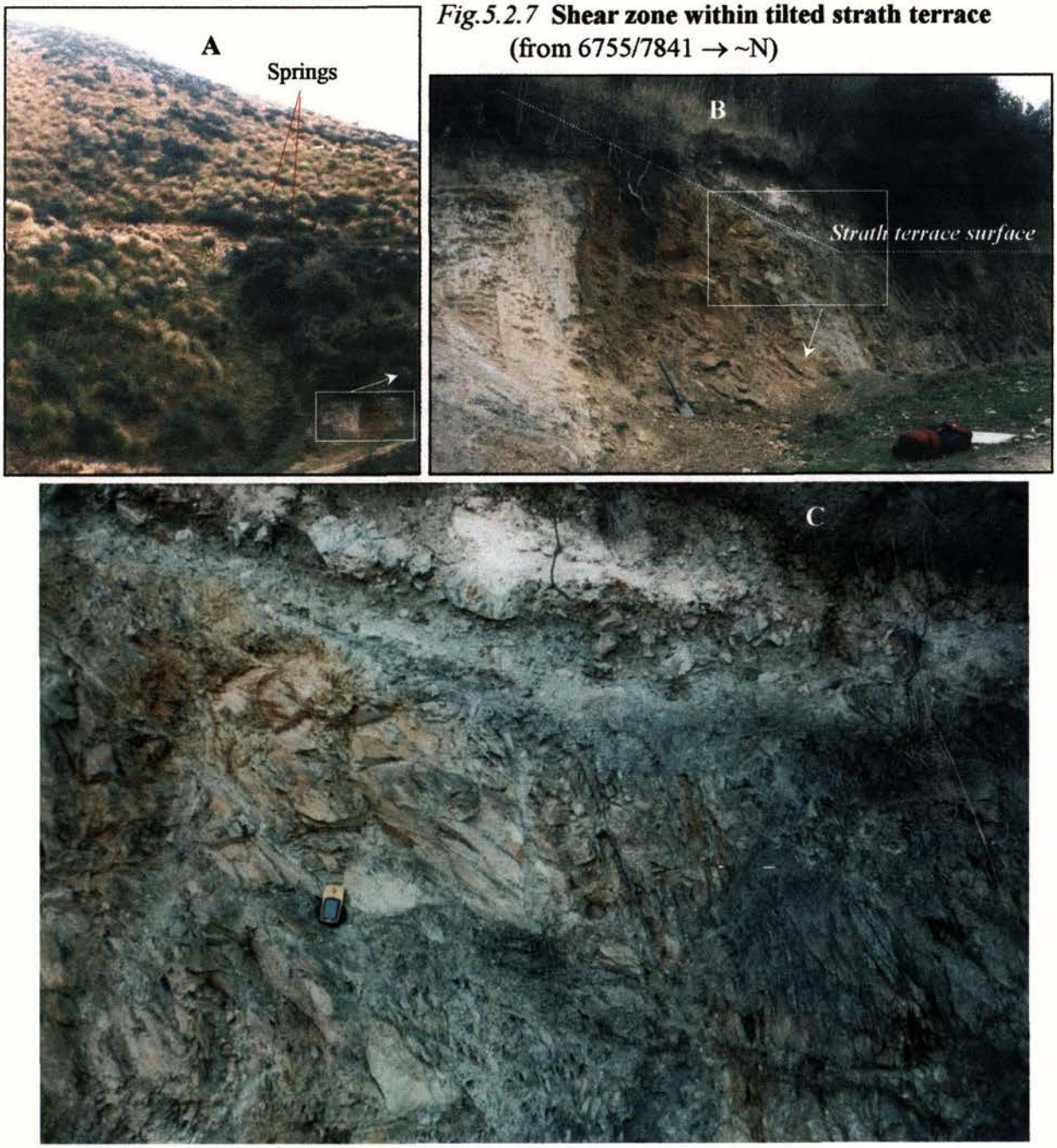

Fig.5.2.7 **Shear zone within tilted strath terrace** (from 6755/7841 → ~N)

This basement shear zone visible in a stream incision at the northern extremity of this field area, aligns with a slope-break on the flanking interfluves and a range-parallel line of stream course disruption. Springs emerge in a line shown in *Fig. 5.2.7*A. The apparent dip of the fault plane is 75°SE, which is close to foliation (210/65 SE), although the foliation bends into the fault over a short distance (*Fig. 5.2.6*). Note the dip change in the strath terrace surface across the fault zone, and lack of evident offset within the alteration zone and overlying kaolinite. Movement on this structure predates deposition of now-incised fan surfaces adjacent to the stream.

5.2.1 Taieri Ridge - Horse Flat Road Section
Fault exposures

Fig5.2.8

Fault beneath tilted strath surface
(from 5635/6936→140°)

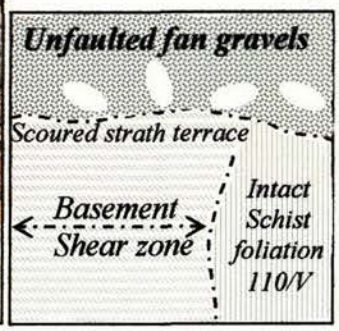

Foliation in unfaulted schist on the right is 110/V. This basement shear zone aligns with slope breaks and range-parallel notches in interfluves, and is within a range-parallel straight section of the stream course (see *Fig.5.2.4*). Fault strike is undetermined, but the dip is sub-vertical, and sub-parallel to schistosity. Extrapolation of a line between here and the location of *Fig. 5.2.7* coincides with many range-parallel stream kinks and interfluve slope breaks (see *Fig.5.2.4*). Faulting hasn't disturbed, and thus pre-dates, overlying fan gravels.

Fig. 5.2.9

(from 5042/5269 → ~S)

East-dipping (~40°) shear zone in west-dipping schist.

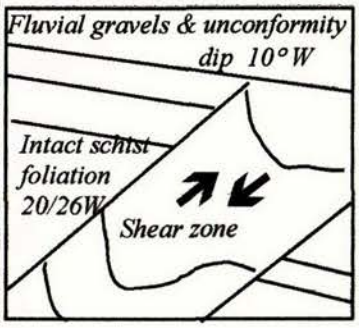

Highly weathered truncated schist surface (intact schist foliation 20/26W) and overlying fluvial gravels are tilted 10°W. This location is a few metres east of the basin axis, thus when compared to the rangefront, the dip of the schist and overlying sediments describe an asymmetric synform, steeper side to the west (see *Fig.5.2.6*). Reverse movement is indicated and faulting hasn't disturbed overlying fine fluvial gravels.

5.2.1 Taieri Ridge - Horse Flat Road Section
Fault exposures

Fig. 5.2.10

West-dipping fault within

Eocene Hogburn Formation

(from 4977/5268 → 60°)

(Visible tape length = 1350mm)

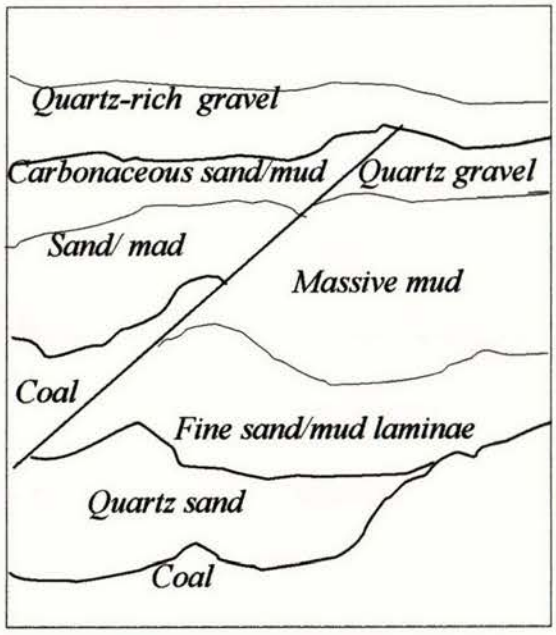

This west-dipping fault plane (10°/40W) with reverse sense of movement is within the Eocene Hogburn Formation just metres west of basin axis. The apparent offset of coal horizons is ~400mm.

Locally, bedding is tilted an average of 10°E. Bedding and fault plane orientations are both opposite to that of *Fig. 5.2.9*, which lies just on the opposite side of the basin axis.

5.2.1 Taieri Ridge – Horse Flat Road
OSL sample sites and surface geometry

Fig.5.2.11 **Lowest terrace surface and OSL sample area** (from 6210/6630 → 90°)

The stream incises along the southern margin of the lowest surface, which is gently tilted south-eastwards. The prominent embankment to the south (left) of the lowest visible surface is a fluvial terrace remnant underlain by Tertiary sediments, which at the rangefront, is 22m above the current stream level. The stream has incised the lowest surface, at the rangefront, to a depth of 2m.

At a distance of 520m from the rangefront (just left of foreground in *Fig.5.2.11*) the higher surface is 5m above stream level, and the stream has incised the lower surface by 1m. The stream loses 14m elevation over this distance giving an average stream gradient of 1:0.027. The average gradient of the lowest surface over the same distance is 1:0.029, and that of the highest surface is 1:0.06. These small differences in average gradient over this distance amount to significant departure from natural depositional slopes, and by proxy, localised uplift.

Older, higher surfaces have increased basin-ward tilt (more differential uplift) and more prominent slope breaks. Subtle deformation (note the bulge below the red arrow in *Fig. 5.2.*11) of the lowest surface aligns with bedding disturbance visible in the banks of the stream incision (see *Figs, 5.2.12 & 5.2.13*). The basement shear zone of *Fig.5.2.8* is just within the gorge (in shadow in *Fig.5.2.11*) and the range-parallel notches in the interfluves are marked with black and white "⬇" symbols.

5.2.1 Taieri Ridge – Horse Flat Road OSL sample sites

Fig.5.2.12 (from 5714/6892 →90°)

Sample Site WLL326 Age: 9.93 ±1.9ka

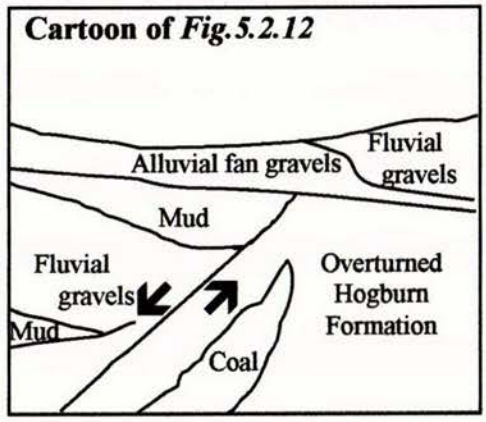

The sample for OSL dating was taken from the location marked ⊗ in the middle of the ~500mm thick mud lens.

Overturned carbonaceous Eocene Hogburn Formation truncates tilted coarse imbricated fluvial gravels and overbank muds. Disruption aligns with a range-parallel 5m step in the lowest surface, up towards the range. This location lies on a range-parallel lineament formed by stream channel deflections (see *Fig.5.2.4.*). The site is 2140mm above current stream level and 850mm below the ground surface, and lies on a sharp inflection point in the stream course.

This date constrains the tectonic activity responsible for the disruption in the bedding to within the last 10ka, and provides an average rate of stream incision since deposition of the overbank mud.

5.2.1 Taieri Ridge – Horse Flat Road OSL sample sites

Fig. 5.2.13 (from 5831/6789 → 60°)

Sample Site WLL 327 Age: 7.14 ± 0.76ka

Sample taken from finely-laminated ~600mm mud layer marked ⊗. Folding within sedimentary layers has produced a subtle terrace surface undulation aligning with this site and visible beneath the red arrow in *Fig.5.2.11*. The sample site is 1800mm above current stream level, which is 2300mm below the terrace surface.

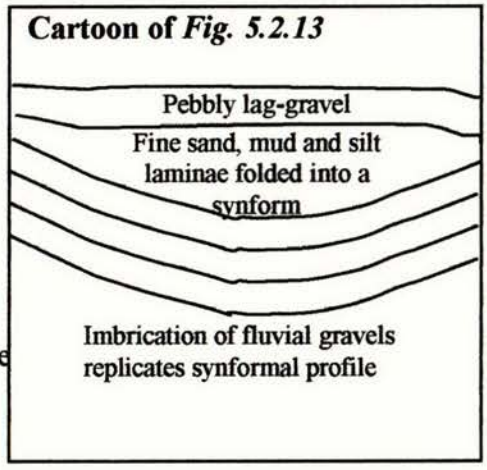

This date constrains the last activity responsible for folding of these lacustrine sediments to within the last 7ka. Bedding within the fine-grained layers is sub-parallel, indicating that folding commenced after deposition of the layers, rather than accompanying their deposition.

5.2.1 Taieri Ridge – Horse Flat Road GPS surface profiles

Fig. 5.2.14A **Location of GPS surface profiles**

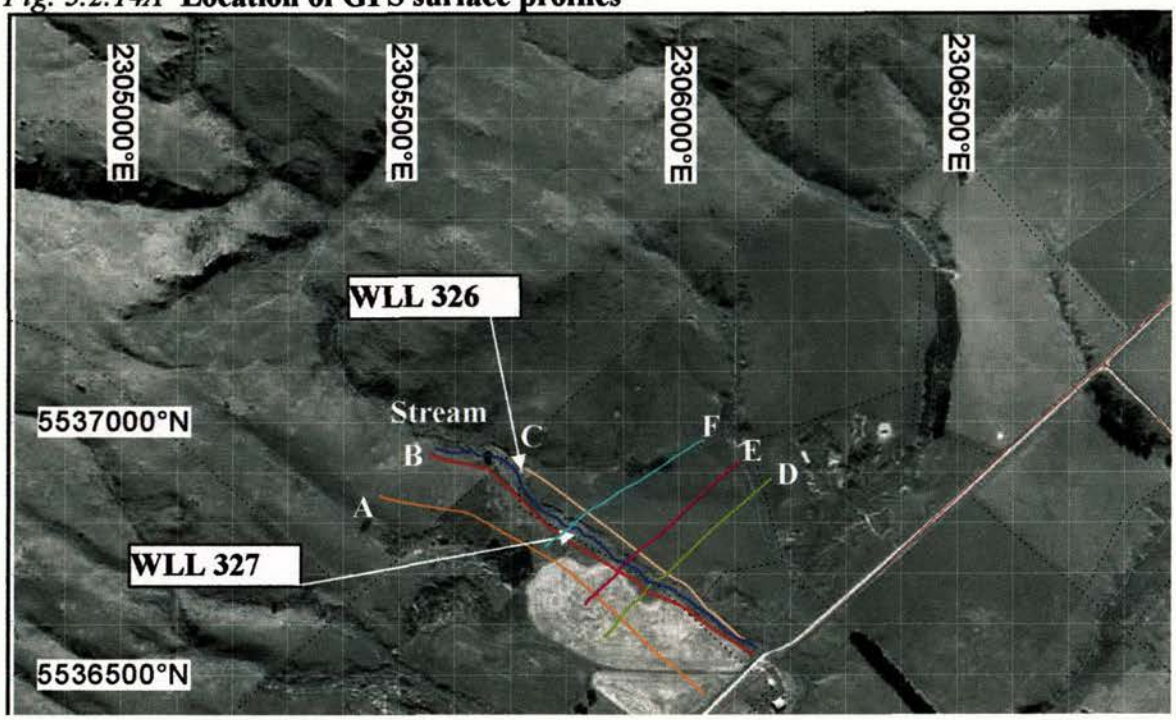

Fig. 5.2.14B **Range-orthogonal profiles**

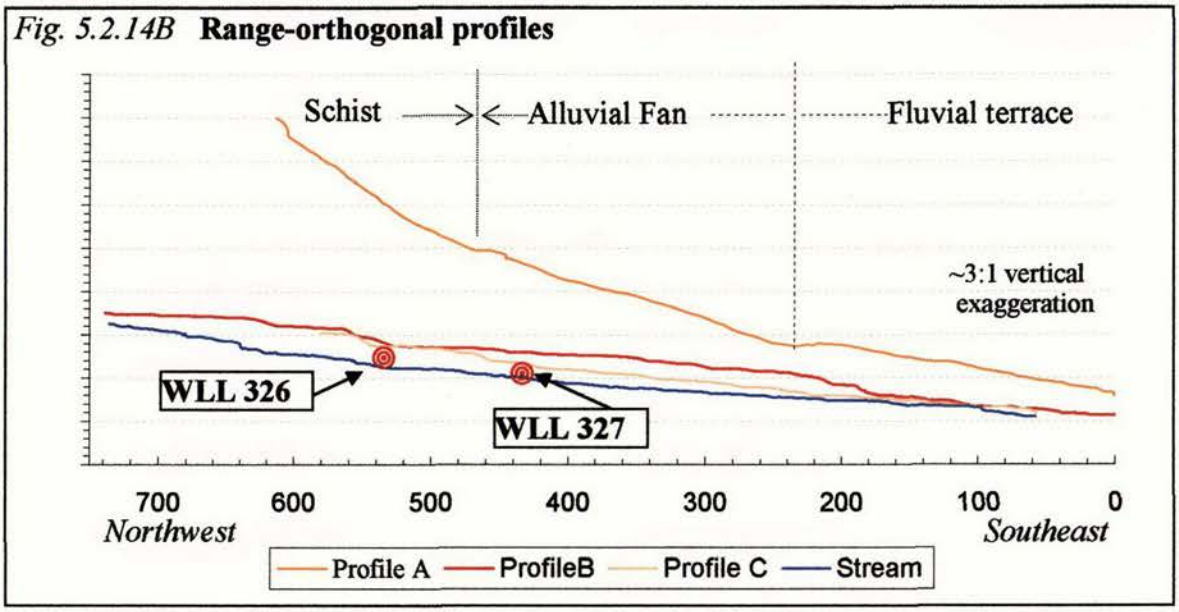

Fig. 5.2.14C **Range-parallel profiles**

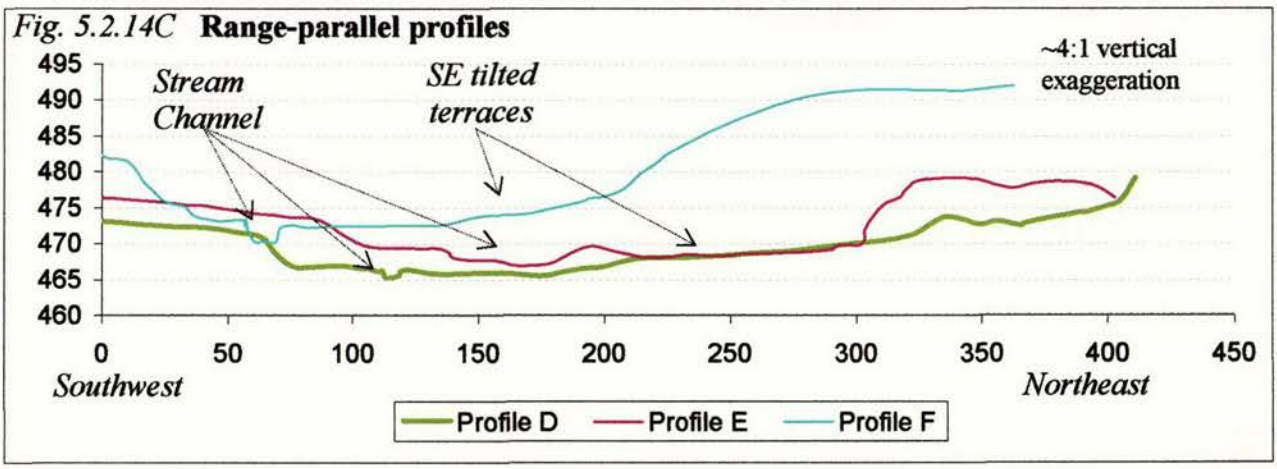

5.2.2 Taieri Ridge - Sheehy Road Section

Fig.5.2.15 **Orthomap and photo locations** (Asterisk is position, arrow is camera azimuth)

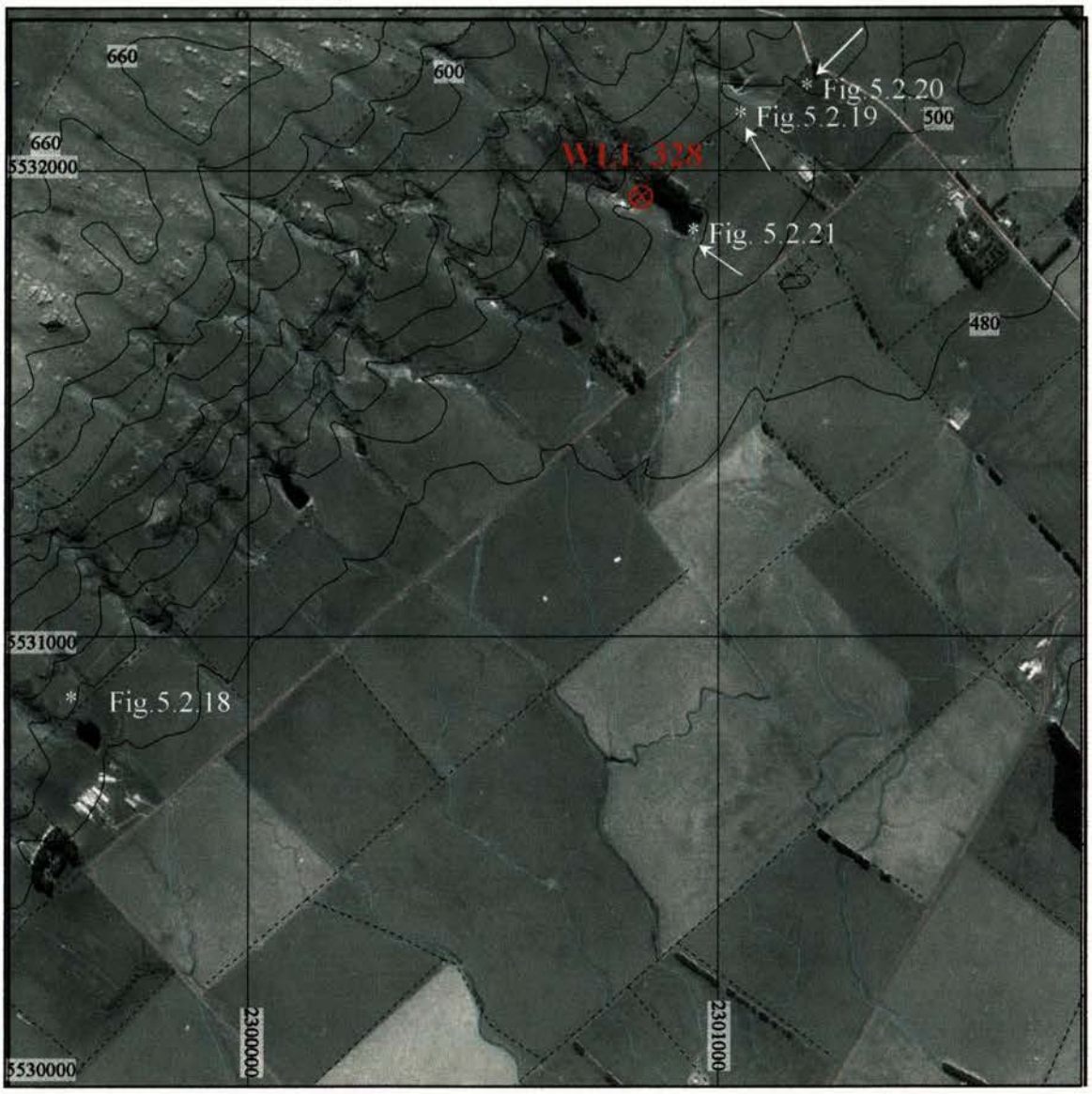

Fig. 5.2.16 **Taieri Ridge rangefront** (from 2400/31700 → SW)

Note change of rangefront slope along strike above the tilted terrace/schist unconformity. The location of the northeast range crest inflection point is arrowed (see next section).

5.2.2 Taieri Ridge - Sheehy Road Section
Structure and sample site

Fig. 5.2.17

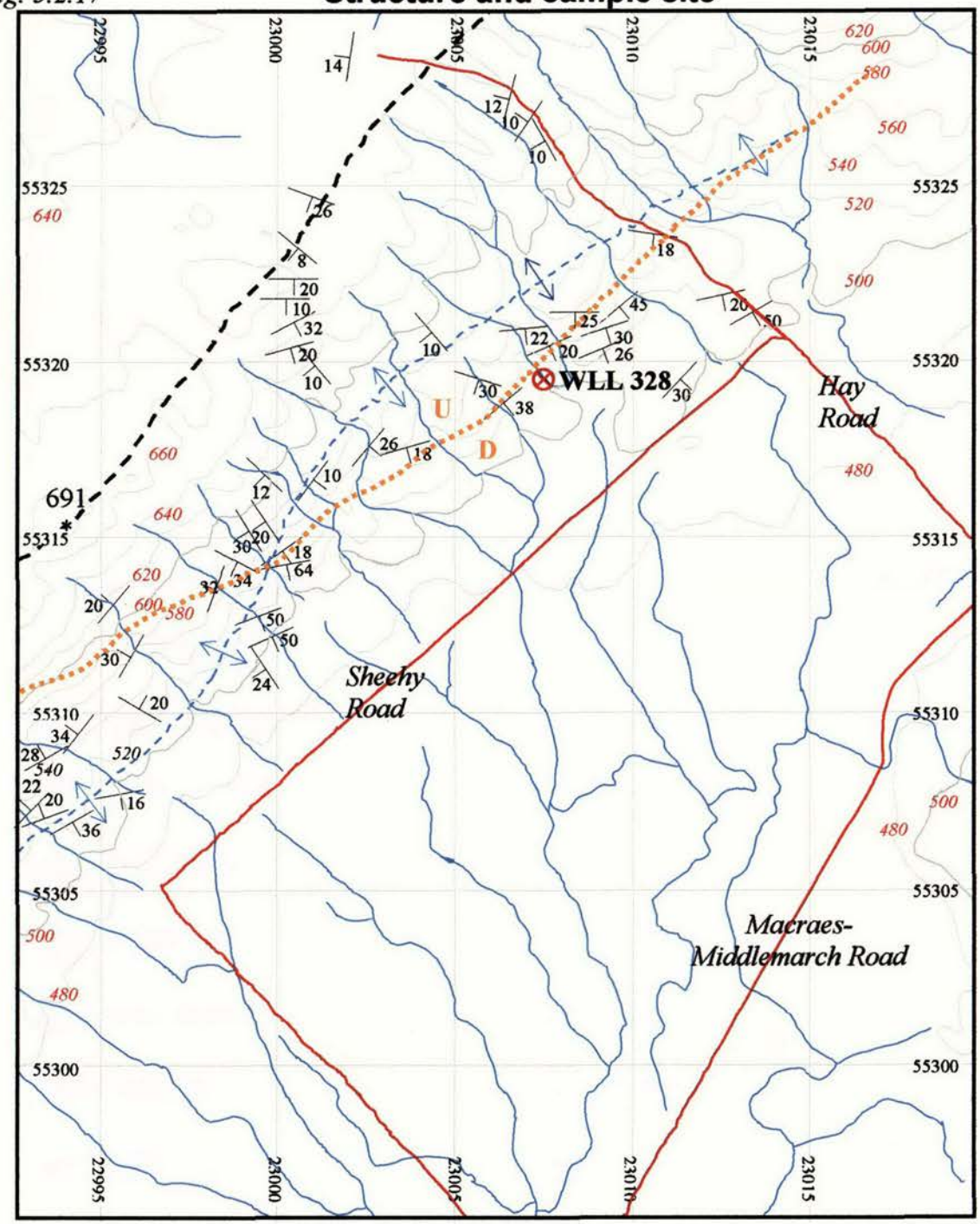

36 Schist strike/dip
Anticline axis
Drainage divide
640 Contour (20m interval)
OSL Sample site **WLL 328** (0805/1935)
Fault
Inferred Fault

5.2.2 Taieri Ridge - Sheehy Road Section range structure

Fig. 5.2.18 **Schist dipping into rangefront, south Sheehy Rd.** (from 99463/30627 → 220°)

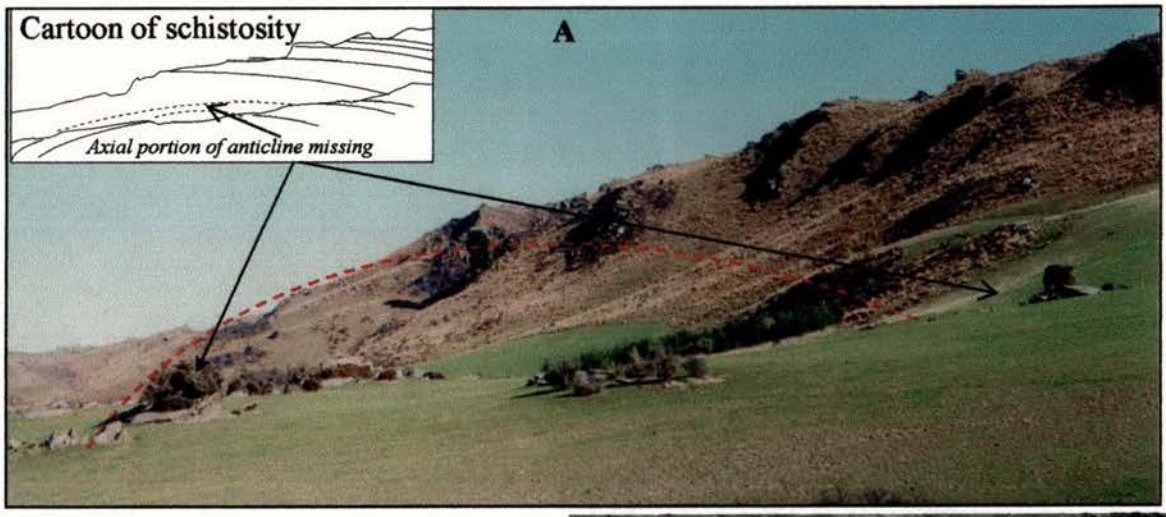

The schistosity in the foreground rocks ↑ describes a truncated asymmetric anticline, steeper limb to southeast (left). In this region the range kinks to the left, changing strike towards the south from ~045° to ~023° (see *Figs. 5.2.3, & 5.2.18B)*. Further to the south-west, at Sheepwash Creek (*Fig. 5.2.3*) the range reverts to a 045° strike, and these features together form a left step in the range.

An interpolation between the line of Deep Dell Creek and an un-named creek on the northwest flank, whose course has a similar strike, intersects the northeast inflection point. A line extrapolated northeast from Sheepwash Creek aligns with a known shear zone running parallel to Deep Dell Creek and intersects the southwest inflection point. All these stream courses are oblique to either component of the regional trellis drainage pattern. These features are marked with ellipses on *Fig.5.2.3*.

Fig.5.2.19 (from 1058/2179 → NNE) At the northern end of the Sheehy Road section the schist foliation strike and dip (060/50°SE) is close to that of the rangefront, in contrast to that above in *Fig.5.2.18*. Here, downslope sliding is evident along foliation planes.

5.2.2 Taieri Ridge - Sheehy Road Section
Tilted terraces

Fig. 5.2.20 **Rangefront terrace deformation** (Outcrop at 0122/3222 → 225°)

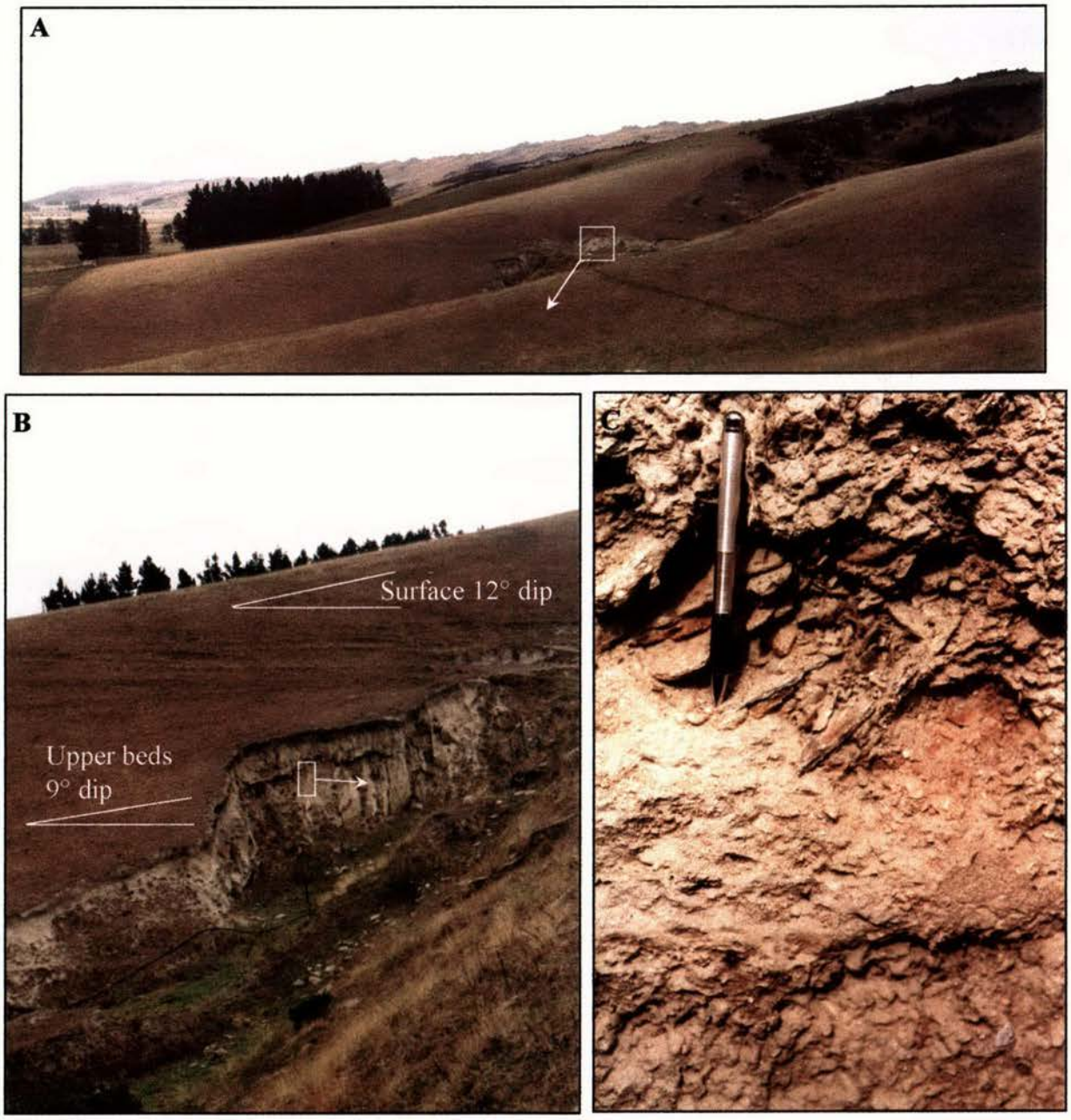

A Slope break on interfluves forms a range-parallel lineament as slope increases towards range (to the right in photo). Note the change in range crest morphology above the pine trees centre-left, which corresponds to the inflection point referred to earlier in figure 5.2.3.

B Bedding dip increases down-section and is discordant with the surface.

C Terrace is formed of sub-rounded schistose fluvial gravel and sand beds with mud lenses. The lowest horizon visible in outcrop is a massive muddy sand layer 800+mm thick. The upper terrace surface is draped in loess, which thins away from the range. Clast imbrication of the gravel (by the pen) indicates a current direction from the northeast.

5.2.2 Taieri Ridge - Sheehy Road Section OSL Sample Site

Fig. 5.2.21 **Rangefront surface disruption and terrace sample site**
(↓ from 00942/31860 → 320°) (↓ from 00760/31906 → 30°)

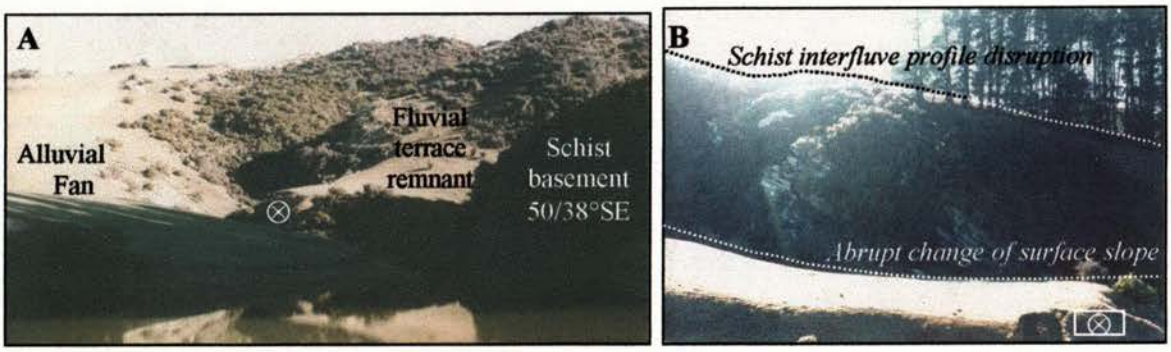

The slope break in the terrace remnant (in B↗) is abrupt and lies on a range-parallel lineament formed by kinks in stream courses and interfluve disruption (see *Fig.5.2.15*). Note the profile of the terrace surface and that of the schist above the terrace remnant in *Fig. 5.2.21B.* The disturbance in the schist interfluve profile is also visible in *Fig. 5.2.20A* just to the right of the pine trees. The line thus formed by the slope break along the interfluves parallels the axis of the anticline, rather than the drainage divide.

Sample site WLL328 (00805/31935) **Age: 12.9 ± 1.1 ka**

The sample is from lacustrine mud (marked '⊗') within the terrace remnant ~800mm below the top surface. The terrace comprises schistose sub-rounded fluvial gravel and sand beds with discordant and disrupted bedding overlain by cm-scale sub-parallel lacustrine mud and silt laminae. This surface above the sample site is 8m higher in elevation than equivalent lacustrine units on the valley floor. Correlatives of this surface remnant occur uplifted in

pockets along the rangefront, and out on the valley floor. Dating provides information on range propagation by virtue of the relative elevation of the individual remnants, and an overall uplift rate from the difference in elevation between the remnants and their correlatives on the valley floor.

5.2.2 Taieri Ridge - Sheehy Road Section

Fig. 5.2.22 **Differential GPS Profiles**

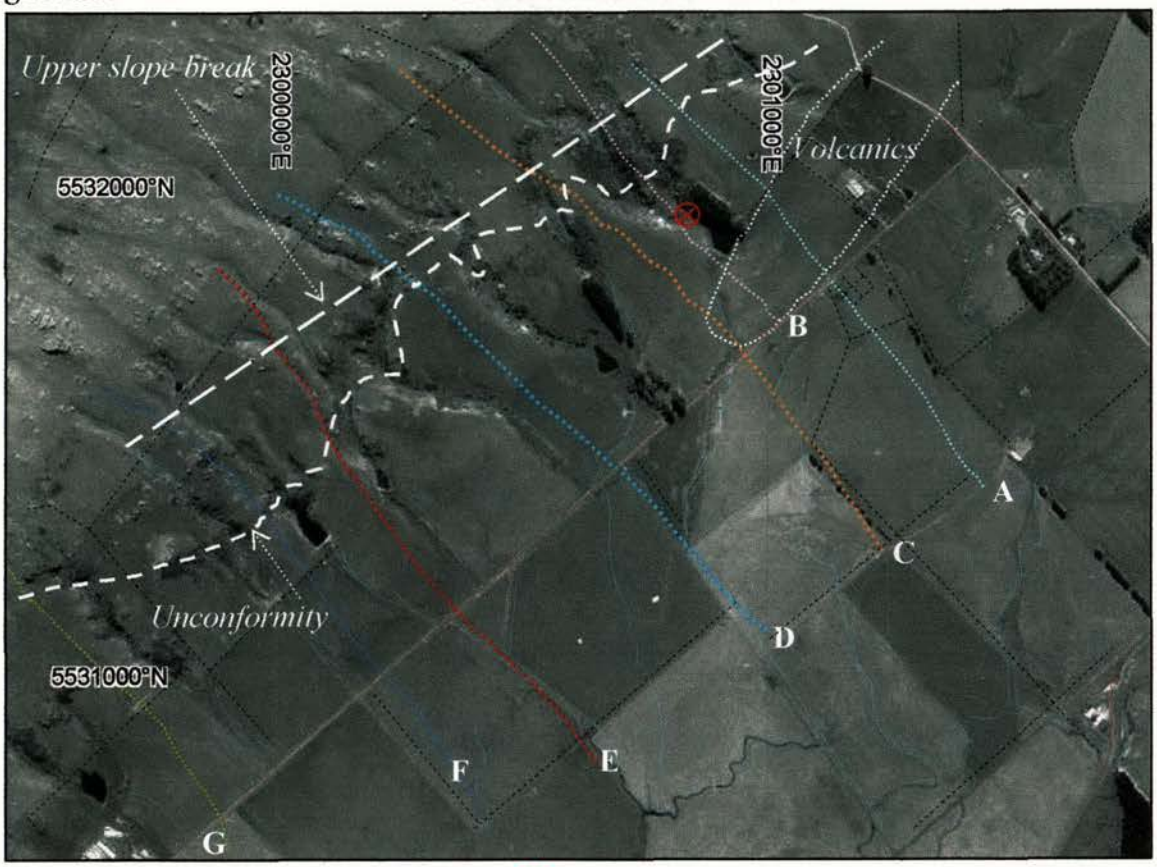

Sample site WLL 328 ⊗

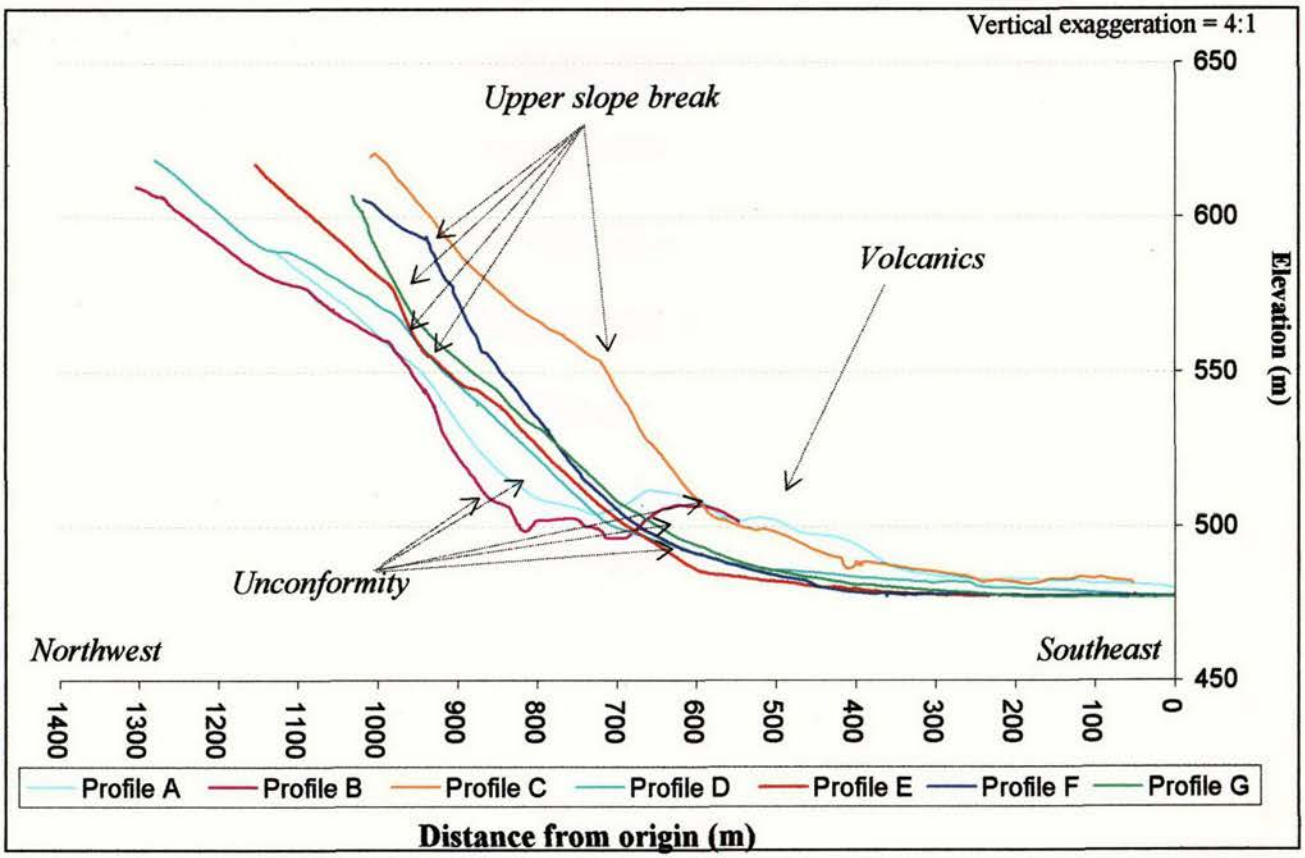

5.2.3 Taieri Ridge Discussion

Multiple generations of deformation are recorded in both the basement and sediments. Basement shear zones observed (*Figs. 5.2.7, 5.2.8, 5.2.9*) have not disturbed overlying sediments, although some tilting is evident. Right-lateral offset in the north-west extension of the shallow-northeast-dipping Mesozoic Hyde-Macraes shear zone (Craw & Chappell, 1999) is consistent with reverse movement on northeast-striking faults, northwest-side up. A deep incision (visible in *Fig.5.2.11,* also see *Fig.5.2.6*) spanning a structural discontinuity within the range may be related to this extension (e.g. Mutch, 1963; Forsyth, 2001).

The inflection points where Taieri Ridge departs from linearity may also be structural discontinuities, and Taieri Ridge may be an amalgamation of at least three discrete en-echelon segments, rather than a single continuous block. This interpretation is supported by anomalous drainage patterns aligning with both inflection points of the ridge and the extrapolation of known faults (see *Fig.5.2.3*). Coalescing of fault segments to form a continuous structure is reported elsewhere in Otago (e.g. Jackson *et al.,* 1996).

Rupture along the total ~30km long Taieri Ridge with a 10-15km thick seismogenic zone would be capable of generating an approximately M_w 6.0-6.5 earthquake (Wells & Coppersmith, 1994; Jackson *et al.,* 1996).

Uplift has both regional and local components. Macraes Flat is approximately 200m higher than the Strath Taieri basin to the west. Isolated remnants of quartz-rich well-sorted gravels, carbonaceous muds and sporadic quartzite sarsen stones point to the erosion of a veneer of Tertiary fluvial and lacustrine sediments prior to late Cenozoic uplift of the whole East Otago area. These are correlatives of the Eocene Hogburn Formation (Williamson, 1933), and Miocene Dunstan and Bannockburn Formations (Douglas, 1986). There are no schist clasts in these well-rounded and well-sorted texturally mature basal sediment remnants indicating local ranges weren't yet uplifted when these were deposited.

Northeast-striking faults are the locus of late Quaternary deformation in the area, with localised differential uplift evinced by angular schist clasts within recycled Tertiary units, blocking and diversion of drainage resulting in Holocene lacustrine sediments within the Macraes-Moonlight depression and, locally, the building of alluvial fans. The relative youth (compared to other ranges in Otago) of Taieri Ridge is apparent by its low relief and minimal stream incision into both the valley sediments and the rangefront schist. The range crest has only been dissected by streams which have exploited inherited structural weaknesses (see *Figs.* 5.2.1, 5.2.11, 5.2.16). Relief on the sub-horizontal range crest is due mainly to late Miocene alkali volcanic peaks, which cap and preserve Tertiary sediments overlying the

schist (Coombs *et al.,* 1986). Another small volcanic intrusion occurs near the intersection of Hay and Sheehy Roads (*Fig. 5.2.17*), which is visible in profiles A, B, and C of *Fig. 5.2.22*. Deformation is distributed across the valley in the form of subtle slope changes, tilts, and small-offsets and folding within sediments. Lineaments are formed of slope breaks both within the schist and at the unconformity (see *Fig.5.2.1*& rangefront profiles *Fig. 5.2.22*). The profiles show (also see *Figs. 5.2.1, 5.2.16*) the location of the unconformity is 2 – 20m above the valley floor and bends upward approaching the range. Surface slopes are reasonable where the surface is an alluvial fan, but outside the depositional realm for fluvial or lacustrine deposits.

The Holocene OSL dates obtained from the three localities are all from units displaying post-depositional deformation. At the Sheehy Road site, the lacustrine sediments pinch out against fan deposits and are elevated 8m above lacustrine correlatives on the valley floor. The OSL date for this sample is 12.9±1.1ka which yields an uplift rate of 0.62mm/yr averaged over the last 12.9ka. This rate seems high, but significant errors may be introduced into strain calculations by a fault dipping steeper than 45°, or enhanced erosion of the valley floor level. For example if the fault dip is increased from 45° (where uplift = shortening) to 50°, 0.62mm/yr of uplift corresponds to 0.56mm/yr of shortening.

The range-parallel GPS profiles of the Horse Flat Road area (*Fig.5.2.14C*) show asymmetric incision patterns, steeper side to the southwest, and a gentle southwest tilt to the lowest terrace surface, to the northeast (right) of the stream channel. Southwest tilting is also evident by the location of the stream along the southwest edge of the terrace system (see *Fig. 5.2.11*). In the range-orthogonal profiles (*Fig.5.2.14B*) the stream profile and the lowest terraces (profiles B and C) all have a subtle (in the profile) gradient change at the location of sample site WLL326, which is visible as a bulge in the terrace surface in *Fig.5.2.11* (see also *Fig.5.2.12*). A tectonic origin for this surface deformation is likely when considered in conjunction with the internal disruption evident in *Figs. 5.2.12* and *5.2.13*. The increasing depth of stream incision approaching the rangefront is also evident in these profiles. The gradient of the fluvial terrace portion of profile A, which is higher and thus older, is divergent from that of the younger terraces. If it is assumed that the streams form depositional terraces with similar surface gradients, then uplift from the northwest is indicated by their departure from parallelism. No single prominent scarp was found that could be the surface expression of a structure responsible for range-scale uplift. The distributed nature of deformation and asymmetry and geometry of the range profile all support the hypothesis that the south-eastern margin of Taieri Ridge is underlain by northwest-dipping reverse fault(s) at depth.

Rock and Pillar Range

5.3 Rock and Pillar Range Overview

Fig.5.3.1 **Southeast rangefront of the Rock and Pillar Range from Macraes-Hyde Road** Photo looking southwest. Note gentle concave-down shape of the range crest, elevation of alluvial fans proximate to highest region of range, and maximum fan incision closest to the range. The surface in the foreground is the shallow-dipping northwest flank of Taieri Ridge.

5.3 Rock and Pillar Range Overview

The Rock and Pillar Range, west of the much smaller Taieri Ridge, rises to 1450m adjacent to Six Mile Creek (*Fig.5.3.3*) over 1000m above the flanking valley floors. In transverse profile it is broadly box-like with steep northwest and southeast flanks and an almost flat central part (*Fig.5.3.1*). The range crest is highest in the centre and gently dips away from the summit toward both ends, thus forming a broad (~20km) flat-topped, elongate (~50km) dome. The range shape closely, but not exactly, mimics schistosity, forming a doubly plunging antiform (Salton, 1993). Jackson *et al.* (1996) used drainage patterns to describe the evolution of the range. The radial drainage pattern and diversion of the Taieri River around the northeast end (see *Figs.5.1, 5.3.2*) are used to imply a north-eastward range propagation direction. Asymmetric incision of north-tilted alluvial fans, steep side to north, all along the southeast rangefront attest to a Quaternary component of uplift. The location of the drainage divide close to the southeast flank is used to infer that the range grew from an initially asymmetric fold structure, like Taieri Ridge (Jackson *et al.*, 1996). Subsequent uplift on the northwest flank required the longer and thus more erosive streams to cut deep gorges once stream capture had provided sufficient catchment to keep pace with uplift.

Fig.5.3.2 **Northeast Rock and Pillar Radial drainage pattern**

The presumption is that range uplift is accommodated on a NW-dipping reverse fault along the southeast rangefront, followed by a later SE-dipping reverse fault along the northwest rangefront. Localised northwest rangefront faulting is evident in small-offset shear zones within the schist (Salton, 1993), and displaced alluvial surfaces, about 4km out from the schist-sediment contact, although surface displacements are less than 10m (Waipiata Fault, Thomson, 1996). On the southeast rangefront, the Hyde fault (Williamson, 1939) is marked on maps as an active structure (e.g. Forsyth, 2001), although a single major fault at the surface is elusive. Two southeast rangefront field areas, (*Fig.5.3.3*) together traversing ~12km, are considered here from which three OSL dates were obtained.

5.3 Rock and Pillar Range Overview

Fig. 5.3.3 **Topography and location of field areas**

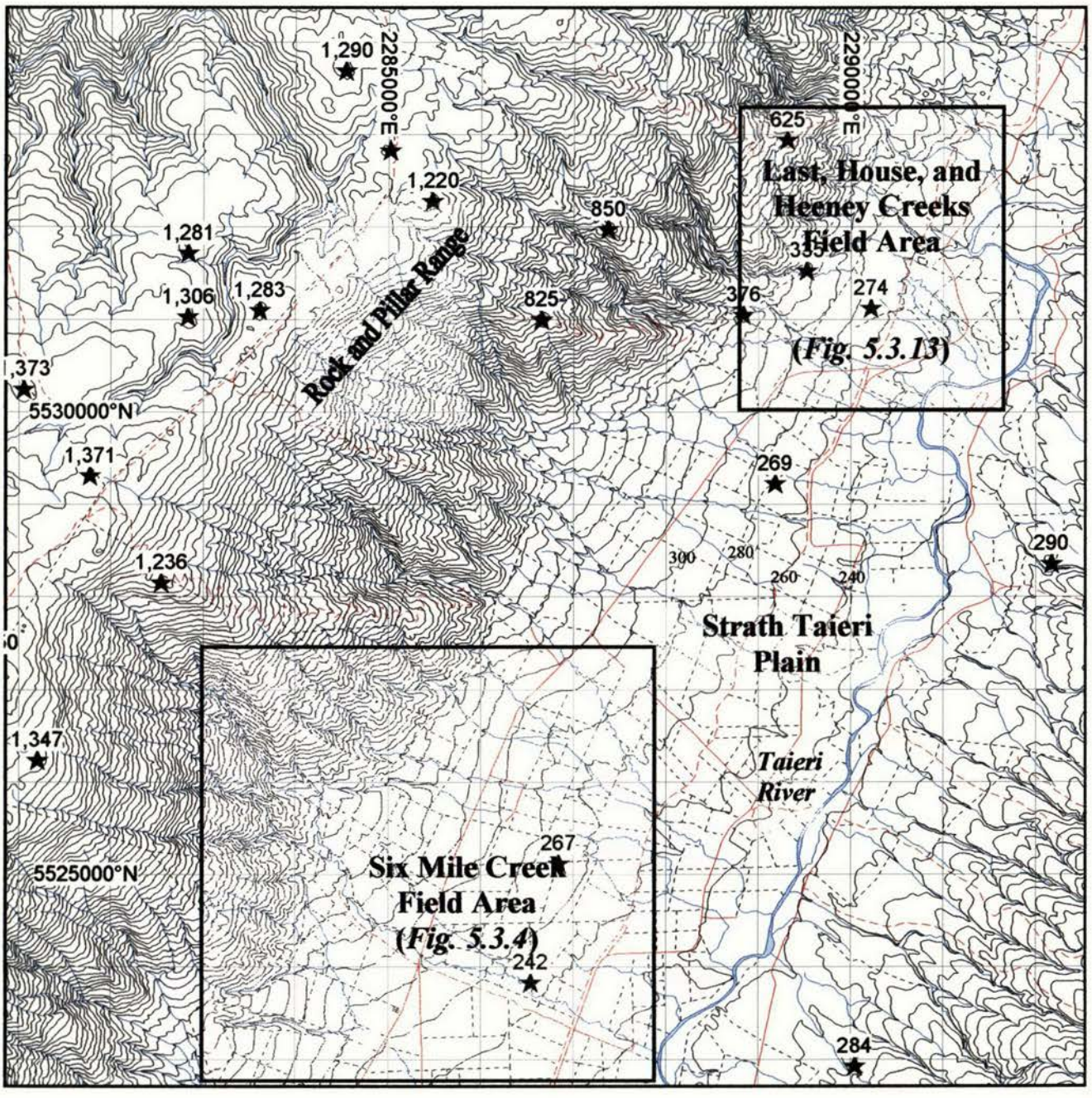

5.3.1 Rock and Pillar Range - Six Mile Creek

Fig.5.3.4 **Orthomap and photo locations** (Asterisk is position, arrow is camera azimuth)

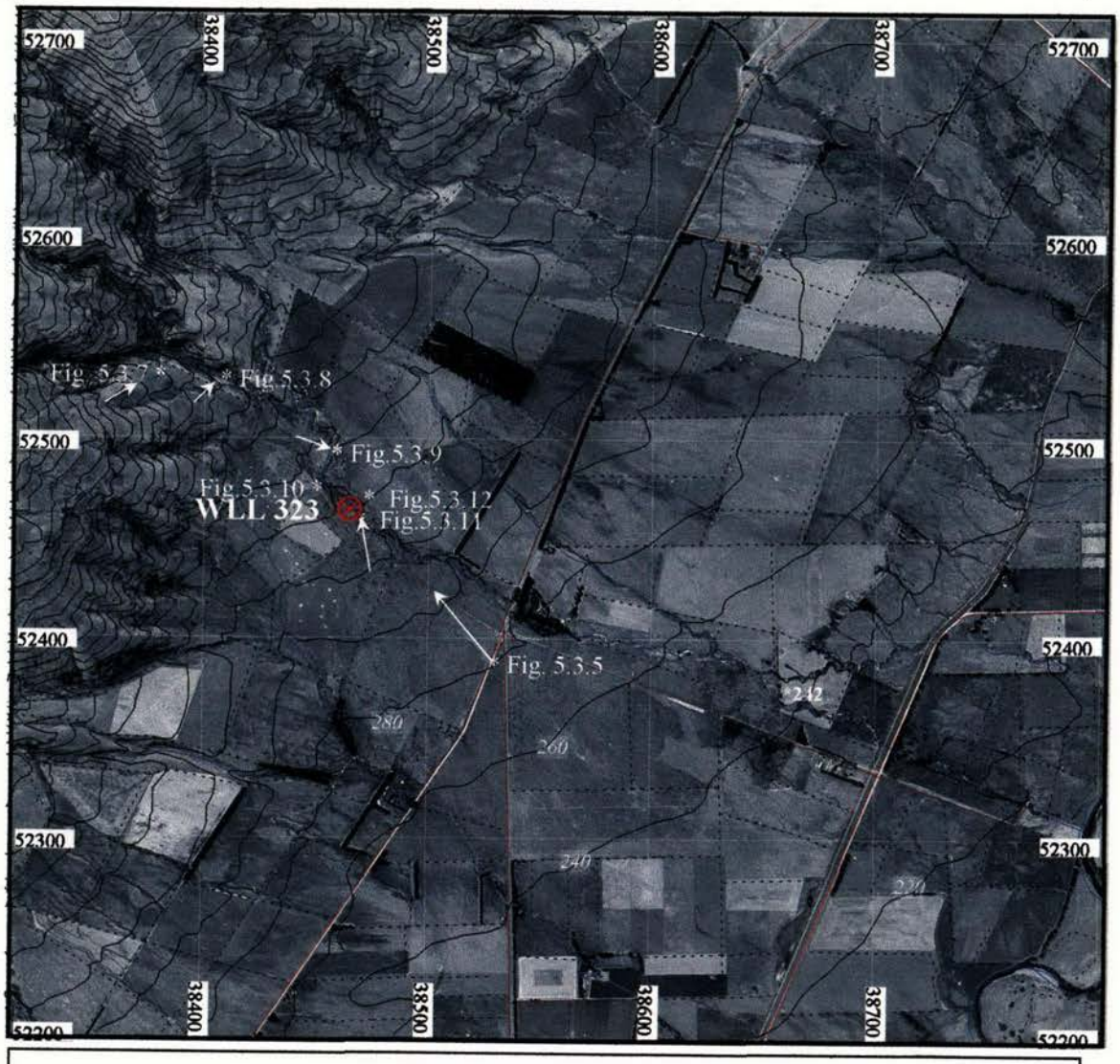

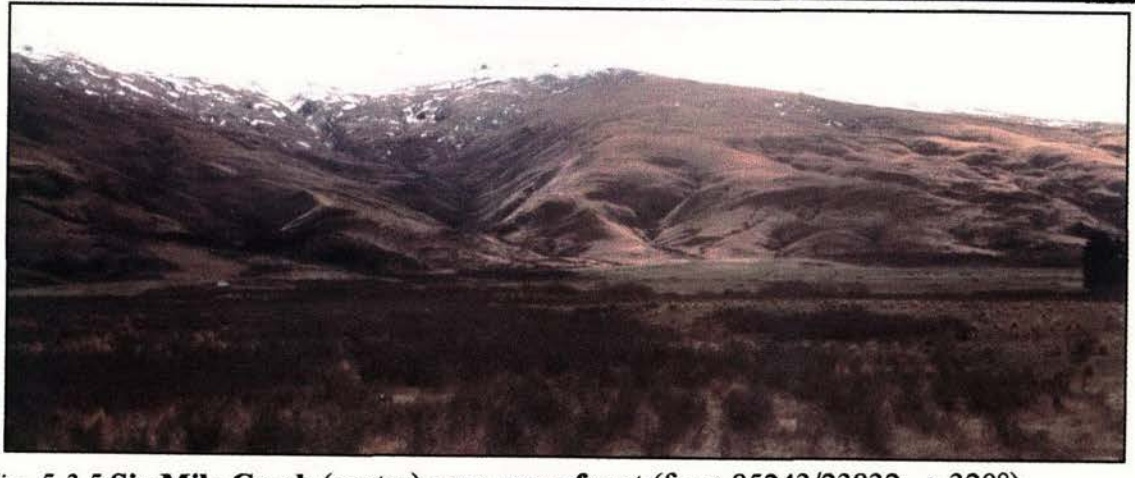

Fig. 5.3.5 **Six Mile Creek** (centre) **area rangefront** (from 85243/23832 → 320°)

An extensive fan has built out ~4km from a deep stream incision into the range and coalesced with neighbouring fans. Stream patterns incising these fans have range-parallel kink segments aligning with subtle surface perturbations and bedding disruption. Multiple terrace remnants within fan incisions record stream adjustments to intermittent range uplift.

5.3.1 Rock and Pillar Range - Six Mile Creek Section

Fig.5.3.6 **Structure and sample location**

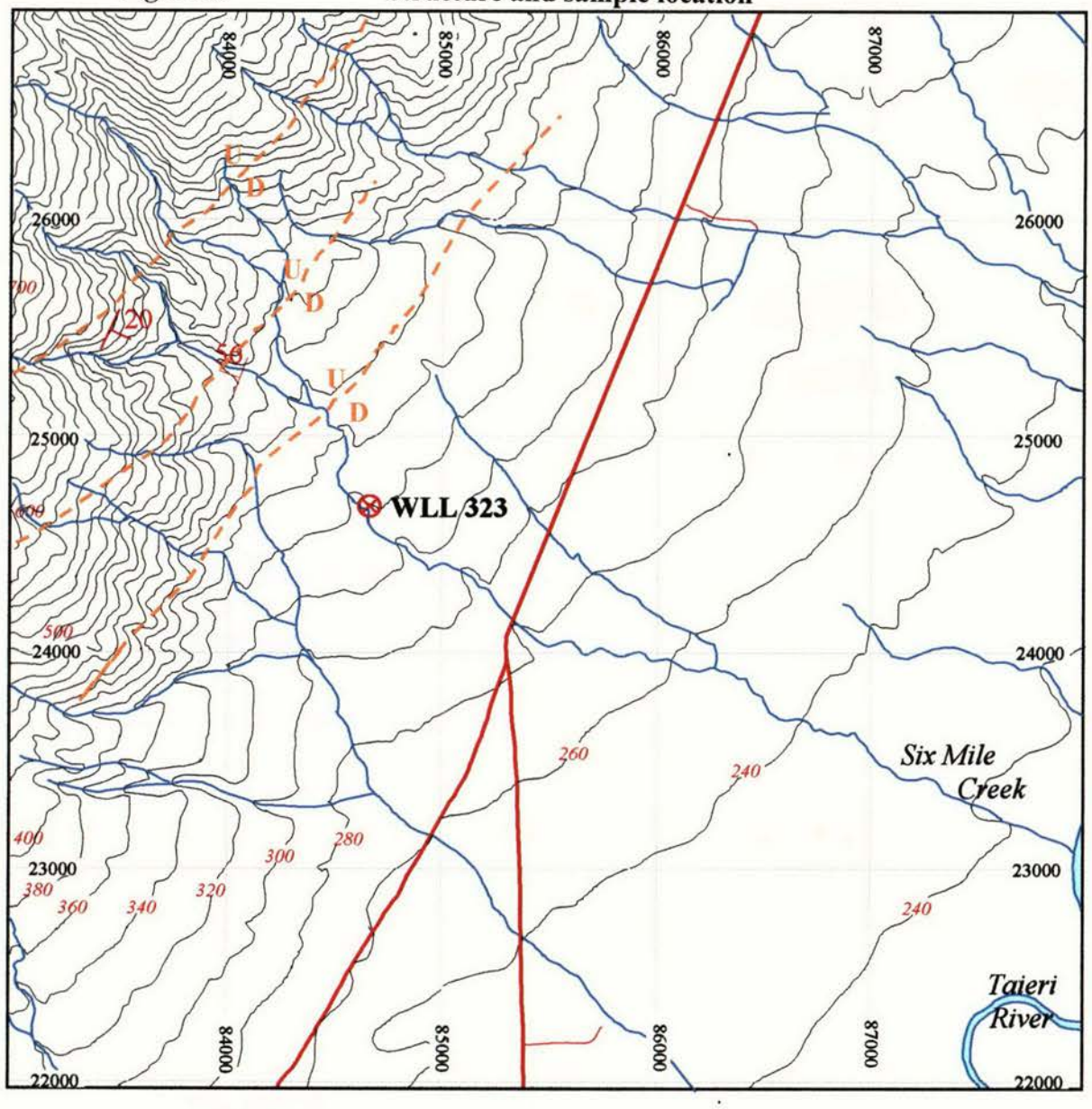

5.3.1 Rock and Pillar Range - Six Mile Creek Rangefront deformation

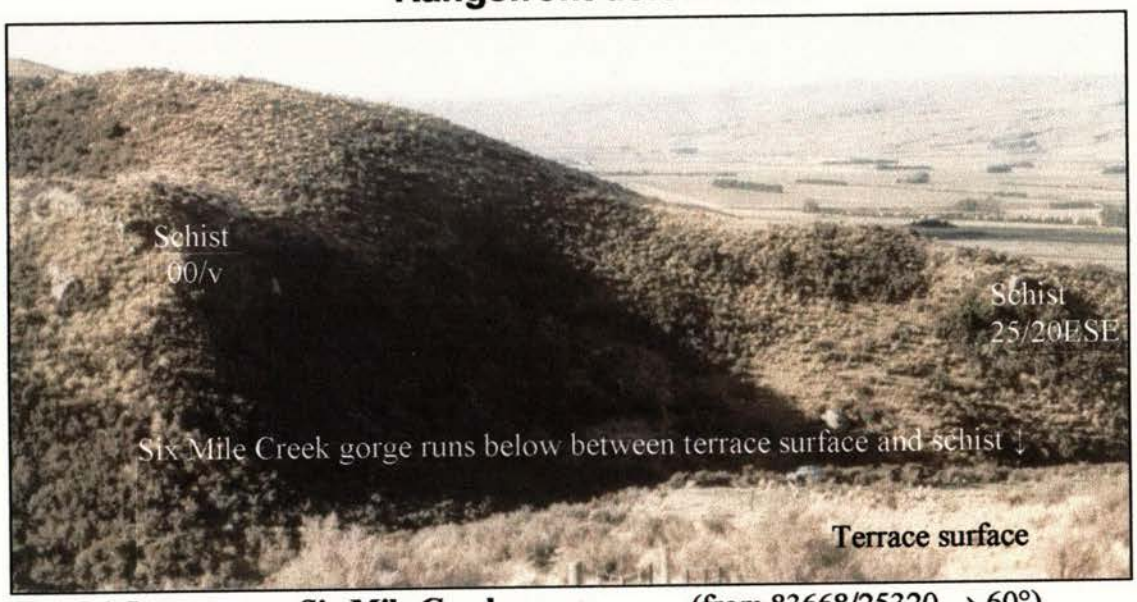

Fig. 5.3.7 **Six Mile Creek gorge** (from 83668/25320 → 60°)

Stepped interfluves, which are common along the rangefront, may be elevated strath terrace remnants (see below, and Heeney Creek section), or a result of differential uplift, i.e. fault offsets. The schist to the left in *Fig.5.3.7* strikes N-S and is sub-vertical whereas on the right it dips ~20°ESE.

Fig.5.3.8 **Shear zone in altered schist strath terrace remnant** (from 84105/25326→ NNE) (Schist 20/56NW) This is located within the Six Mile Creek gorge near the right side of *Fig.5.3.7.* Spade is resting on degraded and tilted (4°ESE) strath terrace surface (marked) above a shear zone in the schist. The shear zone hasn't disturbed the overlying fan deposits and thus predates them. Sense of movement isn't clear, but the dip of the fault is sub-parallel to the schistosity. The location of this shear zone is on a range-parallel lineament formed by stream channel deviation and interfluve deformation. Stream channels to the northeast and southwest (*Figs. 5.3.4, 5.3.6*) contain kinks aligning with this shear zone.

5.3.1 Rock and Pillar Range - Six Mile Creek
Fan processes and deformation

Streams emerging from the range invariably have stepped courses with segments both orthogonal and parallel to the rangefront (see *Fig.5.3.4*). Range-parallel segments often align with bedding and surface disruption, and orthogonal segments always undercut the northern bank, giving asymmetric cross-valley profiles. This is consistent with north-eastward range propagation, and provides excellent vertical sections through the fan. At Six Mile Creek fan, sediments are locally derived, from the Rock and Pillar Range, as judged by clast angularity, composition, and imbrication. Proximal matrix-poor clast-supported winnowed gravels contain hydraulically incompatible clasts deposited in alluvial fan sediment gravity flows. These invariably grade upwards into pebbly planar bedded laminated muds, sands and gravels deposited by fluid gravity flow sheetwash processes. The upper surface is often in scoured contact with chaotic gravels at the base of the next cycle (*Fig.5.3.9* →). Within the fan incision channel are many small depositional fluvial terrace remnants at different elevations (*Fig. 5.3.11*). These incised channel fills form between periodic catastrophic flooding events and serve to decrease the channel gradient, causing flash floods to deposit their coarse (bouldery) fraction due to decreased competency (Blair & McPherson, 1994; *Fig.5.3.10*), if the terrace survives the flood. As the whole fan is tectonically uplifted or tilted, older infill terraces are abandoned as the stream adjusts its long profile in response. Tectonism is thus recorded in both fan surface tilting and disruption plus the elevations of the incised channel fill terrace remnants.

Fig.5.3.9 **Proximal fan section**
(Outcrop at 84558/24960 → 110°)

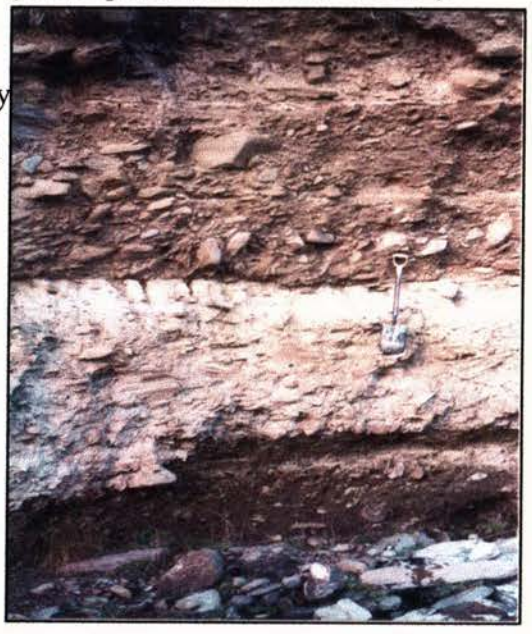

Fig.5.3.10 (Outcrop at 84467/24790)
Channel fill gravels plus boulders

Fig.5.3.11 (from 84625/24647 → 350°)
Multiple channel fill terrace remnants

5.3.1 Rock and Pillar Range - Six Mile Creek Section OSL sample site

Fig.5.3.12 **Sample Site WLL323 Age: 7.47 ± 0.87ka**

(from 84660/24759 → N) (GPS top left for scale)

Sample taken for OSL date from massive sand horizon (marked '⊗') within the lowest-level channel-infill terrace remnant, which is now being incised by Six Mile Creek.

The stream is adjusting its long profile by incision into this depositional terrace in response to gradient change, probably associated with range uplift. The stream is currently 1.7m below the top of this terrace, and 900mm below the site of sample collection.

A date from this horizon constrains rates of change. The coarsening-up of sediments within the terrace remnant above the sample site signal a progressive increase in stream competence and deposition of at least another 800mm of material. Subsequent stream adjustment has now produced incision of 1700mm into the terrace. This yields an absolute minimum uplift/incision rate of 0.23 ± 0.03mm/yr, averaged over the last 7,470 ± 870 years.

5.3.2 Rock and Pillar Range

Last, House, and Heeney Creeks Section

Fig. 5.3.13 **Orthomap and photo locations** (Asterisk is position, arrow is camera azimuth)

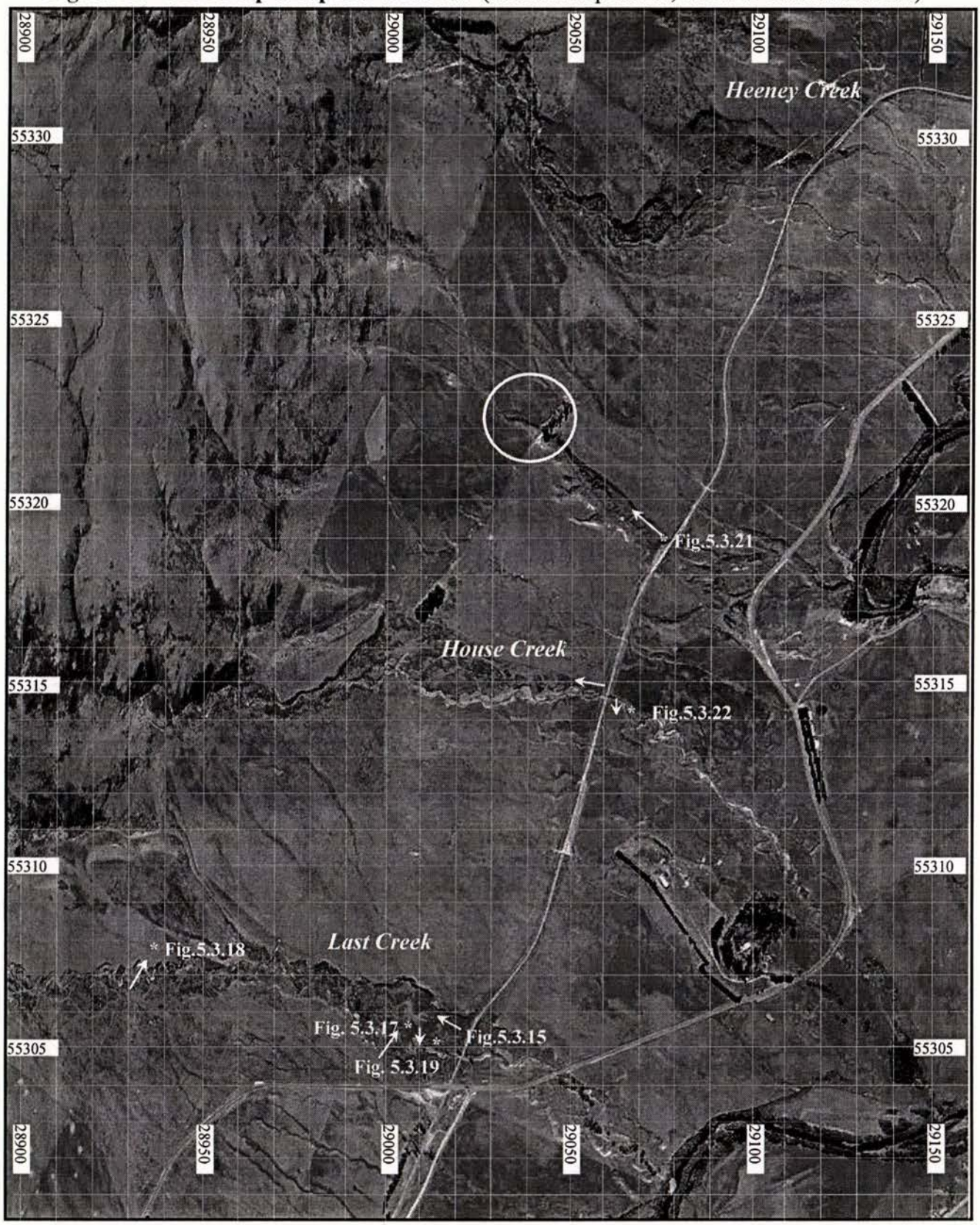

Anomalous stream appearance - refer to page 66

5.3.2 Rock and Pillar Range

Fig. 5.3.14 **Last, House, and Heeney Creeks - Faulting and Sample Sites**

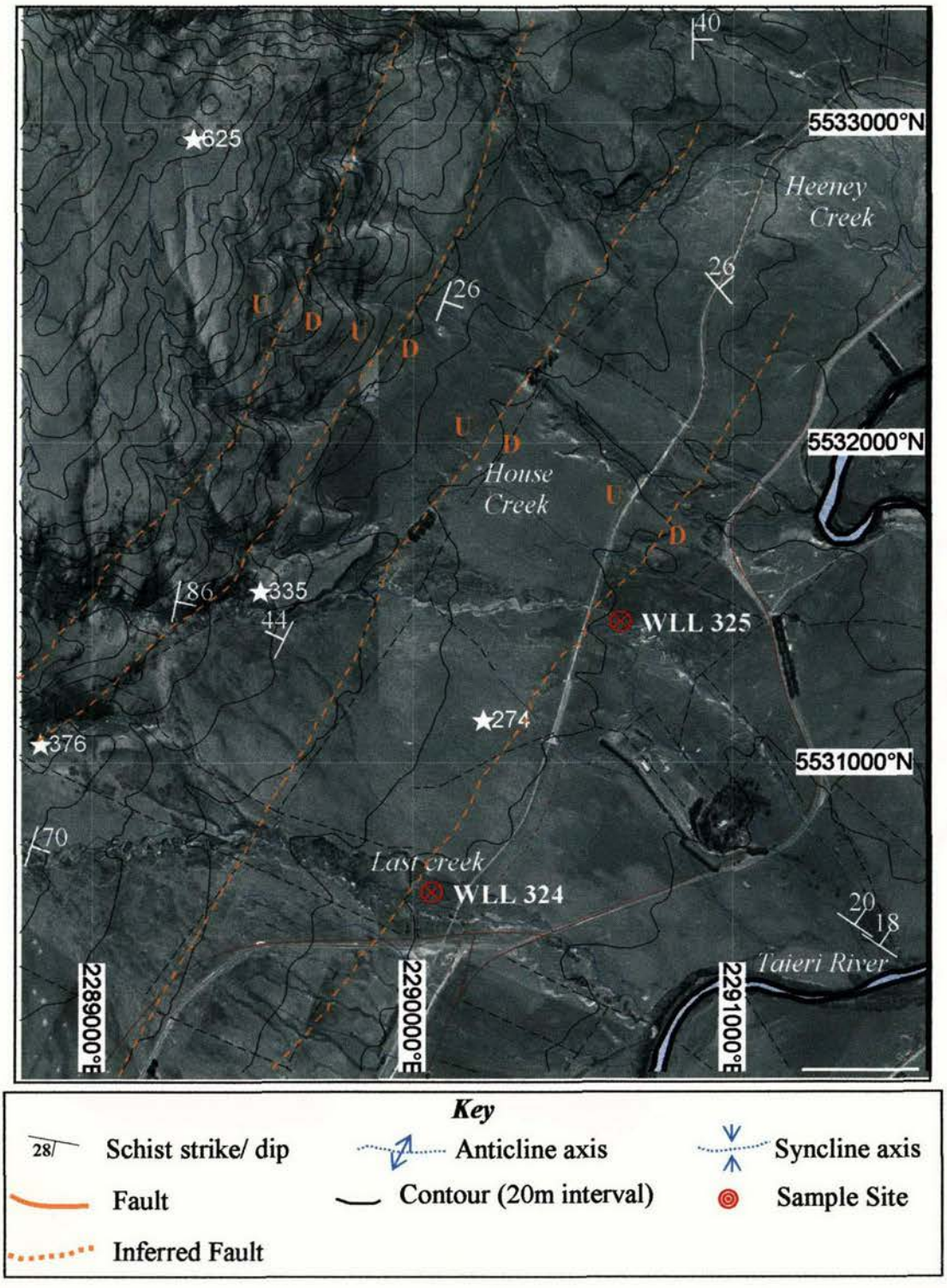

5.3.2 Last Creek area - Geomorphology

Fig.5.3.15 **Last Creek and rangefront** (from 90718/30524 →300°)

Last Creek is incising the large rangefront fan complex, which is tilted gently to the north. Streams incise older, higher fan-incision channel-fill terrace remnants which they have earlier deposited within asymmetric valleys, leaving escarpments on northern (right) side of abandoned channels. This is common to all streams on the Rock and Pillar rangefront in this study. The vertical interval between terrace remnants decreases nearest the current stream level. The oldest escarpment is 23m high, whereas the lowest levels are only ~300mm apart.

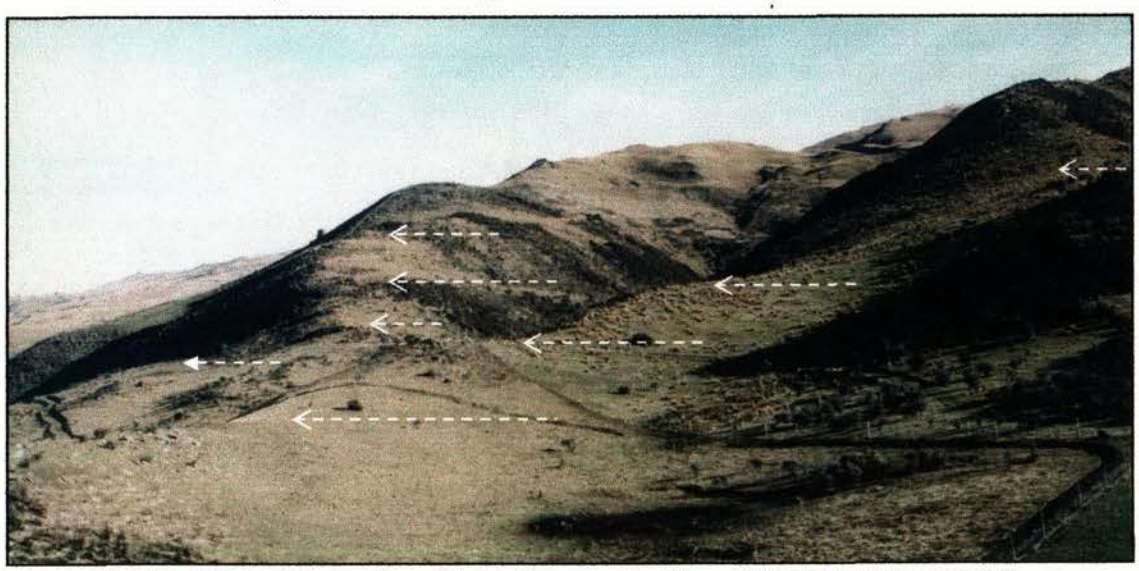

Fig.5.3.16 **Rangefront interfluves** (from 88040/31039 →270°)

These interfluves are central in *Fig.5.3.15* above, and have a decidedly stepped profile. This is common to many interfluves along the southeast Rock and Pillar rangefront and it is possible to correlate step levels between interfluves (marked in *Figs.5.3.15 & 5.3.16*). Some step treads are channel-shaped, i.e. a broad "∪", and others are flat but tilted basinward.

5.3.2 Last Creek area
Rangefront sediment deformation

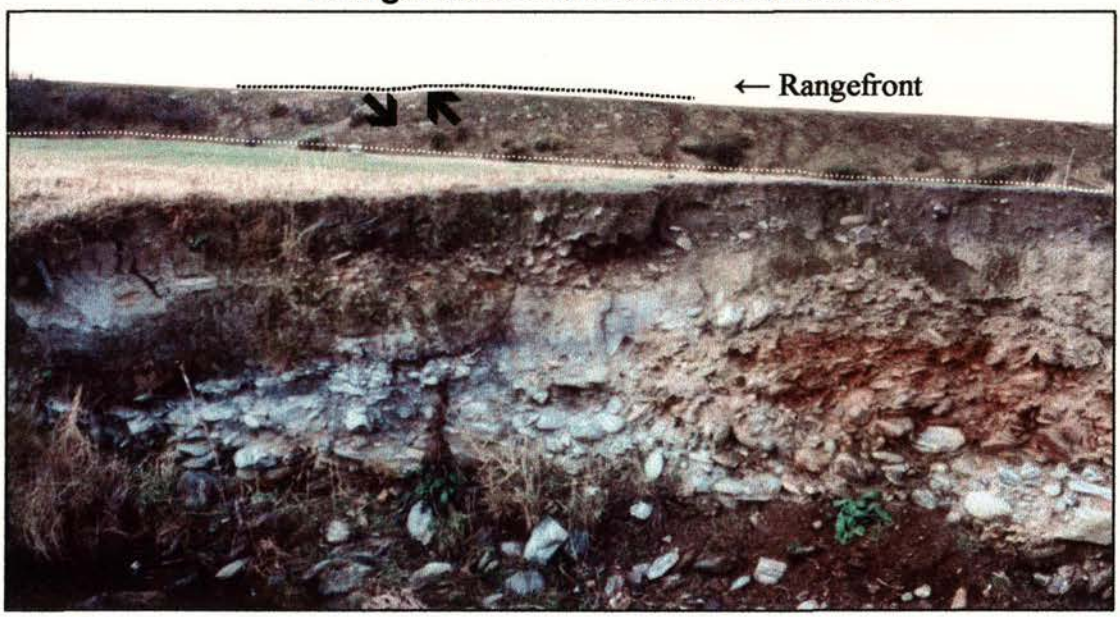

Fig. 5.3.17 **Last Creek bedding and surface disruption** (from 90093/30561 →035°)
Subtle surface distortion (concave down) is mirrored in both infill terrace levels and aligns with a range-parallel stream course kink and internal bedding disruption. Sense of movement is right side up, i.e. antithetic. A range-parallel lineament is formed by stream course inflections aligning with this locality at 1750m from the rangefront.

Fig.5.3.18 **Last Creek bedding disruption** (from 89373/30784 → 30°)
Synthetic movement apparent here (left side up) which is on a range-parallel stream deflection lineament at 1000m from the rangefront.

5.3.2 Rock and Pillar Range
Last Creek area - OSL sample site

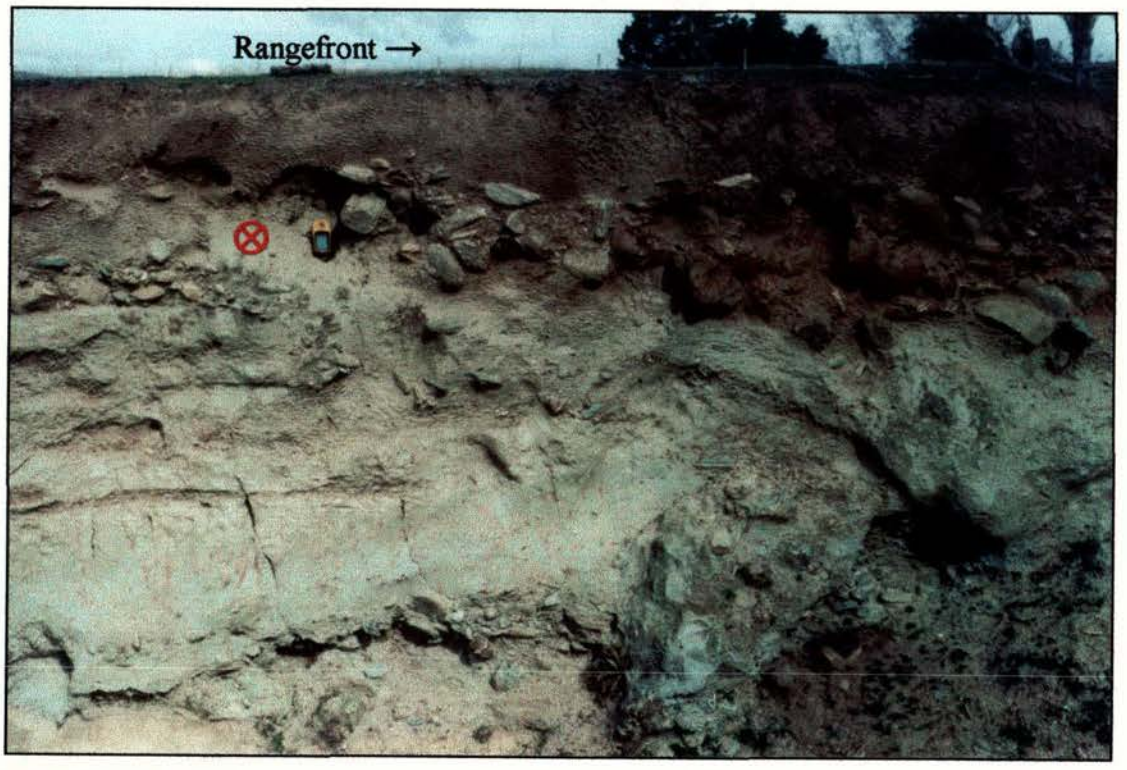

Fig.5.3.19 **Last Creek terrace bedding disruption and sample site** (90132/30523 →S)

Sample site WLL324 Age: 4.26 ± 0.70ka

Sample is quartz and mica-rich fine sand taken from position marked ⊗, just left of the GPS.

The upper surface is 2100mm above present stream level, and the sample site is 400mm from the top. This surface is locally extensive and shows clear evidence for post-depositional deformation. The upper surface is bowed upwards and forms a range-parallel lineament, 2000m from the rangefront, defined by both active and abandoned neighbouring stream course deviations (see *Fig.5.3.13*).

The date from within this surface constrains the incision/uplift rate and gives a maximum age for the deformation.

More evidence of fault-disturbed sediments is found further upstream at 89001/30761, which is 750m from the rangefront, and also lies on a lineament formed of stream diversions.

Disruption also occurs in the schist within the Last Creek gorge. At the gorge mouth the schist foliation is oriented 32/70SE, but 700m upstream at 88876/31145, the foliation strikes N-S and dips 34° *to the west*. A further 600m into the gorge the schist strikes 46° and dips 86°SE. Deformation thus occurs in a zone at least 3km wide orthogonal to the rangefront, from within the range itself out at least 2km.

5.3.2 Rock and Pillar Range
House Creek geomorphology

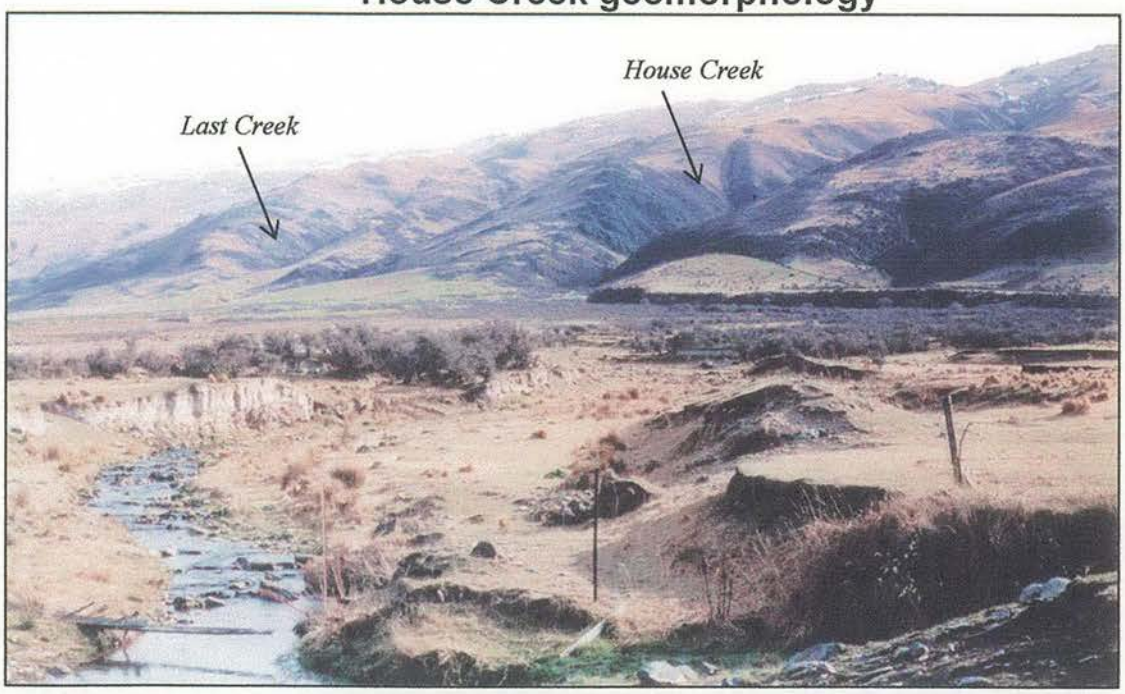

Fig.5.3.20 **House Creek fan and rangefront incision** (from 90609/31494 →280°)
House Creek emerges from the deep incision in mid-photo and a very similar scenario exists to that of Last Creek, which is centre-left. Note the stepped interfluves and largest escarpment in the oldest, highest surface, on the north (right) side.

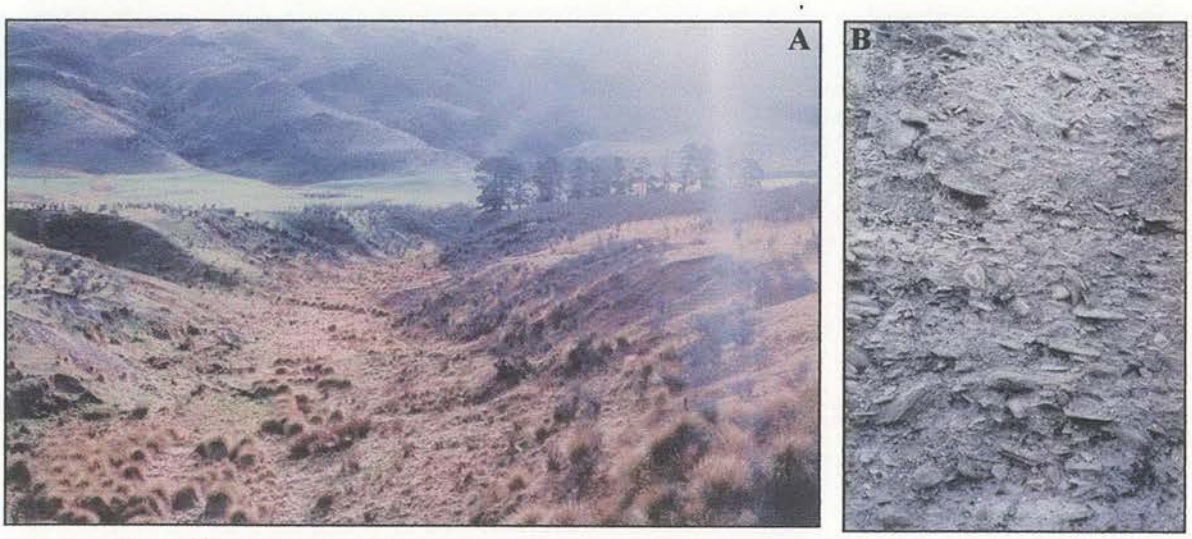

Fig5.3.21 **A. 1st gully N of House Creek B. section through upper surface** (90711/31798)
A This gully just 'appears' in the middle of the fan surface at a point lying on a line between disturbances in House and Heeney Creek stream courses (marked on *Fig.5.3.13*). There is no stream on the fan surface leading into it, and it appears sourced from springs at its head, and there are no channel fill terrace remnants within the incision. (Photo looking towards 310°)
B Section through the top of the left side of **A**, with clasts showing increasing imbrication up-section. Pen is centre left (within red ellipse) for scale.

5.3.2 Rock and Pillar Range
House Creek terrace disruption and OSL sample site

Fig. 5.3.22 **Terrace disruption and sample site** (90687/31425 → 180°)

A Photomosaic of surface and bedding deformation in House Creek fan incision 1500m from the rangefront. Section is 1800mm high, and total sediment thickness to weathered schist basement (schist 30/20°NE) is 2200mm. This lies on an anomalous range-parallel and very straight stream segment, which forms a lineament with similar deflections in neighbouring streams (see *Fig.5.3.13*). Layers are traceable for some distance within terrace exposure. If this is a fault offset, then throw can be gauged from change in elevation of fluvial layers not attributable to stream gradient. This is estimated at 500mm and annotated above.

OSL sample site WLL325 Age: 8.42 ± 0.83ka

Sample device is protruding from the 400mm loess layer sandwiched between fluvial infill channel gravel beds, to the left of the GPS in the photo (inside red circle). Loess deposition of this upper layer post-dates deformation because the loess thickens in the lee of the scarp. The fluvial gravel below the upper loess pre-dates deformation because it bends upwards sub-parallel to the uplifted basal Tertiary sediments (on centre-right in photo above), and c.800mm vertical offset of the fluvial bed over 30m exceeds a natural stream gradient by at least 500mm. Dating the loess gives a minimum age for this deformation.

5.3.2 Rock and pillar Range

Heeney Creek area

Fig.5.3.23 **Orthomap and photo locations** (Asterisk is location, arrow is camera azimuth)

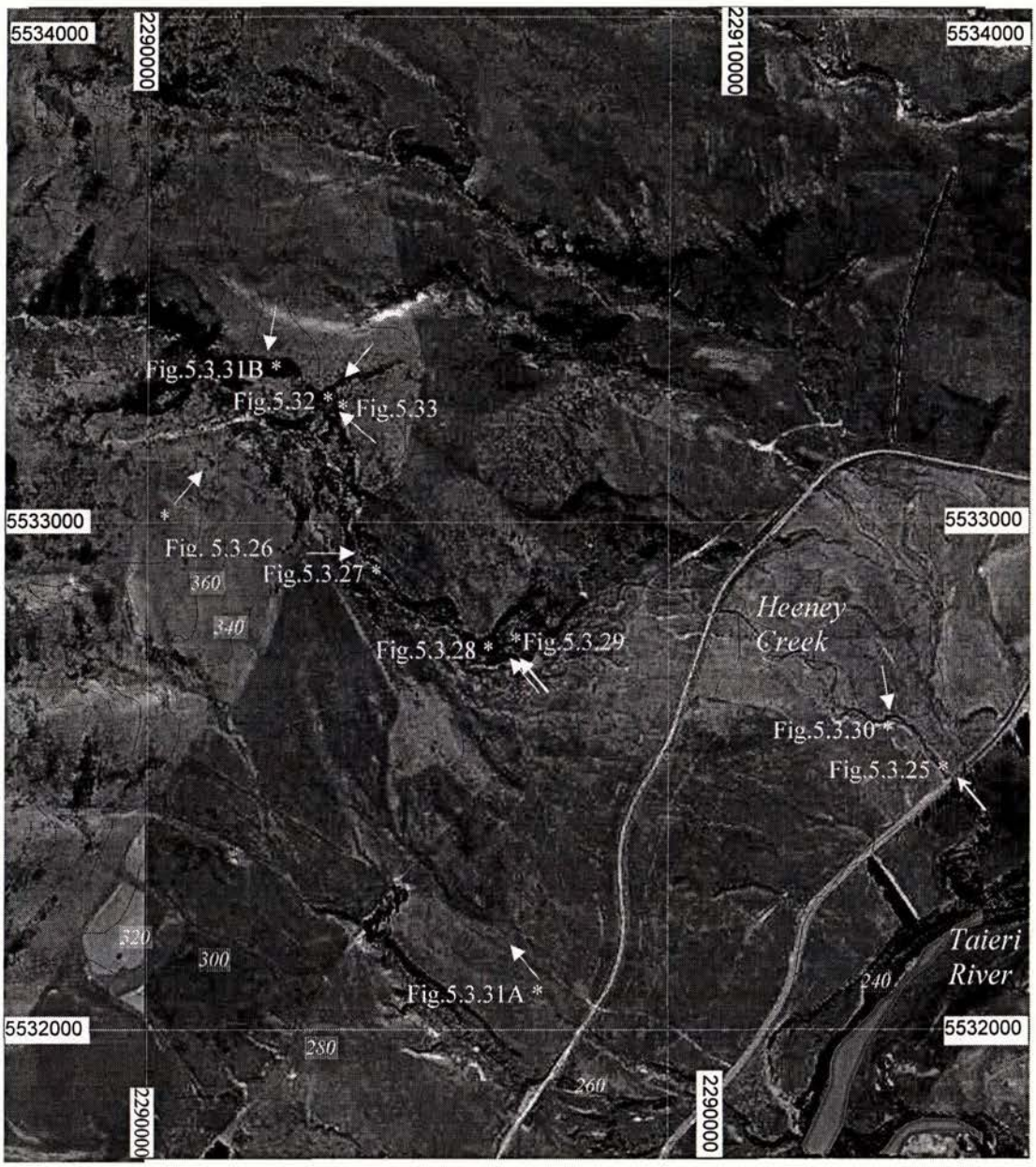

5.3.2 Rock and Pillar Range

Fig. 5.3.24 **Heeney Creek Faulting**

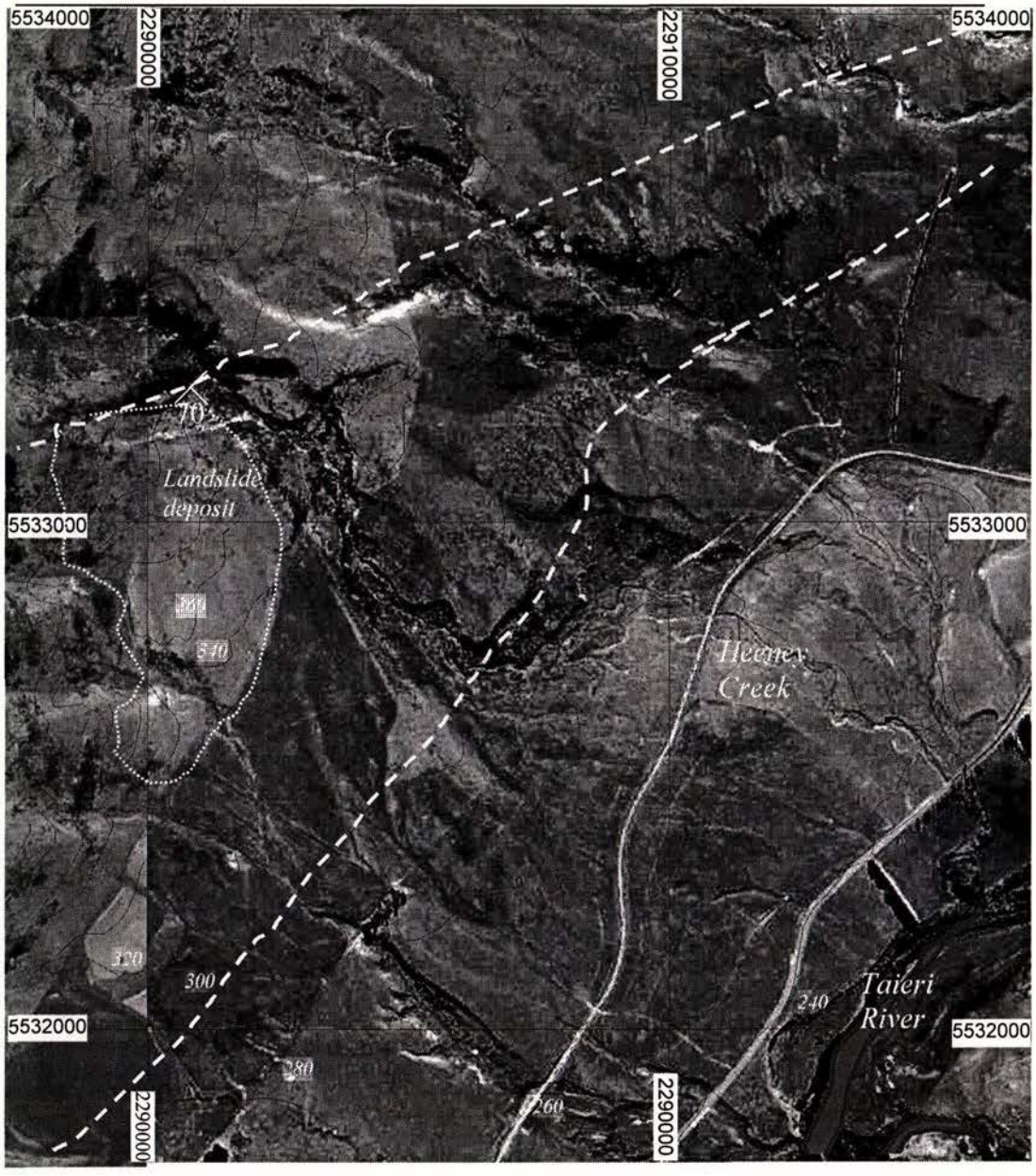

Key

28/ Schist strike/ dip

Fault

Inferred Fault

480 Contour (20m interval)

5.3.2 Rock and Pillar Range

Heeney Creek area – Geomorphology

Fig.5.3.25 **Heeney Creek Rangefront** (from 91563/32492 → 320°)

Ongoing incision into gently north-east tilted fluvial terraces has consistently produced steeper escarpments to the north (right). The height between consecutive terrace treads increases with age, and the lowest and youngest surfaces are in the foreground.

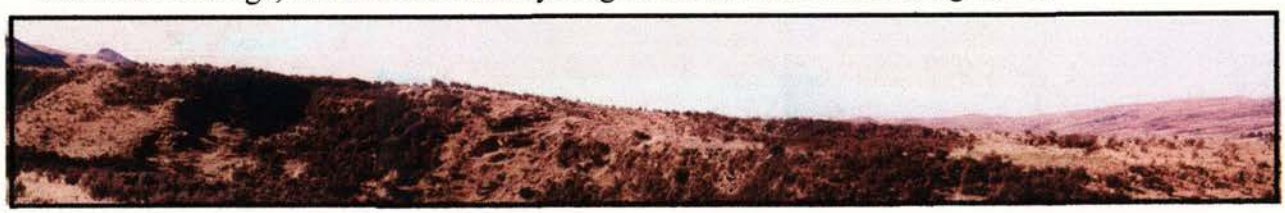

Fig.5.3.26 **Heeney Creek terrace profile** (from 90300/33000 → 40°)

This fluvial terrace section (marked in *Fig.5.3.26* above) has an overall basinward ~8° tilt but with upper surface slope changes, which align with range-parallel stream course deviations in Heeney and neighbouring creeks (see *Fig.5.3.23*). Proximate to the rangefront, Heeney Creek has incised the fan and fluvial terraces to a depth of 30+m.

Fig.5.3.27 **Tilted fluvial gravels and sands unconformably overlain by alluvial fan gravels** (from 90400/32900 → 90°) (2.5m fan gravel section; unconformity marked with white dashed line)

Within the terrace incision, alluvial fan gravels overlie a 10°SE tilted unconformity cut into the fluvial sequence (see *Fig.4.3.27*←). Numerous abandoned channel-infill terrace remnants occur within the stream valley at differing heights. Older, higher remnants have steeper basinward slopes.

5.3.2 Rock and Pillar Range
Heeney Creek area rangefront terrace deformation

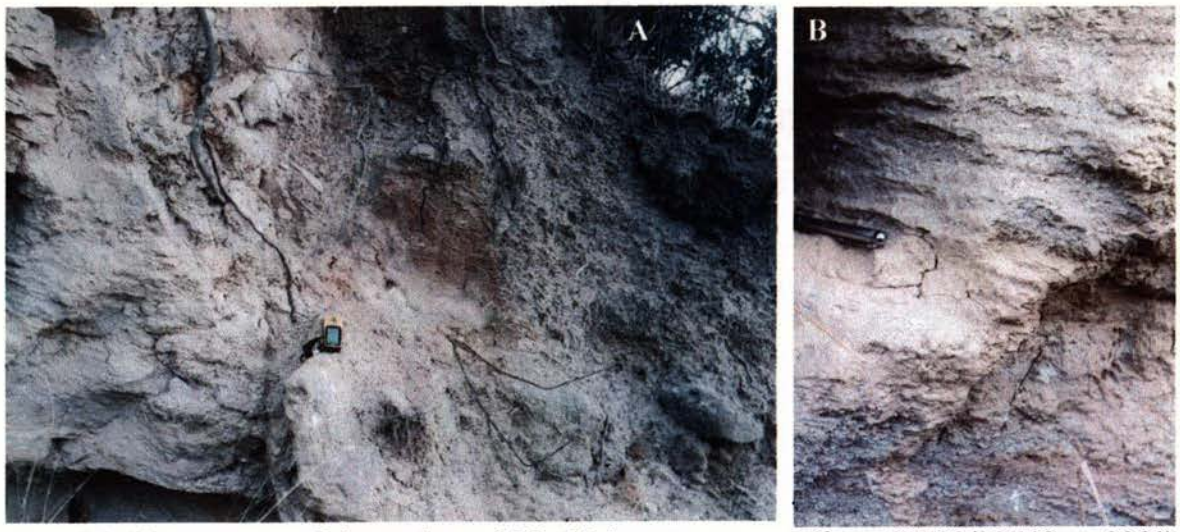

Fig. 5.3.28 **Disruption within high terraces** (from 90709/32748 → 320°)

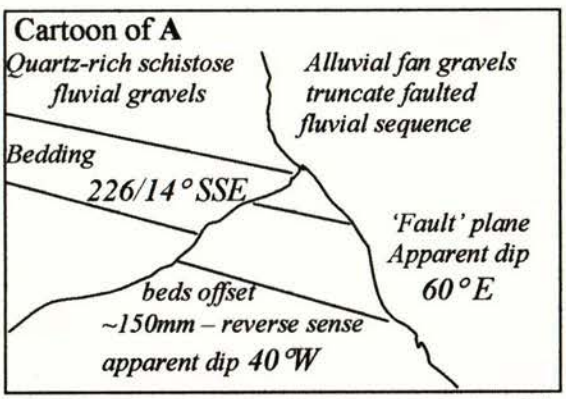

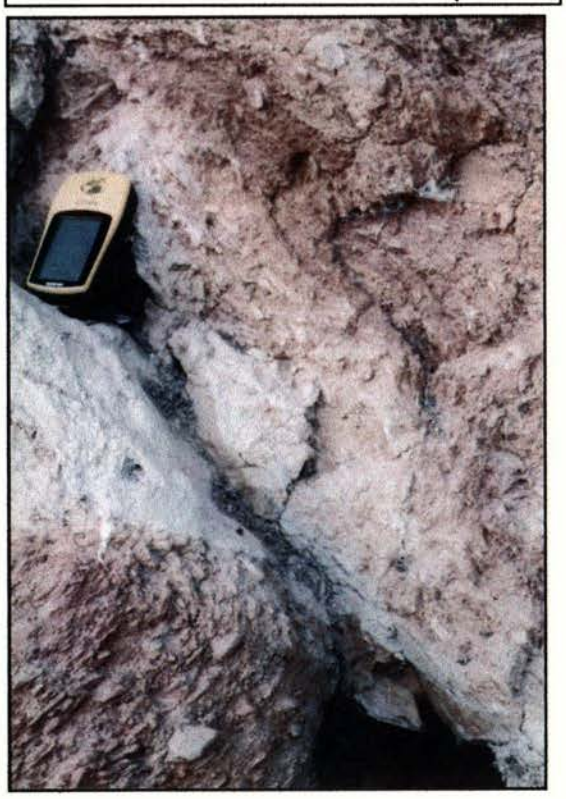

Disruption and tilting of bedding planes within basal quartz-rich fluvial terrace gravels is widespread along this ~200m northeast-striking terrace-section. This is the most prominent of a number of range-parallel northward steps in the stream course which occur between the Heeney Creek gorge mouth and its confluence with the Taieri River (see *Fig.5.3.23*). Abandoned stream courses share this characteristic. Similar deflections in neighbouring streams form a lineament which is 900m from the rangefront. Slope breaks in the terrace profile are coincident with internal bedding disruption and inflection points in the stream courses (see *Fig.5.3.23*).

Fig.5.3.29 **Fault within terrace gravels** (from 90760/32747 → 320°) Bedding planes bend approaching fault plane indicating antithetic reverse movement.

5.3.2 Rock and Pillar Range

Heeney Creek area rangefront deformation

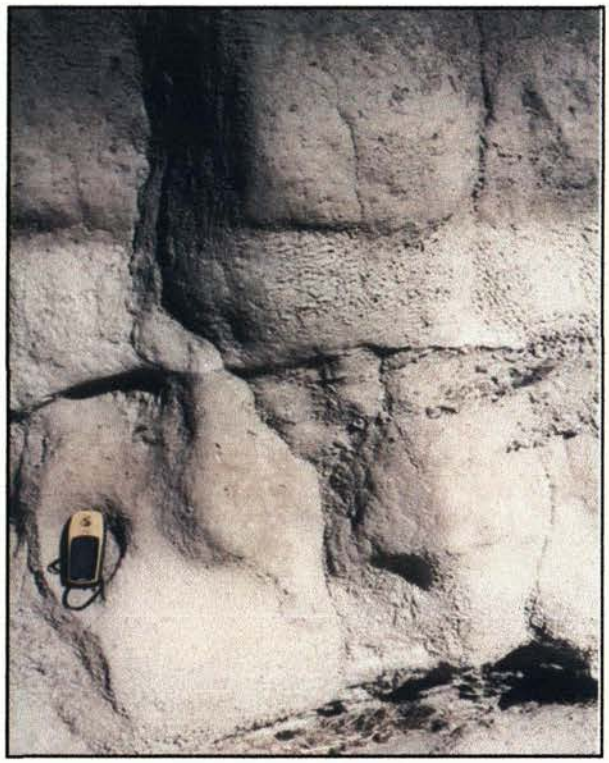

Fig.5.3.30 **Lower terrace section**
(from 91335/32604 → 170°)
This outcrop is a section through the lowest terrace on a range-parallel stream course segment which forms part of a lineament 1.5km from the rangefront unconformity. The dip of the contacts and bedding of the fluvial gravel and loess sequence is divergent and shallows up-section, indicating ongoing uplift to the right (rangeward).

(from 907222/32143 → 320°)

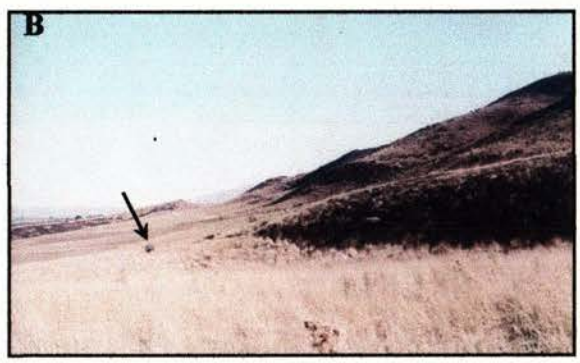

(from 90200/33290 → 190°)

Fig. 5.3.31 **Heeney Creek rangefront landslide**

A large paleo-landslide is immediately to the south (left) of Heeney Creek gorge and has left a lobate 10m high escarpment at its toe (marked in *Fig.5.3.31*A, and aerial view in *Fig.5.3.24*). Vehicle is arrowed in *Fig.5.3.31B* for scale. A line of springs appears at the base of the slide, and the toe is strewn with schist boulders. The upper surface is hummocky with an average slope of 12°, which is 9° less than the overall local rangefront slope of 21°. Stream incision is less developed on the upper surface of the slip, compared to neighbouring areas.

5.3.2 Rock and Pillar Range - Heeney Creek Gorge

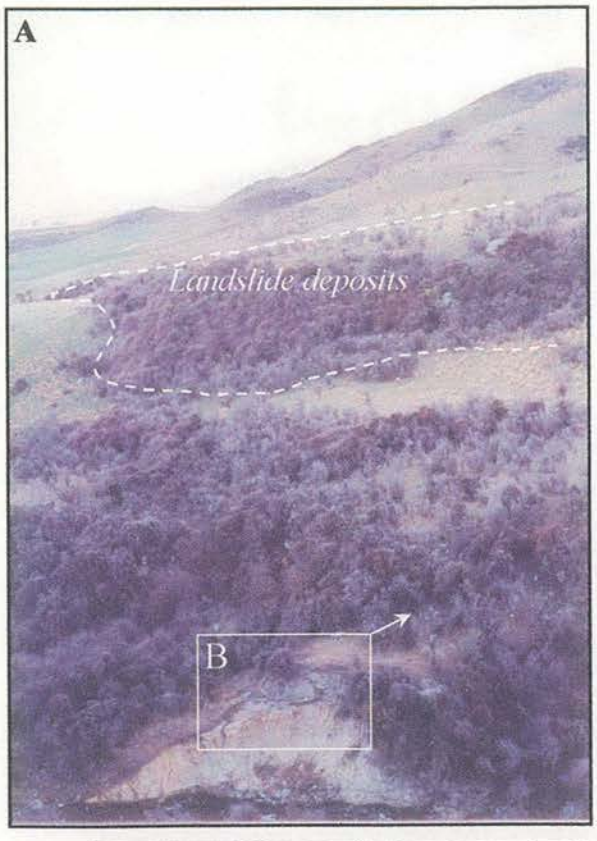

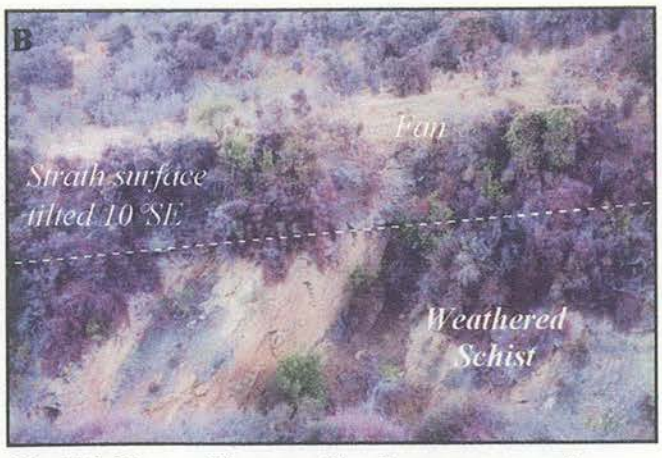

Fig 5.3.32 **Heeney Creek gorge mouth** (from 90407/33146 → 220°)

Fan gravels are deposited directly on weathered and tilted (10°SE) strath surface cut into steeply dipping (70°SE) schist. Note the stepped rangefront profile in *A*. Landslide deposits seen in *Fig.5.3.31* form the upper fan surface.

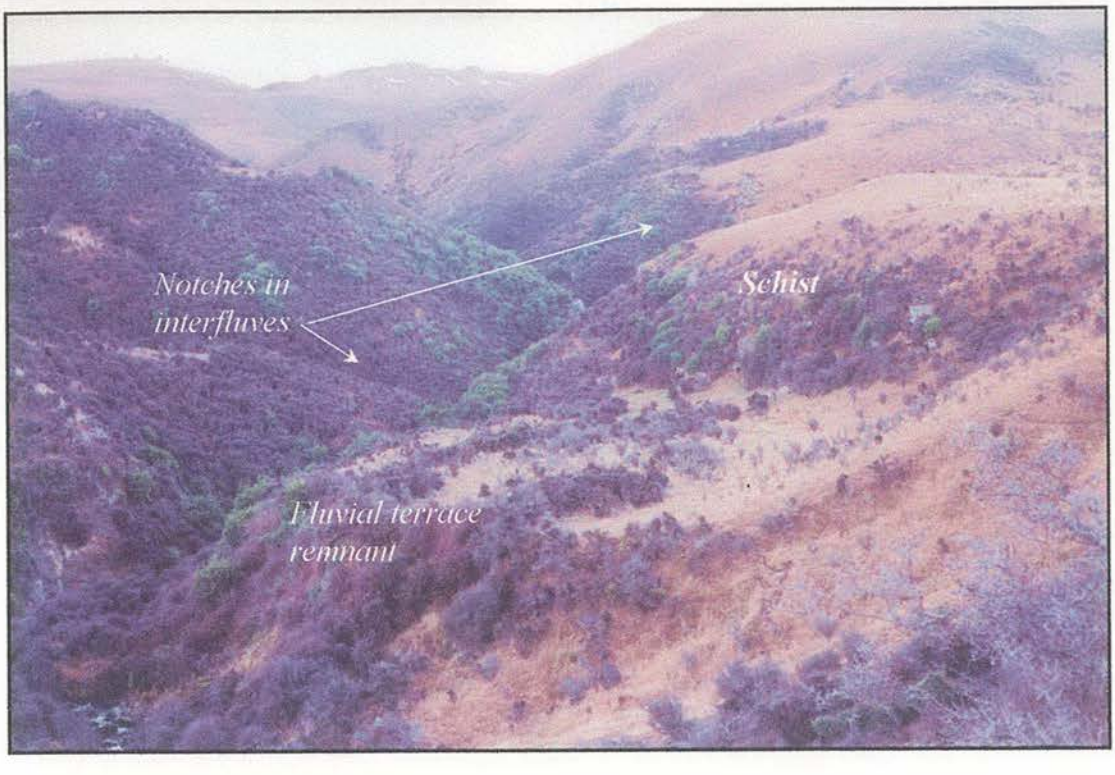

Fig. 5.3.33 **Heeney Creek Gorge** (from 90406/33141 → 310°)

Strath surfaces cut into both fluvial terrace and schist basement have similar across-valley profiles at progressively higher elevations deeper into the gorge. Kinks in the stream course align with notches in the interfluves, which form range-parallel lineaments (see *Fig.5.3.23*).

5.3.3 Rock and Pillar Range – GPS profiles

Fig.5.3.34A **Differential GPS profile locations**

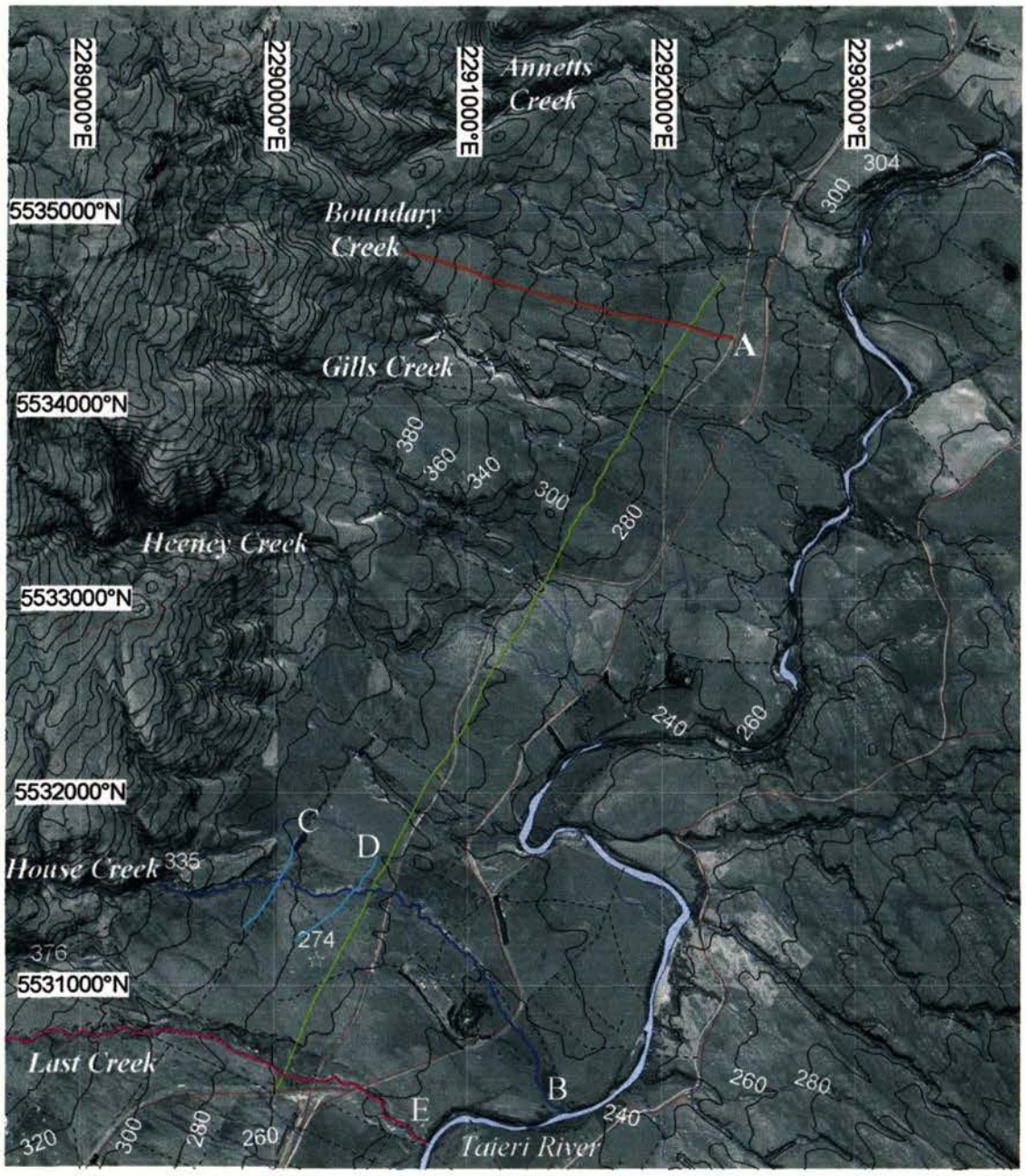

Fig.5.3.34B **Longitudinal rangefront terrace profile**

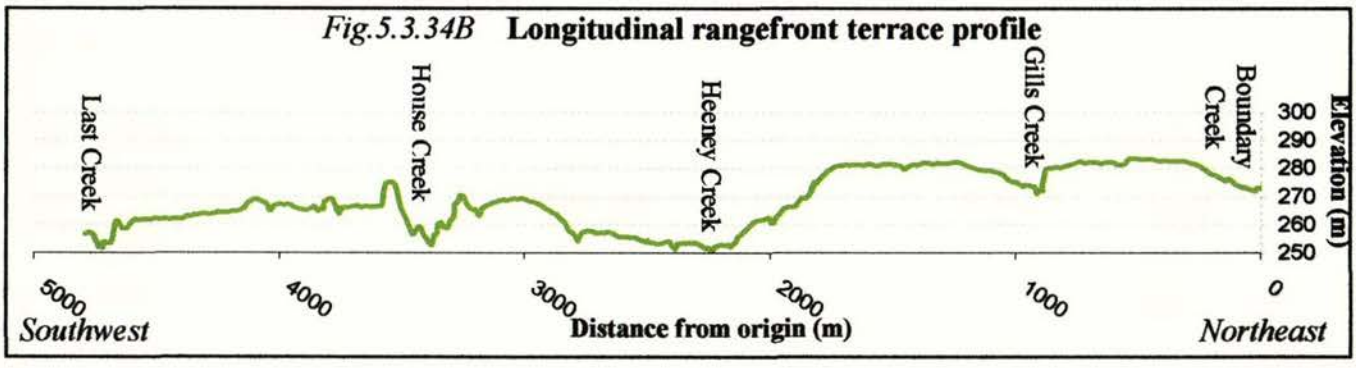

5.3.3 Rock and Pillar Range – GPS profiles

Fig. 5.3.34C **Range-orthogonal differential GPS profiles**

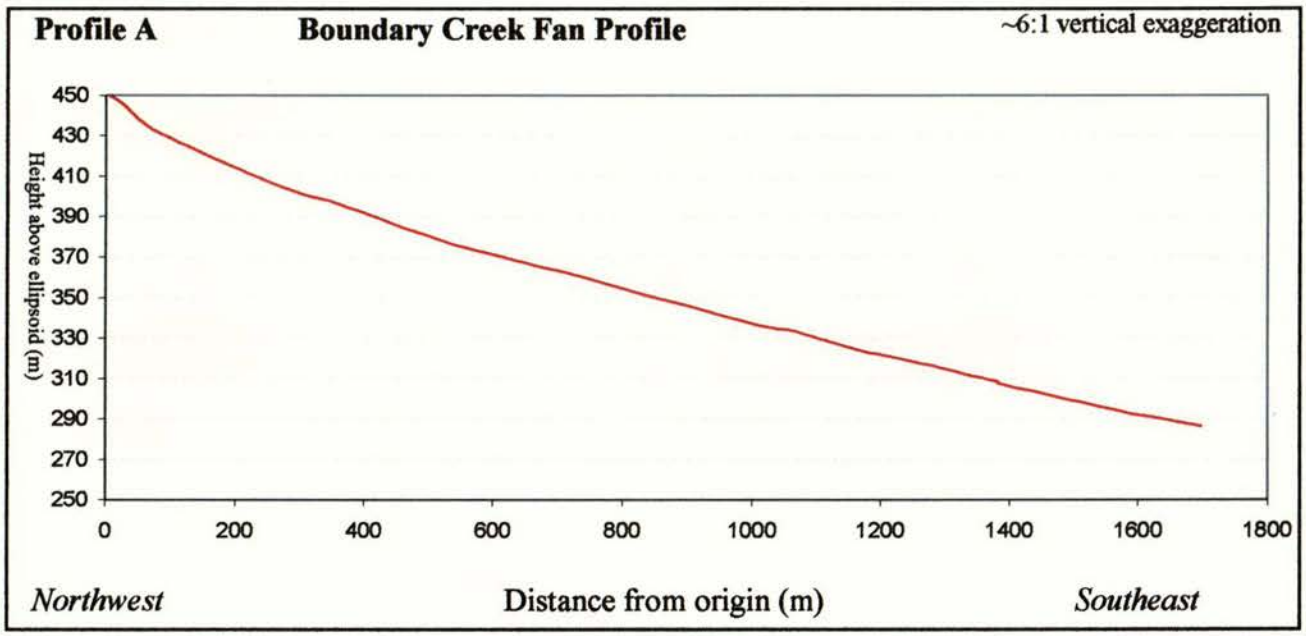

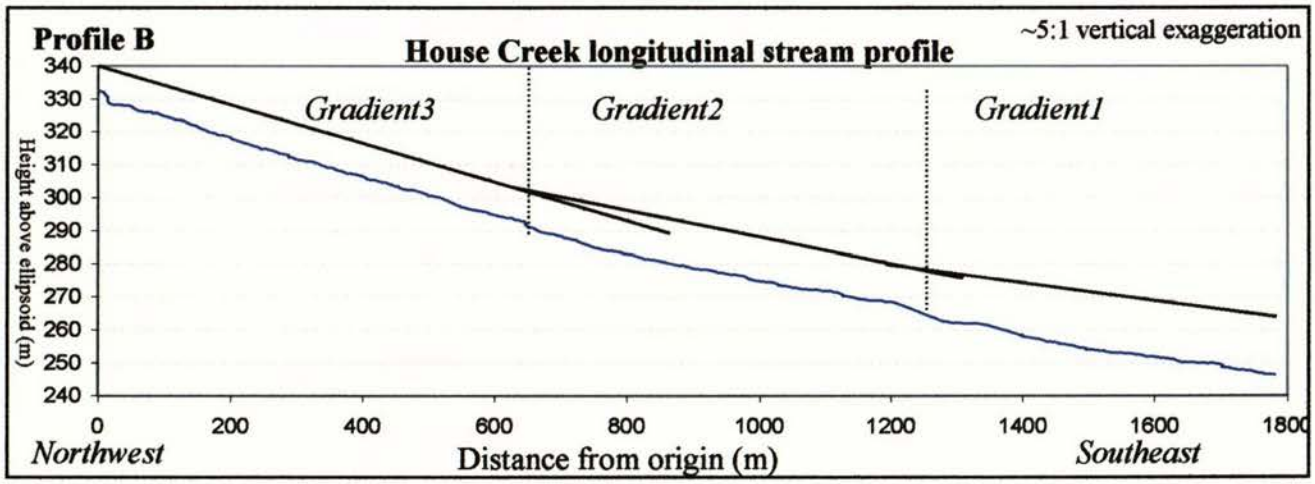

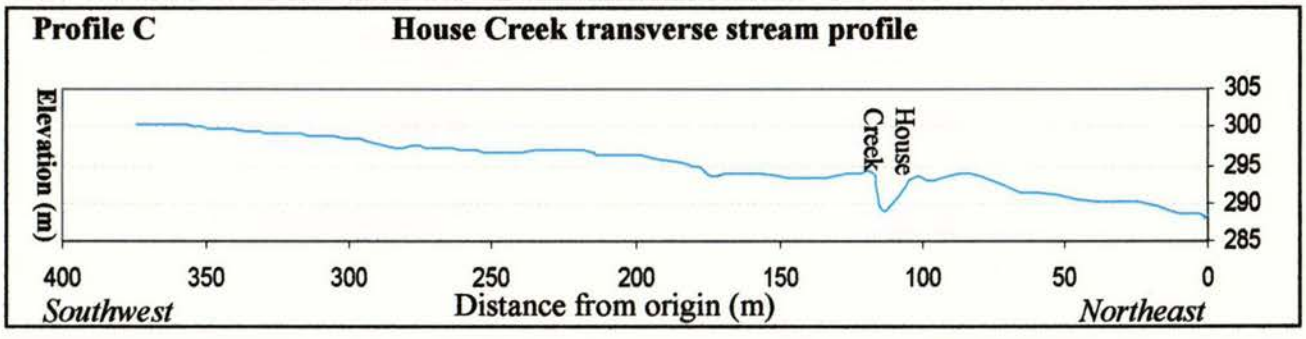

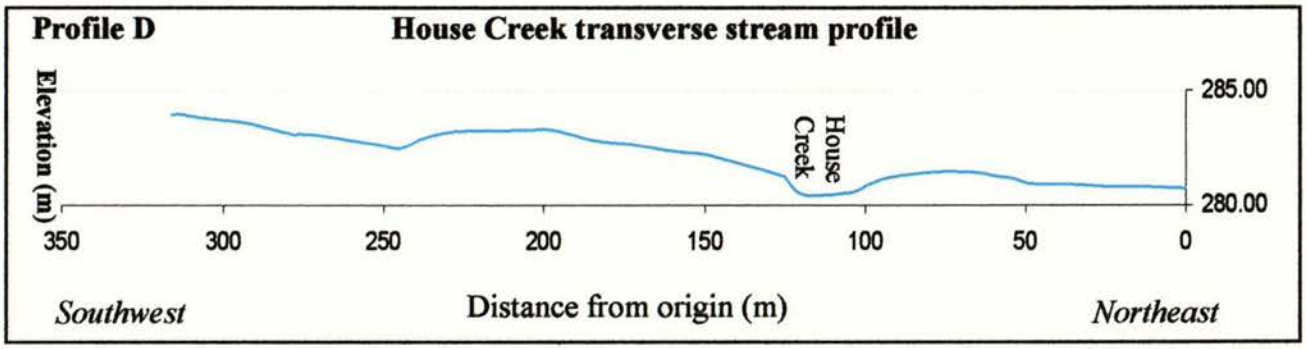

5.3.3 Rock and Pillar Range – GPS profiles

Fig. 5.3.34D **Range-orthogonal differential GPS profiles**

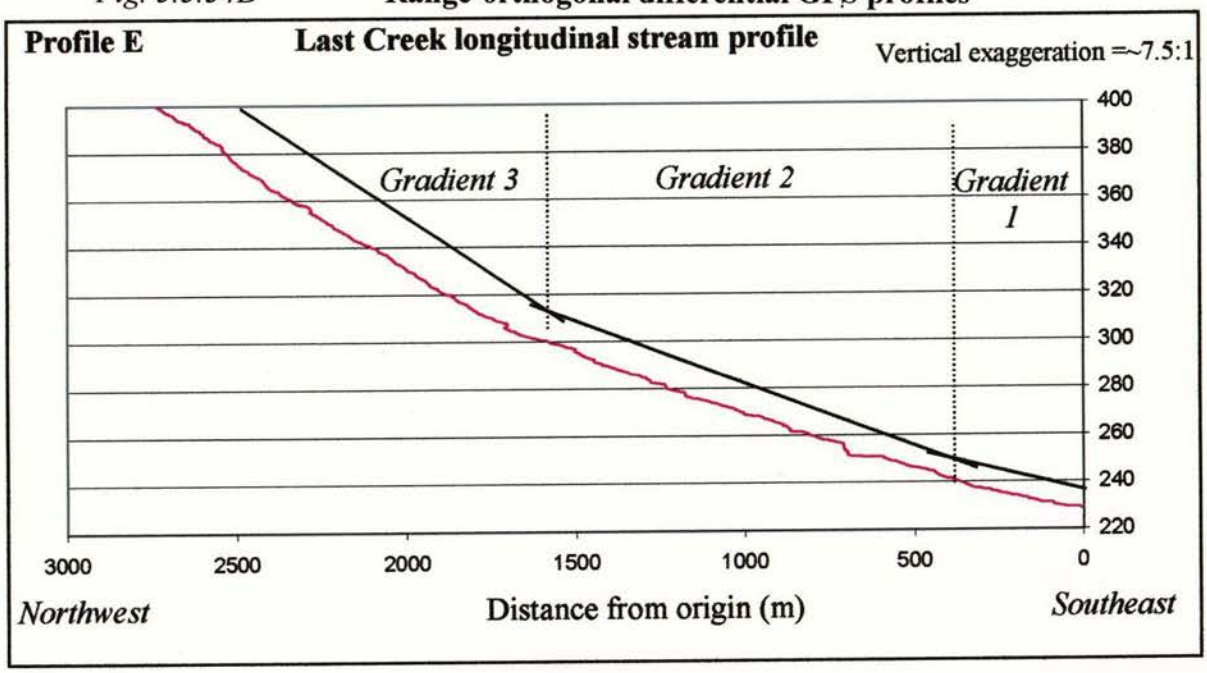

5.4 Rock and Pillar Range DISCUSSION

No single range-scale fault structure was observed at the surface in these field areas, although a through-going active fault is traditionally shown along the southeast rangefront on geological maps (e.g. Forsyth, 2001). Displaced surfaces and bedding and stream course disruption are widespread up to 4km out from the rangefront, and at least some of the structure(s) at depth responsible for this deformation have been active in the Holocene. Sedimentary cover in the basin is generally thin (<<30m, commonly <5; see *Fig. 5.3.22*) and the deformation zone wide (1 - 4km). Possible explanations for these observations include a 'master fault' splaying out at depth, or a bending-moment origin due to flexural slip due to contraction within the schist of the underlying syncline (e.g. Yeats, 1986). However, no evidence for Holocene movement was found on basement shear zones observed within the schist basement of the gorges incised into the rangefront (e.g. *Fig. 5.3.8*). This may represent a migration of fault activity away from the rangefront over time, or be a product of the short residence time of sedimentary evidence within the gorges. Prominent notches and slope breaks in the interfluves aligning with stream course deviations sub-parallel to the rangefront (e.g. Heeney Creek *Figs. 5.3.33, 5.3.34A*) disclose the location of basement faulting, but with no age control.

The longitudinal rangefront terrace profile (*Fig. 5.3.34B*) shows asymmetric incision (steep side to north, also see *Figs. 5.3.15, 5.3.20, 5.3.25*) and gentle north-east tilting of the well-developed large (~5km radial) alluvial fans and fluvial terraces along the southeast rangefront. Steep escarpments on the northeast stream banks occur on all terrace levels and at the current sites of stream incision (see *Figs. 5.3.20, 5.3.25*). The rates of incision are comparable between Six Mile Creek field area (0.23 ± 0.03mm/yr averaged over 7.47 ± 0.87ka) and House Creek (0.20 ± 0.02mm/yr averaged over 8.42 ± 0.83ka). These values are higher than may be expected, but the streams are actively incising in response to relatively recent deformation. Incision would be most vigorous in the earlier stages of stream long-profile adjustment. The stream long-profiles (*Fig. 5.3.34C* profiles B and E) both have a distinct three-fold average gradient division. The location of the gradient inflection points coincides with anomalous stream course deviations, and terrace bedding and surface disruption (*Fig.5.3.17, 5.3.19, 5.3. 22*). The inference is that of the existence of fault structures at depth at or near these localities (sees *Fig. 5.3.14*). This is strengthened by alignment of the head of the 'anomalous stream appearance' (*Figs. 5.3.13, 5.3.21*). There are no obvious streams entering this incision, and water flow appears to be sourced by emergent springs at the head of the valley.

Episodic uplift (or episodic quiescence) is apparent from tilted strath terrace remnants within gorges. In addition, the interfluves are commonly stepped, with increasing basinward slope, up to the range crest (*Figs. 5.3.7, 5.3.16, 5.3.32, 5.3.33*). The stepped interfluves may be degraded strath terrace remnants whose tilt increases with age and elevation. Some of the treads display a channel shape (*Figs. 5.3.16, 5.3.32A*) which may have been cut by a paleo-Taieri River during punctuated uplift of the range.

This range is younger than Pliocene (displaced schist-free Maniototo Conglomerate) but older than Taieri Ridge, based on geomorphologic grounds (well-rounded interfluves, rangefront incisions cutting range crest, greater relief, extensive fan development, radial drainage pattern on northern extremity). Like Taieri Ridge, the Rock and Pillar Range is distinctly sigmoidal in map view and may also be an amalgamation of *en-echelon* segments.

Given the demonstrated Holocene activity along the rangefront, the Hyde Fault should be factored into hazard assessments. The Range is c. 50km long and, assuming a 15km seismogenic zone, would be capable of generating an earthquake of 6.5 – 7.5 magnitude. (Wells & Coppersmith, 1994).

Rough Ridge Group

5.4 Rough Ridge Group Overview

The Rough Ridge Group is a composite system of four interacting antiformal schist ranges lying between the western margin of the Maniototo Plain and the Ida Valley (see *Fig.2.2*).

Fig 5.4.1 **Structural evolution from drainage patterns**

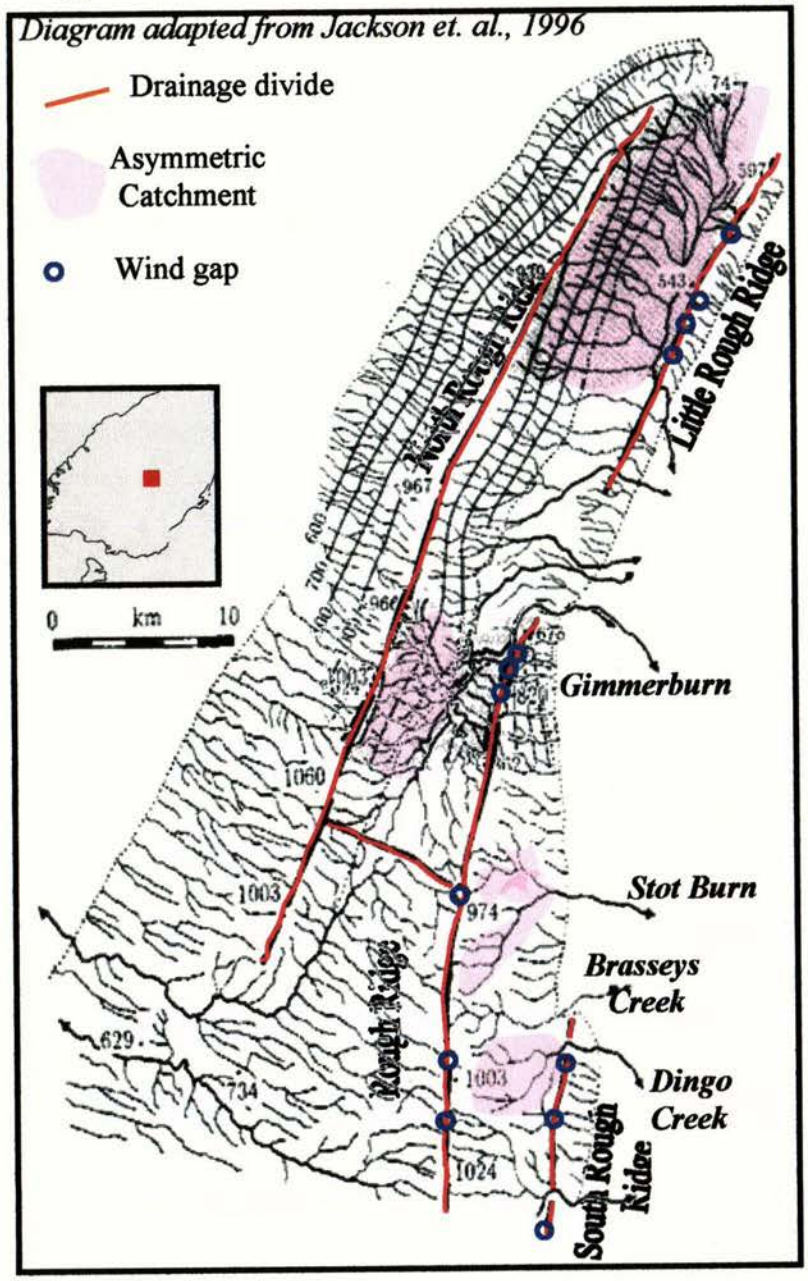

Jackson *et al.,* (1996) used drainage patterns to demonstrate processes involved in fold (and fault) growth and interaction. They determined relative uplift ages of adjacent structures, and their direction of propagation from stream capture patterns, asymmetric catchments, and the elevation of 'wind-gaps'. Wind gaps are former stream channels whose erosive power failed to keep pace with uplift, leaving an elevated incision into the range crest (*Figs 5.4.3, 5.4.8-5.4.11*). They showed how long-term averaged ridge uplift and propagation rates were able to be estimated from the relative elevation and distance between wind gaps. More recently, preliminary data from a joint programme with Cambridge University and CNRS Orsay, France, using cosmogenic ^{10}Be isotope dating of peneplain exhumation, has refined these estimates for South Rough Ridge (Jackson *et al.,* 2002). Their data suggests two clusters of tectonic activity at 150-100ka and 600-400ka separated by a period of relative inactivity. The findings from the three Rough Ridge rangefront areas in this study (see *Fig.5.4.2*) are complementary to the Jackson *et al.,* 2002 study in that they assess deformation at outcrop scale with a main focus on the sedimentary apron younger than ~150ka.

5.4 Rough Ridge Group Overview

Sedimentation

A generalised stratigraphy for the Maniototo is shown at right. The Tertiary units are sporadically preserved both beneath terrace and fan gravels and as isolated remnants. Within the Maniototo, an extensive river terrace system has formed as a result of regional uplift. Where present, Tertiary sediments are commonly in angular unconformty with overlying terrace gravels. All sediments have been locally uplifted and deformed by the emerging rangefronts of the Rough Ridge Group (Jackson *et al.*, 1996). Based mainly on elevation, correaltion of some of the larger terrace surfaces is possible between the three rangefront field areas.

Fig.5.4.2
Generalised schematic Stratigraphy
(modified from Youngson *et al.*, 1998)

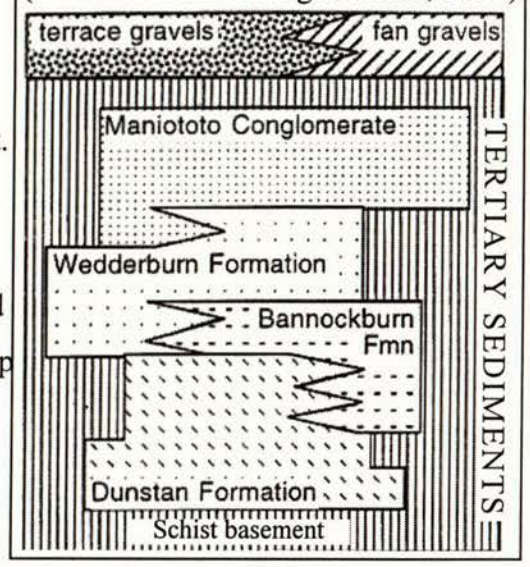

Terraces are mostly composed of schist gravels and recycled tertiary units with a minor greywacke component which increases toward its northeast source. Incision by streams emerging from the rangefront into the uplifted terraces is within asymmetric valleys, steep side to the north. Terrace escarpments on the northern margin of their valleys often have been undercut causing slope failure because streams have a north-lateral component to their incision (see *Fig. 5.4.7*). This is also reflected by northward stream deviation at the rangefront where streams enter the less resistant sedimentary apron (see *Figs. 5.4.3., 5.4.6., & 5.4.7*).

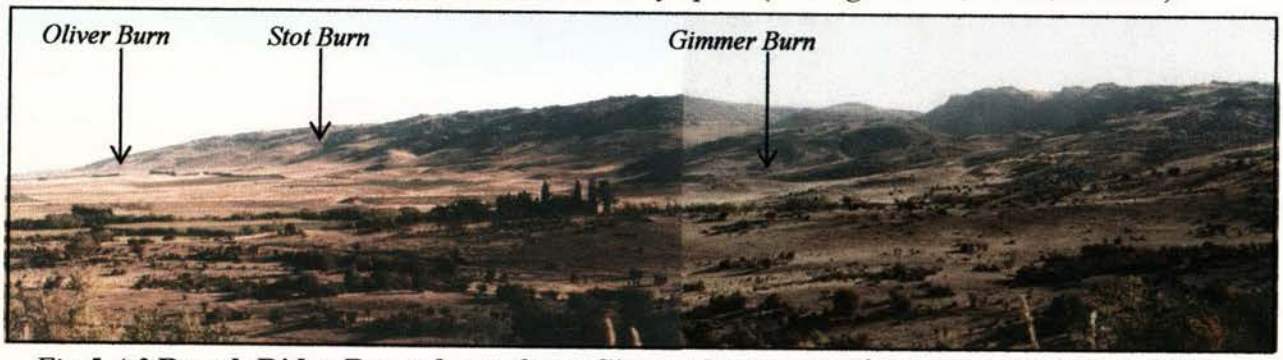

Fig.5.4.3 **Rough Ridge Rangefront, from Gimmerburn area** (from 67810/60000 → 235°)
Rough Ridge occupies an en-echelon left step in the Rough Ridge Group.

Streams emerging from the actively rising rangefront incise tilted, folded and occasionally faulted rangefront sediments. Surface tilting and depth of stream incision both increase toward the rangefront where emergent streams are 40+m below the highest surfaces of the sedimentary apron, and currently incising (see *Fig. 5.4.6*). Deformation is observable within all lithologies across the three Rough Ridge field areas.

5.4 Rough Ridge Group Overview

Fig.5.4.4 **Topography and location of the Rough Ridge Group field areas**

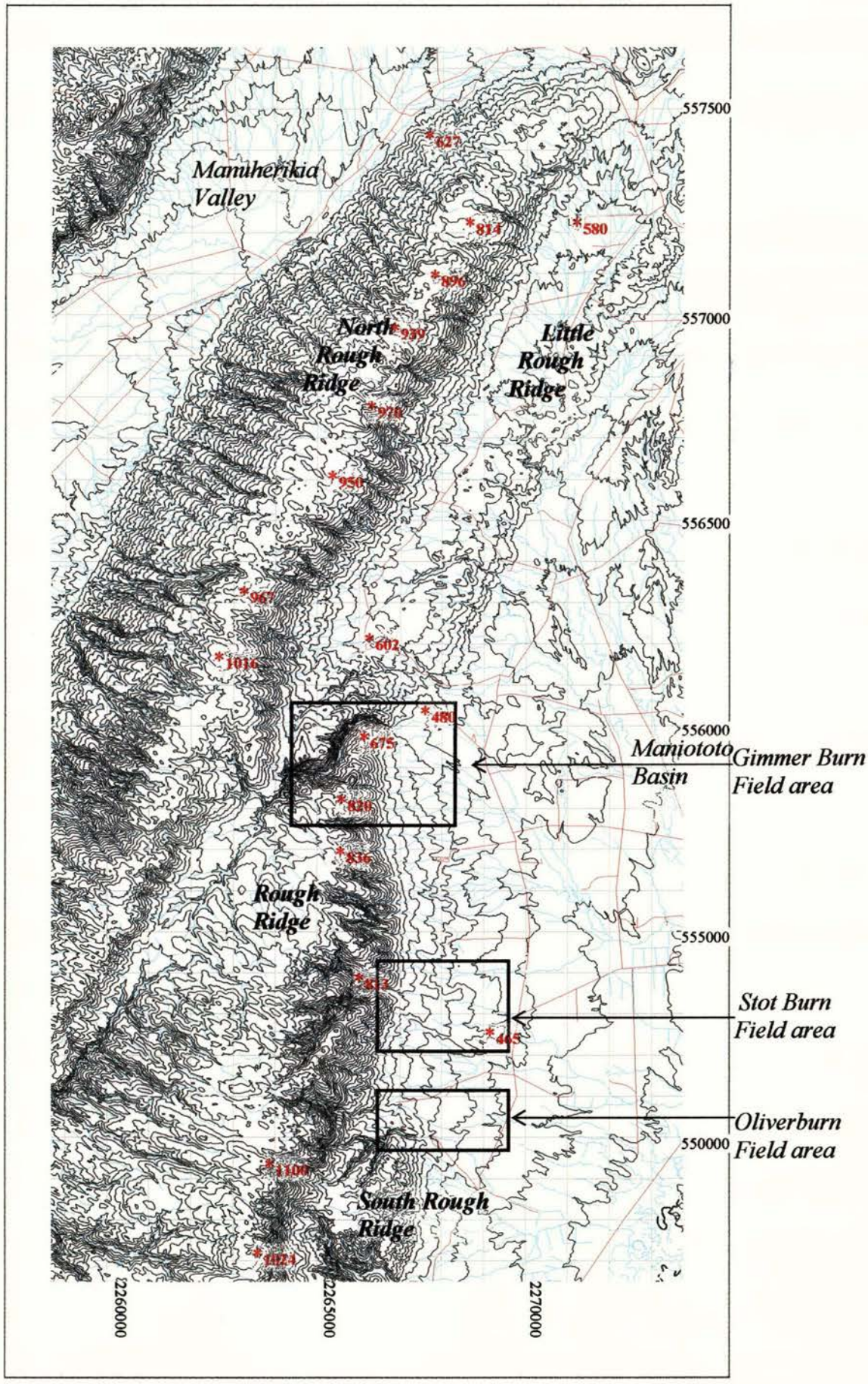

5.4.1 Rough Ridge Gimmer Burn field area

Fig. 5.4.5 **Orthomap and photo locations** (Asterisk is location, arrow is camera azimuth)
O Wind gap (see text for discussion)

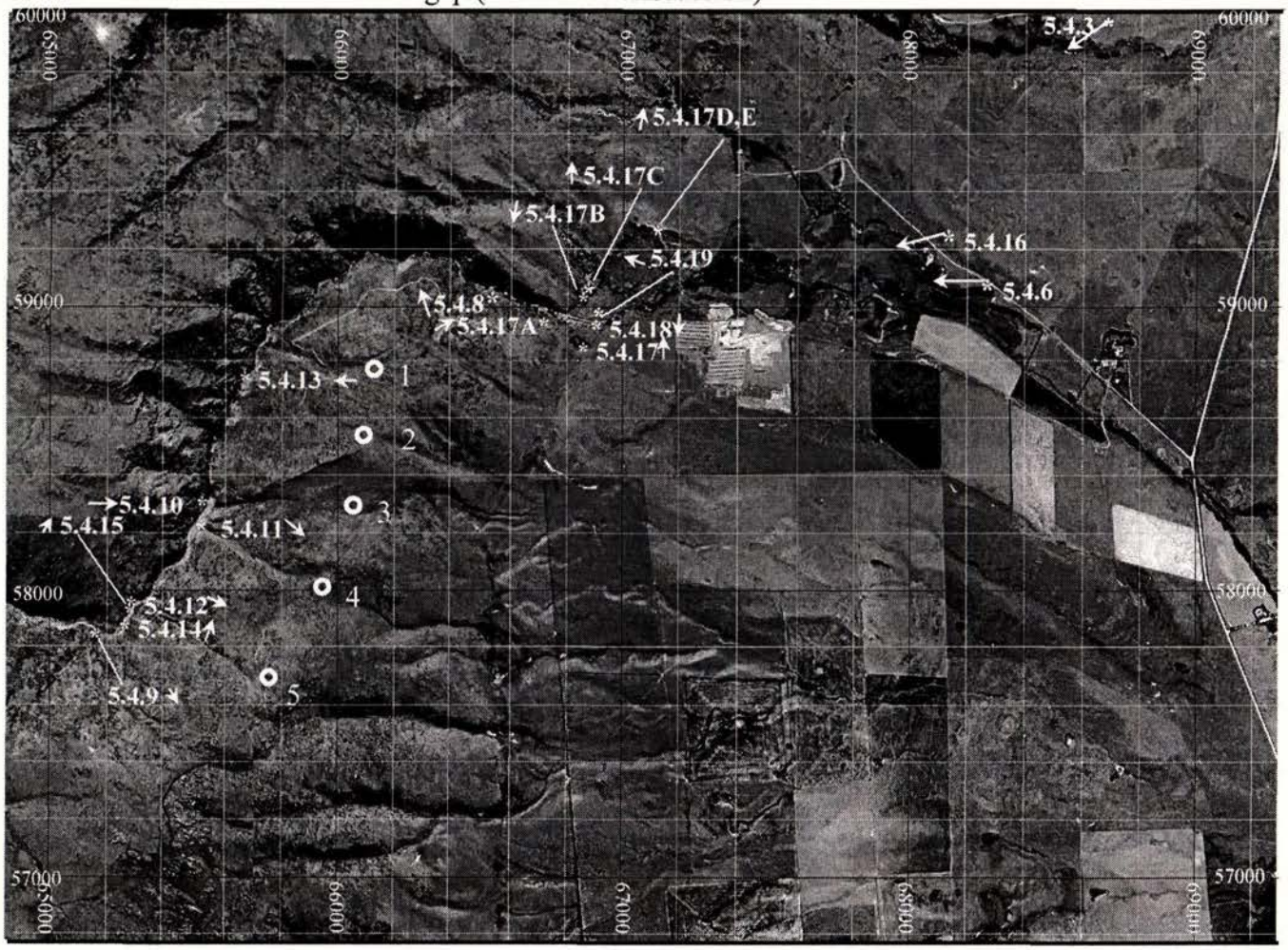

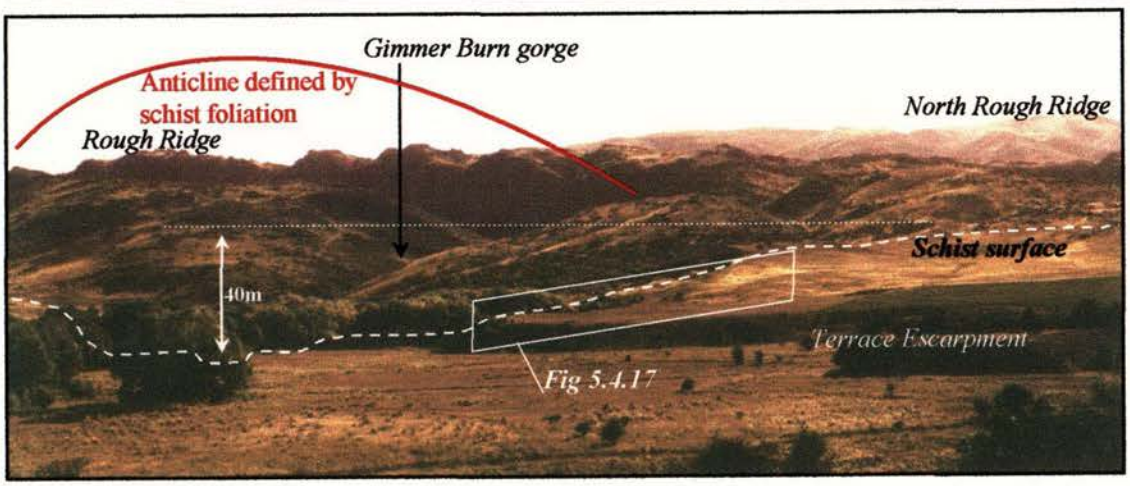

Fig. 5.4.6 **Rough Ridge rangefront showing northward (right) deviating Gimmer Burn incision into uplifted and tilted terrace** (from 68152/59251 → 270°)

The approximate line of where the unconformity is overlain by younger sediments is marked above. Note the increase in slope of the terrace surface toward the rangefront and the abrupt right-side escarpment.

Gimmer Burn field area

Fig. 5.4.5 **Structural orthomap**

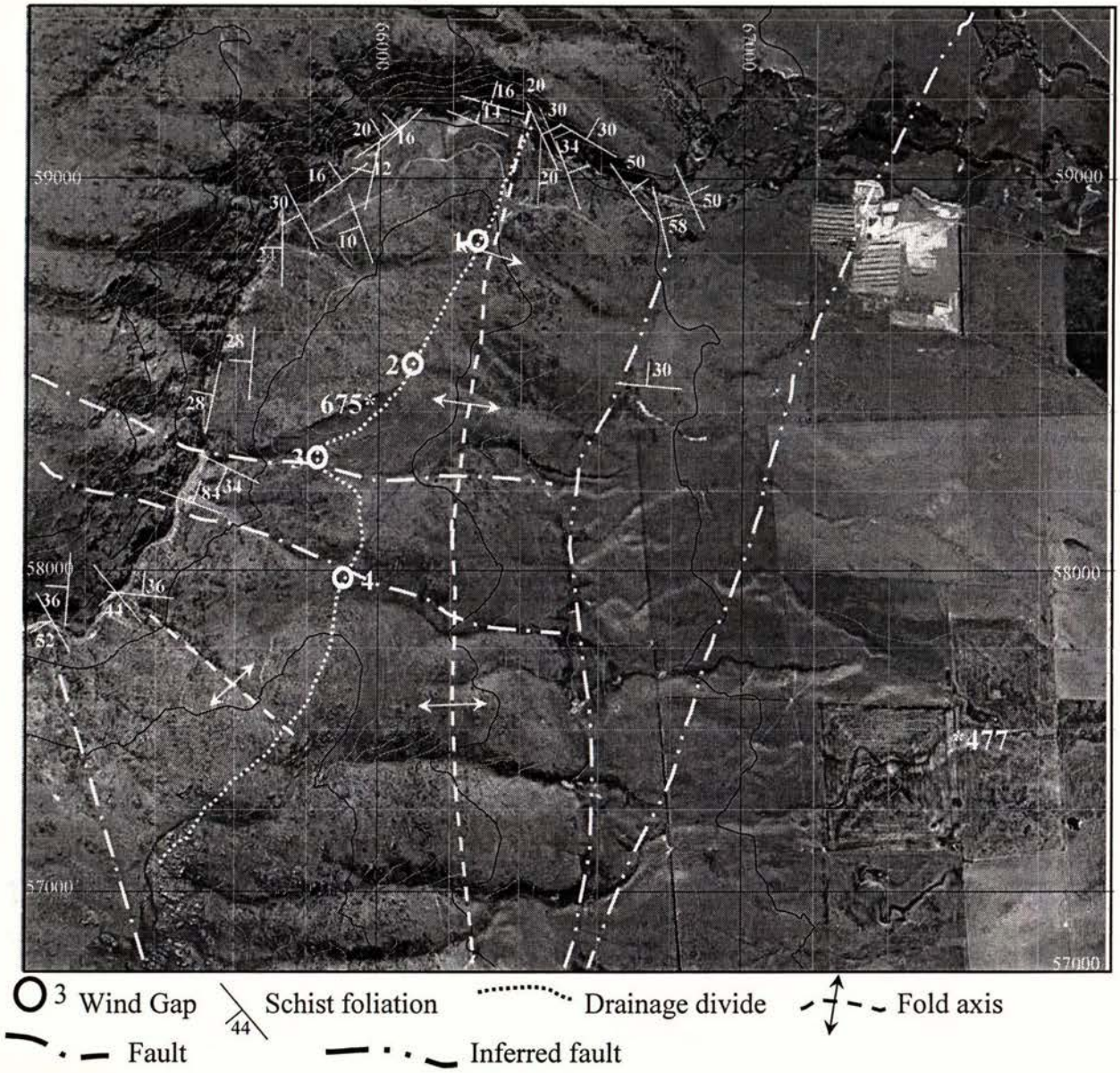

Gimmer Burn is actively incising its schist gorge and is currently up to ~200m below the peneplain surface, permitting observation of structures within the basement. Rough Ridge is a gently NNE-plunging asymmetric anticline, steeper side to east, as described by the foliation of the schist (*Fig. 5.4.6*). The course of Gimmer Burn gorge more or less runs along strike of the schist foliation, so the arcuate northeast gorge extremity approximately maps out the form of the anticline. The azimuth of the entrance to the gorge parallels both the regional NW-SE drainage pattern and that of the drainage entering the gorge from the dissected Rough Ridge. Locally this is approximately orthogonal to the ~NNE-striking drainage divide. On the south-eastern flank of Rough Ridge, bordering the Maniototo Plain, drainage consistently deflects northward a short distance east of the drainage divide.

5.4.1 Rough Ridge
Gimmer Burn gorge – basement faulting

Within the gorge, incision has exposed the axial region of the anticline to a depth of ~80m. A complex multi-generational network of small-offset brittle structures pervades the schist within the axial region. No evidence of a dominant large-offset structure was found in a transect orthogonal to the anticline axis. Anticlinal 'folding' appears to be accomplished by numerous small offsets on ubiquitous joint sets and slip on foliation planes.

Fig. 5.4.8 **Oblique view of the northern gorge wall showing fracture network in the axial region of the Rough Ridge anticline.** (from 66532/59010 → 340°)

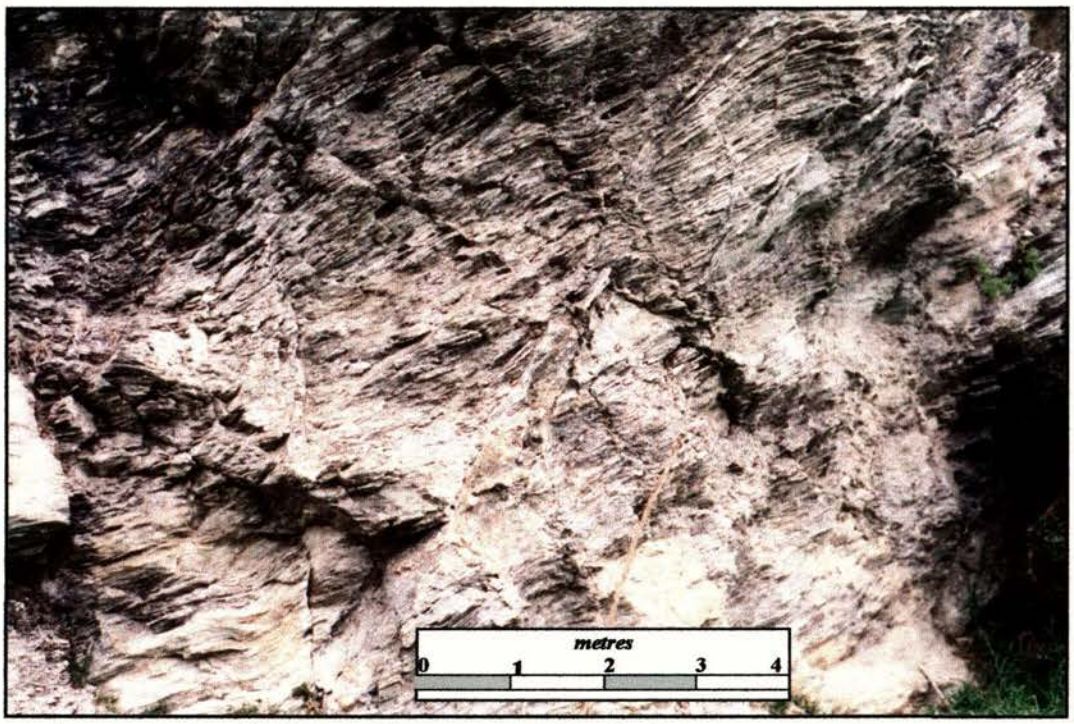

Range-scale structures with larger offsets are present further upstream where the gorge has a ~NNE strike. These align with notches in the range crest and where remarkably straight valleys enter the Gimmer Burn gorge, where schist foliation is often discordant across the valley.

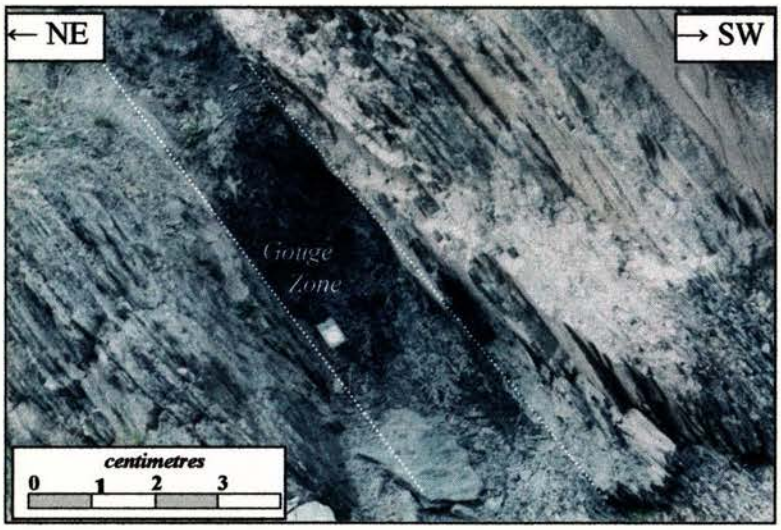

Fig. 5.4.9 **Foliation-parallel shear zone** (from 65025/57877 → 150°). This 350mm wide foliation-parallel gouge zone is oriented 150/52°SW and situated where a valley striking150° intersects the 90° inflection point in Gimmer Burn at the western extremity of this field area.

5.4.1 Rough Ridge
Gimmer Burn Gorge – Wind gaps

A number of wind gaps occur in the Rough Ridge range-crest segment between Gimmer Burn gorge and the rangefront, which are numbered on *Figs.5.4.5. & 5.4.7.* These are inferred to be remnants of the North Rough Ridge consequent drainage pattern of streams subsequently captured by Gimmer Burn (Jackson *et al.,* 1996). Of note is the remarkable linearity of the associated valleys between the wind gap and the now deeply-incised Gimmer Burn gorge. The fact that these stream segments have maintained their antecedent and anomalously straight courses within the flanks of the deep Gimmer Burn incision after such obvious local disturbance in the structural contours of the schist points to a structural control on their location. Some evidence of this is visible from within the gorge, but obscured by sediments on the rangefront.

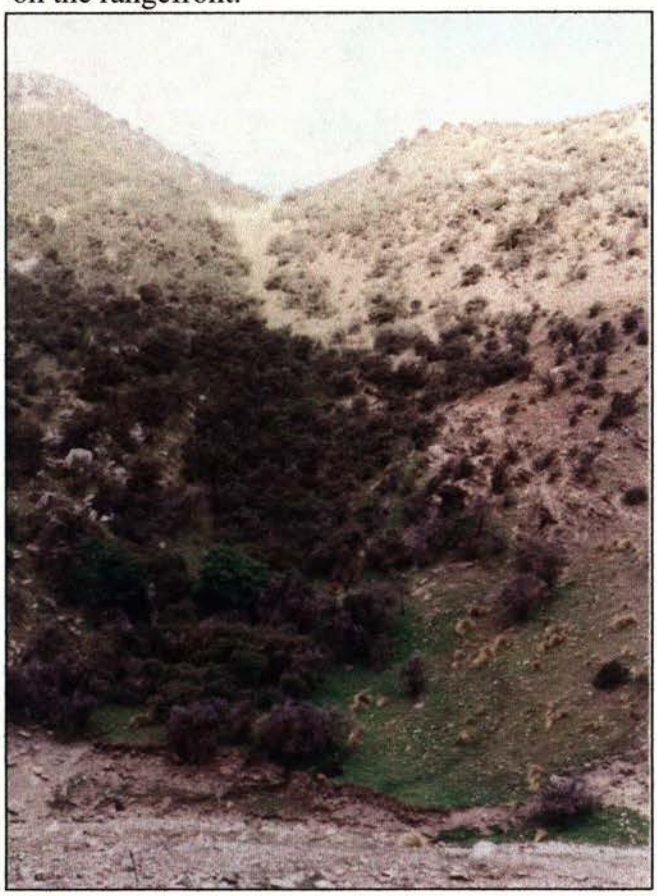

Fig. 5.4.10 (from 65682/58310 →90°)
Wind gap 3 – paleo-Gimmer Burn

The asymmetry of the incision, steeper side to the north-east (left), is common to all wind-gaps in this area, although most pronounced in this one. This wind gap is larger than others in this section with 240m of incision into the range crest. The elevation of the wind gap is 632 ± 0.3m, which is 95m above the Gimmer Burn channel, 320m to the west. The normal trend of wind gaps is to decrease in elevation in the direction of range propagation, however wind gap 3 is ~20m *lower* than wind gap 2, which is ~200m to the northeast (see *Fig.5.4.7*). Wind gap 1, a further ~300m northeast, is at roughly the same elevation as wind gap 3. There is an abrupt inflection point in Gimmer Burn aligning with its confluence with this valley, which strikes at 090°. This strike is anomalous in that it is oblique to both the drainage divide and neighbouring stream courses. Gimmer Burn runs sub-surface between ~50m downstream and ~150m upstream of this confluence, beneath gravel beds which appear to bow up compared to the overall stream gradient.

5.4.1 Rough Ridge
Gimmer Burn Gorge – Wind gaps

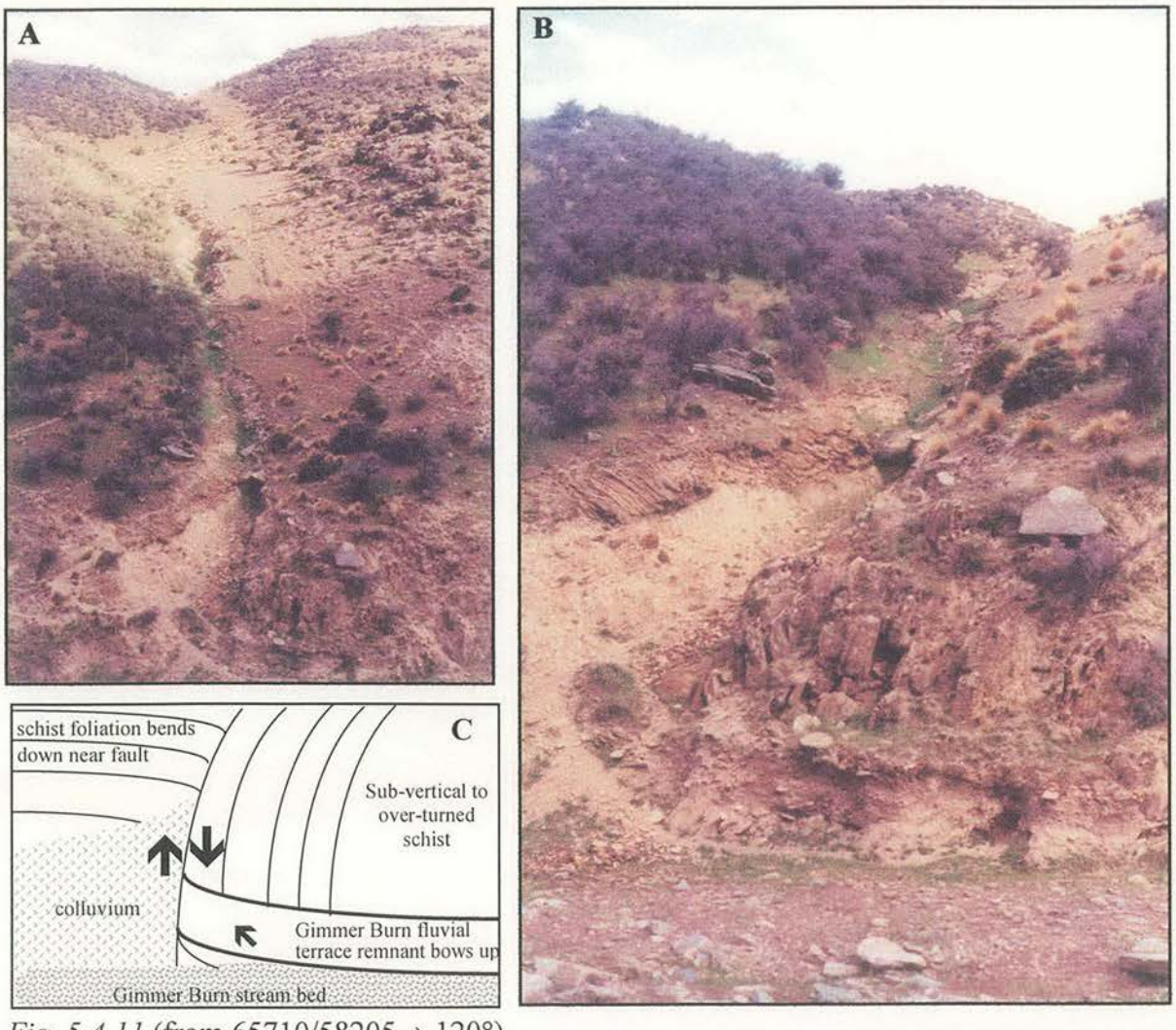

Fig. 5.4.11 (from 65710/58205→ 120°)

Wind gap 4 from Gimmer burn gorge showing the structural influence on its location.

Photo A (↑) shows the linearity of the incision, which strikes 130° , which is orthogonal to the ~40° strike of the drainage divide of both this segment of Rough Ridge and North Rough Ridge. The asymmetry of the incision by the ephemeral stream (centre-shot) appears influenced by the orientation of the schist foliation. The ~35° slope of the north (left) 'bank' reflects the foliation dip of the underlying schist, and a stream preference to erode along foliation planes. The opposing dip (~80° NE) of the schist to the right acts as an obstruction to this preferred incision, and consequently the stream course parallels the foliation of the schist to the right. This stream thus delineates a structural discontinuity defined by schist foliation. Photo B emphasises the discordance of the schist foliation across the gap and the upward tilting of fluvial bed remnants approaching it from the south (right). Movement on this structure is north (left) side up and clearly post-dates deposition of the terrace remnant.

5.4.1 Rough Ridge
Gimmer Burn Gorge – Wind gaps

Fig. 5.4.12A

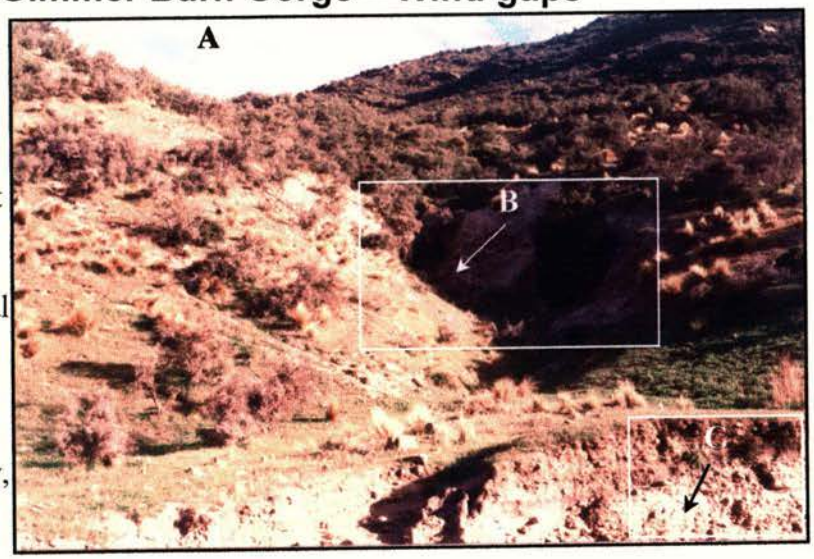

Wind gap 5

(from 65340/57958 → 130°)

This incision is parallel to that of wind gap 4, is also very linear, and also has a structural control on its location. The schist foliation has divergent dip on either side of the valley, thus describing an antiform whose 130° striking axis is occupied by the ephemeral stream.

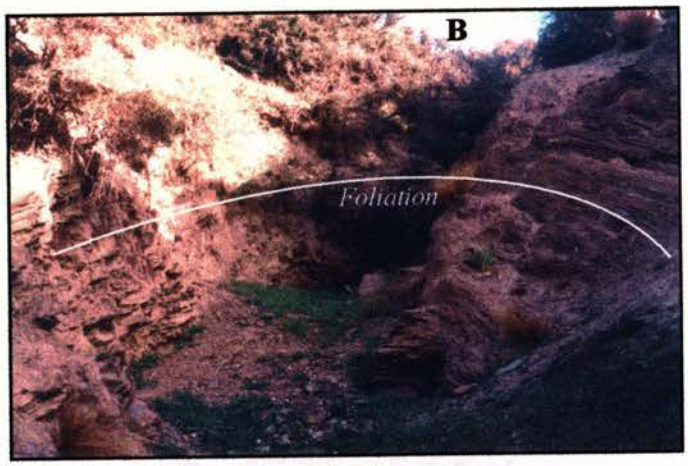

*Fig. 5.4.12.*B

The strike and dip of the incision walls appear coincident with a pervasive joint set, which is sub-vertical, and strikes ~130°. The stream has incised the axial trace of a fold in the schist by exploiting an inherent structural weakness.

*Fig. 5.4.12.*C

Bedding planes and unconformities within this Gimmer Burn fluvial terrace remnant diverge to the south (right), indicating ongoing uplift to the north (left). This is consistent with geomorphologic interpretation of north-east range propagation (Jackson *et al.,* 1996; 2002). There is a repetitive cycle of fluctuating hydraulic conditions responsible for this channel-infill sequence. The clasts within the coarser horizons are hydraulically incompatible, consistent with deposition during catastrophic events. Intervening layers are well-sorted fine-grained quartz-rich sands, near the base, and loess in the upper regions.

5.4.1 Rough Ridge

Gimmer Burn Gorge - Sediment deformation

Numerous small terrace remnants are preserved within Gimmer Burn gorge, which are elevated above present stream level and often distorted. The most common style of terrace deformation observed is bedding planes tilted from original depositional gradients, and dip divergence between progressive bedding planes and unconformities. This is amply illustrated by *Figs 5.4.10 – 5.4.13.*

Fig.5.4.13
(from 65682/58726 → W)

Tilted sequence of fine sand/mud between fluvial gravels with opposite-dipping imbrication

This terrace remant is located in Gimmer Burn gorge on the north-west bank between the channel entrance to wind-gap 3 and the present-day gorge (see *Fig. 5.4.7*). Ongoing uplift and incision has tilted and elevated the whole sequence. The upper surface is tilted 12° to the north and elevated ~1500mm above the present stream level. From clast size and imbrication, the sequence encompasses a stream current direction reversal and a cycle of hydraulic conditions. The imbrication and composition of the basal (in the photo) fluvial gravels indicate deposition by stream of similar magnitude to the present-day Gimmer Burn, but with a southwards current direction. The gradational contact with the overlying sand and mud suggests a progressive waning of stream competance. This is a steep-sided narrow gorge, so the likelihood of overbank mud is diminished. The sharp contact between the sand/mud and upper fluvial gravels signals an increase in stream competence, and the change in clast imbrication signals a switch to current flowing *northwards*, as it does now.

A current reversal over tme within this stream segment would be consistent with a northwards shift in the location of where Gimmer Burn traverses Rough Ridge and exits the range, from the location of wind gap 3 (southwards current), to the present-day gorge (northwards current).

5.4.1 Rough Ridge – Gimmer Burn

Gimmer Burn Gorge - Sediment deformation

Fig. 5.4.14 (from 65321/57935 → 20°)

Normal faulting within fluvial sequence

Fault Plane 50/70°SE, 200mm separation

Fault movement has offset overlying sediment gravity flow deposits, thus post-dating their deposition. The fault plane parallels the strike of the local schist, but has opposing dip, and may be a response to localised slumping into the incision. The cyclic sand/gravel alternations in the fluvial sequence reflect fluctuations in the hydraulic régime. There is an overall up-section increase in clast size signalling an increase in stream competence. The arrival of the uppermost sediment gravity flow gravel layers suggests an increase in local relief.

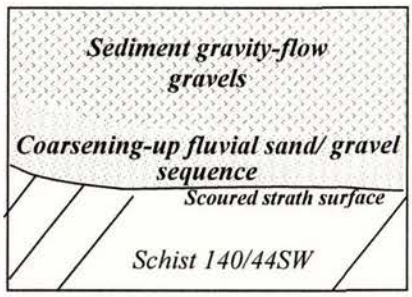

Fig.5.4.15
(from 65682/58726 →30°)

Strath surface cut onto schist in Gimmer Burn gorge

This strath terrace remnant within the gorge is overlain by a coarsening-up fluvial schistose gravel sequence which is in turn overlain by sediment gravity flow gravels of local provenance. To form a strath surface the stream must cut laterally, rather than incise, as it would in response to periods of uplift. The overall upward increase in clast size within the fluvial gravels again reflects an increase in stream competence over time, but after a period of relative tectonic stability, judged from the strath surface.

5.4.1 Rough Ridge – Gimmer Burn

Rangefront terrace incision

Broadly, there are terraces from two separate systems along the rangefront. Range-parallel rivers in their longitudinal valleys have formed the extensive upper-level terraces common to the three Rough Ridge field areas. These have been elevated and abandoned due to regional uplift. Valleys subsequently incising into these older terraces, by streams emergent from Rough Ridge, contain a second system of younger depositional channel-infill terraces. These are sites of aggradation, which migrate in response to sediment supply, local uplift, or lowering of stream base level. As a general rule, because of ongoing uplift, the relative elevation of the terrace surfaces reflects their relative age, i.e. higher means older.

Fig. 5.4.16 **Gimmer Burn rangefront - terrace levels, relative ages incision and wind gaps**

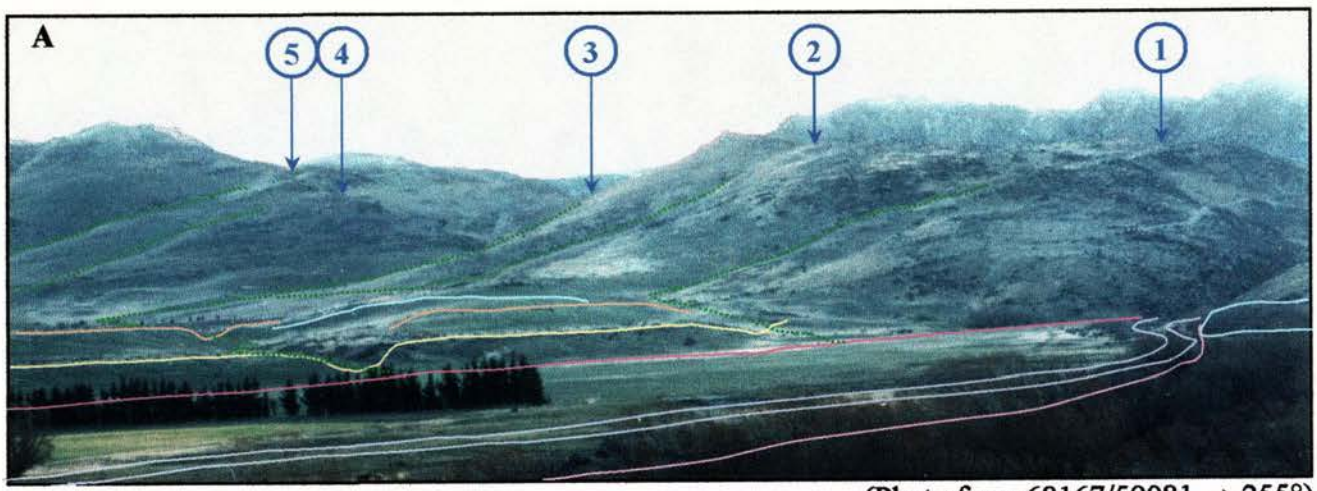

(Photo from 68167/59081 → 255°)

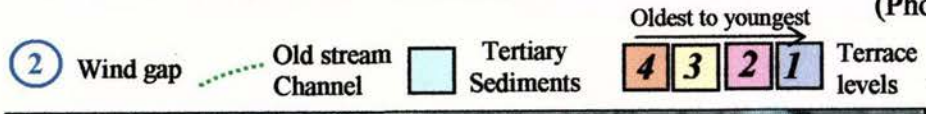

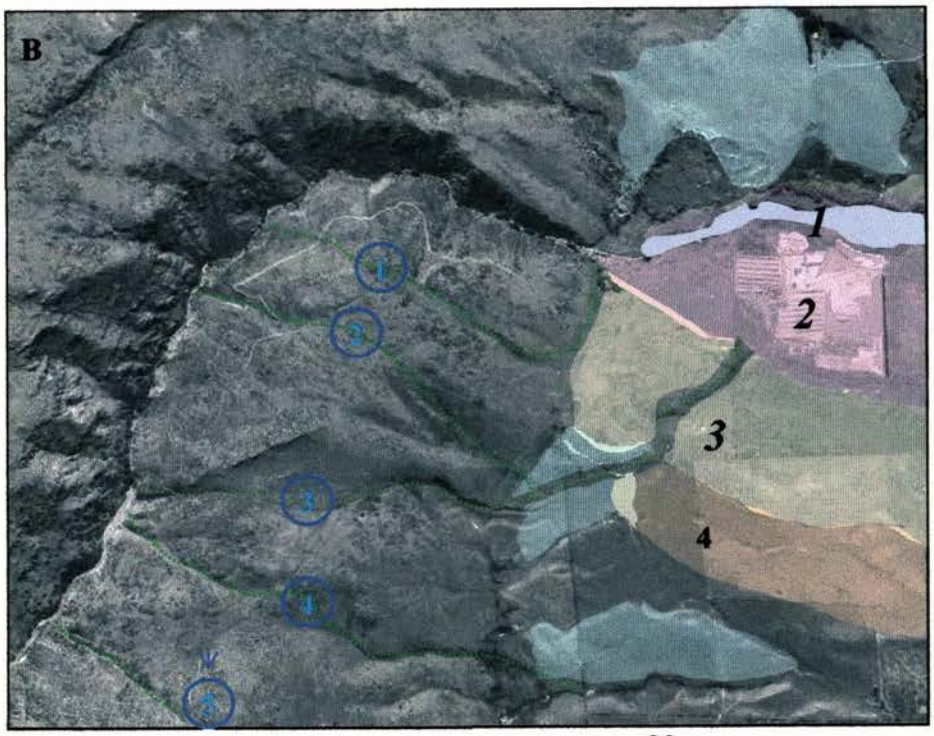

The dominance of wind gap 3 in terms of incision into both the range crest and rangefront terrace system is evident in these figures. The associated channel, to the east, has incised the Tertiary sediments and terrace levels 3 and 4, but not the younger terraces. Stream activity thus pre-dates terraces 1 and 2.

5.4.1 Rough Ridge – Gimmer Burn

Rangefront terrace deformation

In addition to regional and local tilting of the terrace surfaces, internal bedding contains widespread localised faulting, folding, and tilted unconformities. Angular unconformities indicate tectonic movement during the intervening hiatus, and tilted angular unconformities imply longer-term activity.

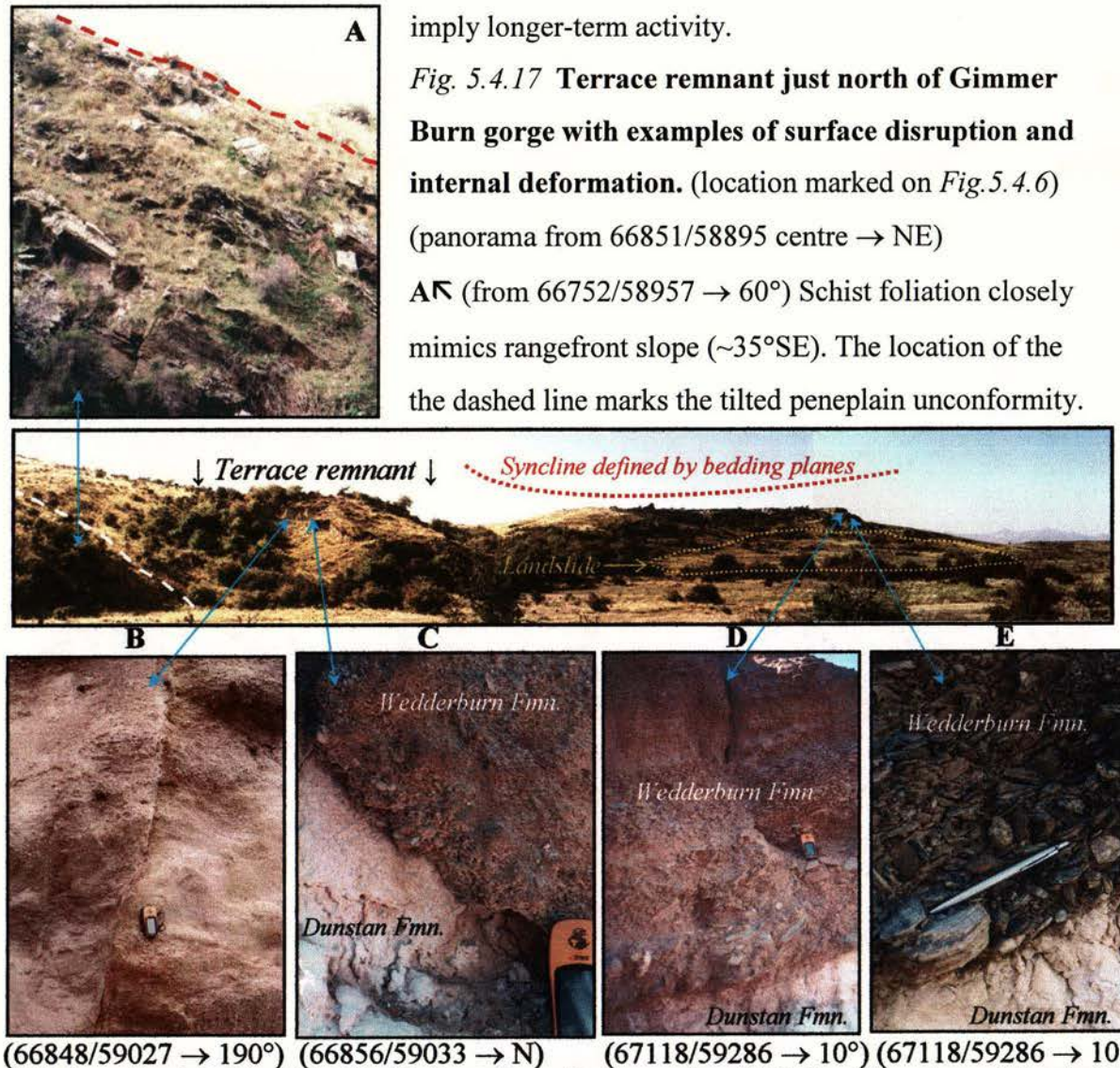

Fig. 5.4.17 **Terrace remnant just north of Gimmer Burn gorge with examples of surface disruption and internal deformation.** (location marked on *Fig.5.4.6*)

(panorama from 66851/58895 centre → NE)

A↖ (from 66752/58957 → 60°) Schist foliation closely mimics rangefront slope (~35°SE). The location of the the dashed line marks the tilted peneplain unconformity.

(66848/59027 → 190°) (66856/59033 → N) (67118/59286 → 10°) (67118/59286 → 10°)

B Sub-vertical fault within Wedderburn formation gravels, which doesn't cut overlying loess.

C Angular unconformity (bedding marked by dashed lines) between Dunstan and overlying Wedderburn Formation dips ~50°SE.

D Angular unconformity between Dunstan and Wedderburn Formations strikes ~30° and dips 20° NW, i.e. opposite to 'C', above. This terrace section is a truncated asymmetric syncline, steeper side to northwest. Note fining-up and bedding divergence within Wedderburn gravels.

E Close-up of Dunstan/Wedderburn contact. Imbrication of Wedderburn Formation suggests a current direction from the northwest.

5.4.1 Rough Ridge – Gimmer Burn
Lower terraces and OSL dating sites

Fig. 5.4.18 **(A) Oldest infill terrace showing surface and bedding distortion (B) and OSL dating site.**

(↑ from 66984/58928 →185°) (↑ from 66980/58918 → 160°)

(A) The embankment is the edge of terrace level 2 in *Fig.5.4.16* and the oldest and highest of the channel-infill terraces within the present-day Gimmer Burn incision into the older high fluvial terraces. Terrace levels 2 and 3 are marked for cross-referencing with previous figures. The strata are a basal imbricated coarse schistose winnowed lag-gravel overlain by a fining up fluvial gravel and loess sequence with an upper winnowed schistose fluvial pebbly lag-gravel. The upper surface of terrace 2 has a gentle range-parallel camber, and overall tilt to the northeast, and overall subtle slope increase approaching the rangefront. The incision containing the lowest infill terrace, which Gimmer Burn is currently incising, runs along the north-eastern margin of this surface, and is deepest (~1200mm) nearest the rangefront.

(B) Sample site WLL 320 Age 5.31 ± 0.52ka

The sample for OSL dating was taken from the site marked ⊗, 400mm below the top surface. A date from this surface places a peg in time between stream activity associated with wind gap 3, and that of the current Gimmer Burn. It is clearly older than the current Gimmer Burn course, and younger than the stream that formed wind gap 3. This provides broad constraints on range uplift and propagation rates when combined with relative elevation, stream gradient and horizontal distance measurements.

In addition, subtle surface tilting may be reasonable evidence of post-depositional tectonic movement, and dating it gives a maximum age for this activity.

5.4.1 Rough Ridge – Gimmer Burn
Lower terraces and OSL dating sites

Fig. 5.4.19 **Gimmer Burn gorge entrance, sample site, and lowest terrace surfaces**

(from 66950/58919 → 290°)

Sample site WLL319 Age 1.30 ± 0.24ka

This is a knick-point in Gimmer Burn stream, which is actively eroding headward into this lowest terrace surface, which is ~1100mm lower than the next terrace level. The sample for OSL dating was taken from 200mm below the top surface at the location marked ⊗ . The strata are fine-grained cm-scale laminated mud and clay beds overlying a coarse clast supported winnowed schist gravel. A date from this site constrains the short-term incision/uplift rate when used in conjunction with the previous sample, WLL320. This allows comparison with medium-term uplift rates, using a date discussed in the next section, and longer-term uplift rates established using wind gap elevations and overall range uplift. In this way it may be possible to isolate in time, periods of enhanced or reduced tectonic activity. These two dates also constrain the duration of the cycle between the two most recent episodes of terrace building, and by proxy, uplift. The location of the division between erosional and depositional environments migrates upstream as the river adjusts its long profile in response to uplift of its catchment (or lowering of base level). The knick-point in the lowest terrace (above in *Fig.5.4.19*) represents active stream long-profile adjustment in response to uplift which must have occurred within the last 1.3 ±0.24ka.

The distributed deformation in this area is likely to be a product of basement structure(s) probably related to those responsible for uplift of Little Rough Ridge and Rough Ridge to the north and south respectively (see *Fig. 5.4.1*).

5.4.2 Rough Ridge

Stot Burn and Oliverburn field areas

Fig.5.4.20 **Orthomap, sample sites, and photo locations**
(Asterisk is position, arrow is camera azimuth)

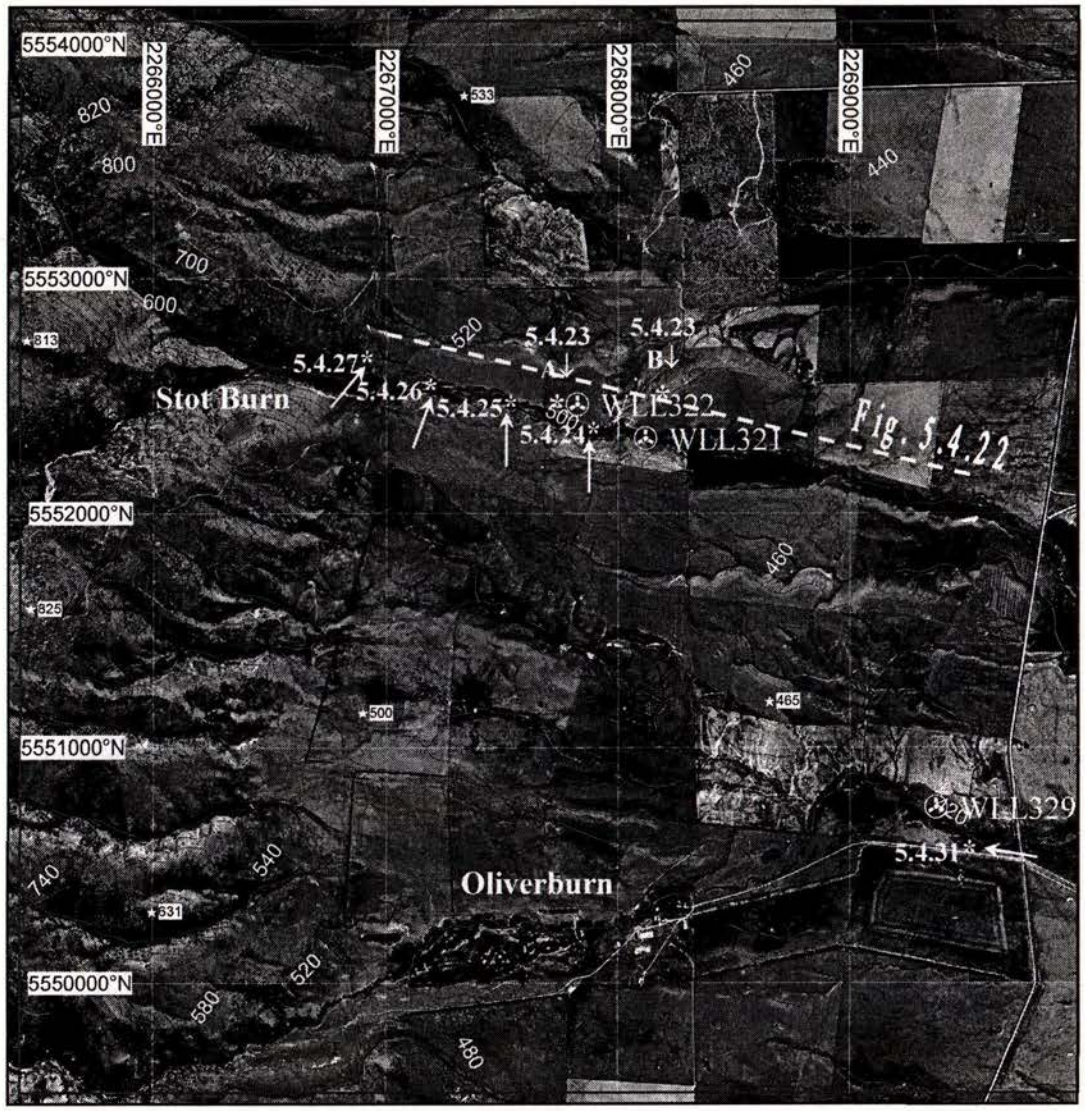

OSL sample site

5.4.2 Rough Ridge

Stot Burn and Oliverburn field areas - Geomorphology

Fig. 5.4.21 **Drainage patterns, divides, and wind gaps**

(Diagram adapted from Jackson et al., 1996; bold streams referred to in text)

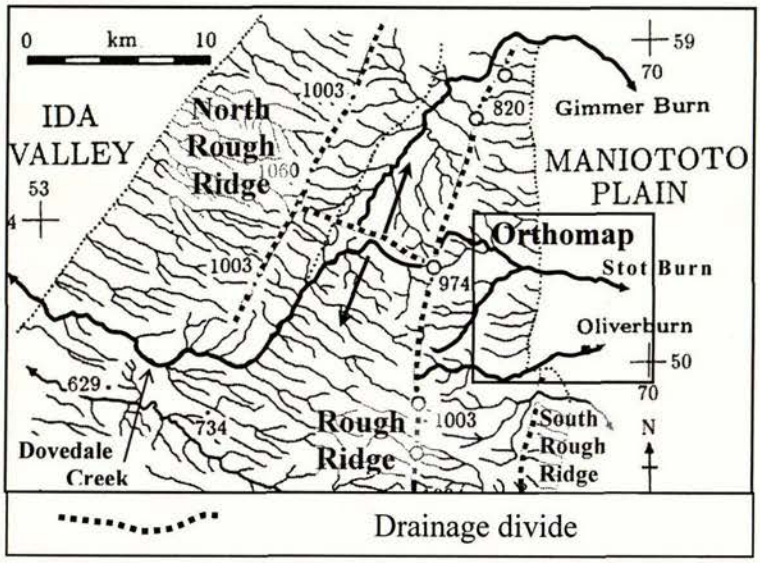

Stot Burn aligns with the NW-SE drainage divide that separates the northward-flowing headwaters of Gimmer Burn from the southward flowing headwaters of Dovedale Creek. Using stream capture patterns, Jackson *et al.*, 1996, concluded that south of this divide Rough Ridge is older than North Rough Ridge, and conversely, north of the divide North Rough Ridge is older than Rough Ridge. Thus in the region of the transverse drainage divide, the northward propagating Rough Ridge has grown past the southward propagating North Rough Ridge (*Fig.5.4.21*). In addition they suggested that the elevation of the North Rough Ridge summit (1060m), near the transverse divide, may in part be due to additional uplift from Rough Ridge. Further south, near Oliverburn Station, the nose of the northward propagating South Rough Ridge anticline (informal name, Jackson *et al.*, 1996) deflects streams northward before it merges with the sedimentary apron. By applying the same reasoning as above, Rough Ridge may have had some additional uplift from the younger South Rough Ridge.

The NNE strike of the drainage divide on Rough Ridge veers to N-S between Stot Burn and Oliverburn (*Fig.5.4.1*). The en-echelon left-stepping Rough Ridge Group is clearly being uplifted on more than one fault at depth. Fault activity on these structures must migrate in time, otherwise all the range segments would be the same age. The evident relative youth of South Rough Ridge and Little Rough Ridge compared to Rough Ridge and North Rough Ridge respectively may represent transference of the location of active faulting with time, or a much slower uplift rate on the frontal ranges.

5.4.2 Rough Ridge

Stot Burn field area – terrace deformation

Fig.5.4.22 **Terrace deformation at Stot Burn** (from 67950/52235 →N)

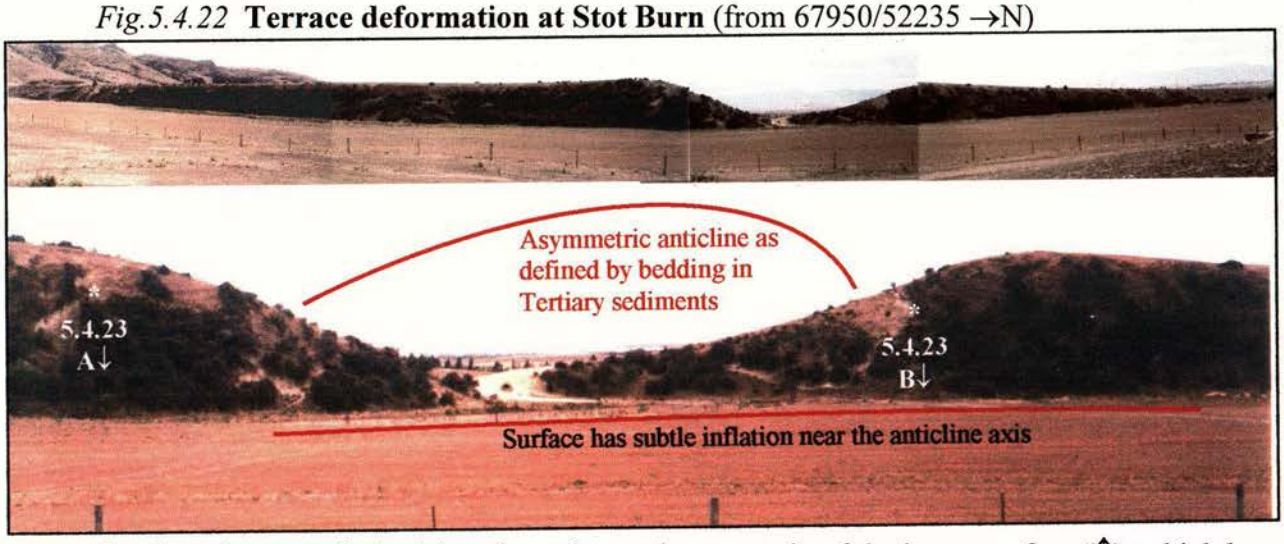

Stot burn is currently incising along the northern margin of the lower surface (↑), which has an overall northward tilt. The steep and remarkably linear ~15m high escarpment forming the high terrace edge occurs only on the northern margin of the valley, as at Gimmer Burn, and Oliverburn (next section). The upper terrace is formed variably of lacustrine and fluvial Tertiary sediments overlain unconformably by ~5m of river gravels. A quartz-rich lag gravel occurs on the upper surface in the 'gap' area, but pinches out a few tens of metres away on either side. Approaching the 'gap' from either side, the upper surface of the high terrace bows noticeably upward. The lower surface has a subtler upward flexure aligning with the centre of the 'gap'. Bedding within the Tertiary sediments describes a N-S striking asymmetric anticline, steeper side to the east. The axis of the anticline aligns with a northward extension of the South Rough Ridge drainage divide (see *Fig.5.4.21*).

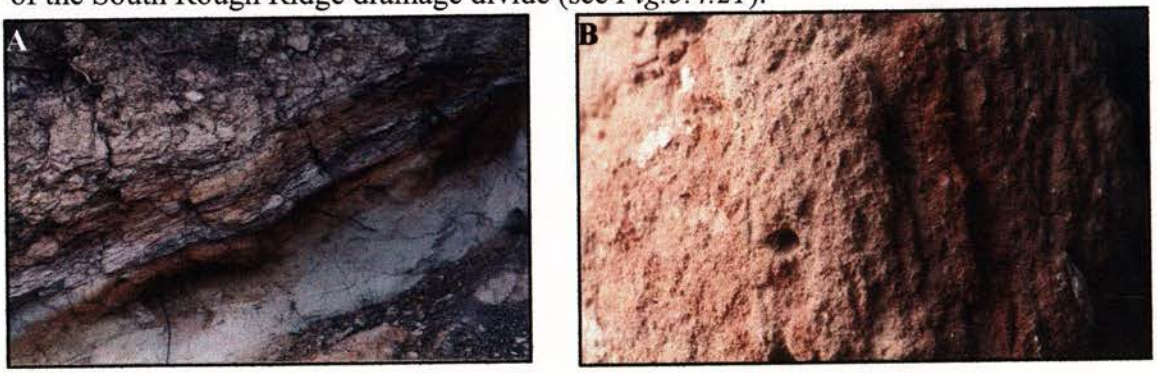

Fig.5.4.23 **Bedding within Tertiary sediments describes an anticline across 'the gap'**

West side of 'gap'
(A) (from 67825/52369 →N)
Bedding in the lacustrine Bannockburn Formation (Miocene) strike N-S and dips 25°W, forming the western anticline limb.

East side of 'gap'.
(B) (from 68000/52373 → N)
Sub-vertical bedding in Wedderburn Formation quartz-rich fluvial gravel strikes N-S and forms the steeper eastern limb of the anticline.

5.4.2 Rough Ridge

Stot Burn field area - Terrace deformation

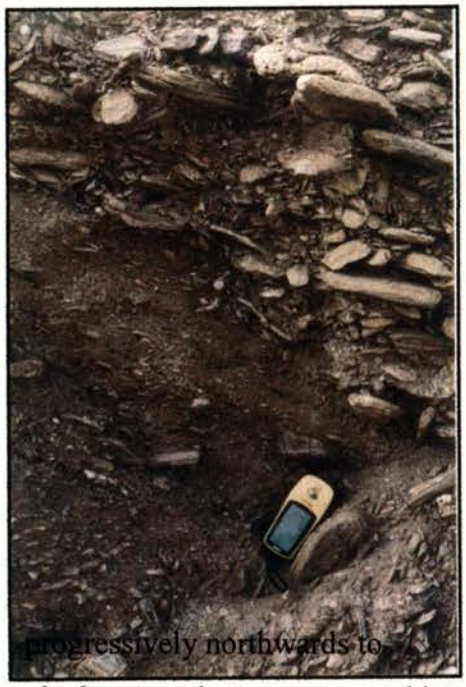

Fig. 5.4.24 **High terrace gravels** (from 67954/52374 → N) Overlying the Tertiary sediments (where present) in angular unconformity are ~5m of schistose gravels and sands with a minor greywacke component. These are southward flowing braided river channel, bar and overbank deposits which form the extensive longitudinal uplifted terrace surfaces prominent in the Maniototo. This high terrace at Stot Burn can be traced along Rough Ridge rangefront between Gimmer Burn and Oliverburn. Maximum high terrace elevation (~520m A.S.L.) occurs in the Stot Burn area, dropping progressively northwards to ~450m at Gimmer Burn. To the south, sediments pinch out against emergent schist at ~480m elevation, near Oliverburn.

Fig.5.4.25 **Fault expression within upper terrace gravels**

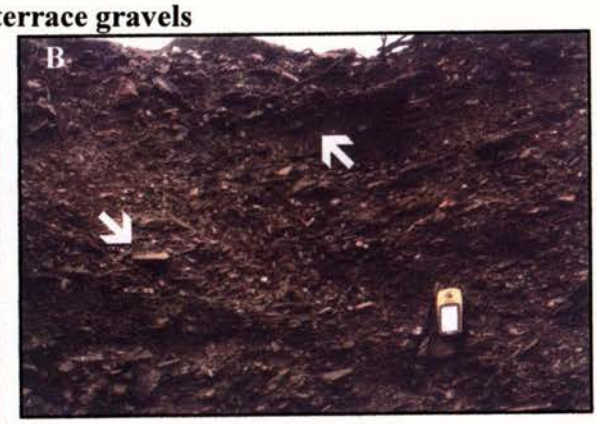

(A) (from 67922/52368 → N) Fault plane dips 30°E and breaks the upper terrace surface, thus post-dates it. The location is ~100m west of 'the gap'. Reverse motion is indicated.

(B) Different view of (A) emphasising the surface break and distributed deformation.

(C) (from 67725/52374 →N) This fault plane dips 23°E and is located ~200m west of A and B. Again, this fault breaks the surface. The dip of both of these fault planes may be shallower than that of their respective underlying basement structures due to fault refraction at the basement/sediment unconformity.

5.4.2 Rough Ridge

Stot Burn field area - Terrace deformation

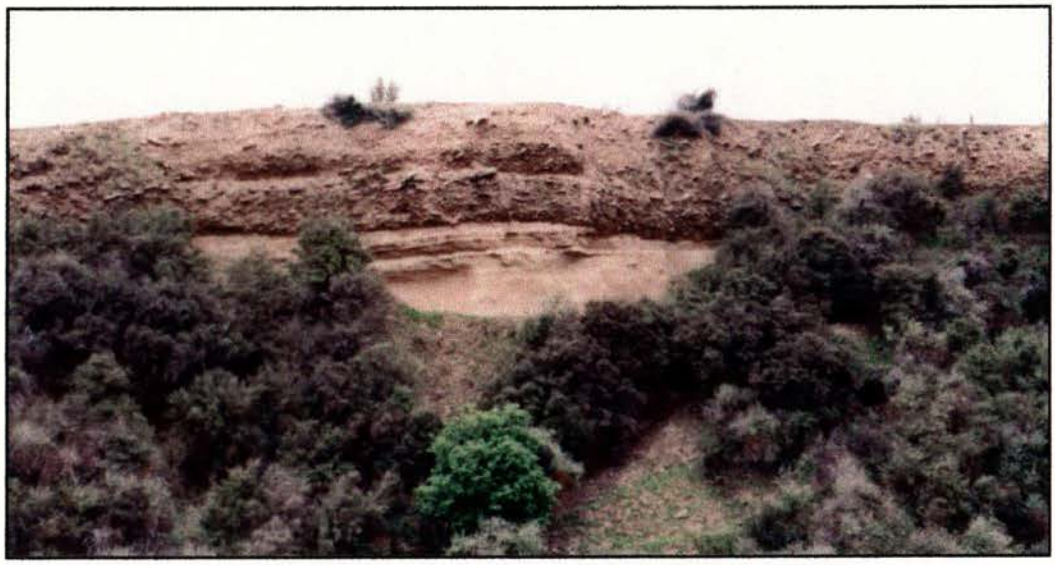

Fig. 5.4.26 ↑ **Stot Burn high terrace showing Tertiary/terrace gravel angular unconformity and upper surface inflation.** (from 67620/52418 → 20°)

Fig.5.4.27 **Stot Burn high terrace showing divergent bedding within Tertiary and offset in the unconformity (in ellipse).**
(from 67532/52439 → 40°)
Internal terrace disruption aligns with more subtle deformation of the lower surface.

Fig.5.4.28 **Deformation within lower-level terrace gravels**
(from 67162/52516 → 20°)
Outcrop is ~1500mm high and bedding is offset ~300mm, with normal movement indicated. This is within the incision by Stot Burn into the lowest terrace level in *Fig.5.4.22*.

5.4.2 Rough Ridge

Stot Burn field area - OSL sample sites

Fig. 5.4.29 **High terrace sample site**

Site 67923/52365

OSL sample site WLL 322 **Age: 129.8 ±19.1ka**

The sample was taken from an indurated overbank mud lens from the site marked '⊗', 2m from the upper terrace surface. This regionally extensive terrace surface correlates across the three Rough Ridge field areas and intersects the Gimmerburn Fault zone of Thomson, (1996). An age from this older, higher surface enables calculation of medium-term uplift/incision rates for comparison with the shorter term rates calculated from Gimmer Burn samples. Along-strike elevation change of this surface not attributable to natural depositional gradient may be useful for assessing a growth rate of the structure(s) responsible for terrace uplift.

Fig. 5.4.30 **Low terrace sample site**

(Site 68115/52346)

OSL sample site WLL321 **Age: 14.2 ±1.4ka**

The sample was taken from the Stot Burn incision into overbank mud 500mm below the upper surface of the lowest terrace level at the location marked '⊗'. This surface shows undulation in the axial region of the anticline, and a subtle gradient change (see *Fig. 5.4.*38E), so a date will give a maximum age for this activity. This surface is locally extensive and also traverses the Gimmerburn Fault Zone of Thomson, (1996) (see *Fig.5.4.32*).

5.4.2 Rough Ridge
Oliverburn field area - OSL sample site

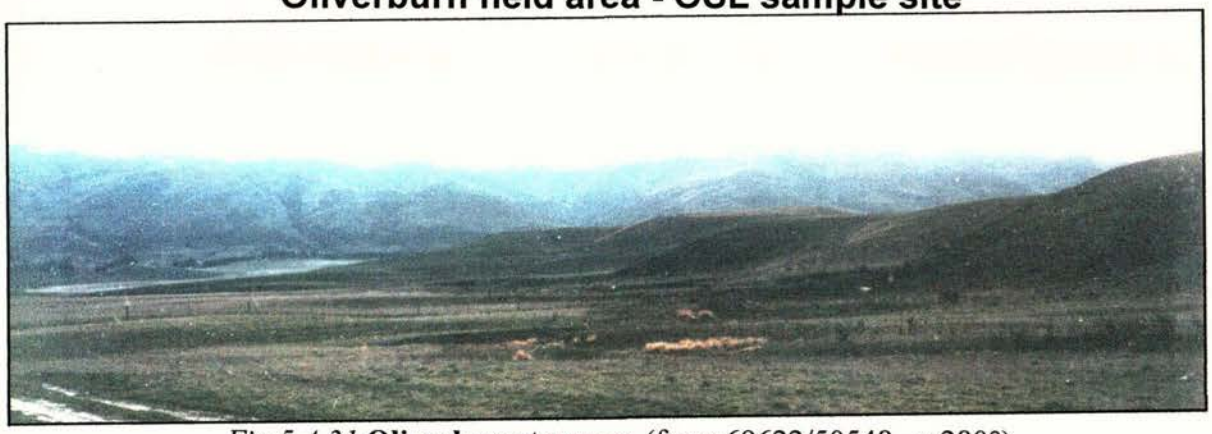

Fig.5.4.31 **Oliverburn terraces** (from 69622/50548 → 280°)

Both terrace surface levels contain range-parallel undulations, which from the air appear as lineaments. Thomson (1996) interpreted some of these as fault scarps forming part of the Gimmerburn fault zone, and the pertinent map scrap is shown at left. Of note is the the alignment of the axis of the Stot Burn anticline with one of Thomson's fault scarps. The next scarp eastwards passes through the Oliverburn field area in the region of *Fig.5.4.29.* Here, the higher terrace, which correlates in elevation with the high terrace at Stot Burn, has numerous slope changes and surface offsets, some of which align with disturbances in the lower level infill-terrace, which may represent faulting at depth.

Fig.5.4.32 ***Portion of Thomson (1996) map***

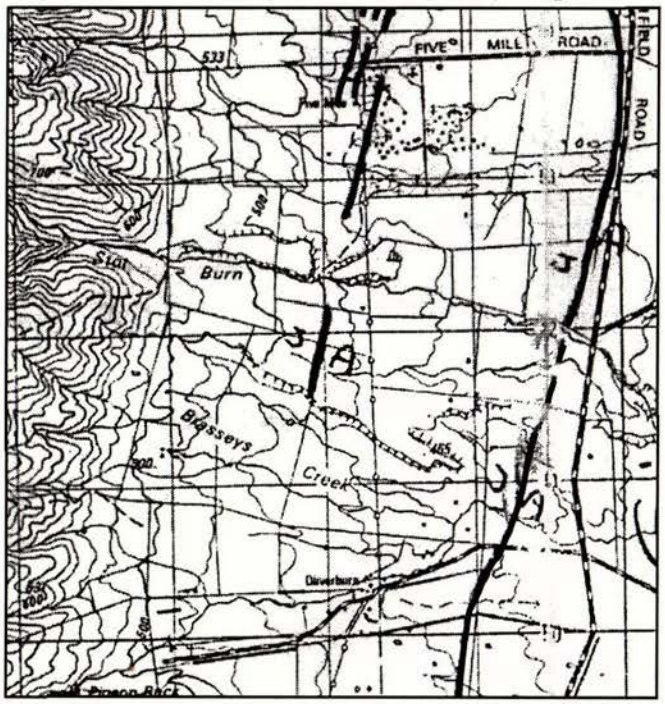

Sample site WLL 329 Age: 2.69 ± 0.27ka

Sample taken from loess 300mm below the surface of the low infill terrace, and marked '⊗'. Dating this surface gives a maximum age of fault activity for this strand of the Gimmer Burn fault zone. A comparison with the ages of surfaces in a similar stratigraphic position, along the rangefront may expose a migration in the timing of infill-terrace formation related to range propagation rate.

Fig.5.4.33 (from 69435/50699 → 270°)

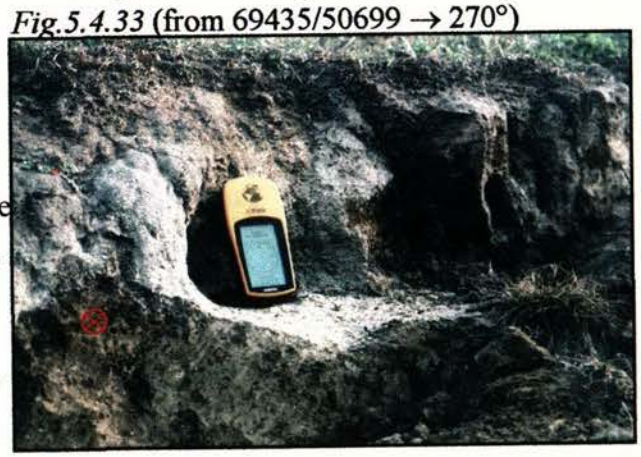

5.4.3 Rough Ridge – North Rough Ridge

Garibaldi Fault

Geological maps commonly show the Garibaldi Fault as a major through-going structure separating North Rough Ridge and Little Rough Ridge (e.g. Bishop, 1979). It is mapped along the western margin of White Sow Valley at the schist/sediment unconformity (see *Fig.5.4.1*). A cursory check of White Sow Valley Road failed to uncover any outcrop evidence of faulting. However where State Highway 85 and Ida Burn traverse the north end of North Rough Ridge, the roadcut / incision permits observation of basement structures obscured by sediments within White Sow Valley. A variety of structures are visible.

← *Fig.5.4.34* (from 72490/74387 →180°)
Low angle thrust sub-parallel to foliation in schist (160/40E). Outcrop is ~4m high.

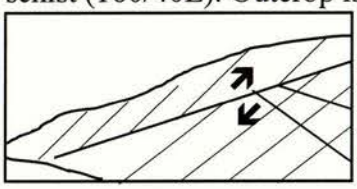

Jointing cuts across foliation

← *Fig.5.4.35* (from 72501/74494 → 60°)
Schist strath surface is bowed up and contains a massive gouge zone under 'intact' schist. Face is ~8m high and surrounding schist is highly altered. This is the north side of the Ida Burn incision through North Rough Ridge.

← *Fig.5.4.36* (from 72510/74473 → 140°)
Orthogonal pervasive joint sets and antithetic shear zone.

← *Fig.5.4.37* (from 72510/74509 → 55°)
Low angle thrust on same orientation as *Fig.5.4.33*, above. Width of gouge zone is ~100mm. Note distributed deformation with foliation bending as fault is approached.

5.4.4 Rough Ridge GPS surface profiles

Fig.5.4.38A **GPS surface profile locations**

Fig.5.4.38B **Profiles A and B – Range-parallel across the mouth of Gimmer Burn**
(Vertical exaggeration = 2.5:1)

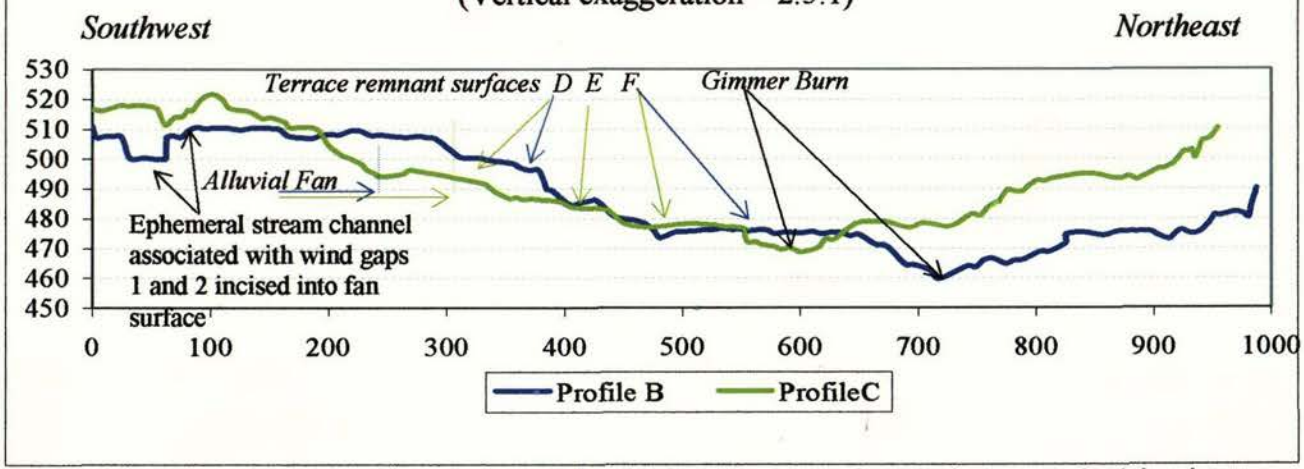

Note the increasing surface slope with older higher terrace surfaces. The stream incision into the fan surface at the southwest end is visible in *Fig.5.4.16*, close to the rangefront.

5.4.4 Rough Ridge GPS surface profiles

Fig. 5.4.38 C **GPS profile A - traverse through wind gap 3 – Gimmer Burn**

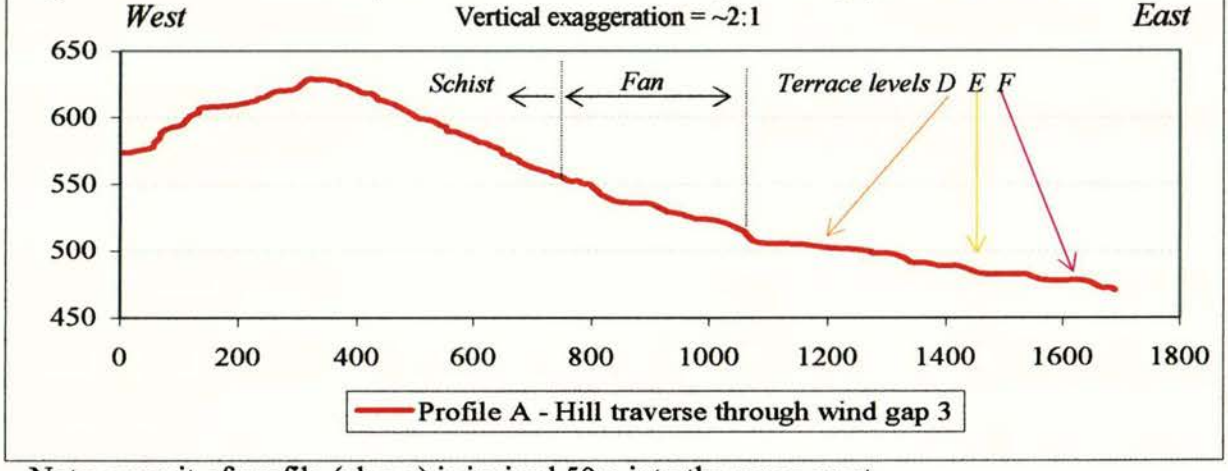

Note summit of profile (above) is incised 50m into the range crest.

Fig.5.4.38D **Range-orthogonal GPS Profiles of three terrace levels at Gimmer Burn**

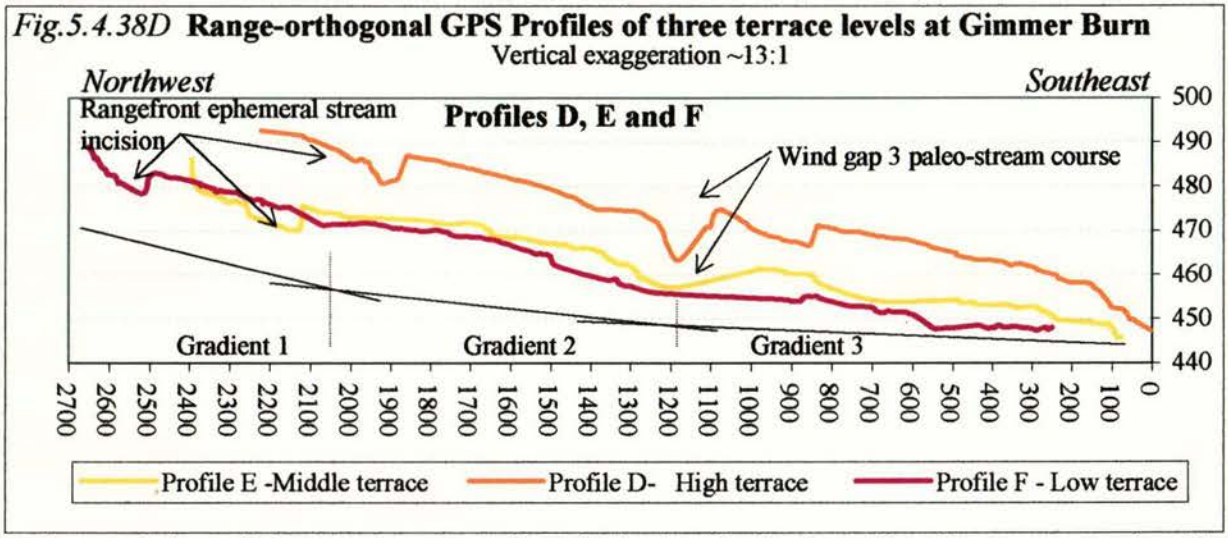

There are three distinct averaged gradients in the longitudinal profiles. One corresponds with the location of the range-parallel segment of the paleochannel associated with wind gap 3, and the other aligns with the knick point in Gimmer Burn in *Fig.5.4.19*.

5.4.38E **Stot Burn Range-orthogonal terrace GPS profiles G and H.**

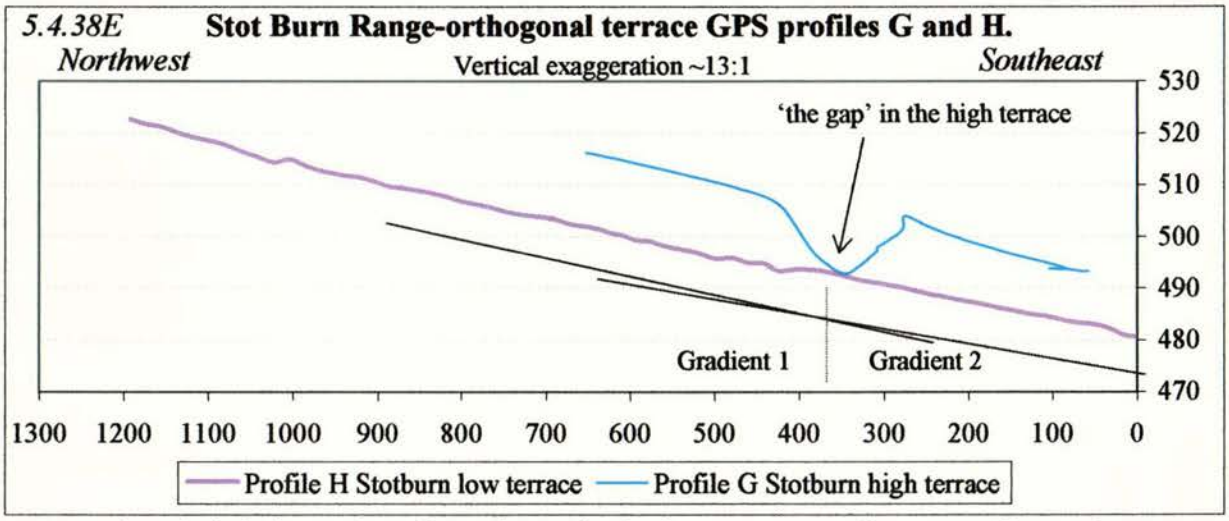

Note the subtle bulge and gradient change in the lower terrace adjacent to 'the gap'.

5.4.5 Rough Ridge Group Discussion

The four interacting members making up the Rough Ridge Group may themselves be composed of amalgamated segments. Suitably orientated structural discontinuities exposed within the gorge have been exploited by streams. These zones of structural weakness are more easily eroded than intact schist, allowing stream courses to persevere in the face of uplift, where they would otherwise be diverted. This leads to the formation of wind gaps, and offers explanation as to why, within the Gimmer Burn gorge, wind gap 3 is at a lower elevation than wind gaps 1 and 2, which are closer to the propagating nose of the anticline (see *Figs. 5.4.7, 5.4.10-12, 5.4.16*). Wind gaps 1 and 2 are probably the product of antecedent streams cut mainly before the uplift of Rough Ridge, and the disturbance in the drainage pattern of the older North Rough Ridge. The inherent weakness at the site of wind gap 3 allowed local incision to keep pace with uplift for a considerable time while the streams at the sites of wind gaps 1 and 2 were elevated and abandoned. Thus wind gap 3 has a much larger relief (~50m) with the saddle at a much lower elevation. The range crest of North Rough Ridge also contains discrete steps related to inherited structures. The deformation uncovered in this investigation indicates that the Rough Ridge Group is accounting for at least some of the required regional convergence. When combined with geomorphologic and geologic observations, the OSL ages obtained provide some constraints on the magnitude and timing of deformation.

Long-term deformation rate

If it is assumed that faults dip at roughly 45°, then uplift equals shortening. Adjacent to Stot Burn, the Rough Ridge summit is 444m above the sedimentary apron. Pleistocene greywacke conglomerates (Maniototo Conglomerate) within the apron contain no component of schist, or paleocurrent indicators to suggest local relief at the time of their deposition. The minimum rate, if uplift started at 2.5Ma would be 0.18mm/yr, and a maximum rate, if uplift started 1.0Ma, of 0.44mm/yr. Published ages of 800ka for sarsen stone exposure on Rough Ridge summit, near Stot Burn would give 0.55mm/yr, although this rate would be a maximum due to possible saturation (Jackson *et al.*, 2002). More recent evidence suggests that while these ages are minima, they are not likely to be substantially greater than 1 million years (J. Jackson, pers. comm., 2003).

Fig.5.4.39A **Assessment of long-term uplift rate**

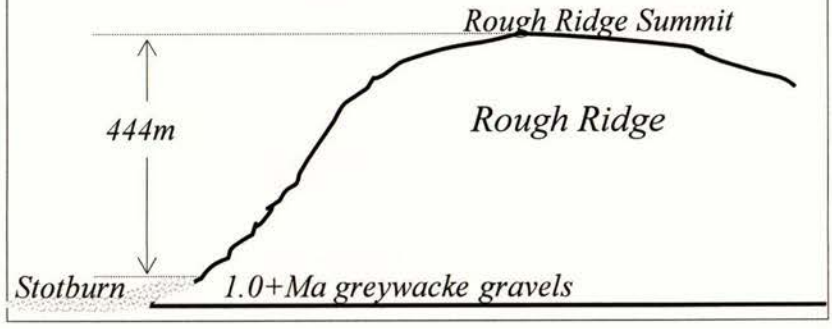

Additional support for this age determination comes from the long-term differential erosion rates between the schist and the sarsen stones. If the ^{10}Be ages erred considerably on the young side due to saturation, then more relief could be expected in the surrounding schist surface. Schist tors adjacent to the sarsen stones are every where between ~5 – 10m high, consistent with 5ka – 1Ma of surface erosion, so the stones may be saturated but unlikely to be much older than 1Ma. The uplift rate therefore is likely to be less than 1.8mm/yr but greater than 0.55mm/yr.

Medium-term uplift rate

At the Gimmer Burn site, the paleo-channel associated with wind gap 3 is truncated by the 5.3ka terrace, so is clearly older than 5.3ka. An equivalent surface to the Stot Burn high terrace dated at 129ka is incised by the paleo-channel which, therefore, must be younger than this surface. The difference in elevation between the 129ka terrace and wind-gap 3 is 116m and subtracting 5m to allow for the natural stream gradient over this distance yields 111m of uplift, or 0.86mm/yr averaged over 129ka.

Fig.5.4.39B **Assessment of medium-term uplift rate**

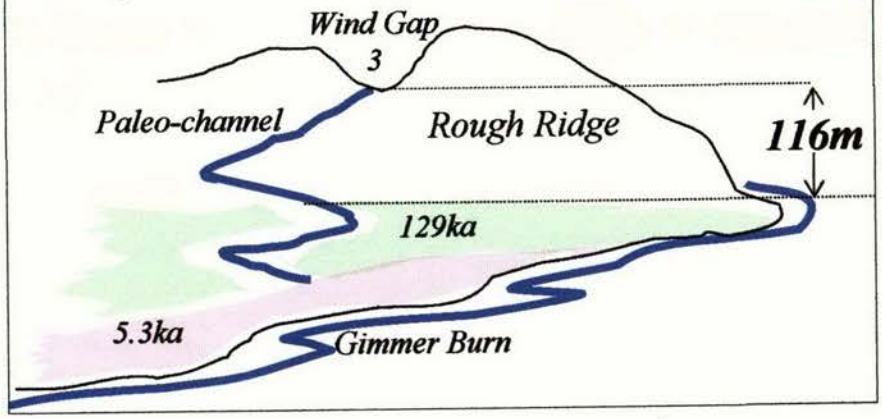

Short-term uplift rate

The difference in age of the two lowest terraces at the mouth of the Gimmer Burn gorge is 4.3ka and the difference in surface elevation is 1100mm. The OSL sample was taken 400mm below the upper surface and 200mm below the lower surface giving a net difference in elevation of 900mm. This gives an incision rate, and by proxy, uplift rate of 0.27mm/yr averaged over the last 4.3ka.

Fig.5.4.39C **Assessment of short-term uplift rate**

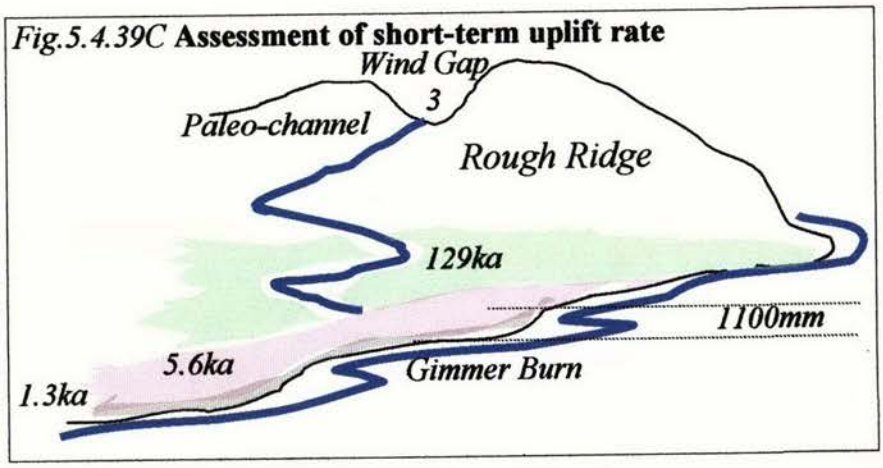

Although all of these rates are founded on a string of assumptions, they are not unrealistic. Even allowing for major errors, it is clear that levels of activity fluctuate over time. These results compare well with those obtained by Jackson *et al.,* (2002) for exposure of the peneplain on South Rough Ridge.

Blackstone Hill

5.5 Blackstone Hill

Overview

Blackstone Hill is a northeast-trending asymmetric schist anticline (steeper side to southeast; *Fig.5.5.2*) situated between the Ida and Manuherikia Valleys (see *Fig.5.5.1*). Together with the Raggedy Range to the southwest, Blackstone Hill forms a topographically continuous ~30km long ridge. Jackson *et al.,* (1996) used drainage patterns to show that Raggedy Range and Blackstone Hill evolved on distinct reverse faults that have now coalesced to form a single continuous ridge. They suggested that uplift of Blackstone Hill is accommodated by two steep-dipping reverse faults at depth, consistent with a fault propagation fold model, and similar to the Rock and Pillar Range.

Markley and Norris (1999) used the progressive tilting of flights of strath terraces on the flanks of Blackstone Hill to show that folding of the peneplain surface has accompanied ongoing late Cenozoic uplift. Their data showed that, in addition to pre-existing planes of weakness, a new generation of fractures has developed in the schist basement to accommodate late Cenozoic deformation. They argue that long-strike variations in topographic expression may be a result of mechanical interference between two generations of folding, namely the Mesozoic Blackstone Hill Nappe (Gray *et al.,* 1995), and the late Cenozoic Blackstone Hill Antiform. From the interpretation of Bouguer gravity data, Markley and Tikoff (2003) proposed along strike variation in either fault dip or depth below the surface might be additional factors in controlling the antiform geometry.

On the northern end of the southeast rangefront of Blackstone Hill, abandoned gold workings provide exposed sections through the sedimentary strata. Tertiary sediments above the schist, where present, consist variably of quartz-rich Dunstan Formation, lacustrine Bannockburn Formation, and fluvial conglomerates of the Wedderburn Formation, and the rounded greywacke Maniototo Conglomerate. Quaternary cover comprises ~10m of fluvial and fan gravels, and loess. Deformation of basement and cover appears localised and complex.

5.5.1 Blackstone Hill

Fig.5.5.1 **Topography and location of field area**

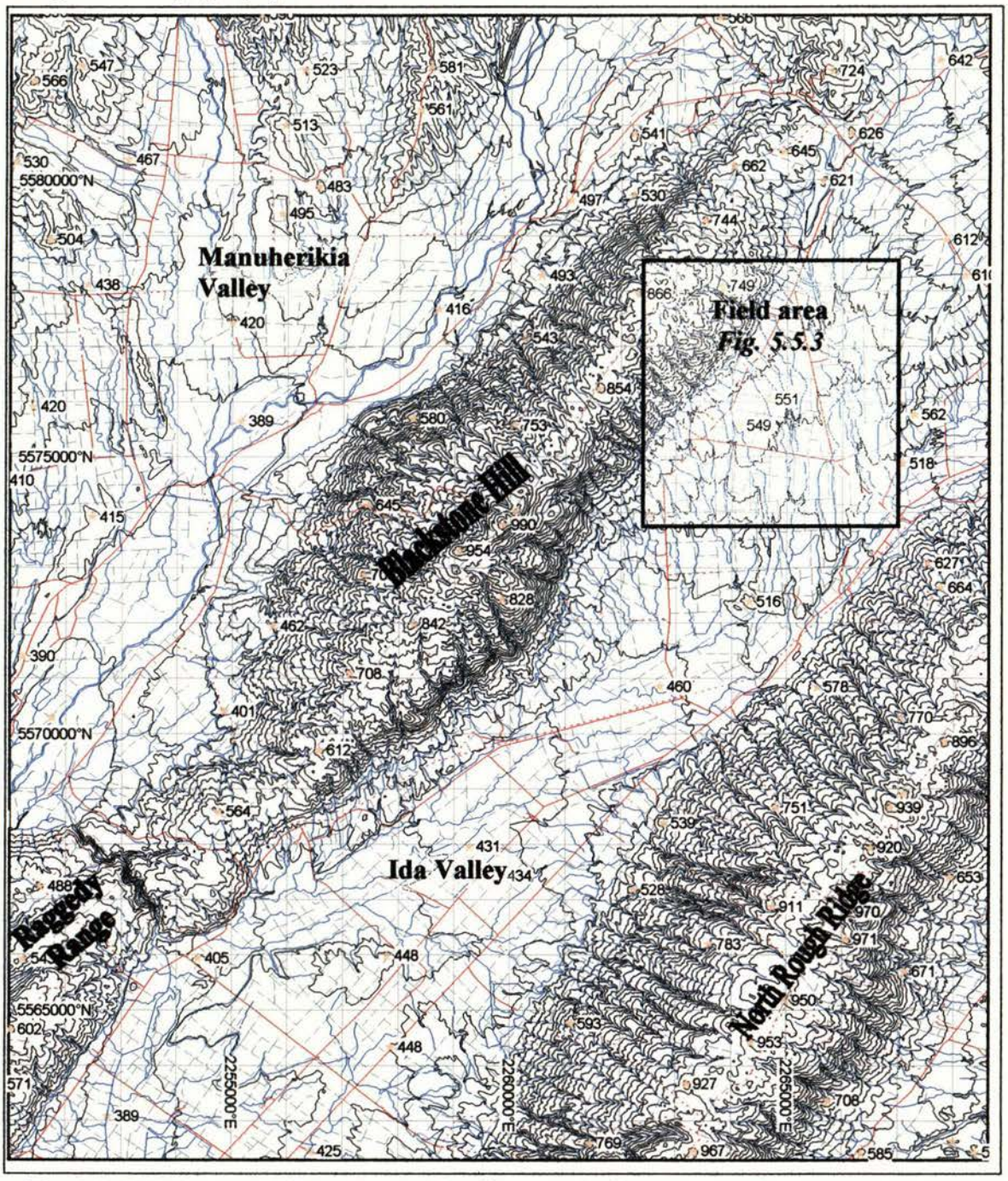

Fig.5.5.2 **Blackstone Hill range profile** (from 52750/63948 →10°)

5.5 Blackstone Hill Overview

Fig.5.5.3 **Orthomap, structure and photo locations**
(asterisk is position, arrow is camera azimuth)

Fig.5.5.4 **Northeast rangefront**
(from 64786/77380 → 290)

Radial drainage patterns on the southwest and northeast tips of Blackstone Hill were used by Jackson *et al.,* (1996) to argue for ridge growth along its axis in both directions. Asymmetric incision into the schist (steeper side to the northeast) suggests northeastwardly range propagation for this segment.

5.5.1 Blackstone Hill

Armitage Diggings

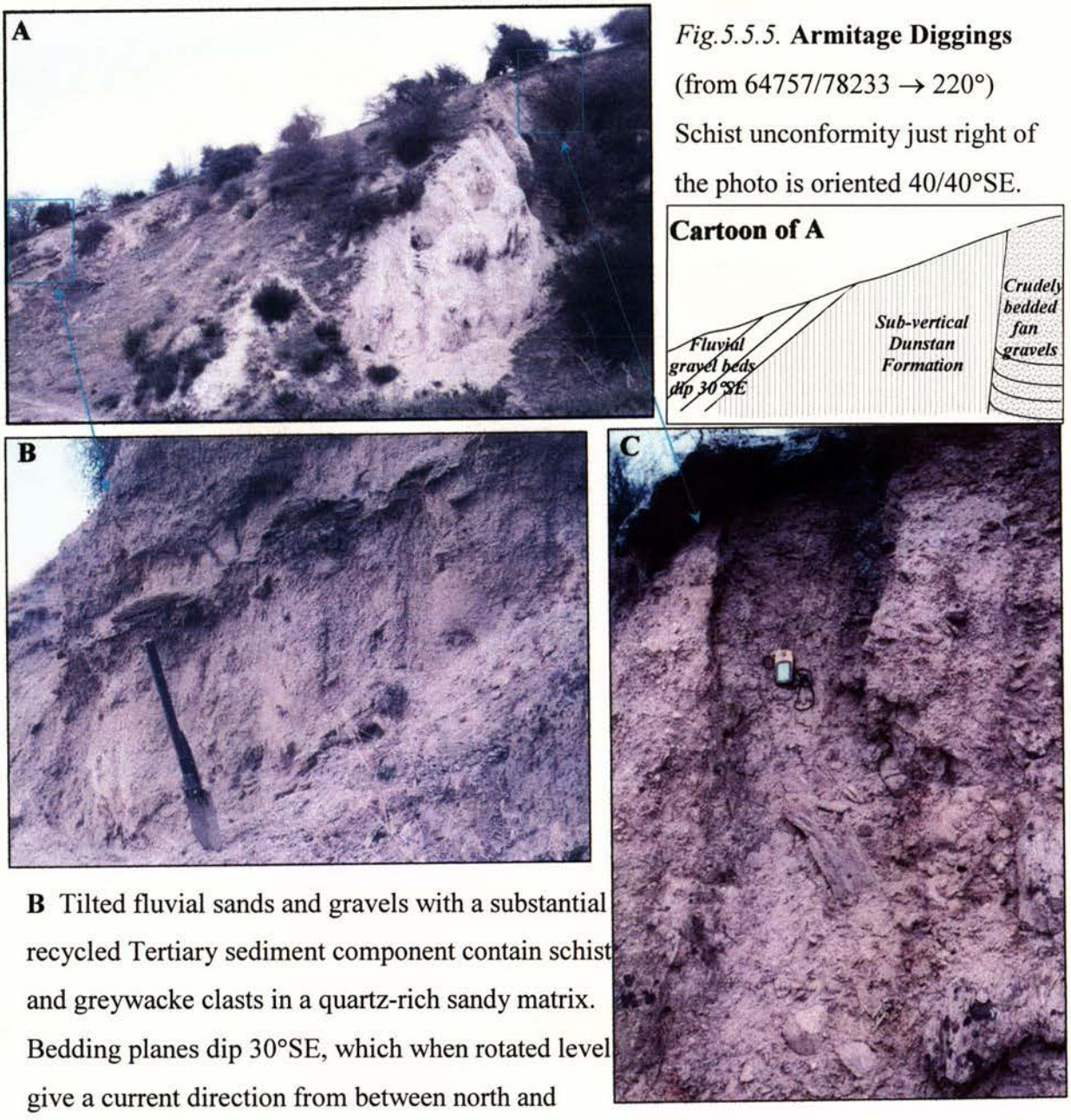

Fig.5.5.5. **Armitage Diggings** (from 64757/78233 → 220°) Schist unconformity just right of the photo is oriented 40/40°SE.

B Tilted fluvial sands and gravels with a substantial recycled Tertiary sediment component contain schist and greywacke clasts in a quartz-rich sandy matrix. Bedding planes dip 30°SE, which when rotated level give a current direction from between north and northeast. They were probably deposited by Ida Burn and have been subsequently uplifted and tilted. The underlying contact with the sub-vertical quartz-rich gravels of the Dunstan Formation dips ~45°SE (see A, above).

C Steeply-dipping contact between sub-vertical Dunstan Formation (left) and crudely bedded fan gravels. The clast-supported fan gravels contain angular pebble to boulder-sized schist clasts with a minor component of sub-rounded greywacke cobbles, which reduces up-section.

5.5.2 Blackstone Hill

Woolshed Diggings

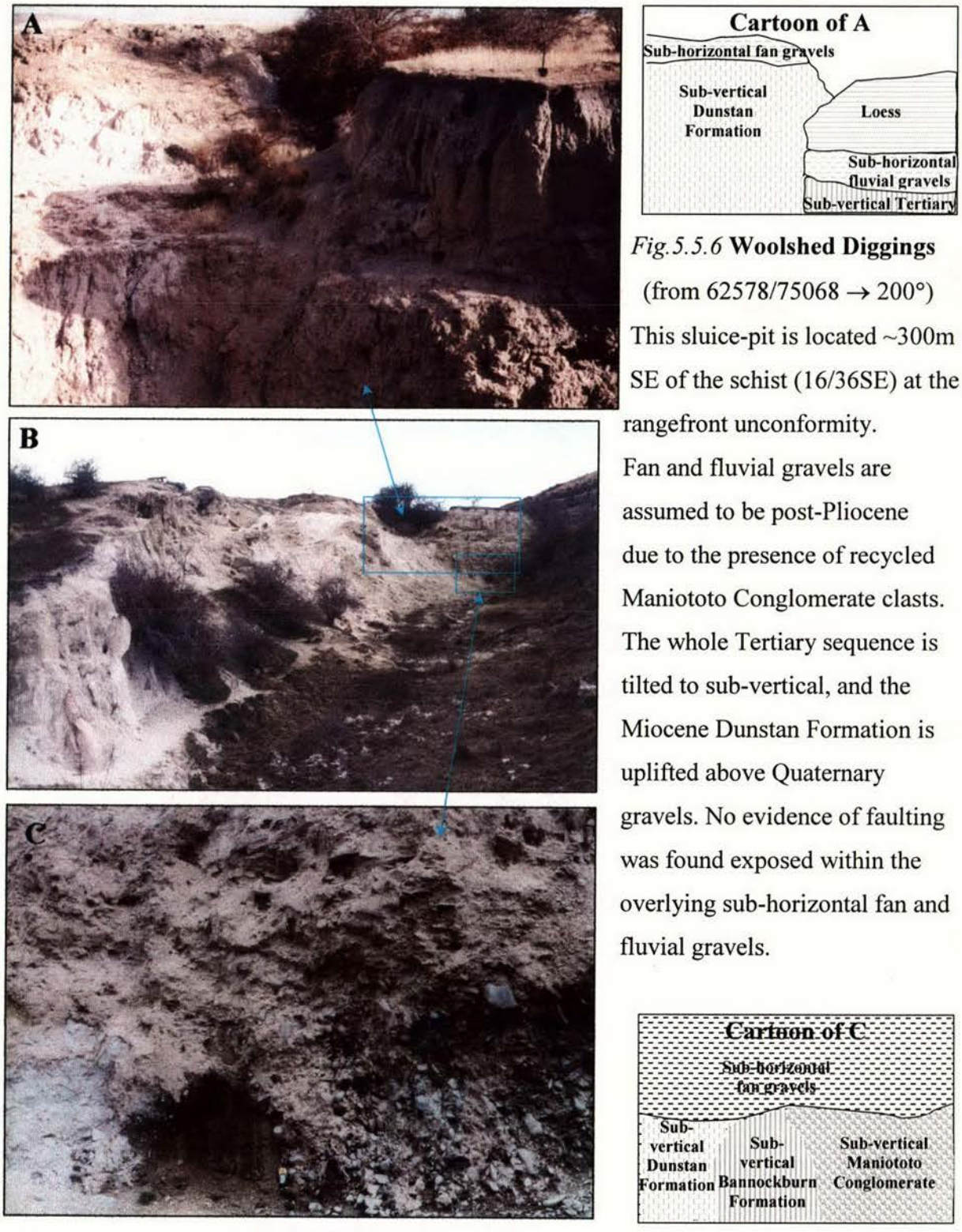

Fig.5.5.6 **Woolshed Diggings** (from 62578/75068 → 200°)

This sluice-pit is located ~300m SE of the schist (16/36SE) at the rangefront unconformity. Fan and fluvial gravels are assumed to be post-Pliocene due to the presence of recycled Maniototo Conglomerate clasts. The whole Tertiary sequence is tilted to sub-vertical, and the Miocene Dunstan Formation is uplifted above Quaternary gravels. No evidence of faulting was found exposed within the overlying sub-horizontal fan and fluvial gravels.

Dunstan Formation deposited directly on the low-relief peneplain surface is the basal sediment in the Ida Valley (Youngson *et al.*, 1998). The schist/sediment unconformity is not visible at this locality but sub-vertical Dunstan Formation between here and Armitage Diggings suggests the peneplain surface below is itself sub-vertical.

5.5.3 Blackstone Hill

Rangefront deformation

Fig.5.5.7 (from 62370/75002 → 230°)
This fluvial/fan gravel and loess sequence is near the top of the strata at Woolshed Diggings, just to the right of *Fig.5.5.5.* Contacts and bedding are sub-horizontal at this locality, which is in contrast to those of the equivalent strata at Armitage Diggings (see *Fig.5.5.4*). Armitage Diggings are situated virtually at the rangefront, whereas Woolshed Diggings are ~200m SE of the emergent schist.

Fig.5.5.8 (from 62420/75053 → 270°)
This outcrop is ~50m from the rangefront, to the east of Woolshed Diggings (see *Fig.5.5.3*)
Bedding within the basal fluvial sequence is sub-horizontal so post-depositional tilting appears minimal. The incoming of overlying quartz-rich alluvial fan gravels signify proximal uplift.

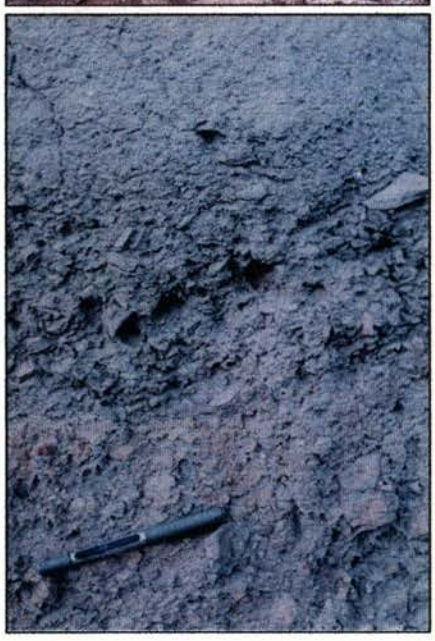

Fig.5.5.9 (from 61839/74671 → 200°)
Bedding planes within this water-race exposure of Bannockburn Formation silt, mud, and gravel are oriented 85/15°SE. Tilting is clearly less advanced here than at Armitage or elsewhere in the Woolshed Diggings, where the same unit is rotated to sub-vertical. This sequence is capped by a ~150mm veneer of angular schistose gravel. Foliation within adjacent schist dips 40° to the southeast.

5.5.4 Blackstone Hill discussion

No OSL samples or GPS surface profiles were taken from Blackstone Hill although the two sites visited near the northeast end of the range show abundant evidence of Quaternary deformation. In the light of field evidence, there are sufficient similarities between the Blackstone Hill rangefront and the others in this study to allow reasonable inferences to be drawn as to the nature and timing of deformation.

The ~SE surface dip of the rangefront sediments increases smoothly approaching the rangefront basement unconformity, with no obvious large range-parallel fault escarpments at the surface. Deformation is distributed in a km-scale zone from within the schist of the range, out into the sediments of the Ida Valley (*Figs.5.5.1, 5.5.10*). On a large scale, the dip of the schist foliation is roughly coincident with the topography, but shows considerable variation along the rangefront. The presence of steeply-dipping to overturned Tertiary and Pliocene sedimentary units at Woolshed Diggings (*Fig.5.5.5*) would suggest that at least locally, the peneplain surface is also steeply dipping, with abundant fault/fold activity within the last 1-2 million years. Less than a kilometre to the southwest, bedding planes within Bannockburn Formation silt and mud dip ~40° to the southeast, suggesting the peneplain surface has a more gentle tilt. Clearly there are basement fault structure(s) between these localities. Proximate to here, the range-front (marked roughly by the position of the water race in *Fig.5.5.10*) steps to the left (marked by dashed black line in *Fig.5.5.10*). This rangefront segment also contains multiple lineaments formed of stream course deviations in the consequent drainage pattern, both within the schist basement and rangefront sediments. Presumably this distributed deformation reflects either multiple fault structures, or splays off a 'master fault' at depth.

Fig. 5.5.10 **Drainage anomalies** (see text)

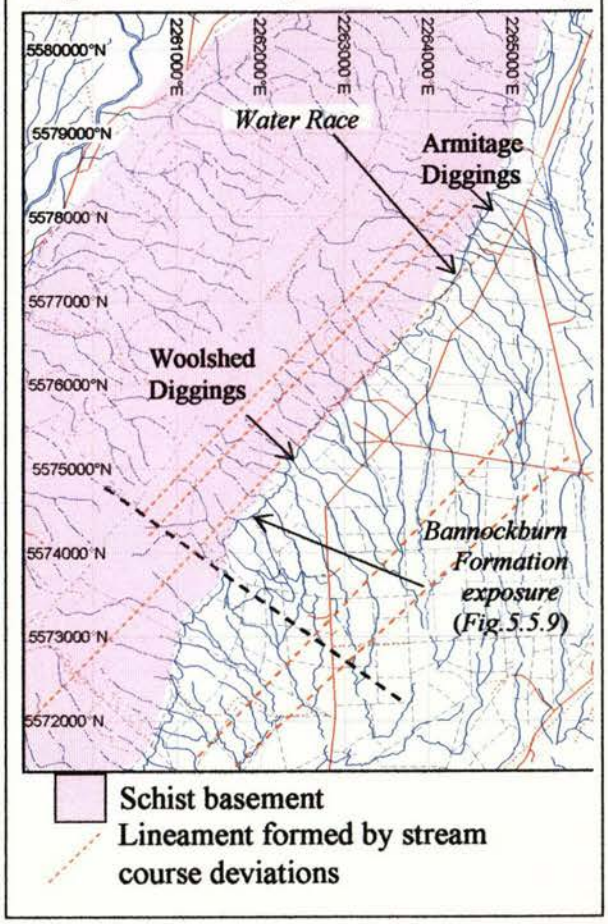

5.6 Dunstan Fault

5.6 Dunstan Fault Overview

The Dunstan fault is a major active reverse fault separating the Dunstan Range and the Manuherikia Basin between St. Bathans and Clyde (~60km), and the western-most of the rangefronts in this study. Maximum uplift of 2000m has occurred on the northwest-dipping fault since the Pliocene, and Late Quaternary activity is discernible within a ~3km wide zone of rangefront sediments (e.g. Beanland *et al.*, 1986)

Dunstan Range and Manuherikia Basin antiform – synform pair

The foliation of the schist defines the Dunstan Range asymmetric antiform. The foliation dips ~20°NW on the western limb; shallows to sub-horizontal at the crest; then steepens progressively to 80° or 90°SE at the foot of the range, forming the steeper southeast limb.

Fig.5.6.1 **Dunstan Range profile looking northeast** (camera position marked in *Fig.5.6.4*)

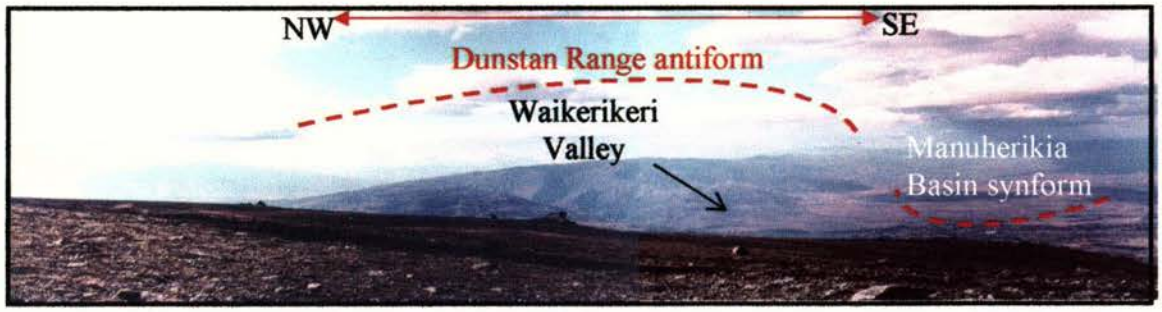

Manuherikia Valley sedimentary structure

The Tertiary sequence in the Manuherikia basin (see *Fig.5.4.2*) forms an asymmetric syncline with a steeply-dipping to overturned northwest limb and a gently dipping southeast limb. Basal Dunstan Formation quartz-gravels are overturned adjacent to the rangefront.

Fig. 5.6.2 (from 22229/55205 → 190°)

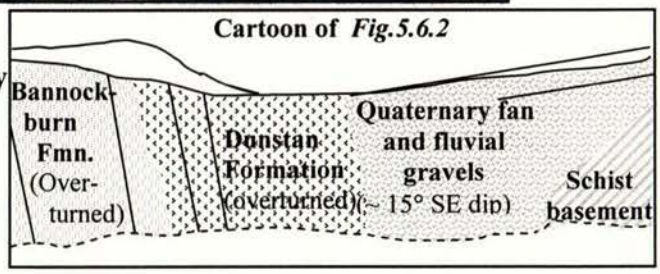

Sediments near the schist unconformity in Waikerikeri Valley

Bannockburn and Dunstan Formations are overturned and separated from the schist basement by a wedge of Quaternary fluvial and fan gravels, in a similar relationship to that of Armitage Diggings on Blackstone Hill. The antithetic bulge in this, and neighbouring terrace surfaces forms part of a range-parallel lineament.

5.6.1 Dunstan Fault

Waikerikeri Valley field area

Fig.5.6.3 **Orthomap, sample site and photo locations**

(asterisk is location, arrow is camera azimuth)

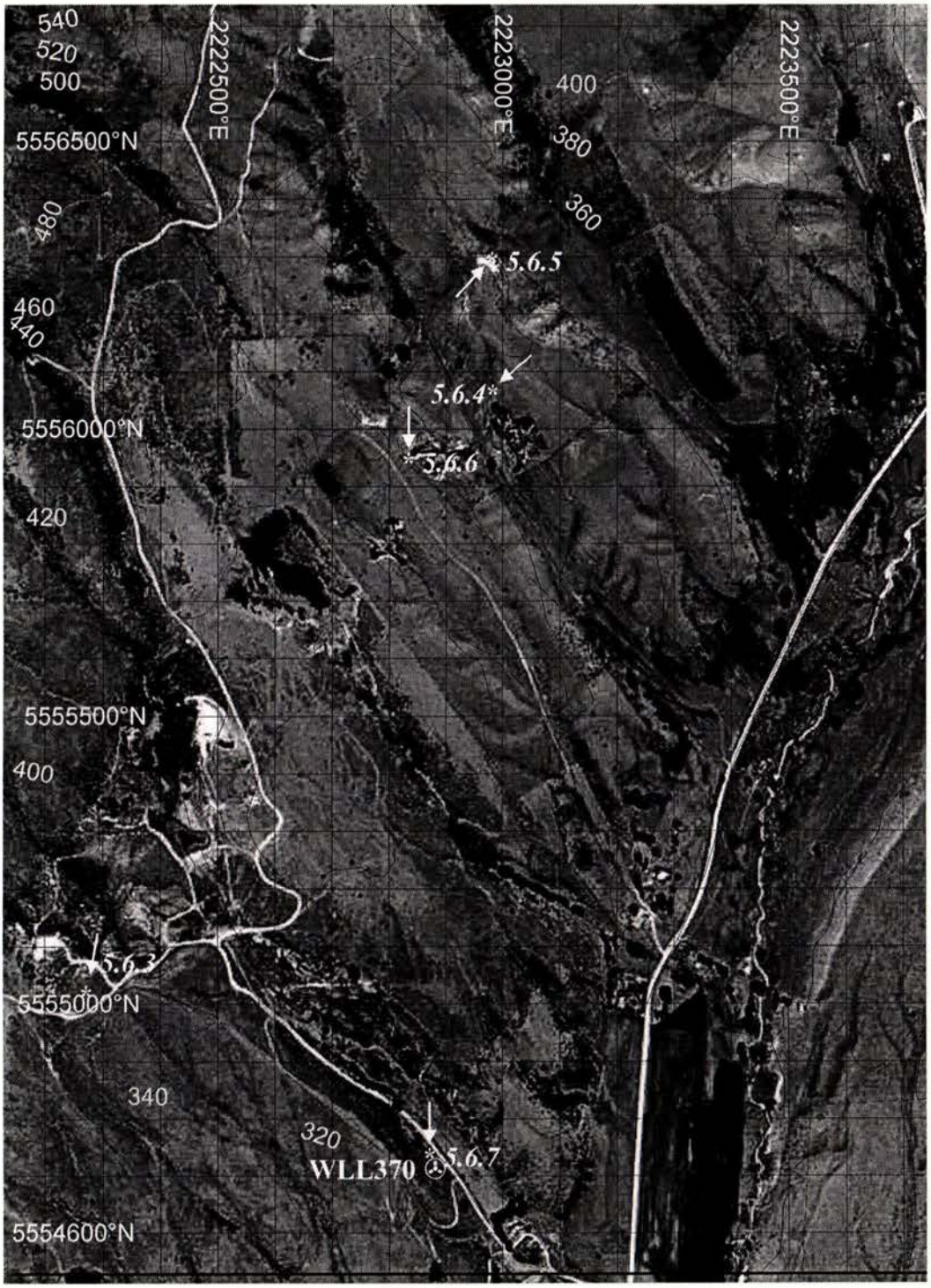

✇ OSL sample site WLL370

5.6.1 Dunstan Fault

Waikerikeri Valley field area deformed terraces

Overlying the Tertiary sequence an extensive fluvial terrace system has formed within the Manuherikia basin, which proximal to the range is interfingered with alluvial fan deposits. The sequence has been elevated, tilted, and incised by streams emerging from the rising Dunstan Range. Within these sites of incision, infill-terraces have formed, have been subsequently tilted, and are currently being incised themselves. Investigations in the Waikerikeri Valley by the New Zealand Geological Survey in 1982 showed the main locus of Quaternary fault activity to be at the topographic discontinuity where schist and Tertiary sediments are in fault contact (Officers of the Geological Survey, 1983, Beanland *et al.*, 1986, *Fig.5.6.2*). Late Quaternary movement is manifest as lineaments formed by subtle range-parallel bulges in the terrace surfaces and drainage diversion within sites of terrace incision ~300m from the rangefront. Two fault traces ~100m apart run sub-parallel to the range and form a horst structure within the terraces.

Fig.5.6.4 **Terrace surface tilting and disruption** (from 22890/55889 → SW)

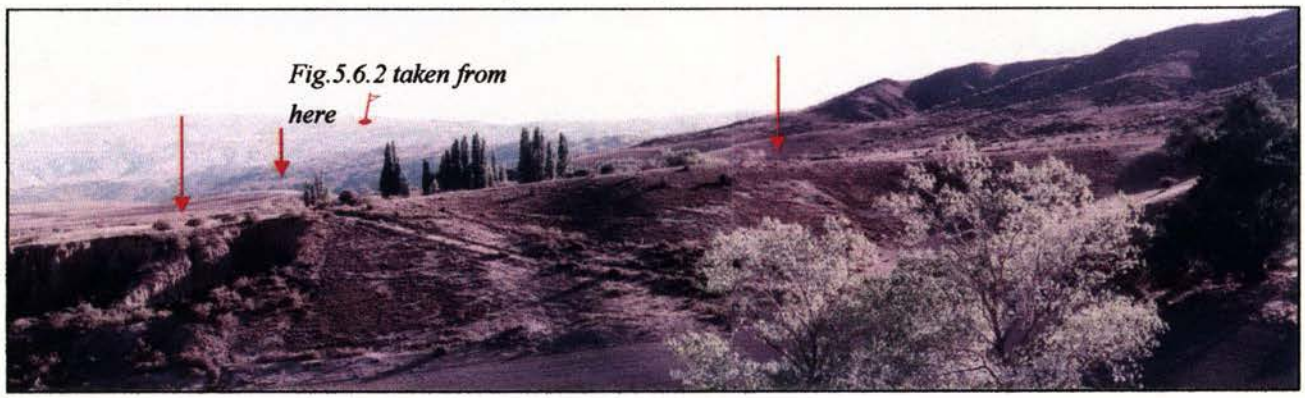

Fig.5.6.5 **Terrace surface disruption** (from 22990/56300 → NNE)

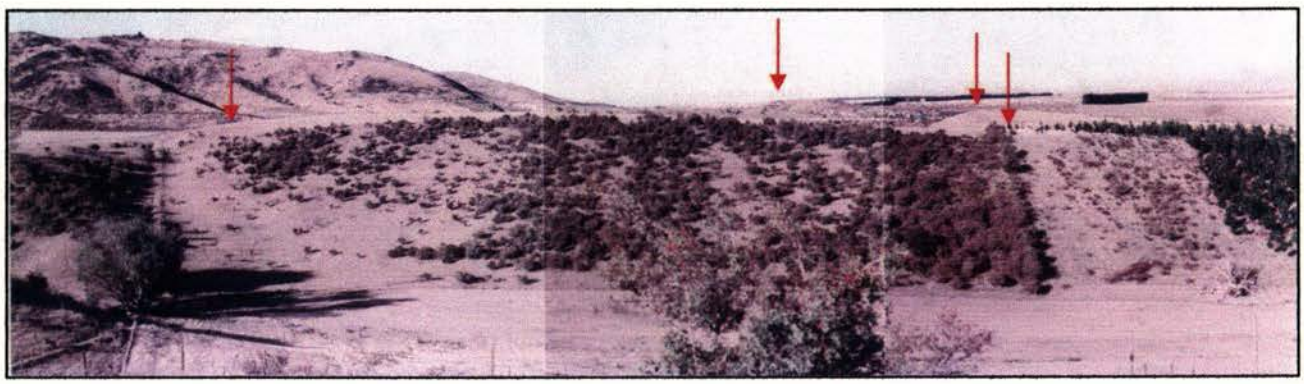

These two photos facing opposite directions along the rangefront show the nature and location of the surface offsets (arrowed) attributed to Late Quaternary fault activity. The lowest surfaces are infill-terraces formed of a combination of reworked older terrace materials, and schist clasts derived from the uplifted Dunstan Range.

5.6.1 Dunstan Fault

Waikerikeri Valley deformed terraces

Fig.5.6.6 **Sections through high terraces showing bedding divergence and tilting.**

(from 22836/55961 → 170°) (from 22876/55969 →180°)

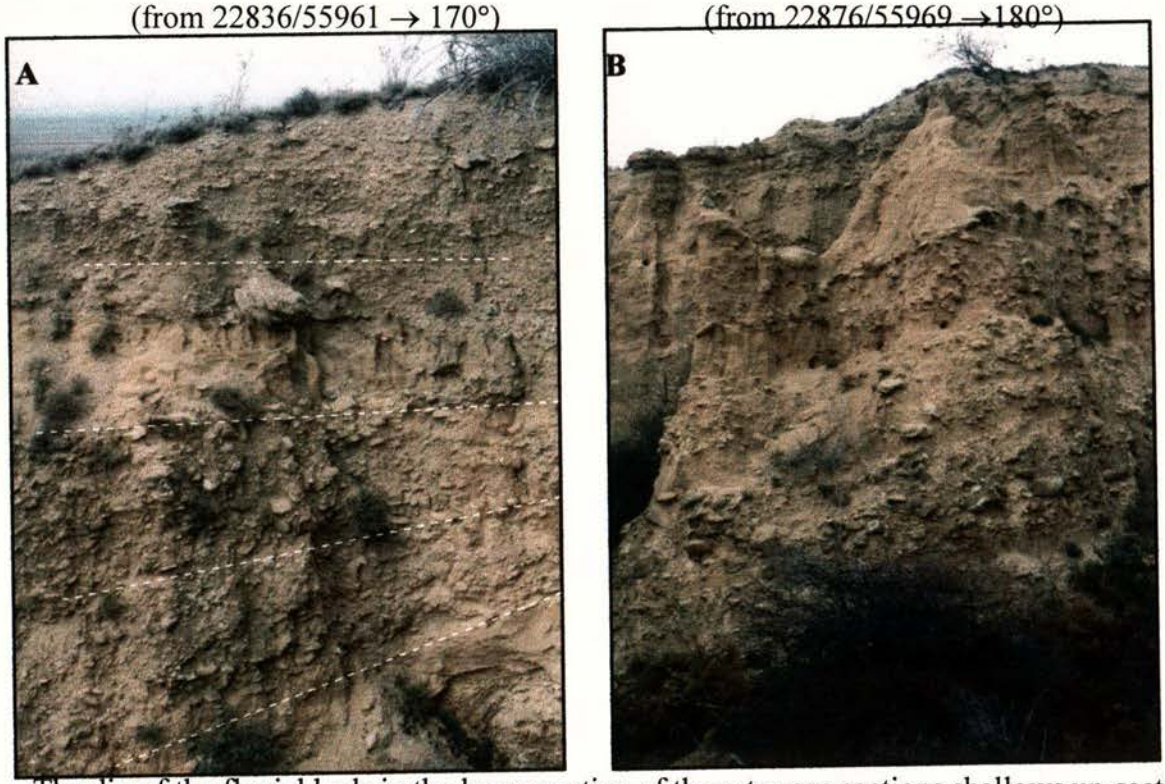

The dip of the fluvial beds in the lower portion of these terrace sections shallows up-section until the prominent loess horizon and a change of depositional regime into alluvial fan deposits. Gravels lower in the sequence contain a higher proportion of rounded greywacke cobbles. This is a consistent pattern in all terrace sections seen in this area.

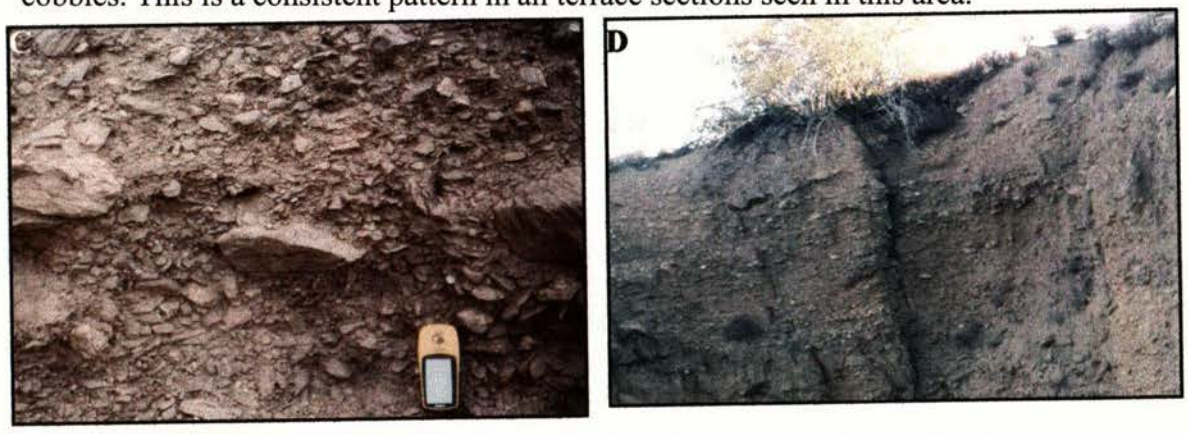

Alluvial fan deposits are either clast-supported sediment gravity flows (C, from the upper section of A), or matrix-supported sheetwash with bedding parallel to the surface (D, from the upper section of B). Both almost exclusively contain angular schist clasts with a minor rounded greywacke cobble component near the basal unconformity with underlying fluvial gravels.

5.6.1 Dunstan Fault

Waikerikeri Valley OSL sample site

Fig.5.6.7 **OSL sample site** (from 22888/54729 → 180°)

Sample WLL330; Age 1.66 ± 0.16ka

The sample was taken from the fine-grained fluvial gravel horizon 400mm from the upper surface of the infill terrace at the location marked '⊗'. This surface correlates with other infill terraces within the incisions into the older alluvial/fluvial terrace sediments of the Waikerikeri fan complex. This is the only generation of infill terrace within these incisions, as there are no older, higher abandoned infill-terrace remnants. The surface deformation of the Waikerikeri fan complex, which defines the trace of late Quaternary fault activity (see *Fig. 5.6.*8, Beanland *et al.*, 1986), aligns with anomalous stream course segments within the infill-terraces. The infill terraces themselves have an anomalously steep basinward tilt (~4°) which may be original as the streams are currently incising the terrace and adjusting their long profile. Thus there is no unequivocal evidence of tectonic deformation of these young infill terraces. Dating this surface gives a minimum age for deformation associated with movement on the Dunstan Fault, and dating of the older higher terraces would give a maximum age, thus constraining the timing of the most recent activity. This latter terrace dating work is currently being undertaken by IGNS (D. Barrell, pers. comm.. 2003).

5.6.1 Dunstan Fault

Fig. 5.6.8 **Location of differential GPS profiles and faults**

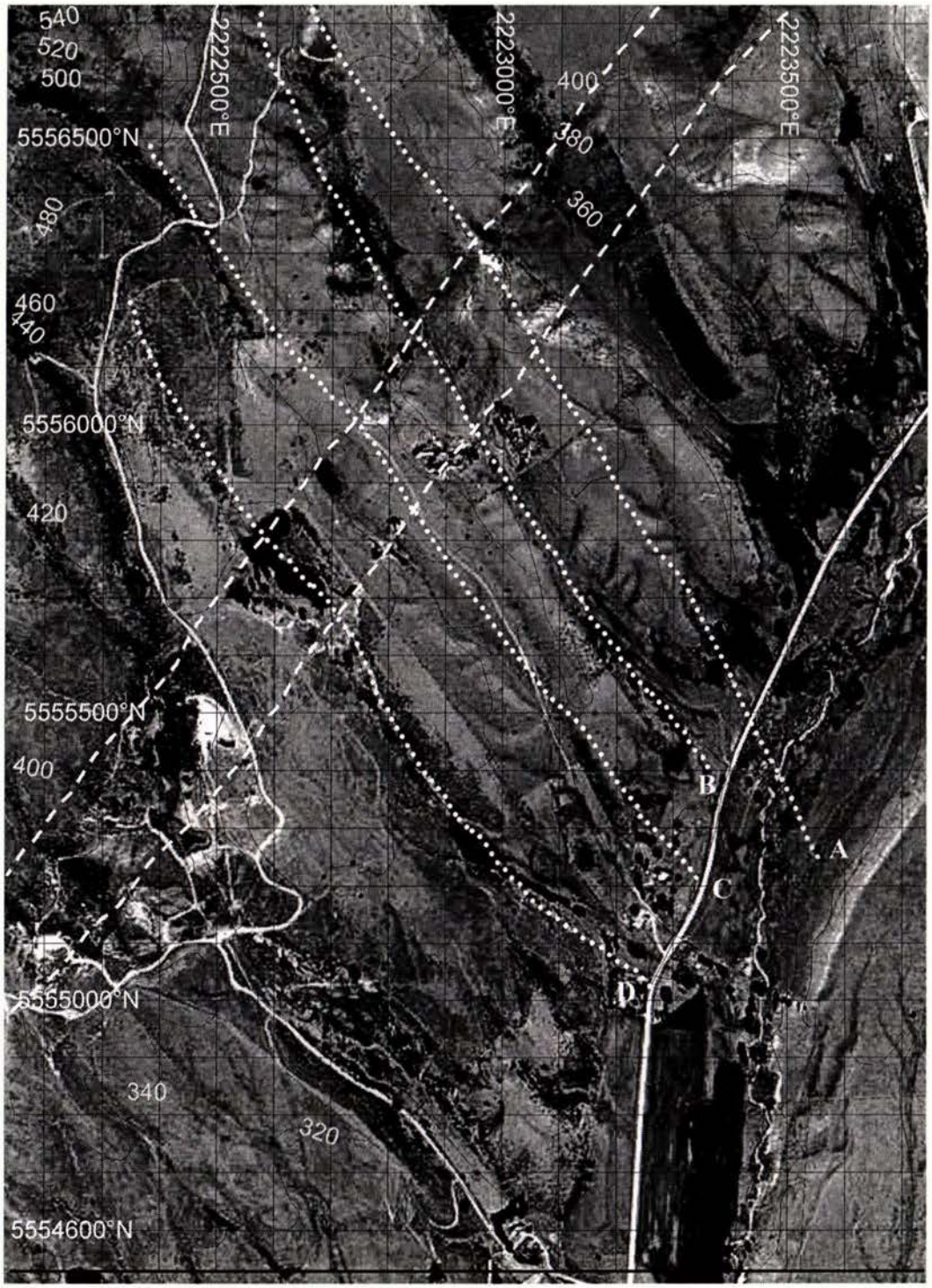

Inferred fault

GPS profile line

5.6.1 Dunstan Fault GPS Profiles

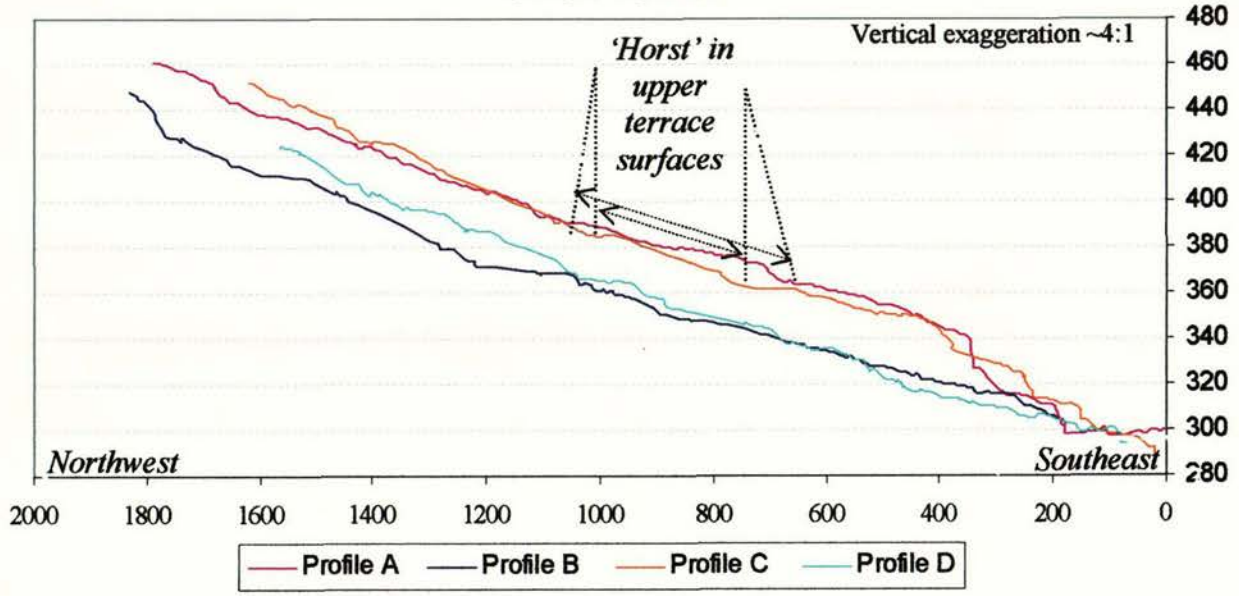

5.6.2 Dunstan Fault Discussion

The upper terrace surfaces show clear evidence for tectonic deformation (profiles A and C, *Figs.5.6.4, 5.6.5*) with multiple surface offsets and the formation of a horst-like structure producing range-parallel lineaments (Beanland *et al.,* 1986, *Fig.5.6.3*). Divergent internal bedding within the high terraces (*Fig. 5.6.6*) signifies ongoing uplift, but there is no clear evidence of tectonic deformation of the young infill terrace. In several places this surface has been disturbed by gold workings and irrigation dams, making the interpretation of surface anomalies equivocal. The surface slope is steeper than a natural stream gradient but the stream is still actively incising the terrace system. IGNS have been obtaining dates from the upper terrace surfaces, but as yet they haven't received their results (D. Barrell pers. comm., June 2004). For completeness we dated the young infill terrace with a view to information exchange. It appears that the activity responsible for upper terrace deformation is older than 1.66 ±0.16ka, but more extensive surface dating is required to further constrain activity on the Dunstan Fault and confirm the earlier work of Beanland *et al.* (1986) and Madin (1988).

6 GPS MEASUREMENTS ACROSS OTAGO FAULT PROVINCE

6 GPS MEASUREMENTS ACROSS OTAGO FAULT PROVINCE

In order to compare long term and short term rates of contraction across the Otago fault province, a direct measurement of shortening using GPS methods was required. Earlier attempts at measuring strain in Otago using triangulation of old networks (Blick 1986; Reilly, 1986; Pearson, 1990, Pearson in Norris et al., 1995) suggested very high strain rates in some areas and low strain rates close to or below the margin of error in others. In particular, the data suggested an anomalous region within central Otago where NW-SE apparent extension was occurring (Blick, 1986; Pearson, 1990). The strain rates shown by some networks are equal to higher than those adjacent to the Alpine Fault (Pearson, 1990), leading Pearson to comment that the measured strain was not commensurate with movement on Otago faults. Because strains were measured in isolated networks, producing an overall shortening across the region is difficult. Also, the triangulation method produces relative strains, rather than displacements, so that true extensions or contractions cannot be determined. Velocity models of Beavan and Haines (1998) are based on data interpolated from campaign GPS surveys (e.g. Beavan et al., 1999) and a few first order survey sites in areas such as the southern South Island where GPS data are few. Their calculated strain rates across the central South island show a NW-SE contraction across the eastern half of the island of around 2.5 mm/yr. Pearson (1995) suggested that the very high strain rates determined by him in central Otago may reflect accumulation of elastic strain which will eventually be released by Alpine Fault movement.

Fig.6.1 **Location of the GPS stations of this study**

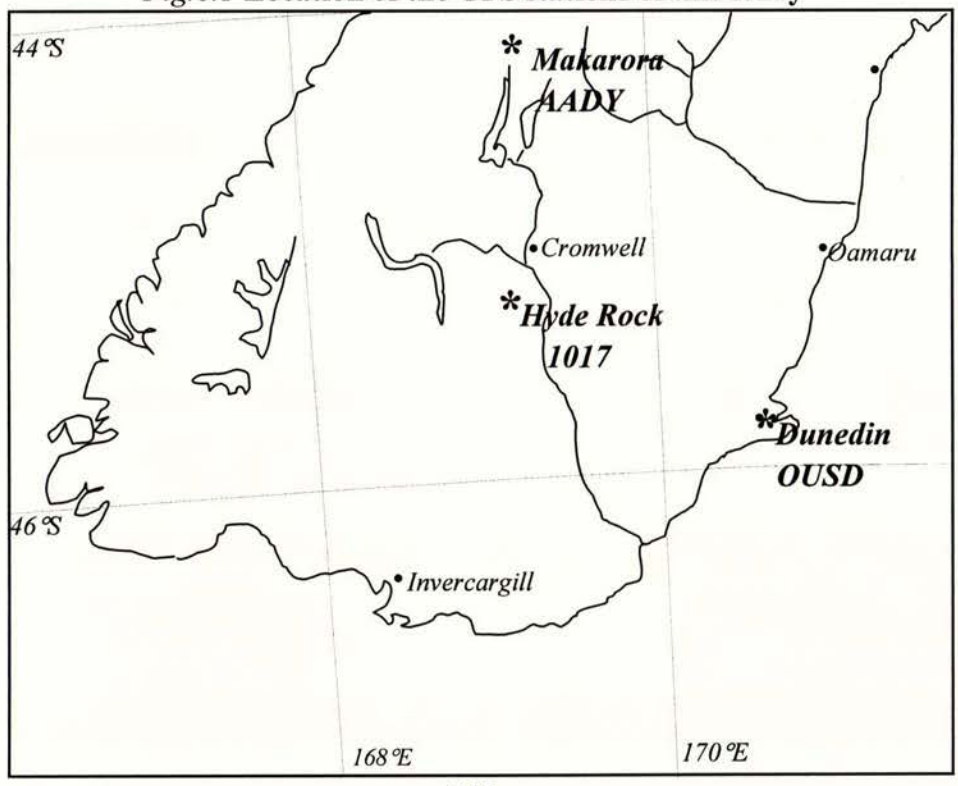

GPS determined strain rate distributions in the central South Island and dislocation modelling by Beavan et al. (1999) would suggest, however, that this effect should not extend east as far as central and east Otago. Because we felt that a knowledge of present day rates of contraction across Otago would add an extra dimension to the study, two trigs were chosen (Trig 1017 Hyde Rock GR 22122/55288; Trig AADY Makarora GR56613/22104; *Fig.* 6.1) that had had periods of GPS occupation on past occasions. Both had extensive occupation during the 1995 Fiordland campaign, and at intervals since. We reoccupied them during April 2003 so that a period of over 8 years is represented by the data. The 2003 measurements were made using Trimble 4700 receivers over 4 to 5 days of occupation at each site. All final results are derived from network solutions using the Bernese GPS package software, and the best models and practice at the time of each campaign. We thank Dr Paul Denys of the Department of Surveying, University of Otago, for assistance with the campaign measurements and for processing the data. The results are presented in Table 6.1.

Table 6.1 **Results from GPS surveys of Trigs at Hyde Rock (1017) and Makarora (AADY).**
COtago 03 are the measurements made during this study.
OUSD is the University of Otago Surveying Department continuous base station.

Campaign	Date	Distance (m) OUSD–1017	σ (m)	Δ distance (mm)	95% conf. interval	Distance (m) OUSD–AADY	σ (m)	Δ distance (mm)	95% conf. interval
Fiord95	21-Feb-95	115587.144	0.0006	4.676	1.2	210950.438	0.0012	9.445	2.4
nzfo95	06-Mar-95	115587.145	0.0094	6.160	18.4				
nzfo96	06-Mar-96	115587.142	0.0098	2.581	19.3				
nzfo97	10-Apr-97	115587.140	0.0111	0.734	21.8				
Haast98	19-Jan-98					210950.431	0.0021	2.654	4.1
nzfo98	07-Sep-98	115587.133	0.009	-6.379	18.5				
Fiord01	10-Feb-01					210950.420	0.0006	-8.478	1.1
COtago03	15-Apr-03	115587.131	0.0020	-7.772	4.0	210950.425	0.0016	-3.621	3.2

The distance between the Otago University Department of Surveying continuous GPS base station (OUSD) and each of the two trigs is calculated for each occupation and the difference from the average distance listed. Makarora (AADY) was occupied on three occasions prior to the present study, all during GPS campaigns and with comparable precisions. Hyde Rock (1017) was occupied on five previous occasions, but apart from the first one in 1995, the precisions are an order of magnitude less. In order to determine a mean annual rate of change in length of the line between OUSD and each of the two trigs, a weighted regression line was fitted to each dataset (*Fig.* 6.2), with weightings inversely proportional to the error bars. For AADY, the best line gives an average contraction rate between Dunedin and Makarora of 2.22 ± 0.88 mm/yr. Although data precision is good, it is not possible to fit a line within error bars of all points. This may be due to some

unknown error on one measurement, to incorrect error bars, or to a non-linear displacement rate over the measurement period. Nevertheless, the data clearly show a contraction of between 1 and 3 mm/yr over this period. The best line through the Hyde Rock data gives a contraction rate between Dunedin and Hyde Rock of 1.58 ± 0.18 mm/yr. Because of the large error bars on all but the 1995 and present measurements, these two are the main influences on the slope of the line. If these two measurements only are used, and a rate calculated directly from them, a contraction rate of 1.53 ± 0.51 mm/yr is obtained. The results are consistent with general estimates of contraction rates of 1-3 mm/yr across the region (e.g. Beavan and Haines,1998, Beavan et al., 1999), with a greater contraction rate between Dunedin and Makarora than between Dunedin and Hyde Rock as would be expected. It should be pointed out that these determinations represent a linear contraction rate only, roughly perpendicular to the main faults. Comparison with shortening determined by fault dip-slip movement is therefore valid. Components of shortening or extension in a NE-SW direction however are not measured, so the existence of the "central Otago shear strain anomaly" of Blick (1986) and Pearson (1990) cannot be ascertained.

The Dunedin-Makarora line crosses the entire Otago fault province and the contraction rate of 2.2 mm/yr is consistent with that derived from fault offsets since the start of the Quaternary (Chapter 1). This in turn suggests a fairly steady-state strain rate across the region over time, which has implications for processes of strain partitioning across the plate boundary. The Dunedin–Hyde Rock contraction rate of 1.58 mm/yr, on the other hand, is higher than the long-term rate expected from fault offsets in East Otago. Although tentative, this may indicate a shifting of deformation eastwards over time. Such migration of deformation towards the foreland is a well-documented pattern in fold-thrust belts (ref. e.g. Boyer and Elliot, 1982; Mulugeta, 1988) and may be related to uplift on the hinterland faults and development of a surface slope (e.g. Davis et al., 1983; Koons, 1995). There is no strong stratigraphic evidence in Otago for a systematic eastwards development of faults, and clearly activity has occurred across the province during the late Quaternary. The data may merely indicate a current increase in strain rate in the east rather than a long-term trend. Nevertheless, this is an interesting result when considered alongside the evidence for surface deformation reported elsewhere in this document.

Fig. 6.2. Plot of difference in length relative to mean length of lines between Dunedin (OUSD) and Hyde Rock (1017) and Makarora (AADY) for the various times of occupation of the two trigs. Weighted regression lines fitted to each dataset (heavy line: OUSD-1017; light line: OUSD-AADY) give average rates of contraction of 1.58 ± 0.18 mm/yr (1017) and 2.22 ± 0.88 mm/yr (AADY).

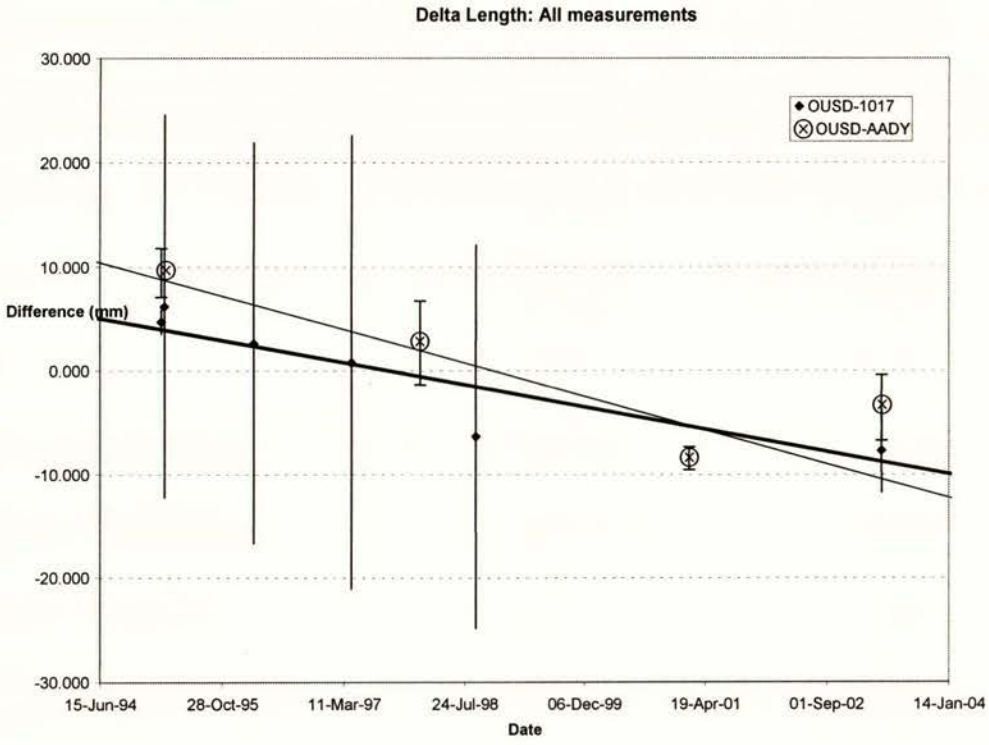

7 GENERAL DISCUSSION

7 DISCUSSION

This study, as discussed in the introduction, was intended to investigate the possibility that faults in central and east Otago are episodically active, with deformation at any one time being restricted to one or two structures and switching between structures over time. While there was no ambition to produce detailed definitive evidence and a comprehensive model, the objectives were rather to obtain data on the range front deformation of some of these structures and carry out preliminary dating of sedimentary units to place constraints on the most recent deformation. The results of the study presented in this report are extremely interesting and have implications for seismic hazard in the region. They indicate, however, that while episodic behaviour of some sort is almost certainly occurring, it is not perhaps as simple as the idealistic models discussed in the introduction.

The questions to be addressed include the following:

- What is the current rate of strain across Otago normal to the fault structures and how does it compare with geologically determined long-term rates?
- What evidence is there for activity on the range fronts in central and east Otago and what constraints can be placed on the age of deformation?
- Is there any evidence for long periods of quiescence on any of the fault structures?
- How do the data on range deformation relate to current strain rates?
- If there is evidence for recent movement on central Otago faults, why aren't well-delineated scarps as found on the Akatore fault more obvious?
- What implications do the data have for seismic hazard in the region?

We discuss each of these in turn below.

1) What is the current rate of strain across Otago normal to the fault structures and how does it compare with geologically determined long-term rates?

From the GPS measurements presented in Chapter 6, a contraction rate of 1.58 mm/yr between Dunedin and Hyde Rock was calculated, and one of 2.2 mm/yr between Dunedin and Makarora. Both estimates are subject to uncertainty. The rate between Dunedin and Makarora is consistent with estimates of long-term contraction across the region (Chapter 1) based on fault displacement data. The Dunedin-Hyde Rock rate is faster than might be expected from the faulting within the area. However, some faults such as the Akatore fault are probably younger than the large faults to the west and there could be a migration of activity from west to east over time.

If we take a contraction rate between Dunedin and Hyde Rock of c. 1.5 mm/yr, and assume that most of this strain is released by faulting within this area, then some 15 m of shortening is required during the Holocene. The Akatore Fault can accommodate around 4 m in the southern part of the area (Litchfield and Norris, 2000) but a comparable fault is required in North Otago if the rate is constant across the region. This still leaves over 10 m. The Dunstan fault has moved during the Holocene (Beanland et al., 1986) and although not crossed by the GPS line, may release some of the strain. This perhaps could release another 2-3 m. This still leaves at least 8 m in the south and 12 m in the north to be taken up. At 1-2 m per event, this requires perhaps 5-10 events on intervening structures during the Holocene. The Titri Fault has not moved since the last interglacial (Litchfield, 2001, Litchfield & Lian, 2004). The North Taieri Fault has possible young scarps (Litchfield, 2000) but no detailed work has been carried out. The remaining structures are those examined during the present study.

2) What evidence is there for activity on the range fronts in central and east Otago and what constraints can be placed on the age of deformation?

As presented in the main body of the report, the investigation has produced evidence for widespread Holocene activity within the region. Taieri Ridge, Rock and Pillar Range and the Rough Ridge group all show evidence for Holocene deformation along their respective range fronts. Dating of deformed terrace and fan deposits show most to be Holocene or latest (post-glacial) Pleistocene. One older surface at the Stot Burn (130 ka) exhibits considerable warping along the line of South Rough Ridge, indicating repeated deformation. This surface is consistent with exposure dating of a correlative terrace deformed over the end of South Rough Ridge at Oliverburn (Jackson et al., 2003). Apart from this example, the data is insufficient to recognize multiple fault events during the Holocene on a single structure. A more extensive investigation including trenching of fault traces would be required.

The evidence acquired during this investigation, therefore, is consistent with the predictions made in (1) above requiring extensive Holocene activity between Dunedin and Alexandra.

3) Is there any evidence for long periods of quiescence on any of the fault structures?

One of the objectives of the study was to see whether any of the structures showed a long time period since the last displacement, for instance like the Titri Fault. None of the faults investigated shows a long period of quiescence since the last displacement. We specifically targeted young deformation because we wanted to constrain the latest fault movements, with the result that data are not extensive enough to determine whether past periods of quiescence occurred. From the

discussion in Chapter 3, simple modeling of episodic behaviour suggests that long periods of quiescence may be the best evidence for non-random episodic behaviour. The data collected during this study suggest that several structures were active during the Holocene and therefore did not show episodic behaviour, at least with respect to each other, during this period. The evidence presented in Chapter 3 for episodic behaviour of Otago faults is still valid, in that several faults do apparently show long periods of quiescence between activity. The present study shows that such behaviour cannot be characterized by displacement restricted to only or two structures throughout the whole region and that patterns of fault activity are more complex.

4) How do the data on range deformation relate to current strain rates?

As discussed under (1) above, the range deformation data are entirely compatible with the short term contraction rate across east Otago, and are consistent with the conclusion that east Otago is currently an area of increased activity.

5) If there is evidence for recent movement on central Otago faults, why aren't well-delineated scarps as found on the Akatore fault more obvious?

This was a question we asked when beginning the study. One reason why most Otago faults weren't mapped as Holocene active structures is because clear well-marked scarps are not evident along their range fronts (although possible subdued scarps have been reported by Thompson, 1996). This contrasts with the Akatore fault, where two displacements in the last 4000 years have left sharp scarps across Holocene surfaces (Litchfield and Norris, 2000). This study has demonstrated that Holocene displacement has occurred on several structures despite the lack of obvious scarps. Surface features are present, as documented earlier, but these are not generally in the form of sharp scarps. The reasons for this have been discussed and are related to two main factors: (i) the reverse, moderate dips of the probable faults lead to slumping and rapid degradation of any surface scarp; and (2) the distributed nature of the deformation over several structures along the range front, leading to small displacements and tilting and folding of deposits. These two features are consistent with the largely folded nature of the central-east Otago ranges (Jackson et al., 1996; Markley and Norris, 1999), in contrast to the much more sharply faulted Akatore ridge.

6) What implications do the data have for seismic hazard in the region?

The data suggest that east Otago is more active than perhaps thought, with multiple events during the Holocene. We cannot consider the Dunstan and Akatore faults to be the only active structures. It is likely that at least some of the investigated structures are potentially as potent sources of

earthquakes as the Akatore Fault, which is usually the one highlighted in seismic hazard analysis. This increases the level of hazard in east Otago. A shortening rate of 1.5 mm/yr across the region would require perhaps one event every 1000 years or so. The Akatore Fault last moved about 1000 years ago. The data collected in this report puts only loose constraints on timing of deformation on other structures, so the time since the last event in the region is uncertain. This makes conditional probabilities difficult to calculate, but it is likely that they are enhanced above the standard Poisson estimate used in most hazard estimates.

More detailed work is required on each of these structures to determine their individual seismic history. As shown by Beanland et al. (1986), such investigations are difficult, but as demonstrated here, OSL dating techniques have provided a potent weapon in placing age constraints on deposits affected by deformation. Thus detailed investigation and trenching studies have potential despite the lack of material for carbon-dating.

CONCLUSIONS

- The current rate of contraction across Otago is consistent with long-term estimates based on fault displacements.
- Rough Ridge, Rock and Pillar, and Taieri Ridge all show evidence for Holocene activity in addition to the Akatore and Dunstan faults. This is compatible with the contraction rate across the region.
- While the arguments for episodic movement on Otago faults remain, the present results show that the behaviour patterns are more complex than those developed at the start of the investigation.
- The data show widespread Holocene activity on east Otago structures and suggest that seismic hazard in the region is perhaps higher than previously envisaged, with several structures presenting hazards. These should be considered in local hazard models.
- Detailed paleoseismic studies are required on east Otago structures to elucidate past activity. The last known event was 1000 yrs BP on the Akatore Fault. The conditional probability of a similar event occurring on one of the east Otago structures is likely to be higher than the Poisson model would indicate.

Acknowledgments

The authors wish to thank the multitude of people who gave freely of their time and expertise, and without whom this project would not have been possible. This includes the many landowners and their families who allowed free access to the field areas.

Special thanks goes to;

Paul Denys, Chris Pearson, Mark Peters, Alistair Neave, and Mike Denham of the Otago University Surveying Department for the use of their equipment, instruction in its use, and assistance with processing data;

Dr. Uwe Rieser and Ningsheng Wang at the Victoria University luminescence laboratory for instruction in sample preparation and free use of their facilities;

James Jackson, Eleanor Bennett (Cambridge University), John Youngson (Otago University) for stimulating and interesting discussions;

Active Earth Processes Group, University of Otago, and the EQC for facilitating the project.

References

Adams, C. J., Graham, I. J., 1997. Age of metamorphism of Otago Schist in eastern Otago and determination of protoliths from initial strontium isotope characteristics. *New Zealand Journal of Geology and Geophysics* 40: 275-286.

Aitken, M. J., 1985. Thermoluminescence dating. Academic Perss, London, 359pp.

Balance, P., 1993. The paleo-Pacific, post-subduction, passive margin thermal relaxation Sequence (Late Cretaceous – Paleogene) of the drifting New Zealand continent. *In*: Balance, P., *ed.* South Pacific sedimentary basins. Sedimentary basins of the world, 2. Amsterdam, Elsevier Science. Pp 93-110.

Beanland, S., Barrow-Hurlbert, S. A., 1988. The Nevis-Cardrona Fault System, central Otago, New Zealand: Late Quaternary tectonics and structural development. *New Zealand Journal of Geology and Geophysics* 31: 337-352.

Beanland, S., Berryman, K. R., 1989. Style and episodicity of late Quaternary activity on the Pisa-Grandview fault zone, central Otago, New Zealand. *New Zealand Journal of Geology and Geophysics* 32: 337-352.

Beanland, S., Berryman, K. R., Hull, A. G., Wood, P. R., 1986. Late Quaternary deformation at the Dunstan Fault, central Otago, New Zealand. In: *Recent crustal movements of the Pacific region* Reilly, W. I., Harford, B. E., (eds.). *Bulletin of the Royal Society of New Zealand* 24: 293-306.

Beanland, S., Forsyth, J., 1988. Structural Geology at the intersection of the Blue Lake and Blackstone Faults, Pennyweight Hill, Central Otago. New Zealand Geological Survey Immediate Report 88/7,1-6.

Beavan, J. and Haines, J., 1998, Contemporary horizontal velocity and strain fields of the Pacific-Australian plate boundary zone through New Zealand: Journal of Geophysical Research, 106, p. 741-770.

Beavan J; Moore M; Pearson C; Henderson M; Parsons B; Bourne S; England; P; Walcott D; Blick G; Darby D, and Hodgkinson K. 1999. Crustal deformation during 1994-1998 due to oblique continental collision in the central Southern Alps, New Zealand, and implications for seismic potential of the Alpine fault. Journal of Geophysical Research. 104: p. 25,232-25,255.

Benson, W. N., 1935. Some landforms in southern New Zealand. *The Australian Geographer* 3: 3-23.

Berryman, K. R., Beanland, S., 1991. Variation in fault behaviour in different tectonic

provinces of New Zealand. *Journal of Structural Geology.* 13: 177-189.

Berryman, K. R., Beanland, S., Cooper, A. F., Cutten., H. N., Norris, R. J., Wood, P. R., 1992. The Alpine Fault, New Zealand: variation in Quaternary structural style and geomorphic expression. *Annales Tectonicæ* 6: 126-163.

Bishop, D. G., 1972. Stratigraphic, structural and metamorphic relationships in the Dansey Pass area, Otago, New Zealand. *New Zealand Journal of Geology and Geophysics* 17: 301-335.

Bishop, D. G., 1974. Progressive metamorphism from prehinite-pumpellyite to greenschist facies in the Dansey Pass area, Otago, New Zealand. *Geological Society of America Bulletin* 83: 3177-3198.

Bishop, D. G., 1979. Sheet S135 – Ranfurly. Geological map of New Zealand 1:63,360. Wellington, New Zealand. Department of Scientific and Industrial Research.

Bishop, D. G., 1994. Extent and regional deformation of the Otago peneplain. Institute of Geological and Nuclear Sciences Science Report 94/1, l0pp.

Bishop, D. G., Bradshaw, J. D., Landis, C. A., 1985. Provisional Terrane Map of South Island, New Zealand. In: *Tectonostratigraphic Terranes of the Circum-Pacific Region,* Howell, D. G. (ed.), *Circum-Pacific of Energy and Mineral Resources, Earth Science Service* 1: 515-521.

Bishop, D. G., Laird M. G., 1976. Stratigraphy and depositional environment of the Kyeburn Formation (Cretaceous), a wedge of coarse terrestrial sediments in Central Otago. *Journal of the Royal Society of New Zealand* 6: 55-71.

Blair, T. C., McPherson, J. G. 1994. Alluvial fans and their natural distinction from rivers based on morphology, hydraulic processes, sedimentary processes, and facies assemblages. *Journal of Sedimentary research* A64, 3: 450-489.

Blick, G.H., 1986, Geodetic determination of crustal strain from old survey data in Central Otago.: Royal Society of New Zealand Bulletin, 24, p. 47-54.

Boyer, S.E. and Elliott, D., 1982, Thrust systems: American Association of Petroleum Geologists Bulletin, v. 66, p. 1196-1230. (Abstract)

Bradshaw, J. D., Andrews, P. B., Adams, C. J. D., 1981. Carboniferous to Cretaceous on The Pacific margin of Gondwana: the Rangitata phase of New Zealand. *In*: Cresswell, M. M., Vella, p. *ed.* Gondwana five: selected papers and abstracts of papers presented at the Fifth International Gondwana Symposium. Rotterdam, A. A. Balkema. Pp 217-221.

Bull, W. B., Cooper, A. F., 1986. Uplifted marine terraces along the Alpine Fault, New

Zealand. *Science 234:1225-1228.*

Coombs, D. S., Cas, R. A., Kawachi, Y., Landis, C. A., McDonough, W. F., Reay, A., 1986. Cenozoic volcanism in north, east, and central Otago. *Royal Society Bulletin* 23: 278-312.

Cotton, C. A., 1917. Block mountains in New Zealand. *American Journal of Science* 44: 250-293.

Cotton, C. A., 1919. Rough Ridge, Otago, and its splintered fault-scarp. *Transactions of the New Zealand Institute* 24:282-285.

Cotton, C. A., 1949. Geomorphology, Wellington New Zealand. Whitcombe and Tombs Limited, 503p.

Craw, D., 1998. Structural boundaries and biotite and garnet 'isograds' in the Otago and Alpine Schists. *Journal of Metamorphic Geology* 16: 395-402.

Craw, D., Chappell, D. A., 1999. Evolution and sulphide mineral occurrences of an Incipient nonmarine sedimentary basin, New Zealand. *Sedimentary Geology* 129:37-50.

Davis, D., Suppe, J., and Dahlen, F.A., 1983, Mechanics of fold-and-thrust belts and accretionary wedges: Journal of Geophysical Research, 88, p. 1153-1172.

Deckert, H., Ring, U., Mortimer, N., 2002. Tectonic significance of Cretaceous bivergent extensional shear zones in the Torlesse accretionary wedge, central Otago Schist, New Zealand. *New Zealand Journal of Geology and Geophysics* 45: 537-547.

DeMets, C., Gordon, R. G., Argus, D. F., Stein, S., 1994. Effect of recent revisions to the geomagnetic reversal time scale on estimates of current plate motions. *Geophysical Research Letters* 21, 2191-2194.

Douglas, B. J., 1986. Lignite resources of Central Otago, New Zealand. Energy Research and development Committee publication P104, Auckland, New Zealand, University of Auckland, 368p.

Forsyth, P. J., *compiler,* 2001. Geology of the Waitaki area. *Institute of Geological and Nuclear Sciences* 1:250,000 *Geological Map* 19. 1 sheet + 64p. Lower Hutt, New Zealand. Institute of Geological and Nuclear Sciences Limited.

French, R. H., 1987. Hydraulic Processes on Alluvial Fans; Amsterdam, Elsevier, 244p.

Gray, D. R., Gregory, R. T., Norris, R. J., Cox, S. C., 1995. Regional scale sheath-folding and heterongeneous distributed shear strain in an evolving nappe pile, Otago schist, New Zealand. Australian Structural Geology and Tectonics Study Group Conference, Clare Valley. *Geological Society of Australia Abstracts* 40: 53-54.

Hutton, C. O., Turner, F. J., 1936. Metamorphic zones in northwest Otago. *Transactions of the Royal Society of New Zealand* 65: 405-406.

Jackson, J., Leeder, M., 1994. Drainage systems and the development of normal faults: an example from Pleasant Valley, Nevada. Journal of Structural Geology 16, 1041-1060.

Jackson, J. A., Norris, R. J., Youngson, J. H., 1996. The structural evolution of fault and fold systems in central Otago: evidence revealed by drainage patterns. *Journal of Structural Geology* 13: 217-235.

Jackson, J. A., Ritz, J., Siame, L., Raisbeck, G., Yiou, F., Norris, R. J., Youngson, J. H., Bennett, E. 2002. Fault growth and landscape development rates in Otago, New Zealand, using in situ cosmogenic ^{10}Be. *Earth and Planetary Science Letters* 195: 185-193.

Koons, P.O., 1995, Modeling the topographic evolution of collisional belts: Annual Reviews of Earth & Planetary Science, 23, p. 375-408.

Korsch, R. J., Wellman, H. W., 1988. The geological evolution of New Zealand and the New Zealand region. *In*: Nairn, A. E., Stehli, F. G., Uyeda, S. *ed.* The ocean basins And their margins, 7b. New York, Plenum Press, Pp. 411-482.

Kneupffer, P. L. K., 1992. Temporal variations in latest Quaternary slip across the Australian-Pacific plate boundary, northeastern South Island, New Zealand. *Tectonics II*: 449-464.

Lee, H-K., Schwarz, H. P., 1996. Electron-spin resonance plateau dating of periodicity of Activity on the San Gabriel fault zone, southern California. Geological Society of America Bulletin 108,735-746.

Le Mesurier, W. E., Landis, C. A., 1996. Mantle-plume activity recorded by low-relief erosion surfaces in West Antarctica and New Zealand. *Geological Society of America Bulletin* 108: 1450-1466.

Litchfield, N. J., 2000. Quaternary deformation at the leading edge of the Otago reverse fault province. *Unpublished PhD thesis held at Otago University.*

Litchfield, N. J., 2001. TheTitri Fault System: Quaternary-active faults near the leading edge of the Otago reverse fault province. *New Zealand Journal of Geology and Geophysics* 44: 517-534.

Litchfield N. J., Lian O. B. 2004. Luminescence age estimates of Pleistocene marine terrace and alluvial fan sediments associated with tectonic activity along coastal Otago, New Zealand. *New Zealand. New Zealand Journal of Geology and Geophysics* 47: p. 29-37.

Litchfield, N. J., Norris, R. J., 2000. Holocene motion on the Akatore Fault, south Otago coast, New Zealand. *New Zealand Journal of Geology and Geophysics* 43: 405-418.

MacKinnon, T. C., 1983. Origin of Torlesse terrane and related rocks, South Island, New Zealand. Geological Society of America Bulletin 94: 967-985.

McLane, M., 1995. Sedimentology. Oxford University Press, 423p.

McSavney, M. J., Thomson, R., Turnbull, I. M., 1992. Timing of relief and Landslides in Central Otago. *In*: Bell, D. H., (*ed.*), Landslides, Sixth International Symposium on Landslides Proceedings. Balkema, Rotterdam, pp 1451-1456.

Madin, I. 1988. Geology and Neotectonics of the Upper Manuherikia Basin, Central Otago, New Zealand. New Zealand Geological Survey Record 27, 1988.

Markley, M., Norris, R. J., 1999. Structure and Neotectonics of the Blackstone Hill Antiform, central Otago, New Zealand. *New Zealand Journal of Geology and Geophysics* 42: 205-218.

Markley, M., Tikoff, B., 2003. Geometry of the folded Otago peneplain surface beneath Ida Valley, Central Otago, New Zealand, from gravity observations. *New Zealand* Journal of Geology and Geophysics 46: 449-456.

Mortimer, N., 1993. Geology of the Otago Schist and adjacent rocks. Scale 1:50,000. *Institute of Geological and Nuclear Sciences Geological Map* 7. Institute of Geological and Nuclear Sciences Ltd. Lower Hutt, New Zealand.

Mortimer, N., 2000. Metamorphic discontinuities in orogenic belts: example of the garnet-biotite-albite zone in the Otago Schist, New Zealand. *International Journal of Earth Sciences* 89: 295-306.

Mortimer, N., Campbell, H. J., 1996. Devonian to Jurassic rocks in New Zealand: Classification, content and Gondwana context. *In*: Guha, P. K. S., Sengupta, S., Ayyasami, K., Gosh, R. N. *ed.* Gondwana nine. New Delhi, Oxford and IBH Publishing. Pp 783-790.

Mulugeta, G., 1988, Modelling the geometry of Coulomb thrust wedges: Journal of Structural Geology, 10, p. 847-859.

Mutch, A. R., Wilson, D. D., 1952.Reversal of movement on the Titri Fault. *New Zealand Journal of Science and Technology* B33: 398-403.

Mutch, A. R., 1963. Sheet 23 - Oamaru. Geological Map of New Zealand 1:250,000, DSIR, Wellington.

Norris, R. J., 1979. A geometric study of finite strain and bending in the South Island. In *The Origin of the Southern Alps,* Walcott, R. I., Cresswell, M. M. (eds.). *Bulletin of* the Royal Society of New Zealand 18: 21-28.

Norris, R. J., Cooper, A. F., 2001. Late Quaternary slip rates and slip partitioning on the Alpine Fault, New Zealand. Journal of Structural Geology 23, 507-520.

Norris, R. J., Koons, P.O., Cooper, A.F., 1987. Aspects of the South Island Collision Zone, Central Otago and the West Coast. *Geological Society of New Zealand Miscellaneous Publication* 37C: 39-88.

Norris, R. J., Koons, P. O., Landis, C. A., 1995. Seismotectonic evaluation of fault structures in east Otago. Unpublished research report to the New Zealand Earthquake Commission, EQC Report 91/53, Wellington.

Officers of the Geological Survey, 1983. Seismotectonic evaluation of the Clyde Dam site. *New Zealand Geological Survey/ EG Report 375.*

Pearson, C., 1990, Extent and significance of the Central Otago shear-strain anomaly: New Zealand Journal of Geology & Geophysics, 33, p. 295-301.

Rees-Jones, R. J., Rink, W. J., Norris, R. J., Litchfield., N. J., 2000. Optical luminescence dating of uplifted marine terraces along the Akatore Fault near Dunedin, South Island, New Zealand. *New Zealand Journal of Geology and Geophysics* 43: 419-424.

Reilly, W.I., 1986, Crustal bending in Otago, New Zealand, from the evidence of geodetic measurements: Royal Society of New Zealand Bulletin, 24, p. 65-73.

Ritter, D.F., Kochel, R. C., Miller, J. R., 1995. Process Geomorphology. W. C. Brown Publishers, 525pp.

Roser, B. P., Cooper, A. F., 1990. Geochemistry and terrane affiliation of Haast Schist from The western Southern Alps, New Zealand. *New Zealand Journal of Geology and Geophysics* 33: 1-10.

Salton, G. G., 1993. An investigation into the Recent deformation of the Rock and Pillar Range. *Unpublished Master of Science thesis held at Otago University.*

Stirling, M. W, 1990. The Old Man Range and Garvie Mountains: tectonic geomorphology of the Central Otago peneplain, New Zealand. *New Zealand Journal of Geology and Geophysics* 33: 233-243.

Stirling, M.W., Rhoades, D., Berryman, K., 1998. Evaluation of Wells and Coppersmith (1194) Earthquake and Fault Relationships in the New Zealand context. EQC Research Report 97-249.

Swan, F. H., 1988. Temporal clustering of paleoseismic events on the Oued Fodda fault, Algeria. Geology 16,1092-1095.

Stein, R. S., King, G. C., 1984. Seismic potential revealed by surface folding: The 1983 Coalinga, California earthquake. *Science* 224: 867-872.

Thomson, R., 1996. Quaternary fault traces, Maniototo Basin. IGNS Immediate Report H41/831.

Turnbull, I. M., *compiler* 2000. Geology of the Wakatipu area. *Institute of Geological and Nuclear Sciences* 1:250,000 *Geological Map* 18. 1 sheet + 72p. Lower Hutt, New Zealand. Institute of Geological and Nuclear Sciences Limited.

Turnbull, I. M., Craw, D., Norris, R. J., 1993. Pre-Miocene and Post-Miocene deformation in the Bannockburn Basin, New Zealand. *New Zealand Journal of Geology and Geophysics* 36: 107-115.

Wallace, R. E., 1987. Grouping and migration of surface faulting and variations in slip rates On faults in the Great Basin Province. Seismological Society of America Bulletin 77, 868-876.

Wang, N., 2001. Optically Stimulated Luminescence Dating Techniques and their Application to Dating the Formation of Late Quaternary Loess in Southern North Island, New Zealand. Unpublished MSc. Thesis held at Victoria University, Wellington, New Zealand.

Wells, D. L., Coppersmith, K. J., 1994. New empirical relationships among magnitude, rupture length, rupture width, rupture area, and surface displacement. Bulletin of the Seismological Society of America, Vol. 84, No.4:974-1002.

Williamson, J. H., 1933. Naseby Subdivision. New Zealand Geological Survey 27th annual Report. Pp. 6-10.

Williamson, J. H., 1939. The geology of the Naseby Subdivision, central Otago, New Zealand. *Geological Survey Bulletin* 39: 141pp.

Wood, B. L., 1962; Sheet 22 – Wakatipu. Geological map of New Zealand 1:250,000. Wellington, New Zealand. Department of Scientific and Industrial Research.

Yardley, B. W. D., 1982. The early metamorphic history of the Haast Schists and related rocks of New Zealand. *Contributions to Mineralogy and Petrology* 81: 317-327.

Yeats, R. S., 1986. Faults related to folding with examples from New Zealand. *Royal Society of New Zealand Bulletin* 24: 273-292.

Yeats, R. S., 1987. Tectonic map of central Otago based on Landsat imagery. *New Zealand Journal of Geology & Geophysics* 30, 261-271.

Youngson, J. H., Craw, D., 1995. Evolution of placer gold deposits during regional uplift, Central Otago, New Zealand. *Economic Geology* 90: 731-745.

Youngson, J. H., Craw, D, Landis, C. A., Schmidt, K. R., 1998. Redefinition and interpretation of late Miocene-Pleistocene terrestrial stratigraphy, Central Otago, New Zealand. *New Zealand Journal of Geology and Geophysics* 41: 51-68.

Appendix

Copy of Luminescence Laboratory Technical Report 04/01

School of earth Sciences

P.O. Box 600, Wellington, New Zealand.

Telephone 64-4-463 5233 Ext. 5345, Facsimile 64-4-463-5186

Determination of sediment deposition ages by Luminescence Dating

Dr. Uwe Rieser

04/01
Technical Report
13th January 2004

SCHOOL OF EARTH SCIENCES
P.O.Box 600, Wellington, New Zealand, Telephone +64-4-463 5233 Ext. 5345, Facsimile+64-4-463-5186

Luminescence Dating of 12 samples / Otago

report by: Dr. Uwe Rieser
Luminescence Dating Laboratory / School of Earth Sciences
Victoria University of Wellington
e-mail: uwe.rieser@vuw.ac.nz
tel: 0064-4-463-6125
fax: 0064-4-463-5186

Summary
12 samples (laboratory code WLL319-WLL330) were submitted for Luminescence Dating by Ross Nichols / Richard Norris (University of Otago). The deposition ages have been determined for all of these samples using the silt fraction. The palaeodose, i.e. the radiation dose accumulated in the sample after the last light exposure (assumed at deposition), was determined by measuring the blue luminescence output during infrared optical stimulation (which selectively stimulates the feldspar fraction). The doserate was estimated on the basis of a low level gammaspectrometry measurement.
All measurements were done in Victoria Universities Dating Laboratory.

Procedure / Luminescence measurements
Sample preparation was done by Ross Nichols himself under extremely subdued safe orange light in a darkroom. Outer surfaces, which may have seen light during sampling, were removed and discarded.
The actual water content and the saturation content were measured using 'fresh' inside material. The samples were treated with 10%HCl to remove carbonates until the reaction stopped, then carefully rinsed with distilled water. Thereafter, all organic matter was destroyed with 10%H_2O_2 until the reaction stopped, then carefully rinsed with distilled water. By treatment with a solution of sodium citrate, sodium bicarbonate and sodium dithionate iron oxide coatings were removed from the mineral grains and then the sample was carefully rinsed again.
The grain size 4-11μm was extracted from the samples in a water-filled (with added dispersing agent to deflocculate clay) measuring cylinder using Stokes' Law. The other fractions were discarded. The samples then are brought into suspension in pure acetone and deposited evenly in a thin layer on 70 aluminum discs (1cm diameter).
Luminescence measurements were done using a standard Riso TL-DA15 measurement system, equipped with Kopp 5-58 and Schott BG39 optical filters to select the luminescence blue band around 410nm. For some samples the Kopp 5-58 was removed to gain more luminescence light, effectively broadening the detection band to 330-600nm. Stimulation was done cw at about 30mW/cm^2 with infrared diodes at 880Δ80nm. β-irradiations were done on a Daybreak 801E $^{90}Sr,^{90}Y$ β-irradiator, calibrated against SFU, Vancouver, Canada to about 3% accuracy. α-irradiations were done on a ^{241}Am irradiator supplied and calibrated by ELSEC, Littlemore, UK.

The Paleodoses were estimated by use of the multiple aliquot additive-dose method (with late-light subtraction). After an initial test-measurement, 30 aliquots were β-irradiated in six groups up to five times of the dose result taken from the test. 9 aliquots were α-irradiated in three groups up to three times of the dose result taken from the test. These 39 disks were stored in the dark for four weeks to relax the crystal lattice after irradiation.

After storage, these 39 disks and 9 unirradiated disks were preheated for 5min at 220C to remove unstable signal components, and then measured for 100sec each, resulting in 39 shinedown curves. These curves were then normalized for their luminescence response, using 0.1s shortshine measurements taken before irradiation from all aliquots.
The luminescence growth curve (β-induced luminescence intensity vs added dose) is then constructed by using the initial 10 seconds of the shine down curves and subtracting the average of the last 20 sec, the so called late light which is thought to be a mixture of background and hardly bleachable components. The shine plateau was checked to be flat after this manipulation. Extrapolation of this growth curve to the dose-axis gives the equivalent dose D_e, which is used as an estimate of the Paleodose.
A similar plot for the alpha-irradiated discs allows an estimate of the α-efficiency, the a-value (Luminescence/dose generated by the α-source divided by the luminescence/dose generated by the β-source).

Fading test
Samples containing feldspars in rare cases show an effect called anomalous fading. This effect inhibits accurate dating of the sample, as the electron traps in the crystal lattice of these feldspars are unable to store the age information over longer periods of time.
None of your samples gave an indication of this problem so far, but a routine test must be carried out after 6 months storage of an irradiated subsample to be sure. Thus, all ages reported below must be seen as preliminary until the fading test has been carried out. You will be notified by e-mail about the result.

Procedure / Gamma spectrometry
The dry, ground and homogenised soil samples were encapsuled in airtight perspex containers and stored for at least 4 weeks. This procedure minimizes the loss of the short-lived noble gas ^{222}Rn and allows ^{226}Ra to reach equilibrium with its daughters ^{214}Pb and ^{214}Bi.

The samples were counted using high resolution gamma spectrometry with a broad energy Ge detector for a minimum time of 24h. The spectra were analysed using GENIE2000 software. The doserate calculation is based on the activity concentration of the nuclides ^{40}K, ^{208}Tl, ^{212}Pb, ^{228}Ac, ^{214}Bi, ^{214}Pb, ^{226}Ra.

Results

Table1: Doserate contribution of cosmic radiation

Sample no.	depth below surface (m)	dD_c/dt (Gy/ka)[1]	Field code
WLL319	0.4	0.2104±0.0105	#4
WLL320	0.4	0.2104±0.0105	#5
WLL321	0.5	0.2075±0.0104	#6
WLL322	2.2	0.1645±0.0082	#7
WLL323	0.6	0.2046±0.0102	#9
WLL324	0.6	0.2046±0.0102	#10
WLL325	0.4	0.2104±0.0105	#11
WLL326	0.85	0.1976±0.0099	#12
WLL327	0.4	0.2104±0.0105	#13
WLL328	0.5	0.2075±0.0104	#14
WLL329	0.9	0.1962±0.0098	#8
WLL330	0.4	0.2104±0.0105	#1

[1] Contribution of cosmic radiation to the total doserate, calculated as proposed by Prescott & Hutton (1994), Radiation Measurements, Vol. 23.

Table2: Radionuclide and water contents

Sample no.	Water content δ[1]	U (µg/g) from ^{234}Th	U (µg/g)[2] from ^{226}Ra, ^{214}Pb, ^{214}Bi	U (µg/g) from ^{210}Pb	Th (µg/g)[2] from ^{208}Tl, ^{212}Pb, ^{228}Ac	K (%)	Field code
*WLL319	1.473	8.93±0.70	3.28±0.06	3.70±0.52	14.0±0.2	2.13±0.05	#4
WLL320	1.302	2.71±0.36	2.38±0.04	2.05±0.34	9.91±0.14	1.91±0.04	#5
WLL321	1.296	2.44±0.32	2.03±0.04	2.15±0.31	8.25±0.12	1.33±0.03	#6
WLL322	1.219	2.29±0.31	1.79±0.03	1.48±0.29	9.04±0.13	1.46±0.03	#7
WLL323	1.306	2.92±0.38	2.48±0.04	2.41±0.36	9.68±0.15	1.67±0.04	#9
WLL324	1.171	2.90±0.35	2.49±0.04	2.56±0.34	9.30±0.14	1.36±0.03	#10
WLL325	1.172	2.71±0.38	2.66±0.05	2.74±0.38	11.7±0.2	1.71±0.04	#11
WLL326	1.243	2.02±0.30	2.01±0.04	2.18±0.30	7.76±0.12	1.67±0.04	#12
*WLL327	1.318	5.18±0.55	3.49±0.06	4.16±0.52	13.2±0.2	2.28±0.05	#13
WLL328	1.307	3.16±0.42	2.42±0.05	2.66±0.40	12.3±0.2	1.93±0.04	#14
WLL329	1.307	2.91±0.38	2.59±0.05	3.20±0.38	9.45±0.15	1.61±0.04	#8
WLL330	1.231	1.91±0.35	2.15±0.04	2.21±0.36	8.75±0.14	1.67±0.04	#1

[1] Ratio wet sample to dry sample weight. Errors assumed 50% of (δ-1).
[2] U and Th-content is calculated from the error weighted mean of the isotope equivalent contents
* A radioactive disequilibrium is significant on a 2σ-level for these samples

Table3: Measured a-value and equivalent dose, doserate and luminescence age

Sample no.	a-value	D_e (Gy)	dD/dt (Gy/ka)	OSL-age (ka)	Field code
[1]WLL319*	0.065±0.009	5.36±0.61	4.13±0.39	1.30±0.24	#4
WLL320*	0.046±0.005	16.6±0.8	3.13±0.26	5.31±0.52	#5
WLL321*	0.044±0.004	34.7±2.0	2.44±0.20	14.2±1.4	#6
WLL322	0.081±0.011	382.7±50.0	2.95±0.20	129.8±19.1	#7
WLL323*	0.036±0.004	21.3±1.7	2.85±0.24	7.47±0.87	#9
[2]WLL324*	0.08±0.02	14.1±2.4	3.31±0.25	4.26±0.79	#10
WLL325*	0.051±0.012	30.6±2.3	3.63±0.23	8.42±0.83	#11
WLL326*	0.067±0.013	29.2±2.7	2.94±0.22	9.93±1.19	#12
[3]WLL327*	0.070±0.010	31.1±1.6	4.36±0.37	7.14±0.76	#13
WLL328*	0.058±0.005	44.3±1.3	3.43±0.29	12.9±1.1	#14
WLL329*	0.063±0.011	8.11±0.44	3.02±0.26	2.69±0.27	#8
WLL330*	0.053±0.007	5.00±0.33	3.02±0.21	1.66±0.16	#1

[1] This sample showed a radioactive disequilibrium, and the given age was corrected accordingly. As the level of disequilibrium over time is unknown, this age is only a better estimate and cannot be seen as the 'true' age. Without correction, i.e. using the Uranium equivalent of ^{226}Ra fi doserate calculation: dD/dt=3.55±0.93 and age=1.51±0.24ka.

[2] The a-value was estimated.

[3] This sample showed a radioactive disequilibrium, and the given age was corrected accordingly. As the level of disequilibrium over time is unknown, this age is only a better estimate and cannot be seen as the 'true' age. Without correction, i.e. using the Uranium equivalent of ^{226}Ra fi doserate calculation: dD/dt=4.18±0.37 and age=7.44±0.76ka.

* These samples showed very low luminescence intensity in the 410nm band. Thus it was decided to use a broadband BG39 filter (330-600nm) for detection.